UNIVERSIDADE D
COIMBRA

Marco António Machado Simões

THE NEUROBEHAVIORAL CORRELATES OF SOCIAL EXPLORATION IN NATURALIST SETTINGS IN NORMAL AND AUTISTIC SUBJECTS

A CLINICAL INFORMATICS APPROACH

Tese no âmbito do Programa de Doutoramento em Ciências e Tecnologias da Informação orientada pelo Professor Doutor Miguel de Sá e Sousa Castelo-Branco e pelo Professor Doutor Paulo Fernando Pereira de Carvalho e apresentada ao Departamento de Engenharia Informática da Faculdade de Ciências e Tecnologia.

Agosto de 2019

Universidade de Coimbra

Faculdade de Ciências e Tecnologia

FACULDADE DE
CIÊNCIAS E TECNOLOGIA
UNIVERSIDADE Đ
COIMBRA

The neurobehavioral correlates of social exploration in naturalist settings in normal and autistic subjects: a clinical informatics approach

Thesis to obtain a Ph.D. degree in Information Sciences and Technologies at the Doctoral Program in Information Sciences and Technologies, supervised by Professor Miguel Castelo-Branco and Professor Paulo de Carvalho, presented at the Department of Informatics Engineering of the Faculty of Sciences and Technology of the University of Coimbra.

Tese no âmbito do Programa de Doutoramento em Ciências e Tecnologias da Informação, orientada pelo Professor Miguel Castelo-Branco e pelo Professor Paulo de Carvalho e apresentada ao Departamento de Engenharia Informática da Faculdade de Ciências e Tecnologia da Universidade de Coimbra.

Marco António Machado Simões

Agosto de 2019

Supervised by: Miguel Castelo-Branco, Ph.D.

Co-Supervised by: Paulo de Carvalho, Ph.D.

The studies presented in this thesis were carried out at the CNC.IBILI / CIBIT-ICNAS (Center for Neuroscience and Cell Biology | Institute for Biomedical Imaging and Life Sciences, Faculty of Medicine / Coimbra Institute for Biomedical Imaging and Translational Research - Institute of Nuclear Sciences Applied to Health), University of Coimbra, Portugal, and were supported by an individual fellowship from the Portuguese Foundation for Science and Technology (SFRH/BD/77044/2011), grants from the Portuguese Foundation for Science and Technology [Grant numbers PTDC/SAU-NSC/113471/2009, UID/NEU/04539/2013--COMPETE, POCI-01-0145-FEDER-007440], the European project BRAINTRAIN-FP7-HEALTH-2013- INNOVATION-1-602186 and the national project AAC Nº13 SI/2011/Hometech/QREN – Compete, cofunded by FEDER.

"Só é tua a loucura \ Onde, com lucidez, te reconheças…"

Miguel Torga

*(**Sifiso**,* Diário XIII, 1977)

Agradecimentos

Esta tese foi enfrentada com uma multitude de apoios que não poderiam ficar por referir.

Em primeiro os participantes que entraram nos estudos aqui apresentados, pois sem eles nada poderia ter sido feito. As instituições ligadas à perturbação do espectro do Autismo com que trabalhei foram incrivelmente prestáveis, proporcionando a aplicação da visão integrada que temos da investigação na sociedade. À APPDA-Coimbra, na pessoa da diretora Elsa Vieira, à APPDA-Viseu, na pessoa da diretora Prazeres Domingues, e à Unidade de Neurodesenvolvimento e Autismo do Hospital Pediátrico de Coimbra, na pesssoa da Professora Doutora Guiomar Oliveira, o meu mais sincero agradecimento.

Aos colegas do IBILI/ICNAS/CIBIT deixo o meu profundo agradecimento. A ténue linha que separa este grupo de trabalho de um grupo de amigos faz com que todos os dias sejam fáceis, não importa os desafios. Um obrigado especial aos colegas dos projetos Braintrain, HomeTech e GameAAL e aos que trabalharam mais diretamente comigo, nomeadamente o Bruno Direito, Susana Mouga, Carlos Amaral, Hélio Gonçalves, Rui Abreu, Miguel Bernardes, Alexandre Sayal e João Castelhano, e os colaboradores mais diretos nas análises de dados infinitas: o João Andrade, a Raquel Monteiro e o – reforço de última hora – Rodolfo Abreu. Pensar no que desbravámos em conjunto deixa-me extremamente orgulhoso.

Aos colegas de doutoramento e amigos do DEI, por toda a boa pressão que me foram colocando e pelos desabafos que partilhámos, o meu muito obrigado. Sabe bem chegar aqui. Também aos amigos de fora do DEI: nem sempre percebemos os problemas uns dos outros, mas sabemos sempre a melhor forma de os fazer esquecer.

Ao Professor Miguel, por todas as condições e autonomia que me proporcionou para desenvolver estes estudos com meios que fazem invejar centros de investigação de topo do mundo, o meu profundo agradecimento. As suas conversas abrem sempre um novo caminho a explorar, uma nova ideia a desenvolver ou um novo projeto a implementar, ao ritmo da mente brilhante que as traz.

Ao Professor Paulo, que se conseguiu adaptar para me proporcionar a orientação necessária nesta área, o meu profundo agradecimento. Guardo com carinho os rabiscos das fórmulas e transformadas que semanalmente criava nas nossas reuniões de orientação.

Sou um privilegiado desde que nasci. Sempre tive os meios que precisei para crescer e, melhor que isso, a educação certa para o saber reconhecer. Se aqui estou devo-o grandemente aos meus pais, José Manuel e Maria do Céu, às minhas irmãs Mariana e Juliana, e à minha restante família. Aprendemos nestes últimos anos as voltas que a vida dá, mas estamos sempre cá para lhes dar a volta, juntos.

Finalmente, a ti, Andreia, meu maior apoio e complemento, deixo O agradecimento. Sem a força que me transmites diariamente o caminho seria muito mais difícil. Olhar para trás e perceber as curvas e escolhas que fizemos para que este passo se pudesse concretizar faz-me olhar o futuro que vamos construir juntos com um grande sorriso nos lábios. Mal o posso esperar.

Abstract

The ability to engage in social interactions is one of the most captivating aspects of human nature. As we develop our social skills throughout life, they become important tools for our integration in the society. However, for some people – like individuals with Autism Spectrum Disorder (ASD) – engagement in adaptive social interactions are far from being intuitive. In this thesis we aimed to better understand core aspects of social interactions in autism and typically developed controls using virtual reality simulations to improve the ecology of experimental paradigms and, with that knowledge, develop techniques to characterize and rehabilitate those deficits.

We focused on the processing of facial expressions (FE), which is a core aspect of social interactions which is often impaired in ASD. We developed an experimental paradigm to address the processing of FEs, using animated dynamic FEs in virtual avatars and a stringent statistical contrast to isolate such type of processing. We were able to identify a brain region over-recruited by the ASD group during the visualization of FEs of the "other": the right precuneus. To the best of our knowledge, this region was never reported as altered for ASD participants in studies with static stimuli, but several tasks requiring perspective taking and theory of mind showed the recruitment of this area, thus confirming the importance of combining ecological stimuli and well-defined statistical contrasts to identify neural correlates of social interactions that would not be retrieved otherwise.

Moreover, we explored the mental imagery of FEs as a mean for brain modulation in ASD, which revealed group differences in the same region identified by the dynamic FE stimuli, especially for the theta frequency band. Furthermore, we identified a group of features extracted from topographical regions correspondent to the right precuneus, from the theta and high-beta/gamma frequency bands, that were able to accurately differentiate the groups, using statistical classifiers. Those features can now be explored as biomarkers to aid the diagnosis or, after further validation studies, as outcome measures of interventions that tackle FE processing deficits.

Furthering the idea of using mental imagery of FEs as a mean of controlling brain activity, we developed a fMRI-based neurofeedback approach that uses this method to modulate activity in the posterior superior temporal sulcus (pSTS) region as a mean for intervention in ASD. We focused our efforts in transferring this approach to an EEG setup, which could be used

in domiciliary settings and with much lower costs. We identified a set of features (at the scalp and source level) that relate to the fMRI localized BOLD activity and combined them with machine learning algorithms to predict the BOLD activity at the pSTS region, while considering different approaches for dealing with the hemodynamic delay. We showed that our proposed feature set (especially the nonlinear ones) improve the prediction accuracy of the literature models and the convolution of the predictors with multiple hemodynamic response functions (HRFs) with variable peak latencies provide a more robust way to deal with the hemodynamic delay of the BOLD signal, since it explores the inter- and intra-subject HRF variability.

Finally, we approached virtual reality as a mean to integrate rehabilitation approaches in ASD. We implemented a paradigm based on a simple social measure – the interpersonal distance – and measured in a real setting and in a virtual replication of the environment. Our results showed a good replicability of the distances measured in the real and virtual environments, with high correlation levels between environments, with a rescaling factor present for the control group (anisometry between real and virtual worlds).

We then developed a pilot interventional study of behavioral training of ASD using a virtual reality serious game. Participants used our system for three sessions where they followed the common steps for taking a bus in the virtual environment. The system measured the electrodermal activity of the participants and automatically adapted the environment noise based on their stress level. We observed a significant improvement in the outcome measures and a reduction of stress during the task. Looking into a possible generalized application of this and future solutions, we developed the *Neurohab* system for therapeutics and clinicians remotely monitoring the performance of the participants along the sessions.

In sum, this thesis aimed at the understanding of social deficits in ASD and aid their rehabilitation, from a clinical informatics perspective, supported on an integrative solution between knowledge derived from neuroimaging and virtual rehabilitation simulations.

Keywords: Autism Spectrum Disorder, EEG, fMRI, Simultaneous EEG-fMRI, Neurofeedback, Biomarker, Mental Imagery, Virtual Rehabilitation, Serious Games.

Resumo

A capacidade de realizar interações sociais adaptativas representa um dos aspetos mais cativantes da cognição humana. As competências sociais que desenvolvemos ao longo da vida são ferramentas importantes para nossa integração na sociedade. No entanto, para algumas pessoas – como os indivíduos com o Perturbação do Espectro do Autismo (PEA) – as interações sociais estão longe de serem executadas de forma intuitiva. Nesta dissertação procurámos entender melhor os aspetos centrais das interações sociais em indivíduos com PEA e com desenvolvimento normal usando simulações de realidade virtual para aumentar a ecologia dos desenhos experimentais e, com esse conhecimento, desenvolver técnicas para caracterizar e reabilitar as dificuldades sociais associadas na PEA.

Focámos o estudo no processamento de expressões faciais (EF), um aspeto central das interações sociais, muitas vezes alterado na PEA. Desenvolvemos um paradigma experimental para abordar o processamento de EFs, usando EFs dinâmicas animadas em avatares virtuais e um contraste estatístico rigoroso para isolar esse tipo de processamento. Com isso identificámos uma região cerebral recrutada excessivamente pelo grupo PEA durante a visualização de EFs no "outro": o precuneus direito. Esta região nunca foi reportada como alterada para participantes com PEA em estudos usando estímulos estáticos, mas várias tarefas que exigiam a tomada de perspetiva do outro e teoria da mente mostraram o recrutamento dessa área, confirmando assim a importância de combinar estímulos ecológicos e contrastes estatísticos bem definidos para identificar correlatos de interações sociais que não seriam visíveis de outra forma.

Além disso, explorámos a imaginação de EFs como um meio para a modulação da atividade cerebral pela PEA, que revelou diferenças de grupo na mesma região, especialmente para a banda de frequência teta. Identificamos também um conjunto de características extraídas de regiões topográficas correspondentes ao precuneus direito, a partir das bandas de frequência teta e beta-alta/gama, capazes de diferenciar com precisão os grupos, utilizando classificadores estatísticos. Essas características podem agora ser exploradas como biomarcadores para auxiliar o diagnóstico ou, após estudos adicionais de validação, como medidas de avaliação de intervenções focadas no processamento de EFs.

Usando a ideia de usar a imaginação de EFs como um meio de controlar a atividade cerebral, desenvolvemos uma abordagem de *neurofeedback* baseada em fMRI que usa este método para

modular a atividade na região posterior do sulco temporal superior (pSTS) como meio de intervenção na PEA. Focámos o trabalho na transferência dessa abordagem para uma configuração de EEG, que poderia ser usada em ambientes domiciliares e com custos muito menores. Identificámos um conjunto de características (ao nível do escalpe e da fonte) relacionados com a atividade BOLD de interesse e combinámo-las com algoritmos de aprendizagem automática para prever esse sinal, considerando diferentes abordagens para lidar com o atraso da resposta hemodinâmica. Mostramos que o conjunto de características proposto (especialmente as não lineares) melhoram a qualidade da predição dos modelos presentes na literatura, e que a convolução dos preditores com múltiplas funções de resposta hemodinâmica com picos de latência variável explora com mais eficiência a variabilidade intra- e inter-indivíduo.

Finalmente, abordámos o uso da realidade virtual para abordagens de reabilitação na PEA. Implementámos um paradigma baseado numa medida social simples – a distância interpessoal – medida num ambiente real e numa replicação virtual desse mesmo ambiente. Os resultados mostraram uma boa replicabilidade das distâncias medidas nos dois ambientes, com níveis de correlação elevados, com o grupo de controlo a apresentar um efeito de reescalonamento (anisometria entre o mundo real e virtual).

Desenvolvemos então um estudo piloto de intervenção na PEA para treino comportamental usando um jogo sério de realidade virtual. Os participantes usaram o sistema em três sessões, nas quais seguiram os passos comuns para viajar de autocarro, num ambiente virtual. O sistema mediu a atividade eletrodérmica dos participantes e adaptou automaticamente o ruído ambiente com base nos seus níveis de stress. Observámos uma melhoria significativa nas medidas de avaliação e uma redução do stress medido durante a tarefa. Projetando a aplicação generalizada desta e outras aplicações, desenvolvemos o sistema *Neurohab* para que terapeutas e clínicos possam monitorizar remotamente o desempenho dos participantes ao longo das sessões.

Em suma, esta tese visou o estudo dos défices sociais na PEA e a sua reabilitação, seguindo uma abordagem de informática clínica, numa solução integrativa apoiada no conhecimento extraído de simulações virtuais ancoradas em técnicas de neuroimagem funcional.

List of Contents

List of Figures

List of Tables

List of Abbreviations

AAS – Average Artifact Subtraction

AAL – Automated Automatic Labeling

ABA – Applied Behavior Analysis

ADDM – Autism and Developmental Disabilities Monitoring

ADHD – Attention Deficit and Hyperactivity Disorder

ApEn – Approximate Entropy

ASD – Autism Spectrum Disorder

ATP – Adenosine Triphosphate

BCI – Brain-Computer Interface

BCG – Ballistocardiogram

BEM – Boundary Element Method

BOLD – Blood-Oxygen-Level Dependent

CAT – Computerized Axial Tomography

CD – Correlation Dimension

CDC – Centers for Disease Control and Prevention

cESI – Continuous EEG Source Imaging

CSD – Current Source Density

CSF – Cerebrospinal Fluid

CT – Computed Tomography

DNNR – Deep Neural Network Regressor

DFA – Detrended Fluctuation Analysis

DSM-5 – Diagnostic and Statistical Manual of Mental Disorders, 5th edition

DTI – Diffusion Tensor Imaging

ECoG – Electrocorticogram

EDA – Electrodermal Activity

EEG – Electroencephalograph

EFP – Electroencephalography Fingerprint

EKG – Electrocardiogram signal

eLORETA – Exact Low Resolution Electromagnetic Tomography

EMBC – Engineering in Medicine and Biology Conference

EPI – Echo Planar Imaging

EPSP – Excitatory Postsynaptic Potential

ERD – Event-Related Desynchronization

ERP – Event-Related Potential

ERS – Event-Related Synchronization

ESI – EEG Source Imaging

FACS – Facial Action Coding System

FA – Flip Angle

FDG – Fluorodeoxyglucose

FDR – False Discovery Rate

FE – Facial Expression

FEM – Finite Element Method

FEPN – Facial Expression Processing Network

FFA – Fusiform Face Area

FG – Fusiform Gyrus

FID – Free Induction Decay

FOV – Field-of-View

FWHM – Full Width Half-Maximum

fMRI – Functional Magnetic Resonance Imaging

fNIRS – Functional Near Infrared Spectroscopy

FSIQ – Full Scale Intelligence Quotient

FWHM – Full Width at Half Maximum

GA – Gradient Artifact

GE – Gradient Echo

GLM – General Linear Model

HRF – Hemodynamic Response Function

ICA – Independent Components Analysis

IEEE – Institute of Electrical and Electronics Engineers

IOG – Inferior Occipital Gyrus

IPD – Interpersonal Distance

IPSP – Inhibitory Postsynaptic Potential

IQ – Intelligence Quotient

JADD – Journal of Autism and Neurodevelopmental Disorders

LFP – Local Field Potential

LORETA – Low Resolution Electromagnetic Tomography

MEG – Magnetoencephalography

MI – Mental Imagery

MPFC – Medial Pre-Frontal Cortex

MPRAGE – Magnetization Prepared Rapid Acquisition Gradient Echo

MR – Magnetic Resonance

MRI – Magnetic Resonance Imaging

mRMR – Minimum Redundancy Maximum Relevance

MSE – Multi-Scale Entropy

NF – Neurofeedback

NVM – Net Magnetization Vector

OFA – Occipital Face Area

OLS – Ordinary Least Squares

PBA – Power Band Activation

PET – Positron Emission Tomography

PIQ – Performance Intelligence Quotient

PSC – Percent Signal Change

PSD – Power Spectrum Density

PSP – Postsynaptic Potential

pSTS – Posterior Superior Temporal Sulcus

RCT – Randomized Control Trial

RF – Radiofrequency

ROI – Region of Interest

RR – Ridge Regression

rt-fMRI – Real-time Functional Magnetic Resonance Imaging

SE – Standard Error

SF – Spectrum Flux

SFI – Spatial Filling Index

SR – Sampling Rate

SpEn – Sample Entropy

SSVEP – Steady-State Visual Evoked Potentials

STFT – Short Time Fourier Transform

STS – Superior Temporal Sulcus

SVM – Support Vector Machine

sLORETA – Standardized Low Resolution Electromagnetic Tomography

SMA – Supplementary Motor Area

SMR – SensoriMotor Rhythms

SnPM – Statistical Nonparametric Mapping

SNR – Signal-to-Noise Ratio

SR – Sampling Rate

STS – Superior Temporal Sulcus

T – Tesla

TAR – Theta/Alpha Ratio

TD – Typically Developed

TE – Echo Time

TPJ – Temporo-Parietal Junction

TR – Repetition Time

USA – United States of America

VIQ – Verbal Intelligence Quotient

VR – Virtual Reality

WNN – Weightless Neural Networks

WiSARD – Wilkes, Stonham and Aleksander Recognition Device

Chapter 1

Introduction

According to the definition of the *American Medical Informatics Association* (AMIA), Medical Informatics is "*the interdisciplinary field that studies and pursues the effective uses of biomedical data, information, and knowledge for scientific inquiry, problem solving and decision making, motivated by efforts to improve human health.*" There are some major sub-fields in medical informatics. Clinical informatics is one of these sub-areas that is concerned with the development of informatics-based services to support health. It deals with all aspects related to the organization and multi-modal and multi-scale analysis of information and its application for clinical decision support. This thesis addresses the current need of creating and applying clinical informatics solutions to the study and rehabilitation of social deficits, especially for the Autism Spectrum Disorder (ASD).

1.1 Motivation

Individuals in the Autism spectrum present persistent deficits in social communication and interaction, as well as restricted and repetitive patterns of behavior and interests (American Psychiatric Association, 2013). These deficits have a major impact in the life of ASD individuals, with implications ranging from the difficulty of establishing empathic relationship to the incapacity of living independently (Van Heijst and Geurts, 2015; Bishop-Fitzpatrick et al., 2017). In this context, any research that helps to understand and improve any of these deficits can have impactful implications on the lives of these individuals (Bohlander et al., 2012; Guivarch et al., 2017). That impact is significant not only at the individual scale but also at a societal level. In the past decades, the number of reported diagnosis have grown exponentially (Baio et al., 2018), with the current estimated prevalence to be 1 out of every 59 children in the United States of America (USA). In Portugal, the most updated prevalence value goes back to 2007 (Oliveira et al., 2007), with 9.2 out of 10000. There are uncertainties regarding the real reason of the increase in diagnosed patients, on whether it represents a true change of the prevalence or is just a consequence of the alterations applied to the diagnosis

methods in the past years along with more people being aware of the existence of this disorder, with studies accounting a contribution of around 60% to those factors (Hansen et al., 2015). Nevertheless, the number of patients that would benefit by improvements in this field is large and keeps increasing every year. Thus, research on understanding and rehabilitating the ASD deficits show great potential both at the individual and population level, especially the ones that can be widely delivered with low costs of application and tailored for the patients' individualized needs, in a personalized health paradigm (pHealth).

When looking for studies focusing the social interaction deficits in the literature, we found that most neuroimaging studies merely look for brain responses to static images, being the use of ecological paradigms still scarce (Monteiro et al., 2017). The need for structured and well-defined experimental settings is contrary to the ecology present in the every-day social interactions. Although we agree that models must be created to understand the reality, and every model is limited in its representative capacity, we believe that virtual reality can be an option to extend the current experimental models in the ecology direction, without losing the control and reproducibility characteristics needed in experimental modeling design. Furthermore, there is evidence for a specific interest (and even preference (Hardy et al., 2002)) of ASD patients in virtual reality or computerized settings, which might ease the acceptance of specific therapeutics that use this mean of administration. Thus, we consider that there is a need and an opportunity to extend ecological validity as an alternative to commonly used neuroimaging tasks, and through that ecology uncover new neural correlates of ASD social deficits.

Concerning the neural correlates of social deficits, there is a clear need for biomarkers in the field. A biomarker is a quantifiable characteristic extracted from biological measures that is able to discriminate disorders or specific deficits. Those biomarkers were traditionally genetic (Goldani et al., 2014), but recently were extended to the neuroimaging field (Anagnostou and Taylor, 2011). The basic idea is to identify features of structural or functional neuroimaging data that function as diagnostic or prognostic markers of the disorder. Most diagnostic and prognostic approaches to ASD and respective core symptoms are made by behavioral observation or neuropsychological evaluation questionnaires answered by the patient and his/her bystanders (parents, teachers, caregivers). As every observation-based metric, it is prone to bias or error, which is partially mitigated by using diversified clinical teams composed of physicians and psychologists to perform diagnosis and prognosis. Therefore, there is a surge

for data analysis techniques able to extract quantifiable metrics that can be used in this field to assist and complement the job of the clinical teams.

In the case of clinical trials – the scientific methodology to validate treatment safety, effects and efficacy – the importance of defining outcome measures that are specific and sensitive to changes in the deficits caused by the treatments is pivotal. In that sense, having biomarkers that can quantify improvements is a core aspect in this field. When designing a clinical trial, teams struggle to find the right outcome measures, usually resorting to neuropsychological evaluation scales which are prone to bias, as mentioned before. In this sense, finding biomarkers that relate directly with the clinical target is nowadays an important research topic, for which neuroimaging has been more and more used (Thal et al., 2006; Anagnostou and Taylor, 2011; Goldani et al., 2014; Ruggeri et al., 2014; Liu and Waterton, 2017).

On the intervention level, there is a growing application of neurofeedback (NF) solutions based on electroencephalography (EEG). However, those interventions still lack scientific validation. Several systematic reviews have investigated this issue (Holtmann et al., 2011; Micoulaud-Franchi et al., 2015; Arns et al., 2017) and show only slight evidence of effects of such interventions in ASD, and some argue that it influences only the symptoms related to the Attention Deficit and Hyperactivity Disorder (ADHD) (Holtmann et al., 2011), a comorbidity of the ASD. The lack of spatial resolution in EEG leads to neurofeedback interventions that use this method to focus on the control of frequency bands of activity (Micoulaud-Franchi et al., 2015). On contrary, the high spatial resolution of functional Magnetic Resonance Imaging (fMRI) allows for a modulation of blood-oxygen-level dependent (BOLD) activity in specific anatomical regions, usually related to the pathophysiology of the disorders (Sitaram et al., 2016). Since the fMRI-based approach is able to target disorder-related localizations, this technique is, arguably, more efficient than the EEG-based approach (Weiskopf et al., 2004). However, due to the costs and higher constrains of using magnetic resonance imaging (Sarracanie et al., 2015), and also being a much more recent technique than the EEG (Kamiya, 1969; Weiskopf et al., 2004), the fMRI neurofeedback approach is not yet fully disseminated.

The costs and setup inflexibility lead to other issues when comparing different neuroimaging-based neurofeedback techniques. For instance, the number of training sessions used for EEG-NF studies is usually superior to 10 (Marzbani et al., 2016), while most fMRI-NF studies use often not more than one session (Shibata et al., 2011). That limits both the widespread

application of fMRI-NF and the efficacy studies of based on this technique. Thus, it would be very beneficial to be able to transfer fMRI-NF protocols to EEG settings. That transfer would potentiate the widespread application of innovative fMRI-NF solutions, make possible domiciliary interventions and pave the way for personalized health solutions.

Despite the great potential application of this solution, it presents big technical challenges to overcome (Biessmann et al., 2011; Abreu et al., 2018). The characteristics of both signals are intrinsically different, and few studies in the literature aimed to transfer neurofeedback paradigms between imaging techniques. Thus, this is still today an open research question.

Another intervention type that has gained traction in the last years is virtual rehabilitation. It consists of using virtual reality (VR) scenarios to train skills in a controlled manner (Parsons et al., 2009; Threapleton et al., 2016). It presents several advantages, namely the full control of the environment, which allows for increasingly change its complexity (Parsons and Cobb, 2011). For instance, this is very important for incremental exposure used in phobias and other disorders (Benbow and Anderson, 2018). In autism, it can be used to adapt the sensorimotor stimuli of the environments to a level tolerable to the patients, and incrementally manipulate it or simply use it to avoid disruption with the training plan (Rizzo and Wiederhold, n.d.; Rothbaum and Hodges, 1999). The virtualization of the environments allows for safely training skills that could, otherwise, endanger the patients, like learning how to cross a street or navigate in a city without the possibility of being hit by a car (Josman et al., 2008). Furthermore, the possibility of training the same task in several different environments might help the generalization of the learned concepts (Parsons and Cobb, 2011).

There are other reasons that make virtual rehabilitation an interesting approach, especially for ASD. There is evidence showing good technology acceptance by patients with this disorder (Hardy et al., 2002), mainly due to the structure and predictability of technology systems, and the fact that VR controls mainly the visual and auditory sensory inputs, which are the preferred sensory channels in ASD (Rao, Shaila and Gagie, 2006), evidence the potential of this field.

However, there is lack of validity demonstrations in the field. Most VR studies use solutions with limited immersion capabilities, with several studies referring to simple computerized interventions to virtual reality environments (Parsons and Cobb, 2011). It is important to establish the VR as a good mean for ASD training and evaluation and, upon that, build solutions that explore the VR potential in this field, since the level of immersion has been

shown to impact the ability to assess and teach social skills to ASD in virtual environments (Miller and Bugnariu, 2016).

An interconnected topic is serious gaming. A serious game is a game that serves a purpose other than entertainment, usually teaching a skill or concept (Ritterfeld et al., 2009). In that field, there is the hypothesis that using gamification techniques – means for retaining the attention and interest of the players – one can increase the success of interventions, by keeping the patients engaged with the intervention (Kapp, 2012). Therefore, combining virtual rehabilitation with serious gaming concepts, one might potentiate the learning effects of the intervention, increasing the engagement and motivation of the patients. There are some studies looking into serious games in ASD (Zakari et al., 2014), but few consider the combination of serious gaming and virtual reality.

Finally, there is the cost motivation. Current cost estimates for raising an ASD child in the USA or the United Kingdom point to over one million dollars throughout the life span (Ganz, 2007; Amendah et al., 2011; Buescher et al., 2014), for which education and behavioral therapy account for more than 50%. This is mostly due to the need of specialized interventions that are, very often, in a one to one basis: one therapist per patient. This option is very demanding in human resources, especially when considering the growth of ASD prevalence. Moreover, most interventions require extensive contact hours, and when left without intervention, there are few resources to train and consolidate the concepts learned. Virtual solutions could contemplate the therapist sessions, with training performed at home. That could even extend the interventions to remote areas where patient associations and intervention solutions are scarce.

1.2 Objectives

This thesis aimed for exploring two main axes of clinical informatics applied to the social cognition in autism: characterization and rehabilitation. Figure 1.1 shows the structure and subdivisions of these objectives.

On the characterization part, we focused on using virtual reality to develop richer and more ecological studies of social cognition to better identify the differences to the typically developed individuals, and develop biomarkers capable of identify those differences, through machine learning.

On the rehabilitation part, we follow two sub-vectors of action: one pointing towards neurofeedback rehabilitation, with the main goal being the transfer of fMRI-based interventions to EEG settings, and another pointing to the use of virtual reality solutions to train social and independent living skills in autism.

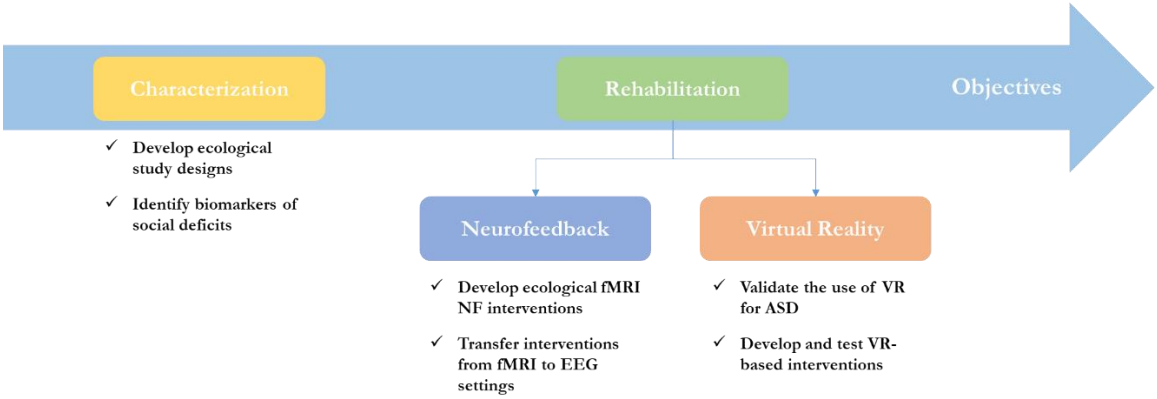

Figure 1.1 - Structure of the objectives of the thesis.

1.3 Contributions and relevance

On the characterization part, we started to explore the use of ecological environments for the study of social characteristics, focusing on facial expressions. We scanned the literature for EEG studies of facial expressions in autism, and verified that most studies used non-ecological stimuli, usually corresponding to still pictures contrasting from blank baselines. We published this analysis as a systematic review in the review Journal of Autism and Neurodevelopmental Disorders (JADD) (Monteiro et al., 2017), where we highlight the need for ecologic studies that use dynamic expressions and better statistical contrasts.

We performed a pilot study in controls showing that evoked potentials of facial expressions were accurately measured in immersive dynamic virtual environments, published in The International Conference on Health Informatics (Simões et al., 2014a). From that study, we moved to the ASD population, with a study published in the Frontiers of Neuroscience journal (Simões et al., 2018b), composed by two parts. The first part consisted of an event-related potential analysis that used dynamic expressions of a virtual character as stimulus, and a contrast of face with emotional expression against the face itself with a neutral expression. This stringent contrast allowed us to identify two event-related potential (ERP) components that showed a higher recruitment of the right *precuneus* region by the ASD group. This was the

first time, to our knowledge, that the right *precuneus* region was implicated in the processing of facial expressions in the ASD population. On the second part of the study, participants performed mental imagery of facial expressions. The study of mental imagery applied to the facial expressions was innovative and relates to the perspective taking and theory of mind, known to be altered in the ASD. Our results showed the over-recruitment of the same region (right *precuneus*) by the ASD participants, both for the ERP and the theta frequency band. We argue that the over-recruitment of this region is a compensatory mechanism for the deficit. Furthermore, we were able to identify a group of features extracted from the EEG signal that were capable of distinguishing the groups with an accuracy of 80%, using machine learning classifiers. We propose those features to be considered as biomarkers, useful for evaluation and prognosis of facial expression deficits.

On the intervention level, since we identified deficits in the processing and mental imagery of facial expressions, we developed a fMRI-based neurofeedback intervention that used the morphing of the imagined facial expression in a virtual human character as feedback to the participant. We used the posterior Superior Temporal Sulcus (pSTS) as target region-of-interest (ROI) for the intervention, since it is known to be related to the processing of facial expressions and to be altered in Autism. Because we were aiming, from the beginning, for transferring this intervention to an EEG setup, we performed an initial study capturing simultaneously EEG and fMRI signals and used them as a validation dataset to test transferring approaches, which we published in the Neuroscience journal (Direito et al., 2019). Our focus, demonstrated in this thesis, was to investigate the transfer possibility for EEG.

For that, we firstly extracted a group of EEG features and checked their individualized correlation with the localized BOLD signal. We published that analysis in the IEEE Engineering in Medicine and Biology Conference (IEEE-EMBC) (Simoes et al., 2015), showing some statistically significant correlations for some features, but with relatively low absolute values. Then, following some research showing a relationship between the alpha band and the BOLD signal, we explored with higher detail that characteristic, with a new publication in the IEEE-EMBC (Simoes et al., 2017, Appendix III). We identified a frontal and a parieto-occipital cluster of alpha variations that statistically significantly correlated with the BOLD signal in the ROIs of the facial expression processing network, but once again, the correlation values were too low to enable the transferring of imaging modalities.

Since individual correlation levels were low, we approached the transfer challenge with machine learning. We replicated an approach published in the NeuroImage journal and increased its efficiency by exploring different delay approaches, a new set of features and new regression techniques, at the scalp and source levels. This result represents a significant advance of the state of the art, since we increased the reconstruction capacity of an established method, currently used in several interventional studies (Noam et al., 2016; Keynan et al., 2019).

On the virtual reality axis, we performed a study using a fully immersive virtual reality setup, where we studied a simple social metric (interpersonal distance) in the real environment and in an exact virtual replication of that environment. We showed that, while the control participants had different behavior in the real and virtual environment, the ASD group had similar behavioral measures in both environments, which, in our opinion, justifies the use of virtual reality environment for interventions and the use of ecological approaches, especially for the ASD population.

With these supporting results, we developed an immersive serious game for training a daily living skill in ASD: how to use the bus as a mean for transportation. That study combined a virtual city where participants had to navigate from one point to another, planning the trip and taking the correct buses to reach the destination, following the bus norms (validate ticket, choose appropriate seats, press the stop button and so on). We measured the behavior (decisions and errors) as well as the stress level through electrodermal activity (EDA) sensors, and saw that, with three sessions of training, participants were able to significantly reduce the number of errors, as well as reducing the level of stress throughout the process. This study was published in the Journal of Medical Internet Research for Serious Games (Simões et al., 2018a).

To have a solution that integrates the serious games, results and implement some gamification techniques, we developed the Neurohab platform, where all those options are provided. We published a short paper in the HCist conference (Simões et al., 2014b) describing that platform, that we believe to have the roots for delivering personalized health solutions to the patients, combining the virtual reality and neurofeedback approaches of interventions, using gamification techniques and monitoring the progress of rehabilitation.

Table 1.1 and Table 1.2 summarize the papers resulting from this thesis. To promote clarity, we selected the core contribution for inclusion in the thesis body, others for inclusion as appendices and others to be referenced, but not included, in the thesis.

Table 1.1 - List of publications directly included in the thesis.

CONTRIBUTION	TYPE	LOCATION
Monteiro R, Simões M, Andrade J, Castelo Branco M (2017) Processing of Facial Expressions in Autism: a Systematic Review of EEG/ERP Evidence. Rev J Autism Dev Disord 4:255–276.	Journal Paper	Chapter 3 Section 3.1
Simões M, Monteiro R, Andrade J, Mouga S, França F, Oliveira G, Carvalho P, Castelo-Branco M (2018) A Novel Biomarker of Compensatory Recruitment of Face Emotional Imagery Networks in Autism Spectrum Disorder. Front Neurosci 12:1–15.	Journal Paper	Chapter 4
Simões M, Lima J, Direito B, Castelhano J, Ferreira C, Carvalho P, Castelo-Branco M (2015) Feature analysis for correlation studies of simultaneous EEG-fMRI data: A proof of concept for neurofeedback approaches. In: 2015 37th Annual International Conference of the IEEE Engineering in Medicine and Biology Society (EMBC), pp 4065–4068. IEEE.	Conference Proceedings Paper	Chapter 5 Section 5.1
Simões, M., Abreu, R., Direito, B., Sayal, A., Castelhano, J., Carvalho, P., Castelo-Branco, M. How much of the BOLD-fMRI signal can be reconstructed by the EEG data: a comparative simultaneous EEG-fMRI study	Journal Paper *	Chapter 5 Section 5.2
Simões, M, Mouga, S, Pereira, A, Gonçalves, H, Oliveira, G, Carvalho, P, Castelo-Branco, M. Virtual reality immersion rescales regulation of interpersonal distance in controls but not in Autism Spectrum Disorder.	Journal Paper *	Chapter 6 Section 6.2
Simões M*, Bernardes M*, Barros F, Castelo-Branco M (2018) Virtual Travel Training for Autism Spectrum Disorder: Proof-of-Concept Interventional Study. JMIR serious games 6:e5.	Journal Paper	Chapter 6 Section 6.3
Direito B, Lima J, Simões M, Sayal A, Sousa T, Luehrs M, Ferreira C, Castelo-Branco M (2019) Targeting dynamic facial processing mechanisms in superior temporal sulcus using a novel fMRI neurofeedback target. Neuroscience 406:97–108.	Journal Paper	Appendix I
Direito, B*, Mouga, S*, Sayal, A, Simões, M, Quental, H, Bernardino, I, Playle, R, McNamara, R, Linden, D, Oliveira, G, Castelo-Branco, M. Training the social brain - clinical and neural effects of an 8-week real-time fMRI neurofeedback Phase IIa Clinical Trial in autism	Journal Paper *	Appendix II
Simões M, Direito B, Lima J, Castelhano J, Ferreira C, Couceiro R, Carvalho P, Castelo-Branco M (2017) Correlated alpha activity with the facial expression processing network in a simultaneous EEG-fMRI experiment. In: 2017 39th Annual International Conference of the IEEE Engineering in Medicine and Biology Society (EMBC), pp 2562–2565. IEEE.	Conference Proceedings Paper	Appendix III
Simões M, Mouga S, Pedrosa F, Carvalho P, Oliveira G, Castelo-Branco M (2014) Neurohab: A Platform for Virtual Training of Daily Living Skills in Autism Spectrum Disorder. Procedia Technol 16:1417–1423.	Conference Proceedings Paper	Appendix IV

* *under review*

Table 1.2 - List of publications not included in the thesis.

CONTRIBUTION	TYPE	CITED IN
Simões M, Amaral C, Carvalho P, Castelo-Branco M (2014) Specific EEG/ERP Responses to Dynamic Facial Expressions in Virtual Reality Environments. In: The International Conference on Health Informatics. IFMBE Proceedings (Zhang Y, ed), pp 331–334 IFMBE Proceedings. Cham: Springer.	Conference Proceedings Paper	Chapter 7
Simões M, Carvalho P, Castelo-Branco M (2012) Virtual reality and brain-computer interface for joint-attention training in autism. Proc 9th Intl Conf Disabil Virtual Real Assoc Technol:507–510.	Conference Proceedings Paper	Chapter 3, 7
Andrade J*, Cecílio J*, Simões M, Sales F, Castelo-Branco M (2017) Separability of motor imagery of the self from interpretation of motor intentions of others at the single trial level: an EEG study. J Neuroeng Rehabil 14:63.	Journal Paper	Chapter 3, 7
Amaral C, Simões M, Mouga S, Andrade J, Castelo-Branco M (2017) A novel Brain Computer Interface for classification of social joint attention in autism and comparison of 3 experimental setups: A feasibility study. J Neurosci Methods 290:105–115.	Journal Paper	Chapter 3, 7
Amaral C, Mouga S, Simões M, Pereira HC, Bernardino I, Quental H, Playle R, McNamara R, Oliveira G, Castelo-Branco M (2018) A feasibility clinical trial to improve social attention in Autistic Spectrum Disorder (ASD) using a brain computer interface. Front Neurosci 12:1–13.	Journal Paper	Chapter 3, 7
Simões M, Amaral C, França F, Carvalho P, Castelo-Branco M (2019) Applying Weightless Neural Networks to a P300-Based Brain-Computer Interface. In: World Congress on Medical Physics and Biomedical Engineering 2018. IFMBE Proceedings (Lhotska L, Sukupova L, Lacković I, Ibbott G, eds), pp 113–117. Singapore: Springer.	Conference Proceedings Paper	Chapter 3, 7
Júlio F, Ribeiro MJ, Patrício M, Malhão A, Pedrosa F, Gonçalves H, Simões M, van Asselen M, Simões MR, Castelo-Branco M, Januário C (2019) A Novel Ecological Approach reveals Early Executive Function Impairments in Huntington's Disease. Front Psychol 10:585.	Journal Paper	Chapter 7
Simões M*, Gonçalves H*, Abreu R, Pinto M, Pereira M, Castelo-Branco M (2019) GameAAL – Gamification applied to ambient assisted living. In: 2019 IEEE International Conference on Serious Games and Applications for Health (SeGAH). Kyoto: IEEE.	Conference Proceedings Paper	Chapter 6, 7
Simões M*, Abreu R*, Gonçalves H, Rodrigues A, Bernardino I, Castelo-Branco M (2019) Serious games for ageing: a pilot interventional study in a cohort of heterogeneous cognitive impairment. In: 2019 IEEE International Conference on Serious Games and Applications for Health (SeGAH). Kyoto: IEEE.	Conference Proceedings Paper	Chapter 6, 7

The contributions of this thesis are transversal to different areas. Combining approaches that explore both the feature engineering and machine learning, as well as serious games and virtual reality are challenging. However, we believe that clinical informatics translational research is the answer to complex problems and exploring the best that each area has to offer is paramount to tackle the challenges that the study of behavioral deficits offers. In the end, we

improved the state of the art on aspects that are basilar for the understanding and rehabilitation of social deficits in ASD.

1.4 Thesis outline

This document is structured in seven chapters. After this introduction, Chapter 2 describes the background topics covered in our work and Chapter 3 the state of the art of the research on them. Chapters 4 to 6 present the studies we performed to achieve the objectives of the thesis. Chapter 4 describes the characterization axis of the work, presenting the EEG study we performed on facial expressions processing and their mental imagery, with biomarker exploration. Chapter 5 covers our efforts in the transfer of a neurofeedback intervention from fMRI to EEG, with an initial feature exploration paper followed by our approach to improve the EEG fingerprint (EFP) method for the neurofeedback transfer, with the exploration of a new feature set, a new method for dealing with the hemodynamic delay of the BOLD signal and improved regression method. Chapter 6 aggregates our efforts on the virtual rehabilitation axis of the thesis. It presents the interpersonal distance study, where we validated the virtual reality setup for training in the ASD population and the pilot intervention study we conducted for training ASD participants on how to take the bus. Finally, Chapter 7 discusses the results and its implications, as well as future steps to follow the line of work of this thesis.

Chapter 2

Background

In this chapter we perform a description of the themes covered in the thesis. Since this is a multidisciplinary work that merges contributions in the clinical, neuroimaging and virtual reality fields, a background contextualization aims to establish the common ground we built upon. We cover first the Autism spectrum disorder, then the neuroimaging techniques we used (EEG and MRI, apart and simultaneously) and finally the concept of virtual reality.

2.1 Autism spectrum disorder

The Autism spectrum disorder (ASD) is a neurodevelopmental disorder characterized by deficits in social interaction and communication, as well as very restrictive interests and repetitive behaviors (American Psychiatric Association, 2013). This disorder was firstly reported by Kanner (1943) in a paper showing a clinical description of 11 children presenting "extreme aloneness from the very beginning of life, not responding to anything that comes to them from the outside world". However, only in the early 80s the disorder was considered independent from schizophrenia being renamed at first to "infantile autism" and in the late 80s to "autism disorder" (Won et al., 2013).

2.1.1 Diagnosis

The fifth edition of the Diagnostic and Statistical Manual of Mental Disorders (DSM-5), which is the current standard reference for the diagnosis of mental and behavioral conditions, provides some examples of the two main axis of symptoms of the ASD. For the social interaction and communication deficits, the provided list of illustrative (not exhaustive) examples states:

1. Deficits in social-emotional reciprocity, ranging, for example, from abnormal social approach and failure of normal back-and-forth conversation; to reduced sharing of interests, emotions or affect; to failure to initiate or respond to social interactions.
2. Deficits in nonverbal communicative behaviors used for social interaction, ranging, for example, from poorly integrated verbal and nonverbal communication; to abnormalities in eye contact and body language or deficits in understanding and use of gestures; to a total lack of facial expressions and nonverbal communication.
3. Deficits in developing, maintaining, and understanding relationships, ranging, for example, from difficulties adjusting behavior to suit various social contexts; to difficulties in sharing imaginative play or in making friends; to absence of interest in peers.

A similar list of illustrative cases is provided for the restricted, repetitive patterns of behaviors, interests or activities, with the diagnosis in this axis to refer the need for identifying at least two of those items, currently manifesting or that have manifested previously during the development of the child:

- Stereotyped or repetitive motor movements, use of objects, or speech (e.g., simple motor stereotypies, lining up toys or flipping objects, echolalia, idiosyncratic phrases).
- Insistence on sameness, inflexible adherence to routines, or ritualized patterns or verbal nonverbal behavior (e.g., extreme distress at small changes, difficulties with transitions, rigid thinking patterns, greeting rituals, need to take same route or eat the same type of food every day).
- Highly restricted, fixated interests that are abnormal in intensity or focus (e.g., strong attachment to or preoccupation with unusual objects, excessively circumscribed or perseverative interest).
- Hyper- or hyporeactivity to sensory input or unusual interests in sensory aspects of the environment (e.g., apparent indifference to pain/temperature, adverse response to specific sounds or textures, excessive smelling or touching of objects, visual fascination with lights or movement).

Accompanied with these items, a level of severity must be defined along with the diagnosis, in accordance to the following table:

Severity Level	Social Communication	Restricted, Repetitive Behaviors
Level 3 "Requiring very substantial support"	Severe deficits in verbal and nonverbal social communication skills cause severe impairments in functioning, very limited initiation of social interactions, and minimal response to social overtures from others. For example, a person with few words of intelligible speech who rarely initiates interaction and, when he or she does, makes unusual approaches to meet needs only and responds to only very direct social approaches.	Inflexibility of behavior, extreme difficulty coping with change, or other restricted/ repetitive behaviors markedly interfere with functioning in all spheres. Great distress/ difficulty changing focus or action
Level 2 "Requiring substantial support"	Marked deficits in verbal and nonverbal social communication skills; social impairments apparent even with supports in place; limited initiation of social interactions; and reduced or abnormal responses to social overtures from others. For example, a person who speaks simple sentences, whose interaction is limited to narrow special interests, and who has markedly odd nonverbal communication.	Inflexibility of behavior, difficulty coping with change, or other restricted/ repetitive behaviors appear frequently enough to be obvious to the casual observer and interfere with functioning in a variety of contexts. Distress and/ or difficulty changing focus or action.
Level 1 "Requiring support"	Without supports in place, deficits in social communication cause noticeable impairments. Difficulty initiating social interactions, and clear examples of atypical or unsuccessful responses to social overtures of others. May appear to have decreased interest in social interactions. For example, a person who is able to speak in full sentences and engages in communication but whose to-and-fro conversation with others fails, and whose attempts to make friends are odd and typically unsuccessful.	Inflexibility of behavior causes significant interference with functioning in one or more contexts. Difficulty switching between activities. Problems of organization and planning hamper independence.

adapted from DSM-5 (American Psychiatric Association, 2013)

Without the existence of definitive biological tests (called biomarkers), the diagnosis is thus based mainly on behavioral and neuropsychological evaluation. The guidelines state that the

symptoms must be present in the early developmental stage, but they may only become fully manifest when social demands exceed limited capacities or may be masked by learned strategies in later life.

2.1.2 Prevalence

The prevalence of Autism Spectrum Disorders is hard to assess, because of the difficulty to conducting full-coverage epidemiological research. It depends on the existence of national-wide institutions of public access and a good cooperation between services and specialized clinical centers, which is frequently hard to establish. However, some studies have been providing some important indicators. In the United States of America, Autism and Developmental Disabilities Monitoring (ADDM) Network from the Centers for Disease Control and Prevention (CDC) have conducted systematic studies for the last decades (Baio et al., 2018), which are summarized in Figure 2.1. These studies have a periodicity of 2 years and cover a total of 14 sites along the USA.

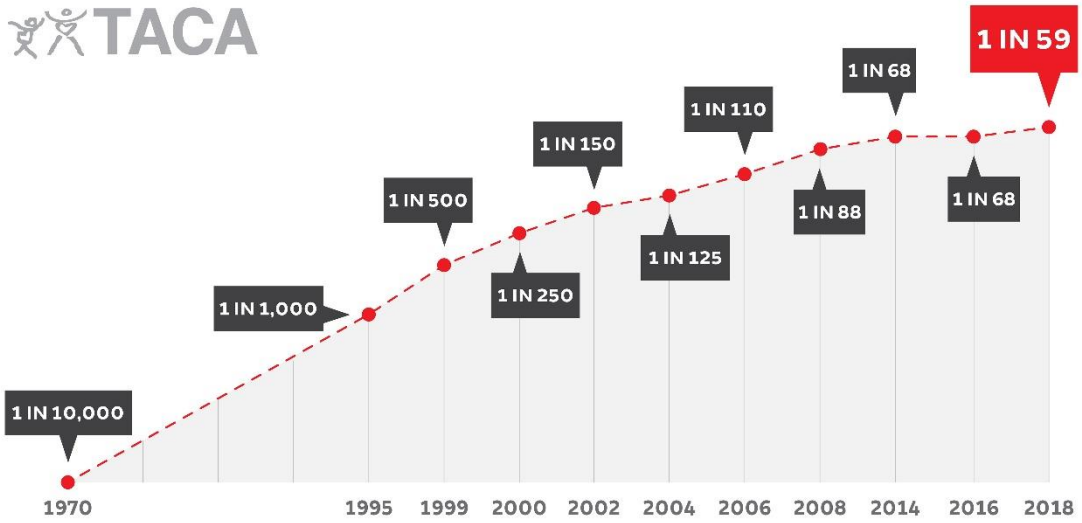

Figure 2.1 – Evolution of ASD prevalence in the USA, measured by the ADDM network of the CDC – adapted from TACA – the autism community in action (*https://tacanow.org/autism-statistics/*).

In Portugal, the only existent study was performed in the main land of Portugal and Azores islands in the year of 2007 by Oliveira and colleagues (Oliveira et al., 2007). It showed a

prevalence of 1 in 1000. This value is significantly inferior (about tenfold) to the USA reported prevalence.

Furthermore, ASDs are reported to occur in all racial, ethnic, and socioeconomic groups. The ADDM reports show higher prevalence in the Caucasian race compared to African-American or Hispanic individuals, but with the ratios Caucasian : African-American and Caucasian : Hispanic decreasing, due to a greater increase of diagnosis of African-American and Hispanic children (Baio et al., 2018). The major variability in the diagnosis is gender, being 4.5 times more common in boys than among girls.

The growth of diagnosed cases in the last few years is a consequence of several factors. The improvement on diagnosis techniques may have contributed to some of the apparent increase on the prevalence, along with the increase of the general awareness on autism. Some studies have tried to quantify the impact of the changes of the diagnostic criteria in the increase of reported prevalence, estimating a contribution of around 60% (Hansen et al., 2015). Therefore, despite this major contribution, other effects (like environmental causes) cannot be discarded.

There is a list of comorbidities that often occur with ASD. About 70% of the cases show at least one comorbidity and 40% show two or more comorbidities (Simonoff et al., 2008). Between the most common comorbidities are anxiety, attention deficit and hyperactivity disorder (ADHD), intellectual disability and epilepsy. Those comorbidities harden sometimes the diagnosis, since the traits of ASDs often overlap with symptoms of other disorders and the characteristics of ASDs make traditional diagnostic procedures difficult (Bauman, 2010).

2.1.3 Treatment

Currently, there is no known cure for ASD. However, some interventions can help improving significantly the quality of life of ASD patients and of their bystanders. These interventions usually need to be performed by a trained specialist and must be consistently recurrent for improving results. These needs are very expensive and cause a strong socio-economic impact on the families. Cost estimates for raising an ASD individual surpass the value of one million USA dollars throughout life (estimates for the USA and the United Kingdom) (Ganz, 2007; Amendah et al., 2011; Buescher et al., 2014). In this cost estimates, education and behavioral therapy account for more than 50%. The largest cost components identified for children are

special education services and loss of productivity of the parents. For adults, residential care or supportive living accommodation and loss of individual productivity are the highest cost components. Medical costs are higher for adults than for children (Buescher et al., 2014).

There is a clear deficit of pharmacology responses to ASD. Although the use of psychotropic pharmacotherapy in individuals with ASD is comparable to schizophrenia or ADHD (about 50%), the pharmacotherapy in ASD focus mainly non-core symptoms and significant psychiatric comorbidities (Jobski et al., 2017). The most common medications used are risperidone and aripiprazole for tackling challenging and repetitive behaviors (McPheeters et al., 2011). With few pharmacological responses, behavioral therapies play an important role in managing the disorder.

Therapies often follow the Applied Behavior Analysis (ABA) structure, an approach based on the analysis of behavior and reinforcement in the structure of antecedent, behavior, consequence. This procedure has shown some interesting results, and is considered an evidence-based best practice treatment for ASD by the American Psychological Association (Slocum et al., 2014). However, the interventions following this procedure must be intensive, from 25 to 40 hours per week (Roane et al., 2016), most of the times in a one-on-one basis between the therapist and the patient. This kind of therapy is extremely expensive to support, considering both cost to the families and even at the societal level, with the continued increase in prevalence. This opens space to new therapies following domiciliary or remote training to step in and complement the one-on-one therapies, providing means to individualized and independent training.

2.2 Neuroimaging: a window to the brain

Neuroimaging is a term used to describe any experimental technique measuring human (or animal) brain structure or function, directly or indirectly (Brammer, 2009).

For the structure of brain, the oldest technique is the computed tomography (CT) scan, formerly known as computerized axial tomography (CAT) scan, which uses several X-ray measurements taken from different angles to create cross-sectional images of the brain. It has been surpassed by the magnetic resonance imaging technique (MRI), which produces detailed structural information where grey matter (neuronal cell populations) and white matter (myelinated tracts) are visible to the naked eye (Bunge and Kahn, 2010). New techniques, such as diffusion tensor imaging (DTI), focus on mapping those myelinated tracks.

Despite the importance of structural neuroimaging, our work focuses on the functional aspects of the brain. Thus, there is a greater interest of functional neuroimaging techniques, which capture where and when neuronal activity in the brain is associated to a specific cognitive task. There is a greater variety of techniques for assessing brain function, which can be divided into two categories: direct measures of electrical activity of brain firing and indirect measures of brain activity, supported by the assumption that neuronal activity is directly supported by increased blood flow and metabolic activity (Bunge and Kahn, 2010). Into the direct measure category fall the electroencephalography (EEG) and the magnetoencephalography (MEG) techniques, which provide greater time resolution (when neuronal activity happens), but fall short of specifically localizing the activity (where), due to the ill-posed structure of the source localization problem, the attenuation of the brain signals until they reach the sensors located at the scalp and the complexity of the neuroanatomical models needed for performing the localization of source activity (da Silva, 2009; Awan et al., 2018). This topic is further discussed in section 0. On the category of indirect measures, one can mention functional MRI (fMRI), the functional near infrared spectroscopy (fNIRS) and the positron emission tomography (PET). The former two (fMRI and fNIRS) measure the blood-oxygen-level dependent response (BOLD) signal and the latter (PET) is based on mapping metabolic activity (if fluorodeoxyglucose (FDG) is used) or perfusion ($H_2{}^{15}O$), using radioactive tracers. Therefore, PET is the most intrusive technique, since it requires a radiopharmaceutical compound to be injected in the patients' veins and for some cases even arterial sampling to derive arterial input functions. Since the two first techniques depend

always on the hemodynamic response, they are considered indirect techniques, because what is measured is not the real activity but the result of the changes in the cerebral blood flow caused by neuronal activity. This principle is called neuro-vascular coupling. Due to their indirect nature, a time delay is always present, in addition to lower time resolution, but usually offer a very good spatial resolution (where brain activity occurs). fNIRS has advantages in cost and portability over fMRI, but it cannot measure cortical activity more than 4cm deep and has poorer spatial resolution.

In this thesis we used the EEG and fMRI techniques, both separated and combined. We will now further discuss their characteristics.

2.2.1 Electroencephalogram

The existence of the electrical activity of the brain was firstly identified by Richard Canton in 1875 (Canton, 1875), a discovery reported for the brains of monkeys and rabbits. Only four decades later, in the late 20s, Hans Berger reported a way to record the electrical activity from the human brain (Berger, 1929). Despite being almost one century old, the electroencephalogram (EEG) took a considered amount of time to be accepted as a method to assess brain function in health and disease (da Silva, 2009), mostly due to the large complexity of the underlying system of neural generators and the attenuation suffered from the signal until it reaches the sensors.

The measured EEG activity is composed by the summed electrical activities of populations of neurons, from the cortex. Neurons are excitable cells with characteristic intrinsic electrical properties and their activity produces electrical and magnetic fields. Each neuron is composed by the dendrites (input from other neurons signals), the soma (cell body) with the nucleus, the axon and the axon terminals (Figure 2.2). Axon terminals of other neurons are connected to the neuron dendrites and soma, and through that connections the neuron receives its input information.

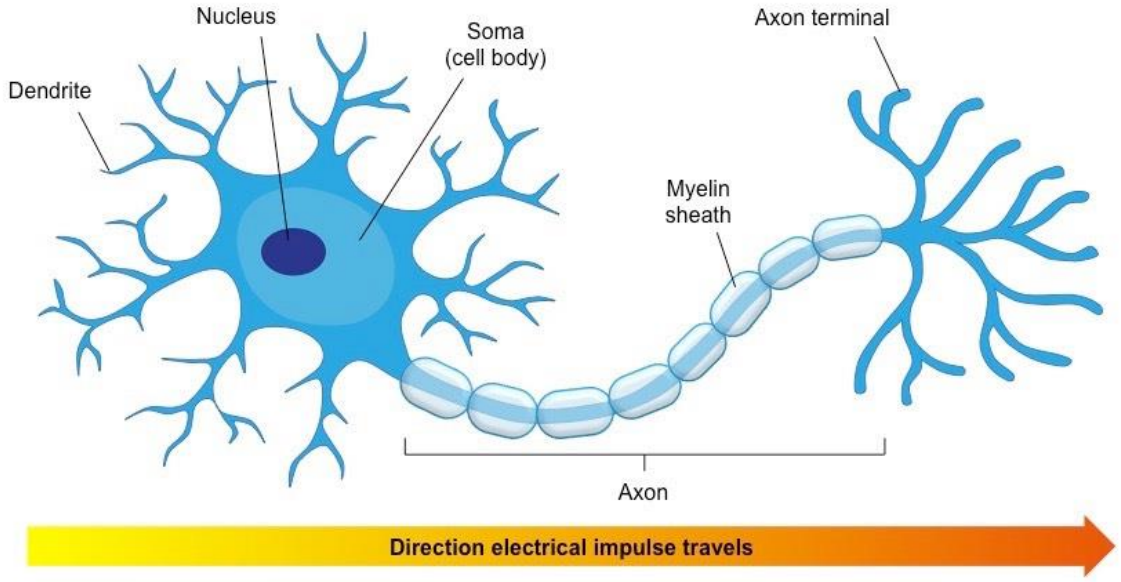

Figure 2.2 – Schematic of the structure of a neuron. This model is a simplification of the neuron cell, showing the main elements (dendrites, soma, nucleus, axon and axon terminals) - adapted from Arizona State University's *Ask a Biologist* page "A Nervous Journey" (*https://askabiologist.asu.edu/neuron-anatomy*).

Like any other cell in the human body, membranes of neurons are positively charged in the extracellular space, and negatively charged in the intracellular space, generating a rest potential of around -70 mV of voltage in the neuron cell. However, each time one neuron receives a synapse from other neuron, the cell potential and the surrounding extracellular potential fluctuates, causing what is called a postsynaptic potential (PSP). That connections can be excitatory, which increase the membrane potential (excitatory postsynaptic potentials - EPSP), or inhibitory, which decrease the membrane potential (inhibitory postsynaptic potentials - IPSP). When the membrane potential reaches the -55 mV threshold (which may vary according to neuron type), an action potential is fired and passed through the axon up to the axon terminals, connecting to other neurons. During the action potential, the membrane potential rises to +30 mV and then drops quickly down to below -70 mV, until it normalizes at the rest potential (Figure 2.3). All of this happens in less than 2ms (Brandeis et al., 2010). That variations in the neuron membrane are made mainly through the selective permeability of the neuron membrane to potassium (K+) and sodium (Na+) ions, through voltage gated sodium channels, leaking potassium channels, and the sodium-potassium pumps.

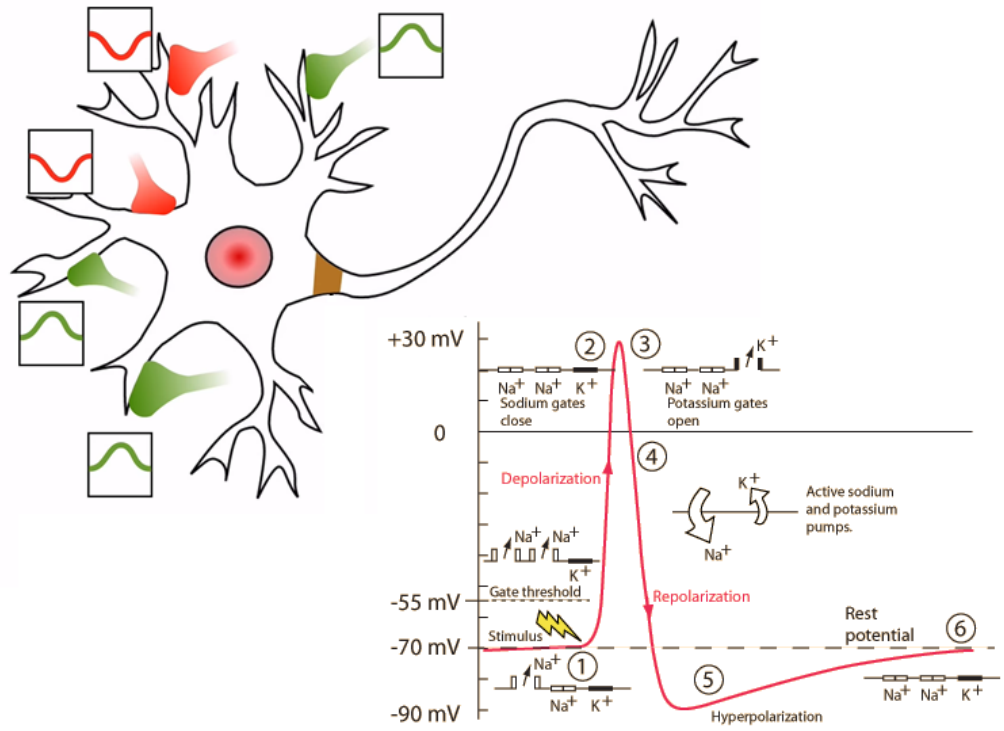

Figure 2.3 – Representation of a neuron receiving signals from other neurons connected to it, and the action potential. The left can be represented as an analogue region, where the voltage floats until the membrane reaches the -55mV threshold (typical of most neurons), and the right part, the axon, can be considered digital, since it follows the "all or none" rule, meaning that when the threshold is reached, it passes the voltage all the way to the axon terminals and a synapse occurs between the neuron and the ones it is connected to. – adapted from Ka Xiong Charand – HyperPhysics Action Potential (*http://hyperphysics.phy-astr.gsu.edu/hbase/Biology/actpot.html*).

The action and postsynaptic potentials of several nearby neurons produce an electrophysiological signal in their extracellular space (local field potential – LFP). As previously referred, for a sensor to be able to capture electrical activity of the neurons, a large population of neurons must activate synchronously and with the same orientation, orthogonal to the skull. Since action potentials are very fast and almost never overlap, EEG measures are composed mostly by the variations of the PSPs (graded potentials). Regarding the orientation, most of the signal captured by the sensors is generated in the pyramidal cells (Spruston, 2008), Although all neuron types contribute to the extracellular field, the shape of the cell influences their relative contribution. Pyramidal cells have long, thick apical dendrites that can generate strong dipoles along the axis between the dendrites and the soma. Such dipoles generate an open field, due to the considerable spatial separation between the active sink (or the source)

and the return currents. Thus, pyramidal cells are the greater contributors to the extracellular field. (Figure 2.4).

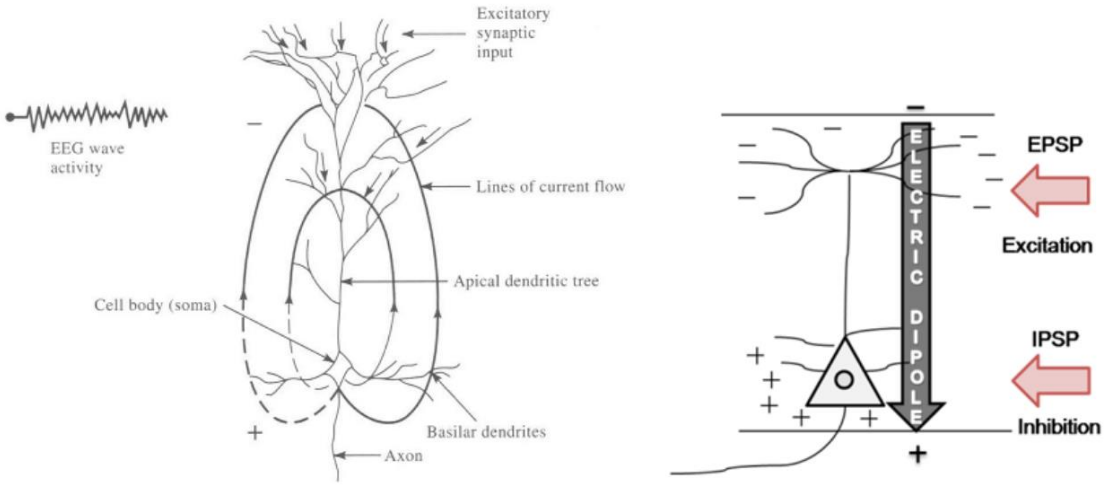

Figure 2.4 – Diagram of a pyramid cell and the correspondent dipole it generates – adapted from (Abtahi, 2011).

EEG activity can be measured locally with implanted depth microelectrodes, from the cortical surface (electrocorticogram – ECoG) or even from the scalp (EEG) (Buzsáki et al., 2012) – see Figure 2.5 for a graphical hierarchy of the brain layers. Since the signal gets attenuated by the different layers, the deeper the sensor the better the signal-to-noise ratio (SNR). However, ECoG and deep electrodes are very intrusive and require a medical surgery to be implanted in the patients, so it is only performed in cases of disease (like epilepsy) where the possible benefits overrule the risks. In this thesis, we worked mainly with scalp EEG. Scalp EEG is a mixture of local field potentials (LFP) generated at several brain locations, which generate two types of electrical activity: rhythmic and arrhythmic (Michel and Brandeis, 2010).

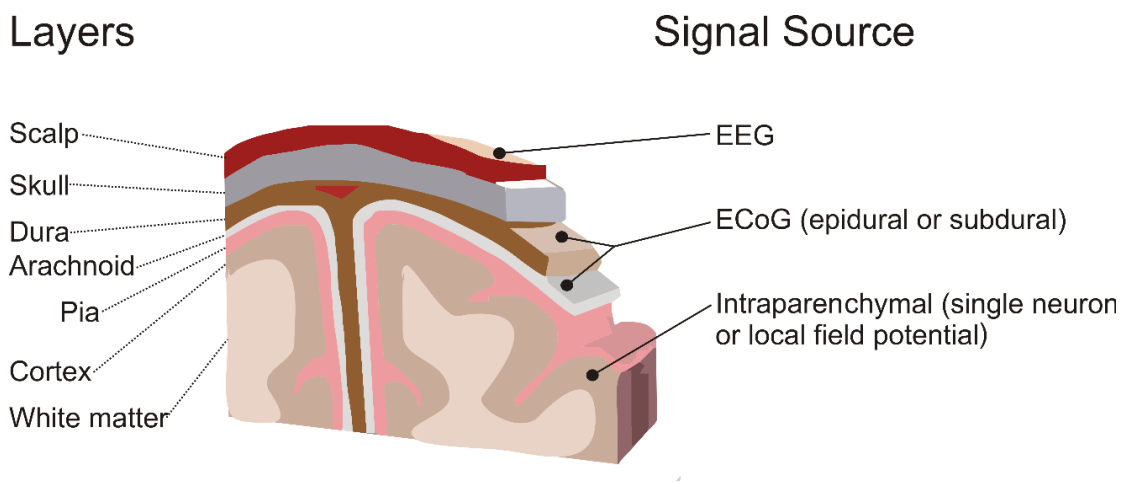

Figure 2.5 – Layers of the brain and the type of signals measured at each level. EEG is measured at the scalp, ECoG at epidural or subdural levels and implanted microelectrodes at the intraparenchymal space. – adapted from (Leuthardt et al., 2009).

2.2.1.1 EEG rhythmic activity

Neural activity in the central nervous system can happen in repetitive patterns, called oscillations. Oscillatory activity is generated at the cortex in many ways, either within individual neurons or driven by interactions between neurons. In individual neurons it can be found either by oscillations in membrane potential or by rhythmic patterns of action potentials, which then produce oscillatory activation of post-synaptic neurons. Considering large groups of neurons, their synchronized activity gives rise to oscillations that can be observed at the scalp. Despite oscillatory activity of the measured EEG being identified since the first recordings, only in the mid-seventies the different frequency bands were stratified and a taxonomy was defined by the International Federation of Societies for Electroencephalography and Clinical Neurophysiology, driven by pragmatic clinical considerations (IFSECN, 1974). Berger has firstly identified the alpha activity, so the subsequently discovered frequency bands followed the same nomenclature and were labeled with Greek letters. The identified bands and respective nomenclature are still in use today (delta: 0.5–4 hertz; theta: 4–8 hertz; alpha: 8–13 hertz: beta: 13–30 hertz; gamma: >30 hertz). Besides a significant inter-subject variability, brain rhythms identifiable in the EEG signal are highly dependent on the age and behavioral state of the measured individual, particularly the alertness level (da Silva, 2009). Brain rhythms are believed to provide a mechanism for coordinating activity within and across brain regions (Zheng and Colgin, 2015).

Power Spectrum Distribution

The power of the brain electrical field potentials follows an inverse relation with the frequency, meaning that the power tends to decrease with increasing frequency, following the power-law function

$$P \propto \frac{1}{f^{\beta}} \tag{2.1}$$

where P is power, f is frequency, and β is the power-law exponent, typically in the range of 0 to 3 (He, 2014).

Delta oscillations

Delta waves are defined as rhythms with frequencies below 4 Hz (IFSECN, 1974). They are usually present in some phases of sleep (slow wave sleep) in human adults. In wakefulness, it is present in young children, but in adults it is mainly found in pathological states (Michel and Brandeis, 2010).

Theta oscillations

Theta waves oscillations present a frequency range of 4 to 8 Hz (IFSECN, 1974). Found more often in infancy and childhood, they are also present in drowsiness and during sleep. For adults in a wakefulness state, theta activity can be found at mid-frontal electrodes related to cognitive activities, especially cognitive control and working memory (Maurer et al., 2014; Eschmann et al., 2018). The theta band has been found at posterior sites, especially related to memory retrieval (Walden et al., 2014) and a relation between frontal and parietal theta has been reported associated to willed attention (Rajan et al., 2018). Changes in theta are often correlated with power changes in the alpha oscillations, and they are usually analyzed as the theta/alpha ratio (TAR) (Imperatori et al., 2017). Theta rhythms during wakefulness are different from the ones during sleep.

Alpha oscillations

The alpha rhythm was the first one to be described, since it has been found in the first EEG studies of Hans Berger (1929). This EEG rhythm was thoroughly explored by the famous Portuguese scientist Fernando Lopes da Silva, both in dogs and humans (Lopes Da Silva and Storm Van Leeuwen, 1977; Lopes Da Silva et al., 1997; da Silva, 2009). It comprises

oscillations between 8 and 13 Hz (IFSECN, 1974) and represents the most prominent oscillatory frequency over occipital cortex during rest and with eyes closed, which supports the idea that it is an idling rhythm involved in the active suppression of sensory input (Michel and Brandeis, 2010; van Diepen and Mazaheri, 2017). Furthermore, the alpha activity is suppressed after eye opening, visual stimulus presentation or simply additional mental activity, which reinforces that hypothesis. But the alpha is not specific to the visual cortex. Alpha oscillations also occur over frontal cortex as well as over the auditory cortex, sensory motor cortex and the supplementary motor area (SMA). This version of the alpha rhythm is named the mu rhythm, and is suppressed by the performance of activity or simply by the mental imagery of it (Pfurtscheller and Neuper, 1997; McFarland et al., 2000; Neuper et al., 2009). This alpha suppression was broadly linked with cortical activation, in an inverse relation. However, there is task-related evidence that the alpha rhythm also plays important roles in regulating the timing and temporal resolution of perception and are strongly associated with top-down control and may help the transmission of neural "predictions" to visual cortex (for a review of the alpha roles, please refer to the work of Clayton and colleagues (2018)). Therefore, as for the other rhythms, there is no single source of alpha activity in the brain, since alpha rhythms appear in different brain areas and have different behavioral significance.

Beta oscillations

Even in Berger first reports, he made a distinction between the large alpha waves from small fast oscillations he called "beta waves". Beta activity is present in the frequency range from 15 to approximately 30 Hz (IFSECN, 1974) and its role in coordination between regions has been implicated in numerous functions, including sensory perception, selective attention, and motor planning and initiation (Sherman et al., 2016). Beta activity is a strong predictor of perceptual and motor performance and, in sensorimotor cortex, beta rhythms have been linked to anticipation of visual stimuli that cue a subsequent motor response (Kilavik et al., 2013) , and are visible during motor activity. Thus again, as for the other frequency bands, beta activity has several different functions and generators, depending also on the functional state of the brain (Michel and Brandeis, 2010).

Gamma oscillations

Gamma rhythms are usually attributed to sensory and cognitive brain functions. They range from around 30 to 80 Hz. Gamma oscillations can reflect a state of high neuronal excitability

involved in complex brain processes, binding the activity of distributed neuron populations (engaged networks) (Jia and Kohn, 2011), and are associated to several cognitive processes, including perceptual decision (Castelhano et al., 2017), working memory (Pesaran et al., 2002) and learning (Bauer et al., 2007). As for the other frequency bands, distinct gamma frequency sub-bands reflect different neural substrates and cognitive mechanisms (Castelhano et al., 2014).

Overall, the rhythmic activity depends on the mental state of the subject in a broad sense, and variations in the rhythms are observed linked to specific mental processes. Therefore, it is possible to modulate it based on stimuli or events that provoke variations in the EEG spectrum through stimuli experienced by the subject. Depending on the response to those stimuli/events, oscillatory activity can be either enhanced — event-related synchronization (ERS) — or suppressed— event-related desynchronization (ERD) (Neuper et al., 2009; Formaggio et al., 2010). The detection of those variations can be exploited by algorithms and converted to commands for external devices or applications, a technique known as brain-computer interface (BCI), that we further describe in section 3.2.1.1.

2.2.1.2 EEG arrhythmic activity

The second type of EEG activity we find is arrhythmic activity. The most studied case of arrhythmic activity is the response to stimuli, for which populations of neurons produce a synchronized activation or deactivation, time-locked to the event / stimuli. Those are called event-related potentials (ERP).

The ERPs are difficult to measure because their amplitude is usually one order of magnitude lower than that of ongoing EEG. To separate the ERPs from the ongoing signal, and assuming that they are independent, several responses to the same stimuli have to be recorded. Considering *K* EEG single trials responses to the same type of event or stimulus, each with *N* samples along the time, represented in the matrix *y* of dimension [K, N], its signal-to-noise ratio (SNR) can be estimated, as suggested by Lemm and colleagues (2006), using the formula

$$SNR(y) = 10\ log \frac{Var_n(E_k[y])}{E_k[\ Var_n(y_k - E_k[y])]} \tag{2.2}$$

where Var_n is the variance of the signal along the N time samples and E_k is the mean over the K trials.

Averaging the signal over the trials increases the SNR. The mathematical justification is based on two assumptions:

1. The K signals contain ERP responses of invariable shape and latency, time-locked to the stimulus,

2. The noise can be approximated by a zero mean Gaussian random process of variance σ^2, uncorrelated between trials and not time-locked to the event. This includes both noise and ongoing EEG activity, independent of the stimulus.

Based on these assumptions, the averaging method can be described by

$$\bar{x}(n) = \frac{1}{K}\sum_{k=1}^{K} x_k(n) = s(n) + \frac{1}{K}\varepsilon_k(n) \tag{2.3}$$

where $\bar{x}$ is the averaged signal over K event-locked trials, s is the signal that is constant between the trials (ERP) and ε_k the noise on the segment k, which includes the ongoing EEG activity. Because of assumption 2, the mean of the noise is 0 and, therefore, when K increases, the noise will tend to its mean, leaving the signal $\bar{x} \approx$ s.

The implications of this method include the fact that, for one to visualize and analyze it an ERP, the same event/stimulus must be repeated several times (usually about 100 repetitions per condition), which hardens the experimental conditions (studies have to be both long and repetitive). However, especially for the field of brain-computer interfaces (BCI) that we describe in section 3.2.1.1, few repetitions are considered, and machine learning algorithms are used to extract the information that the human eye cannot see. Pires and colleagues (2008) performed a study on the effect of changing the amount of averaged trials on the error rate for a P300-based BCI using a Bayesian classifier, and found a monotonic decrease in the false positive, false negative and error rate as the number of averaged signals increased. This result highlights the efficacy of the averaging method in increasing the SNR of the ERPs and reinforces the need for trading off SNR for duration and repetitiveness of the experimental paradigms. Although few trials are used in the classification approaches, it should be noted that for BCIs, the objective is to identify the presence of the ERP, not to study its morphology. Therefore, it can use substantially less trials than the ones needed for pure neuroscientific

studies, where the aim is to characterize the brain response to the stimulus as well as their timing and morphology.

Another important issue is the intrinsic trial-to-trial variability that, through (2.3) are also averaged out. This problem as gain increasing interest and some studies and approaches now look into modeling or, at least, measure trial-to-trial variability in their analysis (Delorme et al., 2015).

2.2.1.3 Source localization of EEG activity

As mentioned before, the signals captured at the scalp include a mixture of several brain sources of activity. In order to study the neural correlates of specific brain processes measured at the scalp, it is important to estimate the regions from where the measured signals are generated. That process is called source localization.

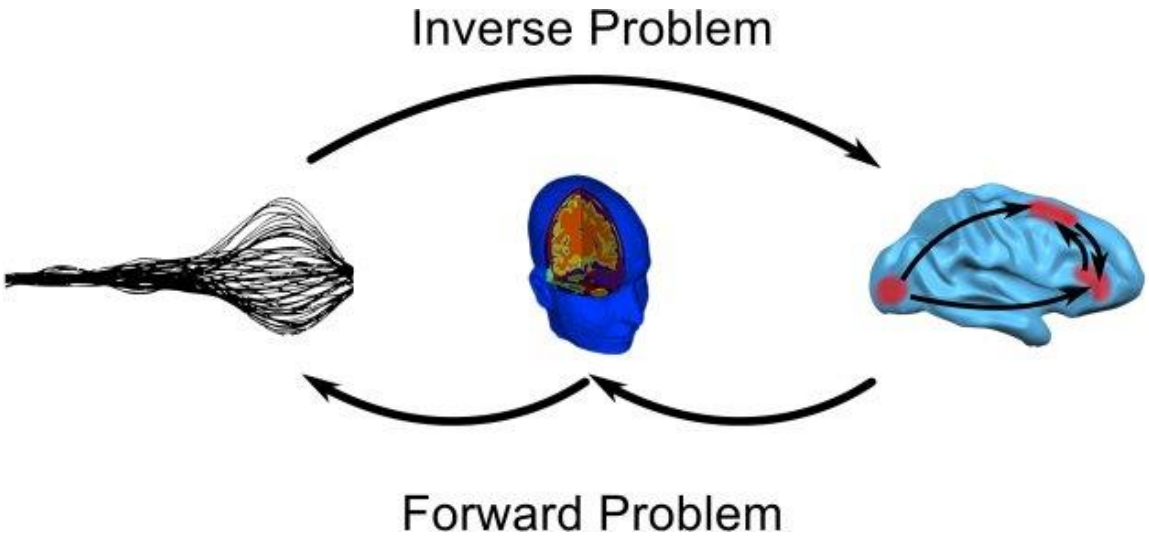

Figure 2.6 - Schematic representation of the forward and inverse problem. The forward problem consists in modeling the signal propagation from the sources up to the sensors at the scalp, whilst the inverse problem localizes the sources of activity based on the signal measured at the sensors. – adapted from (Belaoucha, 2017).

In this field there are two well-known and related problems, called the forward problem and the inverse problem (see Figure 2.6). The forward problem consists in modeling the brain structure such that one can simulate the propagation of a source signal generated in a specific location of the cortex up until it reaches the sensors at the scalp. In sum, the forward problem responds to the question: "given an electrical source at location L, what is the potential

measure at the electrodes E" (Hallez et al., 2007). This procedure is performed for several locations, in order to cover significantly all possible brain locations. Then, solved the forward problem, the inverse problem consists of going from a measured EEG signal and finding which location brain location generated that signal. In sum, the inverse problem answers to the question: "given this potential measure in the electrodes E at the scalp, which location L generated it" (Grech et al., 2008).

The forward problem

The forward problem addresses the calculation of the electric potential that reaches the scalp for a known configuration of sources, given that the physical properties (conductivities) of the head tissues are known. The problem can be formalized as

$$\Phi = \mathrm{K}\,\mathrm{J} + \varepsilon \tag{2.4}$$

being $\Phi \in \mathbb{R}_{N_E \mathrm{x} 1}$ the electric potentials measured at the scalp, $\mathrm{K} \in \mathbb{R}_{\mathrm{N}_E \mathrm{x} 3\mathrm{N}_S}$ the leadfield matrix, $\mathrm{J} \in \mathbb{R}_{3\mathrm{N}_S \mathrm{x} 1}$ the current source density (CSD), and $\varepsilon \in \mathbb{R}_{N_E \mathrm{x} 1}$ an array with a repeated arbitrary constants representing the noise of the measurement. N_E represents the number of electrodes at the scalp, N_S the number of possible source activities. Since the source activity generates the signal in a specific direction, each J_l contains three values, containing the intensity in the direction of each axis x, y and z. Thus,

$$J = \{J_{1,x}, \quad J_{1,y}, \quad J_{1,z}, \quad J_{2,x}, \quad J_{2,y}, \quad J_{2,z}, \ldots, \quad J_{Ns,x}, \quad J_{Ns,y}, \quad J_{Ns,z}\} \tag{2.5}$$

and K contains, for each e $\epsilon\, [1, N_E]$, the mapping of all J sources to the electrode e.

The forward problem consists of computing the *leadfield* matrix K. To do so, one must create a model of the brain, considering the different electrical conductivities of different tissues, as well as the morphology of the head itself. There are two types of models used for this computation: the finite-element method (FEM) and the boundary element method (BEM).

The BEM method models the head as a volume conductor consisting of compartments with constant, isotropic conductivities, in a shell form, where currents flow from the inside surface to the outside. This way, the forward problem can be transformed into a boundary integral equation, which can then be solved numerically. The most simplistic BEM solutions include three concentric spheres, simulating the different layers of the head. However, assuming

isotropy in each head compartment is inaccurate, since anisotropy is present in several cases, e.g., in the white or gray matter compartment. That simplification influences source analysis, as has been shown (Güllmar et al., 2010), but the errors induced by the disregard for anisotropy are smaller than other modelling errors, like misclassified tissue or the use of non-realistic head models. Additionally, most current BEM implementations are restricted to nested shell topographies. The FEM solutions do not suffer from several of those problems, since they represent complex models that (usually) consider more aspects of the head anatomy than the BEM models. However, there are studies pointing towards the good performance of some BEM algorithms, even when compared with FEM implementations (Vorwerk et al., 2012).

The inverse problem

The inverse problem consists of, given the electrode potentials at the scalp, find the source generator(s) of that activity. That implies to invert the equation (2.4). Assuming the noise to be white, Gaussian and zero-mean, that inversion can be represented as

$$J = K^{-1}\Phi \tag{2.6}$$

However, this corresponds to an ill-posed problem, since the number of possible sources is much greater than the number of sensors at the scalp, and different solutions can give rise to the same signal measurements at the scalp.

There are several methods to solve the inverse problem, which can be subdivided in equivalent dipole methods and linear distributed methods.

The dipole methods assume that a given scalp measurement is exclusively explained by a limited number of sources, smaller than the number of electrodes to ensure the solution is unique. The forward model is computed for estimating the scalp potentials by a single dipole at a specific position, orientation and strength. The result is compared with the measured signal with a similarity metric, and the process is repeated for every dipole position, orientation and strength, to select the dipole that better represent the observed signal (Gulrajani et al., 1984). This search through the solution space increases exponentially in complexity when one considers more than one dipole. Moreover, identifying the correct number of dipoles is usually impossible without some *a priori* knowledge about the physiological mechanisms underlying

the scalp potentials under analysis (Bai and He, 2005). Therefore, solutions that do not need this information (linear distributed models) are usually preferred over this method.

Linear distributed source models are the most common used models to solve the inverse problem. Their main advantage is the fact they do not need *a priori* information regarding the number of sources. For these models, the source space is a 3D grid covering the cortical grey matter, rendering each cell a possible source of activity. Since their positions are fixed, their orientation and strength must still be estimated, and so it is possible to represent the scalp recordings as a linear combination of the source amplitudes. Nevertheless, and on contrary to the equivalent dipole models, distributed models have more sources than sensors, thus some constrains must be defined that allow the selection of the 'optimum' solution. Several methods have been suggested, being some of the most widely adopted the minimum norm estimate (MNE) and its variations, LORETA, sLORETA, VARETA, S-MAP, ST-MAP, Backus-Gilbert, LAURA, Shrinking LORETA FOCUSS -SLF, SSLOFO and ALF for non-parametric methods, and beamforming techniques, BESA, subspace techniques like MUSIC and its derivatives, FINES, simulated annealing and computational intelligence algorithms for parametric methods. A comprehensive revision of those methods is provided by Grech and colleagues (2008) and, more recently, by Awan et al. (2018). The former study performs a simulation analysis comparing all the methods and identifies sLORETA method as the best solution in terms of both localization error and ghost sources, while the latter focus more on recent advances on new methods, still poorly consolidated in the literature.

2.2.2 Magnetic resonance imaging

Magnetic Resonance Imaging (MRI) is a technology that uses strong magnetic fields, magnetic field gradients, and radio waves to generate images of the organs in the body. It manipulated the magnetic properties of the hydrogen nucleus (one proton), since the hydrogen is present in water and fat, which is present in most of our body tissues in different concentrations (Huettel et al., 2004).

2.2.2.1 Longitudinal magnetization

Each hydrogen proton is spinning around an axis, thus creating a tiny magnetic field. So, we can look at each proton as a very small magnetic bar that, under normal circumstances, is align

randomly across the body. However, when placed under the influence of a strong magnetic field ($\vec{B}_0$), the spin axis of each hydrogen proton aligns parallel or anti-parallel to that strong magnetic field direction. The preferred alignment direction is the one that requires less energy, so more protons align parallel to $\vec{B}_0$ than antiparallel. This excess of protons aligned with B_0 produces a net magnetic effect called the net magnetization vector (NMV) $\vec{M}$ that aligns with the main magnetic field. The difference is typically small but depends on the strength of B0 and the temperature of the measured tissue. So, if the B0 strength increases, more magnetic moments align with B0 since the energy needed to oppose it is higher. Therefore, the NMV increases (Berger, 2002).

For the magnetic moment of the protons to align with the B0 field, they perform a precession movement around the B_0 axis. The angular momentum vector of the proton precesses about the external field axis with an angular frequency known as the Larmor frequency, described (in MHz) by

$$\omega_0 = \gamma B_0 \tag{2.7}$$

where γ is the gyromagnetic ratio, a constant of the nuclear species of the matter (e.g. hydrogen), and B_0 is the main magnetic field strength. The strength of the magnetic field is measured in units of Tesla (T), and 1T is equivalent to approximately 20 000 times the magnetic field of the earth. The gyromagnetic ratio of the hydrogen proton is 42.6 MHz/T. As seen in (2.7), the Larmor frequency ω_0 is proportional to the strength of $\vec{B}_0$ (Currie et al., 2013).

2.2.2.2 Transverse magnetization

Since $\vec{M}$ is aligned to $\vec{B}_0$, it cannot be measured. But it is possible to apply a radiofrequency (RF) pulse (B_1) transversal to B_0, at the same frequency as ω_0, which will disturb the protons so they fall out of alignment with B_0. That disturbance happens by the transfer of energy from the RF pulse to the proton, which occurs only if the RF pulse has the same frequency as the precession frequency (ω_0), a phenomenon called resonance. The $\vec{M}$ vector is tilted onto the transverse plane relative to $\vec{B}_0$ by a specific angle, called flip angle, given by

$$\alpha = \gamma B_1 \tau \tag{2.8}$$

where τ is the exposure duration of the nuclei to B_1. Therefore, it is possible to control the flip angle that we apply to the protons. This RF pulse is generated by an electromagnetic coil known as the transmitter coil, but mostly referred as the RF coil. The titled $\vec{M}$ can be decomposed into two separate components: a longitudinal magnetization component $\vec{M}_z$, along the direction of $\vec{B}_0$ (conventionally assumed as z axis), consequence of the transition between parallel and antiparallel directions of the protons nuclei magnetization vectors due to the increase of their energy state, and a transverse magnetization component $\vec{M}_{xy}$, precessing around the z axis, consequence of the phase synchronization of the proton spins induced by the RF pulse (Currie et al., 2013).

After the application of the RF pulse, protons go back gradually to their equilibrium state, in a process called "relaxation". Relaxation occurs in two different ways: the longitudinal magnetization returns gradually to its original value, a process named longitudinal or T1 ('Time' 1) relaxation, and the transverse magnetization begins to disappear, a process called transverse or T2 ('Time' 2) relaxation. Following the Faraday law of induction, a change in the magnetic flux experienced by a coil induces an electromotive force (EMF), that can be detected by receiver coils (Huettel et al., 2004).

2.2.2.3 Relaxation processes

The energy received through the resonance process makes some protons to transition from the parallel state to the antiparallel, which changes the $\vec{M}_z$ vector. After the RF pulse, the protons transition back gradually to their equilibrium state M_0. To return to that lower energy state, protons exchange energy with their surroundings. The rate at which that process occurs depends on the sampling tissue. For instance, fat and water recover the equilibrium at different rates. So, different tissues have different T_1 values, but the relaxation process follows an exponential with time constant T_1 given by

$$M_z(t) = M_0 - (M_0 - M_z(0))e^{-\frac{t}{T_1}} \tag{2.9}$$

where M_0 is the original magnetization value (prior to the RF pulse) and $M_z(0)$ is the value longitudinal magnetization value of $\vec{M}$ after the RF pulse. If the RF pulse produces a flip angle of 90º, $M_z(0)$ becomes 0 and (2.9) can be simplified into

$$M_z(t) = M_0(1 - e^{-\frac{t}{T_1}}) \tag{2.10}$$

So, the T_1 value corresponds to the time it takes for the tissue to recovers $(1 - e^{-1}) \approx 63\%$ of its original longitudinal magnetization value (see Figure 2.7). The imaging method takes advantage of the different T_1 values of different tissues to generate images with different levels of intensity for different tissues, depending on the time after the RF pulse that the image is captured.

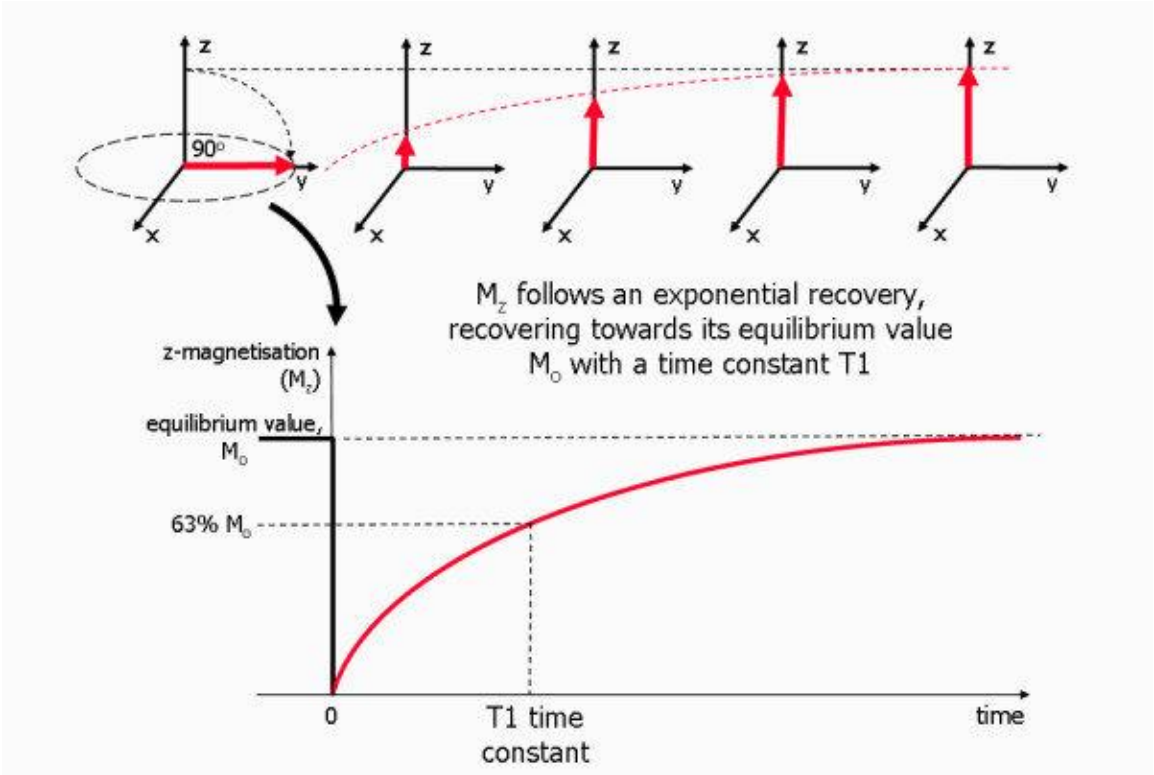

Figure 2.7 - T1 relaxation illustrations, showing the recovery of the longitudinal magnetization of $\vec{M}$ across time – adapted from (Ridgway, 2010).

Another consequence of the RF pulse is that it synchronizes the phase of the spins, so after the pulse all protons spin with the same phase, generating an $\vec{M}_{xy}$ component that is spinning

around $\vec{B}_0$. Before the pulse, at the equilibrium state, protons spin at random phases and, therefore, their magnetizations in the *xy* plan sums to 0 since they cancel each other out.

After the RF pulse, the spins will gradually fall out of phase with each other, thus decreasing the $\vec{M}_{xy}$ component. This reduction of the M_{xy} value in function of the time is given by

$$M_{xy}(t) = M_{xy}(0)e^{-\frac{t}{T_2}} \tag{2.11}$$

having $M_{xy}(0)$ representing the transverse magnetization after the RF pulse (instant 0). If the pulse produces a flip angle of 90º, $M_{xy}(0)$ will be equal to M_0, since the longitudinal magnetization is fully transposed the transversal plan ($M_z(0) = 0$, $M_{xy}(0) = M_0$). For the duration of T2, the transverse magnetization is reduced in $e^{-1} \approx 37\%$.

However, in reality the spins dephase quicker than T2, due to inhomogeneity in the magnetic field B_0 and differences in magnetic susceptibility between tissues present in the sample. Those tissue differences are particularly important in regions in contact with blood vessels containing paramagnetic hemoglobin. This quicker decay is called T2* relaxation.

The relaxation processes in $\vec{M}$ are, thus, summarized in three equations (known as the Block equations):

$$\begin{aligned} \frac{dM_x}{dt} &= \gamma(M_y B_0 - M_z B_1 \sin\omega t) - \frac{M_x}{T_2} \\ \frac{dM_y}{dt} &= \gamma(M_z B_1 \cos\omega t - M_x B_0) - \frac{M_y}{T_2} \\ \frac{dM_z}{dt} &= \gamma(M_x B_1 \sin\omega t - M_z B_1 \cos\omega t) - \frac{M_z - M_0}{T_1} \end{aligned} \tag{2.12}$$

The relaxation times are highly dependent on the local characteristics of the tissues under imaging. Since different tissues have different T_1 and T_2 times, they will present different levels of magnetization at time X, thus creating contrasts in the MR images. Carefully crafted acquisition parameters (such as echo time, repetition time or the flip angle) generate T_1-, T_2- and T_2*-weighted MR images that show the different soft tissues in the human body, in health and disease.

So, after the RF pulse, the $\vec{M}$ net magnetic vector is precessing around $\vec{B}_0$ at the Larmor frequency. Thus, though Faraday's law of induction, a RF receiver coil detects the electric

voltage induced by the moving magnetic field $\vec{M}$. This signal is called a Free Induction Decay (FID) and an illustration is provided in Figure 2.8.

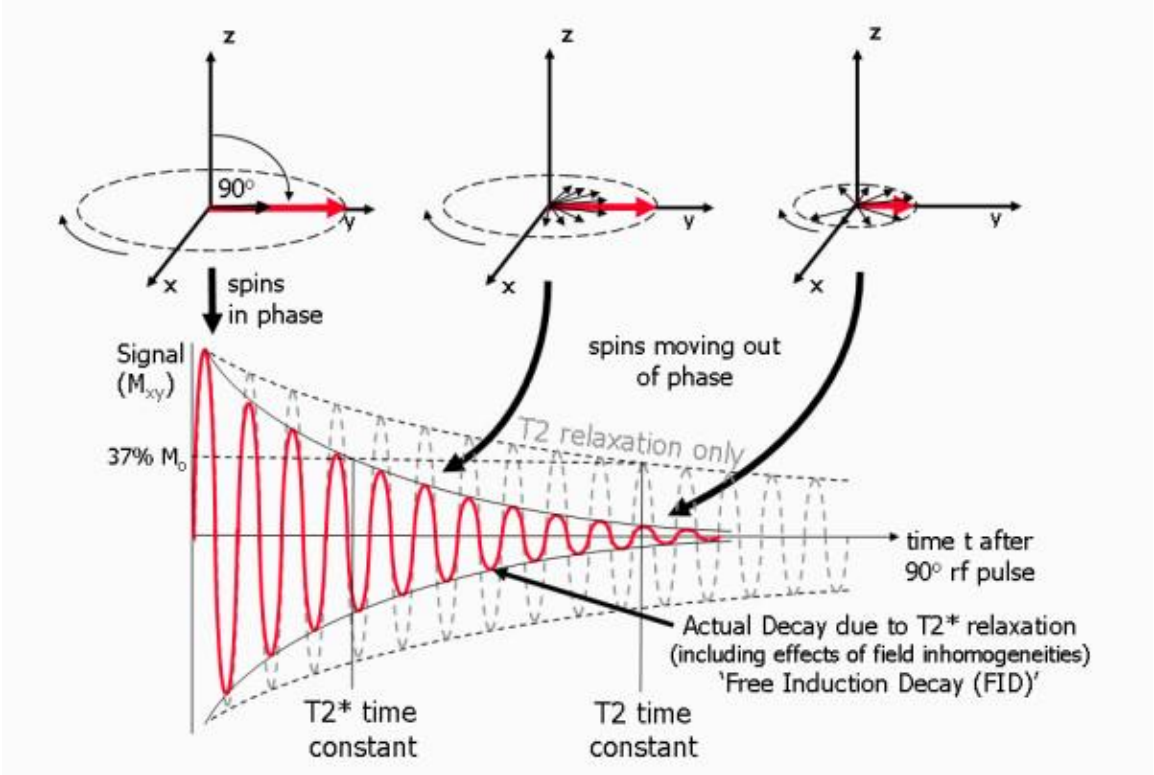

Figure 2.8 – T_2* and T_2 relaxation illustration, showing the effect of the de-phasing of nuclear spins through time, in the transverse plan XY – adapted from (Ridgway, 2010).

Although the FID can be detected directly as an MR signal, usually the MR generates and measures the signal in the form of an echo, because of the magnetic field gradients used to localize and encode the MR signals in space cause additional de-phasing in the nuclear spins which disrupts the FID. There are two commonly used types of echoes: gradient echoes and spin echoes. To spatially encode the FID measured signals, magnetic gradient fields are used (generated by the gradient coils in the MR machine). Magnetic field gradients produce a change in field strength (and, consequentially, the Larmor frequency of the nuclear spins) along a particular direction. Three gradients (G_z, G_x, G_y) are applied along the z, x and y axis, respectively, to spatially localize the measured signal. The G_z gradient generates a monotonic variation along the z axis, which allows the RF pulse to target the frequency of a specific slice (a plane transversal to the z axis). Therefore, only the protons in that slice will be influenced by the RF pulse. The G_z gradient is often called the Slice Select Gradient. The spatial encoding for the XY plane is achieved by using the gradients in the x and y plane to create changes in

the frequency and phase characteristics of the FID signal, respectively. The phase encoding is performed before the signal acquisition (but after the RF pulse) and consists of using G_y to change the frequency of the protons' spins depending on their position (where the magnetic field increases, the frequency of precession is higher, and where it decreases, the frequency is lower). After the gradient is switched off, the relative phase of the protons' spins has changed by an amount that is linear dependent on their position along the y axis (known as the phase encoding direction). After the phase encoding, the frequency encoding starts and, at the same time, the signal is recorded. The G_x will, similarly to the G_y, produce a change in the frequency of the protons based on their position along the x axis (called frequency encoding direction). This is called the frequency encoding. So, for a specific slice, one acquires a signal that can be decomposed in frequency and phase to positions of the xy plane. The process is repeated several times with variations in the strength of the phase gradient, and each acquisition is decomposed to what is called the k-space. Then, a 2D Fourier transform applied to the k-space data is able to construct the MR image of the targeted slice. The process is repeated for the remaining slices to cover the full volume of interest to be imaged (Berger, 2002; Huettel et al., 2004; Ridgway, 2010).

2.2.2.4 Functional Magnetic Resonance Imaging

Functional Magnetic Resonance Imaging (fMRI) is supported by the neurovascular coupling concept: the property that states that there is an increase of cerebral blood flow wherever and whenever neuronal activity occurs. Neuronal activity consumes energy in the form of adenosine triphosphate (ATP), a nucleotide produced from glycolytic oxygenation of glucose, which generates carbon dioxide as a by-product of its production. Therefore, an activated brain region causes a variation in the cerebral metabolic rate of oxygen (Buxton and Frank, 1997). The vascular system responds with an increasing affluence of glucose and oxygen to provide for the energetic demands of those brain cells, thus restoring the homeostasis of the system (Buxton et al., 1998). This process causes a change of the relative levels of oxyhemoglobin and deoxyhemoglobin (oxygenated or deoxygenated blood) that can be measured through their differential magnetic susceptibility, since oxygenated blood shows different magnetic properties than deoxygenated blood. When fully oxygenated, hemoglobin is diamagnetic and magnetically indistinguishable from brain tissue, but fully deoxygenated haemoglobin is highly paramagnetic, with 4 unpaired electrons. This paramagnetism results in local gradients in magnetic field whose strength depends on the deoxyhemoglobin

concentration (Glover, 2011). Therefore, images can be created using the deoxygenated haemoglobin paramagnetism as result of brain activity, with the so-called blood-oxygen-level dependent (BOLD) contrast.

This hemodynamic response to an increase of activity in the brain is not instantaneous. In fact, the process of restoring the homeostasis takes several seconds to complete. The maximum level of deoxygenation peaks around 5 to 6 seconds after the trigger of brain activity, and after that the deoxygenation process stops and oxygenation takes place, up to 15 to 18 seconds, where an undershoot occurs. This undershoot is a reduction, relative to the baseline, of the BOLD signal after the end of the stimulus, which can persist several seconds before the signal returns to baseline. There is some debate around this effect (van Zijl et al., 2012), with the most common theories arguing a slow recovery of the cerebral blood volume, a slow recovery of the cerebral metabolic rate of oxygen or even an undershoot of the cerebral blood flow (Liu et al., 2019). Nevertheless, these variations are detected by the BOLD signal and, transformed to a function over time, became the so-called hemodynamic response function (HRF). Figure 2.9 describes the canonical version of the function, since several variations can be found between individuals (Handwerker et al., 2004) or pathologies (Hanlon et al., 2016).

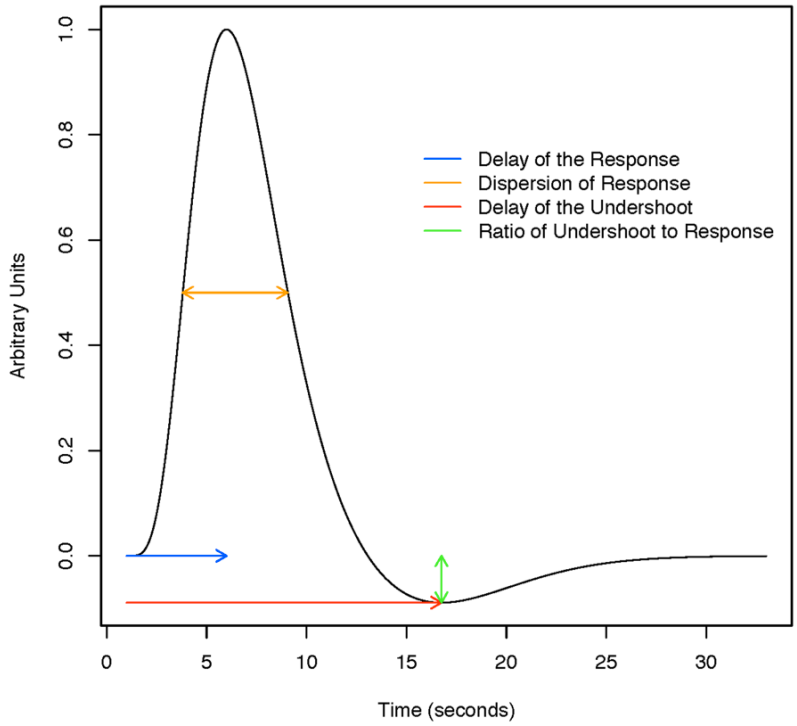

Figure 2.9 – Morphology of the canonic Hemodynamic Response Function (HRF) over time, specifying its main characteristics – adapted from (Eloyan et al., 2014).

The link between brain activity and blood flow, the basilar principle of the fMRI method, was first discovered by Roy and Sherrington in 1890. Next, Pauling and Coryell discovered the magnetic properties of deoxygenated and oxygenated blood, and their differences, during the year of 1936. Ogawa and colleagues, in 1990, figured out how to explore this principle using MRI, at the time used only for structural imaging, introducing the BOLD contrast. Ogawa and colleagues proved this principle in rodents in that same year, Belliveau et al. (1991) explored this principle using a ferromagnetic contrast injected into the participants, but the first studies using BOLD in humans occurred in 1992: one by Kwong and colleagues, one by the Ogawa group and the third one by Bandettini and colleagues (Bandettini et al., 1992; Kwong et al., 1992; Ogawa et al., 1992).

2.2.3 Simultaneous EEG-fMRI

As seen above, each imaging modality presents some significant drawbacks. On the one hand, EEG presents poor spatial resolution, which limits the localization of neuronal activity, and a low SNR, which requires long and repetitive experimental structures to overcome it. On the

other hand, fMRI presents poor time resolution, being limited by the hemodynamic response timings and hardware constraints, as well as its costs and setup inflexibility, which limit its large-scale application. In that sense, efforts have been made to combine both methods, aiming to obtain the best of both worlds: the temporal resolution of EEG with the spatial resolution of fMRI. The first tests of combined EEG-fMRI measurements appeared soon after the invention of fMRI, driven by the need to map epileptic brain activity. So, the first study was performed in 1993 by John Ives and colleagues in Boston, USA (Ives et al., 1993). The main driver of this was the need for noninvasively localize the epileptic focus, which even today remains a significant challenge.

The first difficulty in combined EEG-fMRI acquisitions is the noise contamination the EEG signal suffers. Ensuring EEG data quality in an EEG-fMRI experiment is a crucial step of the process. There are two main artifacts affecting the EEG signal inside the MR machine: the gradient artifact (GA) and the ballistocardiogram (BCG) artifact (also called pulse artifact – PA) (Ferreira et al., 2016).

2.2.3.1 Gradient artifact correction

The gradient artifact is an interference in the EEG signal caused by the switching on and off of magnetic field gradients of the MR machine. A variation of the magnetic flux applied to a conducting circuit causes an electromagnetic current, according to Faraday law of induction. That current affects the head of the subject and the EEG equipment (sensors and wires), creating very large variations on the measured signals that occlude the brain activity of the subject. Depending on the type of MR imaging sequence, the changes in the gradient will be different. The most common case the 2D multi-slice Echo Planar Imaging (EPI) sequence, for which the gradients are rapidly switched on and off for the acquisition of each imaging slice. That process generates an artifact in the EEG signal through the electromagnetic induction phenomena, as previously described. This artifact is usually called Gradient Artifact (GA).

GA shows much higher amplitudes than the small neurophysiology-based EEG measures, which make the EEG signal unrecognizable during MRI acquisition periods (for an example of this type of artifact, refer to Figure 2.10). Several solutions have been proposed to attenuate the effects of the GA at the source. One approach to minimize the magnitude of the GA is to lay out and immobilize the EEG leads, twisting the leads or modifying the lead paths, using

a bipolar electrode configuration, and using a head vacuum cushion (Mullinger et al., 2014). Even adjusting the position of the subject within the MR scanner attenuates the GA amplitude (Mullinger et al., 2011). Other options have been proposed at the hardware level, with Chowdhury and colleagues suggesting the use of an EEG cap with electrodes on an external layer that record the GA separately from the EEG, allowing then to make a subtraction between the signals recorded by internal and corresponding external electrodes, reducing the artifact (Chowdhury et al., 2014). Although these solutions perform a considerable attenuation of the GA, its effective suppression must be performed with post processing signal approaches.

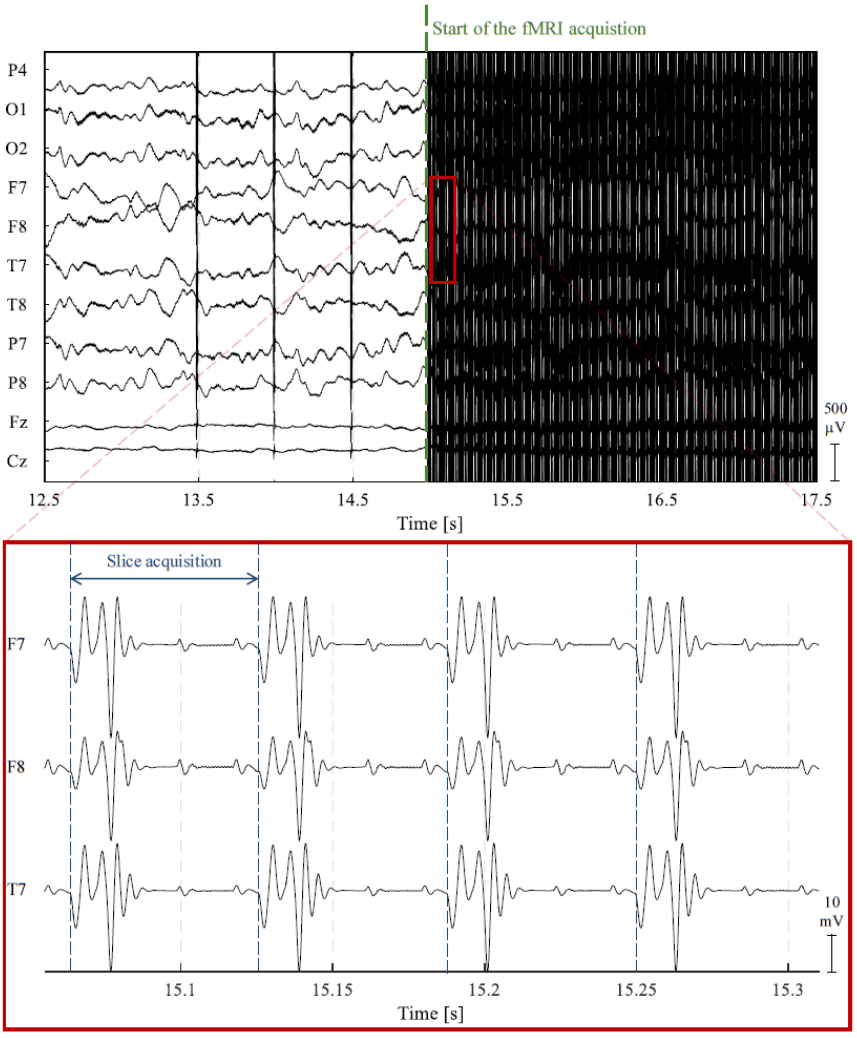

Figure 2.10 - Example of EEG data with and without the contamination by the Gradient Artifact. A zoomed view of the GA shows the repetitive nature of the artifact, which is explored by the template subtraction methods. – adapted from (Abreu et al., 2018).

Targeting the GA at the post processing phase is challenging, since the amplitude of the GA exceeds the physiological measures significantly and contain components in the EEG frequency range. There is an important result showing that the gradient-switching-related impulse response function can be modeled as a linear and time invariant system (Felblinger et al., 1999). Thus, one can assume that the GAs are additive, and therefore can be removed independently from other artifacts. With that established, average artifact subtraction (AAS) methodologies can be applied, which are currently the most used approaches to remove the GA from the signal. The process explores the assumption that the GA is periodic and stationary to create an average template from several occurrences, which are then subtracted from the signal to restore the neurophysiological signal, due to the additive property mentioned above.

The quality of the reconstruction achieved by AAS methods depends on the EEG sample frequency, since timing correctly the windows for creating the average template and its subtraction have crucial importance and depend also on the absence of head movement by the participant. To target the first dependence, very high frequencies are used for EEG recording (above 5KHz), and synchronized with the clock frequency of the MR machine (Mandelkow et al., 2006). To avoid head motion, besides immobilizing the movement as much as possible with head cushions, Allen and colleagues proposed a template approach that is still used as the most effective way to remove GA in post processing (Allen et al., 2000). Additional to the template subtraction, an adaptive noise cancelation (ANC) filter is applied. The small head motions of the subjects and the system vibrations add a stochastic component to GA, characterized by random artifact fluctuations on the EEG. Since morphologies and amplitudes of the GA (template) systematically differ between EEG channels, because of the different positions and orientations of the electrodes and cables with respect to the gradients (among other factors), the GA template calculation and the corresponding GA correction is performed for each channel separately. Specific targeting that component, some variations of the original method have been proposed, considering moving or weighted averages for the creation of the template, for instance. For an overview of different approaches, please refer to (Eichele et al., 2010).

2.2.3.2 Pulse artifact correction

Concerning the pulse-related artifact (PA), the ballistocardiogram (BCG) component is usually clearly visible after the GA rejection. Besides existing also outside the scanner, the BCG artifact presents a much larger amplitude inside the scanner. This is believed to be a consequence of cardiac-related electrode movement, due to expansions and contractions of scalp arteries between systolic and diastolic phase (Vanderperren et al., 2010). Those movements, occurring under the B_0 magnetic field, generate an electric current due to Faraday's law of induction. The stronger the B_0 magnetic field, the higher the BCG artifact amplitude (Debener et al., 2008). Inside the MR machine and, therefore, under the influence of the B_0 magnetic field, the cardiac pulse generates an artifact of approximately 10Hz and bellow (Allen et al., 2000).

There are several putative mechanisms that cause the PA, with the stronger candidates being cardiac-pulse-driven head rotation, the Hall effect[1] due to pulsatile blood flow and pulse-driven expansion of the scalp. The main contributor to PA seems to be cardiac-pulse-driven head rotation, but the variance of PA across cardiac cycles is more influenced by the Hall effect of pulsatile blood flow (Mullinger et al., 2013).

The correction approaches to this artifact can be divided into two main categories: template subtraction and blind source separation (Vanderperren et al., 2010). The template subtraction method is similar to the AAS method for the GA correction, with variations on the process of template creation, to account for temporal variability. The different approaches include median-filtering (Ellingson et al., 2004), Gaussian weighted averaging (Goldman et al., 2000) or the use of an optimal basis set (OBS) of PCA components (Niazy et al., 2005; Marino et al., 2018), for each channel. These approaches depend also on the identification of the QRS complexes on the EEG, which can be made through peak detection algorithms or using a modified Teager energy operator (Kim et al., 2004). For the blind source separation approach different methods have been employed, such as, for example, the canonical correlation analysis (Assecondi et al., 2009), but the most commonly used is, by far, the independent component analysis (ICA) (Mullinger et al., 2013). The process relies on the fact that BCG activity is independent of neuronal activity, and thus could be separated from each other given

[1] The Hall effect is the production of a voltage difference (the Hall voltage) across an electrical conductor, transverse to an electric current in the conductor and to an applied magnetic field perpendicular to the current (Hall, 1879).

enough sensors. The independent components (ICs) containing BCG-related activity are discarded and the remaining components are re-projected in the original data, thus removing the contribution of the discarded ICs. However, most ICA algorithms assume spatial stationarity, ignoring the spatio-temporal variability of the BCG artifact. Nevertheless, due to the limitations of alternative methods (Vanderperren et al., 2010), ICA-based approaches are usually used. An interesting approach has been suggested using a combination of both approaches, applying AAS or OBS on the IC projections instead of excluding the ICs, which yield an improvement compared to the currently most used methods (Abreu et al., 2016). A different approach has also been recently applied, modeling the BCG using likelihood-based regression techniques, with promising results (Krishnaswamy et al., 2016).

2.2.3.3 Simultaneous EEG-fMRI analysis

When considering simultaneously acquired EEG-fMRI analysis, different strategies have been used. There are three main approaches in the literature: i) symmetric fusion techniques, where a common generation model is constructed to explain both the EEG and fMRI data, ii) fMRI-constrained EEG source localization, using the fMRI data to limit search space of the inverse solution and iii) EEG-informed fMRI analysis, using EEG features, convolved with the HRF, to identify regions that correlate significantly the BOLD activity with those EEG features (Lei et al., 2012).

In theory, the most interesting approach would be the symmetrical fusion, which considers both signals without constraining any of them. However, it implies the creation of a common temporal forward or generative model that links the underlying neuronal activity to the measured hemodynamic and electrical responses (Mullinger and Bowtell, 2011), which is difficult to develop. Model-driven fusion approaches use frameworks like dynamic causal models or neural field models to create neurophysiologically grounded solutions, whose inversion might give some insights into the origin of neuronal activity and its mediation through intrinsic and extrinsic connections. Due to the difficulty of developing such models, most fusion approaches use joint EEG/fMRI ICA decompositions in a data-driven approach to integrate the two modalities (Lei et al., 2012).

fMRI data can be used to provide spatial constraints when localizing sources of EEG activity. This idea is grounded on the premise that the origins of EEG are linked to regions of increased BOLD signal, which has been shown in a couple of combined EEG/fMRI studies that,

analyzing the EEG and fMRI data independently, identified the same sources of activity (Mulert et al., 2004; Mullinger and Bowtell, 2011). However, the use of fMRI to constrain the source localization of EEG should be handled with care, due to 1) deep sources of brain activity, which appear in the fMRI data and do not manifest in EEG due to its strong dependence of the depth of the source, 2) particular sources of EEG activity might generate low metabolic demand and, therefore, there may not be a corresponding BOLD response and 4) an EEG signal may correlate to either positive or negative BOLD fluctuations, making it difficult to impose source constraints on the EEG (Ritter and Villringer, 2006). Nevertheless, given that those issues are taken into account, one can still use fMRI as a weight factor for the source localization, thus only guiding the process, which has been shown to help the localization process (Wan et al., 2008).

Finally, and probably the most used integration analysis technique, is the EEG-informed fMRI analysis. For this technique, the common approach is to extract a time course representative of the phenomenon one wants to study from the EEG signal and use it as a regressor for the general linear model (GLM) analysis of the fMRI signal. That representation is often achieved using temporal or spectral features (Abreu et al., 2018). In the temporal domain, the simplest case is the use of boxcar functions to select periods of interest (Thornton et al., 2010) or, in task-related analysis with event-related potentials (ERPs), to use features from those ERPs, at each trial (e.g., peak amplitude and/or latency) (Nguyen and Cunnington, 2014). For the spectral domain, the typical approach is to compute the time-frequency decomposition of the EEG signal and extract the power of specific bands over time (Abreu et al., 2018). By including the power values over different EEG bands in the GLM analysis, one can investigate their individual contributions to the BOLD signal (de Munck et al., 2009). To account for the spatial representations of EEG phenomenon in the scalp, techniques like clustering, ICA or topographic time-frequency decomposition are usually employed (Yuan et al., 2012; Schwab et al., 2015). Functional connectivity methods have also been used as priors for the fMRI analysis, including partial direct coherence, phase synchronization index or global field synchronization (Abreu et al., 2018). Some studies have also addressed the EEG-fMRI combination in terms of connectivity in both signals, meaning to link connectivity measures in the EEG to dynamic functional connectivity measures in the BOLD signal, instead of the BOLD signal itself (Tagliazucchi and Laufs, 2015).

In the scope of this thesis, the EEG-fMRI combination is addressed in a transfer way: we aim to find EEG characteristics that correlate with the BOLD activity in a specific location. This

is different from the usual EEG-informed fMRI approach, in the way that we do not seek to identify which regions best correlate to an observed EEG phenomenon, but instead to identify which EEG phenomenon correlate with the BOLD activity we observe in a specific region. Studies using this approach are scarce in the literature. There is one Israeli group that developed a method to map EEG time-frequency decompositions to the BOLD activity in the amygdala, to use in relaxation neurofeedback tasks (Meir-Hasson et al., 2014, 2016). They named this method EEG Finger-Print (EFP) and it consists of mapping the EEG time-frequency decomposition of several delayed signals to the observed BOLD signal, using a ridge regression model. They find interesting correlation values for both the visual cortex and what they claimed to be the amygdala signal (please refer to the end of section 3.2.1.2 for further details).

2.3 Virtual reality

According to the definition presented by Craig and colleagues in Developing Virtual Reality Applications (2009), Virtual Reality (VR) is a term that applies to computer simulations that create an image of a world that appears to our senses in much the same way we perceive the real world (or "physical" reality) . In order to convince the brain that the synthetic world is authentic, the computer simulation monitors the movements of the participants and adjusts the sensory displays in a manner that delivers the feeling of being immersed in the simulation. Since sight is, for most people, the dominant perceptual sense, it is the aspect of reality most frequently addressed in VR. Other important components for one's perceptual experience are sounds and tactile feedback. Although smell and taste play important roles in our daily life, they have been less exploited in VR due to the complexity of the required technology (Gutiérrez A. et al., 2008).

The VR technological steps started around the mid 50's, with the cinematographer Morton Heilig's Sensorama, patented in 1962. This was an arcade-like cabinet featuring stereo speakers, a stereoscopic 3D display, fans, smell generators and a vibrating chair, designed for immerse the viewer completely in the film. Heilig also patented a head-mounted display (HMD) device, called the Telesphere Mask, in 1960. In 1965 Ivan Sutherland presents a paper describing the "ultimate display", where he details the concept of a virtual world viewed through an HMD which replicated reality so accurately that the viewer would not be able to distinguish between it and the reality, and included means for the user to interact with objects (Sutherland, 1965).

VR technology continued to be developed throughout the 1970s, but mostly in universities and research centers. The 1980s saw a boom in VR research and commercialization, but the technology was not ready to fulfil the expectations. The most common problems were unreliable hardware, slow computers and cyber sickness (Gutiérrez A. et al., 2008). In the early 1990s, a change of paradigm in VR interfaces occurred with the design of the CAVE (Cruz-Neira et al., 1992). The CAVE is a room with graphics projected from behind the walls in stereo to provide a depth cue. The projected images create a wider field-of-view (FOV) than that of an HMD and has the benefit of instead of using a heavy headset, the user only needs some (lightweight) stereo glasses.

The first decades of the 21st century saw a major, rapid advancement in the development of virtual reality. Computer technology, especially small and powerful mobile technologies, have exploded while prices were constantly driven down. The rise of smartphones with high-density displays and 3D graphics capabilities enabled a generation of lightweight and practical virtual reality devices. The video game industry also continued to drive the development of consumer virtual reality, delivering depth sensing cameras, motion controllers and natural human interfaces. The Oculus Rift, which started as a Kickstarter campaign in 2012, showed that was possible to create lightweight easy-to-wear HMDs and re-opened the HMD development and commercial market, which several companies to follow, bringing momentum to the area (Sony, Google, Facebook, Samsung, HTC and more).

The immersion quality of an experience is measured by the level of fidelity, concerning all sensory modalities, that a VR system can provide. Thus, immersion is objective, measurable, and depends only on the technology used by the VR system. Presence, however, refers to the human reaction to that immersion and represents the psychological sense of being inside the virtual environment (Sanchez-Vives and Slater, 2005). Characteristics that have an impact on the presence in a virtual environment (VE) include:

- Display parameters - graphics frame-rate, latency, head tracking, stereopsis (stereoscopic vision), geometric field of view,
- Visual realism,
- Sound,
- Haptics - technology with tactile feedback (e.g. game controller vibration),
- Visual body representation,
- Body engagement - using body motion as input.

Thus, immersion and presence are the two main factors that influence VR experiences and, regarding immersion, VR systems can be divided into three different categories (Gutiérrez A. et al., 2008), namely:

- non-immersive - systems using desktop-based VR (e.g. video games),
- semi-immersive - systems using large projection screens (e.g. CAVE),
- fully-immersive - systems using head-mounted displays (HMD) (e.g. Oculus Rift, HTC Vibe, etc).

Figure 2.11 shows example snapshots of the different types of immersion from our lab.

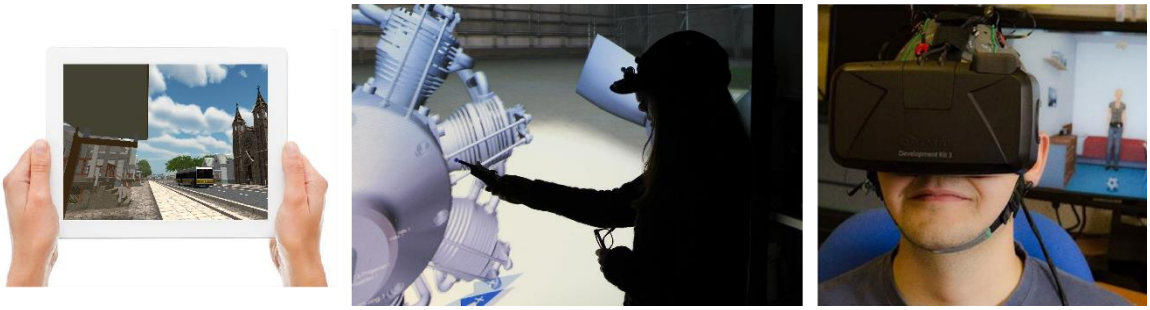

Figure 2.11 - Examples of the three types of immersion in virtual reality. at the left, a non-immersive system (tablet). In the middle, a semi-immersive system (3D projection with position tracking). At the right, a fully-immersive system (a head-mounted display).

2.3.1 Virtual rehabilitation

Virtual rehabilitation represents the combination of computers, special interfaces, and simulation exercises used to train patients in an engaging and motivating way (Burdea et al., 2007). The advances in VR technology, along with respective cost reductions, supported the development of more usable, useful, and accessible VR systems that have been explored to target a wide range of physical, psychological, and cognitive rehabilitation concerns and research questions (Rizzo and Kim, 2005). VR characteristics potentiate the creation of systematic human testing, training, and treatment environments that allow for the precise control of complex, immersive, dynamic 3D stimulus presentations, enabling sophisticated interactions, behavioral tracking, and performance recording.

Mostly due to its capacities of recreating real environments while keeping control of the events, virtual reality has been widely applied as rehabilitation tool in several pathologies, including post-traumatic stress disorders (PTSD) (Cukor et al., 2015), anxiety disorders (Benbow and Anderson, 2018), physical (Edmans et al., 2006; Piquepaille, 2010) and cognitive rehabilitation (Coyle et al., 2015). For reviews on the level of evidence of the clinical applications of VR, please refer to (Parsons et al., 2009; Mishkind et al., 2017; Powers and Rothbaum, 2019). In the case of ASD, there are some aspects of VR that make it particularly interesting (Strickland, 1997; Goodwin, 2008; Bellani et al., 2011; Parsons and Cobb, 2011):

- **Controllable Input Stimuli:** virtual environments can be simplified to the level of input stimulation tolerable by the user. Distortions in elements can take place to match the user expectations or abilities. Distracting visual elements and sounds can be

removed and introduced in a slow, regulated way. Moreover, the level and number of non-verbal and verbal features of communication can be directly controlled and manipulated.

- **Modification for Generalization:** minimal modification across similar scenes may allow generalization and decreased rigidity. For instance, one can train to shop for groceries in different virtual grocery stores, following the same procedure and thus helping to learn the procedure independently of grocery store. This is a property of major importance, because it dictates the relevance of the application for the user's real life.
- **Safer Learning Situation:** a virtual learning world provides a less hazardous and more forgiving environment for developing skills associated with activities of daily living. Mistakes are less catastrophic, and the environments can be made progressively more complex until realistic scenes to help individuals function safely and comfortably in the real world.
- **A Primarily Visual/Auditory World:** the VR systems used nowadays use especially visual and auditory stimuli. Particularly with autism, sight and sound have been effective in teaching abstract concepts. Studies show that the autistic individuals thought patterns are primarily visual.
- **Preferred Computer Interactions:** the complexity of social interaction can interfere when teaching individuals with social disorders. Establishing influence over the child is an often-difficult step where human interaction can be so disruptive that learning is not possible. These children respond well to structured, explicit, consistent expectations and challenge provided by computers. Moreover, interaction can take many forms and face-to-face communication can be avoided, which many people with autism might find particularly threatening (users may communicate via their avatars).

It is worth mentioning that most virtual rehabilitation interventions categorize themselves as virtual reality interventions but the large majority consist solely on computerized interventions (Lorenzo et al., 2016). Fully immersive interventions are still scarce.

2.3.1.1 Serious gaming

One type of virtual rehabilitation that has gain traction in the last years is serious games. A serious game is a game whose objective is not recreational, but rather to train or develop a

skill or knowledge (R. Michael and L. Chen, 2006). Thus, the primary purpose of serious games can be, but are not limited to, education, training, human resource management, and health improvement. This way, serious games are designed to educate, train, or change behavior as they entertain players.

Most serious games use computer or tablet platforms, since they are more disseminated in the market. Some virtual reality serious games can be found in the literature, but they are scarce (Zakari et al., 2014). A recent review by Lau and colleagues (2017) found that serious games as interventions for reducing mental health problems appears feasible, but there is a limited number of randomized control trials (RCTs) that systematically test the effects of serious games. More RCTs are needed to determine the effectiveness of serious games in pathologies like ASD. The heterogeneous characteristics of this population make it an interesting target of these games, since the levels of difficulty or complexity can be gradually adapted to the participants' performance and, through gamification principles, keep the user engaged in the learning process. Gamification is the process that leverages the innate desires of people to mastery, competition, achievement and status (among others) to engage them in the game (Lieberoth, 2015). These strategies usually use rewards, points, achievement badges, leaderboards levels or virtual currencies (Kapp, 2012). Through these strategies, players are impelled to progress and achieve new results in the game which, when applied to serious games, means the development or training of some skill or knowledge.

Chapter 3

State of the art

This chapter covers the current knowledge of the two axes of this thesis: characterization and rehabilitation of social deficits in ASD. On the characterization part, we describe how social deficits in ASD are studied nowadays and explain how adding more ecology to the experimental paradigms might help to unveil neural mechanisms that are masked in current studies due to the great simplification imposed on experimental setups. Furthermore, we explore the current known biomarkers associated with ASD social processing deficits.

The rehabilitation part is subdivided into the two main areas of that axis: neuroimaging-based and virtual reality-based interventions. On the neuroimaging-based interventions axis we cover the current brain-computer interfaces and neurofeedback studies that tried to rehabilitate ASD patients. We then explain why the transfer of fMRI neurofeedback interventions to EEG is an important step to generalize and improve the application of neurofeedback interventions. On the virtual reality-based interventions, we highlight studies that focus on the training of social skills on ASD individuals. Particularly with the development of mobile technologies, several serious games have appeared but with poor validation. Furthermore, we emphasize that most of studies use non-immersive technology (like tablets or desktop applications) and could benefit from using virtual reality to improve the sense of presence, performing the training in realistic environments and, thus, improving the chances for generalization of the learnt concepts into the real world.

3.1 Studying social deficits

Being the social deficits a core area of ASD symptomatology, there is a large area of research investigating them. Although ASD is heterogeneous in etiology and symptoms, social behavior deficits unrelated to cognitive dysfunction represent a common central feature and they alone are specific to ASD. So, social deficits are likely to be most informative with respect to modeling the pathophysiology of the disorder (Schultz, 2005). Studies types range from purely behavioral to neuroimaging assessments (EEG and fMRI), with several research groups focusing on eye-tracking analysis of behavior (Billeci et al., 2017).

Social deficits are found throughout child development. In ASD newborns there is evidence for lack of innate preference and impaired selective attention to human voice over other sounds and human faces over other stimuli (Barak and Feng, 2016). Diminished social preferences in auditory and visual stimuli can be observed throughout infancy, for stimuli like biological motion, human speech or facial expression (Chawarska et al., 2007; Paul et al., 2007; Klin et al., 2015). Another indicator of social interaction deficit is the inability of following joint-attention cues. Joint-attention is the process by which two individuals share the focus on an object or element. This skill is impaired in most cases of ASD and is related to later development of other skills like language or pretend play (Charman, 2003; Dawson et al., 2004; Vivanti et al., 2017; Adamson et al., 2019).

Social impairments follow though the development of the child, especially after language acquisition. In typically developed children, the increased ability to communicate verbally with others results in more complex social behavior, including shared play and interactions with other children. Since these abilities are impaired in ASD children, social interactions deficits are conspicuous during this phase and are usually the triggers to test the children for ASD (Barak and Feng, 2016). These impairments in social interaction are manifested throughout the life-course of ASD individuals.

One key aspect of social interactions is the understanding and correct identification of facial expressions of the others. Faces represent a critical source of visual information for social perception, conveying relevant information about identity and emotional states of others (Kanwisher and Yovel, 2006). Since the first months of life, children are able to process facial cues, like facial expressions. The ability to interpret these social signals represents an essential skill in child development and, therefore, a basic condition for the development of the ability

to engage in successful social interactions early in life (Bayless et al., 2011). Specialized neural systems have evolved for rapid perceptual analysis of emotional face expressions, which is essential for decoding the feelings of others (Akechi et al., 2010). Thus, facially expressed emotions have an important role in the regulation of contextual interactions between individuals and their environment. In this thesis, we focus on the facial expression processing aspect of social interaction. Although face processing deficits (as a whole) in ASD have been fairly covered in the literature, both by behavioral (Tanaka and Sung, 2016) and neuroimaging (Tavares et al., 2016) approaches, understanding of facial expression processing presents up until today some challenges, especially from the neuroimaging perspective, that we address in our work.

Neuroscientific studies have been able to identify specific brain areas and neural circuits involved in face processing (Apicella et al., 2013). From those regions, two different neural systems were identified as responsible for face recognition: a **core** system, that processes the early visual face properties, consists of three bilateral regions in occipito-temporal cortex (Haxby et al., 2000), and an **extended** system, which includes a number of regions with distinct functional specializations (Benuzzi et al., 2007; Apicella et al., 2013; Tye et al., 2014). The **core** system includes the inferior occipital gyrus (IOG), the lateral portion of the fusiform gyrus (FG) and the superior temporal sulcus (STS) (Haxby et al., 2000; Batty et al., 2011). IOG and FG mediate the encoding of faces, while STS is involved in the perception of social signals derived from faces, such as direction of gaze, facial expressions, and dynamic changes in face identity (i.e., a face morphing into another face) (O'Connor et al., 2005; de Jong et al., 2008; Akechi et al., 2010).

In recent years, many behavioral studies have been conducted focusing the face processing in ASD, but there is a lot of variability in the results regarding the deficits in recognizing emotional facial expressions (Rump et al., 2009). Some studies suggest that the ability is intact (Castelli, 2005; Jones et al., 2011), whereas others found profound deficits relative to TD children (Rump et al., 2009; Akechi et al., 2010; Apicella et al., 2013; Lerner et al., 2013). Nevertheless, there is evidence for face-processing differences in individuals with ASD relative to TD children. While TD individuals process faces holistically, individuals with ASD appear to prefer to use analytical-processing strategies (O'Connor et al., 2005).

It is crucial to determine where and when processing of neural information of emotion displayed by faces is disrupted in ASD, as an important step towards understanding the

neurobiological basis of social and emotional deficits that these individuals display (Wong et al., 2008). To do that, the high temporal resolution of EEG makes it a particularly appropriate technique for studying the time course of emotional processes (Lerner et al., 2013). Event-related potentials (ERPs) are particularly applicable to the study of face processing since faces evoke a distinct pattern of electrical brain activity. Several studies have showed some ERP components that are preferentially activated by faces. The most common, the N170, is recorded over the occipito-temporal cortex (critical for social perception, including FG and STS) and is greater in the right than the left hemisphere (Apicella et al., 2013; Tye et al., 2014). It is characterized by a negative slope that peaks at approximately 170 ms post-stimulus presentation. Another two ERP components are usually present in responses to face stimuli: the vertex positive potential (VPP), a fronto-central concomitant positive deflection of the N170, which is also sensitive to processing of faces (Luo et al., 2010; Sel et al., 2015); and also the early posterior negativity (EPN), a component that slopes negatively in response to emotional facial expression stimuli relative to neutral stimuli (Rellecke et al., 2013).

Although those components are associated with face processing, it is still unclear how they are influenced by facial expressions. Abnormal ERP responses to emotional face expressions have been reported in ASD: consistent alterations are demonstrated for the N170 component in response to facial stimuli (Dawson et al., 2002, 2005; McPartland et al., 2004; Webb et al., 2006); with delayed and reduced N170 ERP components to emotional facial expression stimuli (de Haan et al., 1998; Batty and Taylor, 2003; Eimer et al., 2003; McPartland et al., 2004; O'Connor et al., 2005; Webb et al., 2006; Blau et al., 2007; Wong et al., 2008; Batty et al., 2011; Lerner et al., 2013); reduced N170 component by fear compared to TD individuals (de Jong et al., 2008) and larger amplitude compared to neutral facial expressions (Batty and Taylor, 2003; Eimer et al., 2003; Akechi et al., 2010; Wagner et al., 2013). Nevertheless, other studies report no differences in ERP components but rather in source localization of face related activity (Eimer and Holmes, 2001; Eimer et al., 2003; Wong et al., 2008; Tye et al., 2014)(Eimer and Holmes, 2001)(Eimer and Holmes, 2001)(Eimer and Holmes, 2001)(Eimer and Holmes, 2001)(Eimer and Holmes, 2001). The same uncertainty applies to the VPP. Some studies report that this ERP component is affected by emotional facial expression contrasts (Luo et al., 2010; Sel et al., 2015), whether others find the opposite (De Taeye et al., 2015; Shim et al., 2016).

To clarify the state-of-the-art regarding the facial expressions deficits in ASD, we conducted a systematic review on EEG studies that addressed facial expressions processing in this

disorder (Monteiro et al., 2017). We conducted article selection according to Preferred Reporting Items for Systematic Reviews and Meta-Analyses (PRISMA) (Moher et al., 2009). The procedure is detailed in the flowchart present in Figure 3.1.

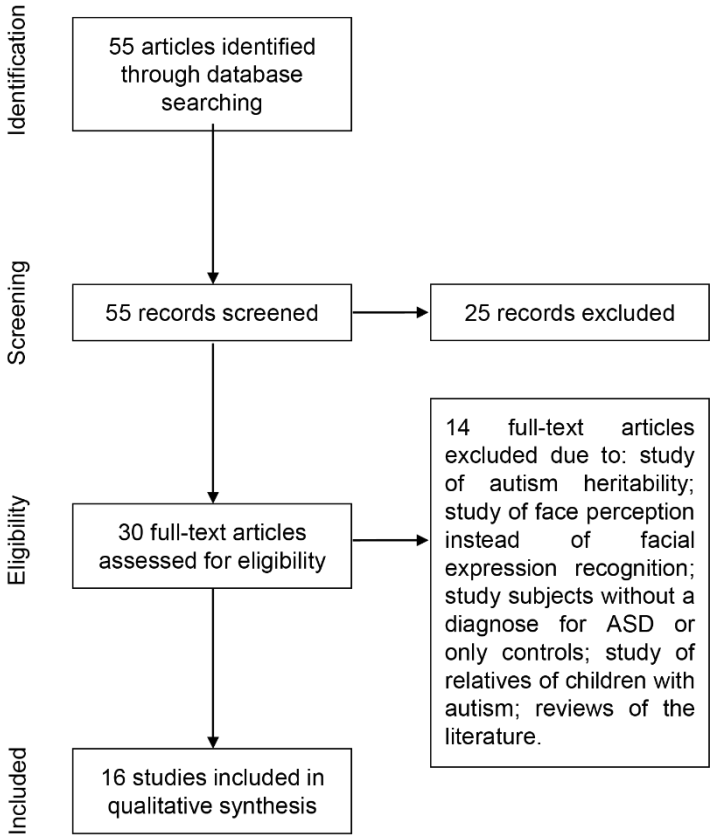

Figure 3.1 – PRISMA flow diagram of the article screening and selection process.

After the application of the article screening and selection criteria, only 16 articles were available for further analysis. Most of the studies reviewed reported consistent findings, including: group differences; emotion and emotion by group interactions; source localization effects; and correlations between behavioral performance and ERP component signals. Significant group differences, found in some of the reviewed studies, point towards some disruption in processes involved in emotional face processing in ASD individuals, essentially due to deficits in early stages of visual processing (Batty et al., 2011; Luckhardt et al., 2014). Although for the first ERP components (P1 and N170) we found concordant results, that is only true for global group differences, for a maximum of three studies. Therefore, the findings regarding ASD facial expression processing deficits are not very robust yet. This scenario is

even worse when considering the later potentials (P2, N400, VPP, etc.), where none of the differences were reported by more than one study.

Group differences and emotion by group interactions reported in the studies reviewed in Monteiro et al (2017) provide evidence that individuals with ASD process emotional facial expressions differently than TD individuals. However, the main emotion effects found for both groups suggest that, in most of the cases, individuals with ASD perform at the same level as TD individuals, possibly through the use of compensatory mechanisms they have developed (Harms et al., 2010). In other words, neurophysiological differences may reflect more a matter of cognitive style rather than a true deficit (Happe, 1999).

3.1.1 The need for more ecological approaches

Assessing emotional expression processing impairments in ASD individuals using static photographic stimuli depicting facial expressions, as almost all of the studies reviewed did, may represent a problem, because this type of stimulus could be learned explicitly in the context of therapeutic interventions (Harms et al., 2010). Dynamic morphing of facial expressions, representing emotional expressions of differing intensity, are more ecologically valid than static presentations and are more likely to induce the same response as subtle facial expressions in daily life social interactions (Harms et al., 2010). Thus, this type of stimulus may be more sensitive to group differences between ASD and TD individuals and should be included in future research, as a way to better connect behavioral clinical research and neural processing of emotional information (Harms et al., 2010).

While it is clear that simplifications of reality must be created for us to be able to conduct systematic experimental studies, in the case of studying social domains (like facial expression processing) that simplification might be disruptive, since social interactions and theory of mind (the ability to interpret others' beliefs, intentions and emotions) depend, most of the time, on the interpretation of subtle social nuances of the other (Brewer et al., 2017). Therefore, we believe that virtual reality can serve as a balanced medium, where structured and fully controllable environments can be developed to mimic some aspects of reality, while keeping its ecology.

Based on our systematic review, all EEG studies rely on blank baselines followed by the presentation of a still picture. This experimental design loses the ecology of real life facial

expression interactions in two aspects. Firstly, the absence of dynamism in the facial expression. In real-life interactions, facial expressions are portrayed in a dynamic way, where the face of the individual expressing the emotion gradually morphs between facial expressions at distinct intensity levels. Secondly, the transition from blank baseline to face with expression merges the responses to the face itself (as a visual objects) with the specific responses to the facial expressions per se. With controlled virtual environments, experimental designs can be defined to structure transitions from faces without expressions to faces with expressions, thus creating stringent contrasts that isolate the responses to the facial expressions themselves.

3.1.2 Biomarkers of social impairments

There is a lack of biological tests (biomarkers) to diagnose or even characterize ASD. Biomarkers can be defined as biological variables associated with the disorder or disease and measurable directly in the patient or in his/her derived biological samples using sensitive and reliable quantitative procedures (Ruggeri et al., 2014).

There is a clear heritability factor in autism, since monozygotic twins show much higher concordance rates of ASDs (92%) than dizygotic twins (10%) (Goldani et al., 2014), which supports the theory of a genetic etiology of the ASD (Won et al., 2013). But despite being highly heritable, the heterogeneous clinical symptomology and genetic architecture of ASD make difficult the identification of common genetic factors. Although several genetic mutations have been associated with the presence of autism, no common genetic variants that increase the risk of ASD have been identified, other than some clear genetic disorders such as fragile X, for example, of which phenotypes meet the ASD category description. ASD is, therefore, an etiologically heterogeneous disorder with no single genetic mutation accounting for more than 1 to 2% of ASD cases (Abrahams and Geschwind, 2008).

With limited causal information available from the field of genetics, this led the science community to investigate other research avenues. More recently, neuroimaging studies have been used to characterize the ASD (Goldani et al., 2014). Early-accelerated brain volume growth has been identified in ASD, with a 10% increase in brain volume identified in toddlers, but followed by a plateau in volumetric changes during adolescence, ultimately leading to adult brain volumes that fall within the range of typically developing controls (Anagnostou and Taylor, 2011). However, there is also some evidence for enlarged total brain volume in adolescence and adulthood (Freitag et al., 2009; Hernandez et al., 2015).

There are some MRI studies showing structural abnormalities in the ASD brain, but there is too much variability between studies to derive a structural biomarker. For instance, studies show an increased volume of the caudate in ASD, and a relation between its volume and the severity of repetitive behaviors (Hollander et al., 2005). However, the little replicability of structural findings led to the exploration of functional abnormalities using electrophysiological and functional Magnetic Resonance Imaging (fMRI) studies.

The fMRI research applied to ASD represents a large field of study. Most of fMRI findings point towards connectivity deficits, especially between fontal-posterior regions (Li et al., 2017), mostly identified in resting-state measures. However, there is interest in identifying biomarkers that are specific of the social mechanisms of the brain, and thus task-specific differences between ASD groups and controls must be assessed. Considering task-specific studies on the social networks of the brain, we can divide the studies into face processing, biological motion, theory of mind and the reward network.

Face processing studies showed that viewing faces elicits activity in the bilateral fusiform face area (FFA), lateral occipital cortex (occipital face area – OFA), posterior STS and amygdala (Fox et al., 2009). It was originally proposed that ASD individuals show reduced activation to faces in the fusiform gyrus (FFA region) (Corbett et al., 2009; Kleinhans et al., 2011), but brain activity in these areas may be mediated by extrinsic factors that increase attention. For example, if ASD individuals are cued to look to the eyes of the faces activity in FFA increases (Davies et al., 2011), and the level of activity is correlated with the amount of time spent looking to the eyes of face stimuli (Dalton et al., 2005). Therefore, these studies suggest that the original findings of hypoactive responses to faces in ASD are due to either avoidance of or lack of attention to the eye area.

The ability to process biological motion (movement that is not mechanical but rather human, like walking or moving body parts as the hands, mouth, eyes, etc.) has been associated with the STS region, inferior frontal gyrus, amygdala and visual areas like the fusiform gyrus (Herrington et al., 2011). In ASD, STS hypoactivation has been consistently reported associated to biological motion or social tasks that involve biological motion processing (like detecting dynamic facial expressions) (Kaiser et al., 2010; Shih et al., 2011; Hotier et al., 2017).

Theory of mind is the ability of attributing mental states and intentions to others. This skill elicits neural activity in the STS, temporo-parietal junction (TPJ), medial prefrontal cortex

(MPFC), and temporal poles. There are studies showing abnormal activation patterns in all of these areas (Hernandez et al., 2015).

Finally, the reward network associated to social interactions. In humans, social cues such as smiles are processed early in infancy and appear to be highly rewarding, biasing attention toward such cues. One general theory of autism postulates that reduced social motivation underlies the development of autism (Chevallier et al., 2012). The reward network includes the anterior cingulate cortex, orbitofrontal cortex, and ventral striatum (Kohls et al., 2013). Those regions have shown aberrant activity during monetary reward tasks, and those differences in the striatum were also found during social reward tasks (viewing happy faces) (Scott-Van Zeeland et al., 2010; Delmonte et al., 2012).

Overall, there is increasing evidence for the temporal regions, like the STS, to play a crucial role in the social processing deficits in autism. However, variability of results makes it difficult to generalize neuroimaging biomarkers from these social networks, especially because many regions showing reduced activity under certain conditions can show typical responses when attention is explicitly directed to the task at hand, when the salience of the stimuli is increased, or when stimuli or tasks are more personally relevant to the individual (Hernandez et al., 2015).

Regarding EEG-based biomarkers, several studies have investigated EEG patterns that may differentiate individuals with ASD from age-matched typically developing controls. Not surprisingly, because of the wide range in ages and phenotype of the ASD group being studied, no single EEG biomarker has been identified that consistently distinguishes individuals with ASD from those without ASD (Jeste et al., 2015). Although most of the studies usually recur to linear EEG measures (like the amplitude of event-related potentials or frequency measures in the different bands of the spectrum), Bosl and collegues (2018) showed recently that the nonlinear characteristics of the EEG signals can be explored as diagnosis tools (in particular when combined with machine learning algorithms).

Some studies of functional connectivity have identified a general pattern of short-range under-connectivity and long-range over-connectivity in ASD, with results varying based on regions and frequency bands of interest (Coben et al., 2008; Duffy and Als, 2012; Schwartz et al., 2017). Signal complexity measures, like multi-scale entropy (MSE), have been used to differentiate ASD to TD individuals (J. et al., 2014).

However, those measures represent group differences that are not specific to social interaction deficits, since they are extracted in resting-state activity. Task-related measures provide better insights on the mechanisms behind the perceived deficits in social interactions. Some studies focus on the face processing network and investigate event-related potentials (ERPs) characteristics (amplitude and latencies of their components' peaks), and differences have been found in those ERP components on the face processing network (Dawson et al., 2005). However, some studies fail to replicate those differences, with too much heterogeneity confounding the results (Monteiro et al., 2017). Another EEG component linked to the social deficits (usually associated with the mirror-neurons system) is the reduced suppression of the mu rhythm (~11Hz) when observing actions of others (Oberman et al., 2005). Most studies, however, only analyze group differences and do not evaluate the potential of those metrics as biomarkers (Jeste et al., 2015).

In Chapter 4 we describe our approach to the study of social deficits, including the use of computerized dynamic stimuli to increase ecological validity and the search for biomarkers related to the abnormal processing of those stimuli.

3.2 Rehabilitating social deficits

As seen in section 2.1.3, therapies for ASD rehabilitation usually follow the Applied Behavior Analysis (ABA) structure, an approach based on the analysis of behavior and reinforcement in the structure of antecedent, behavior, based on consequences. However, those interventions are intensive in time and resources – from 25 to 40 hours per week (Roane et al., 2016) and, most of the times, in a one-on-one basis between the therapist and the patient – which are, in most cases, impossible to implement. This way, other solutions which complement this type of interventions have been raising increased interest in the community. We divide those interventions into two main axes: neuroimaging-based interventions and virtual rehabilitation interventions.

3.2.1 Neuroimaging-based interventions

Considering the neuroimaging-based interventions, there are mainly two types: brain-computer interfaces and neurofeedback paradigms.

3.2.1.1 Brain-Computer Interfaces

A Brain-Computer Interface (BCI) – also called Direct Neural Interface or Brain Machine Interface – is a direct pathway between the brain and an external device (Figure 3.2). Its basilar concept is to interpret brain signals in order to allow communication or interaction with the external world through the thoughts of its user (Hammon and de Sa, 2007). As suggested by Pfurtscheller and colleagues (2010), a BCI application must exhibit the four following components:

1) **Direct recording:** the BCI must rely at least partly on direct measures of brain activity, such as through electrical potentials, magnetic fields, or hemodynamic changes.
2) **Real time processing:** the signal processing must occur online and yield a communication or control signal.
3) **Intentional control:** the user must perform an intentional, goal-directed mental action to control, such as imagining movement or focusing on a stimulus.
4) **Feedback:** goal-directed feedback, about the success or failure of the control, must be provided to the user.

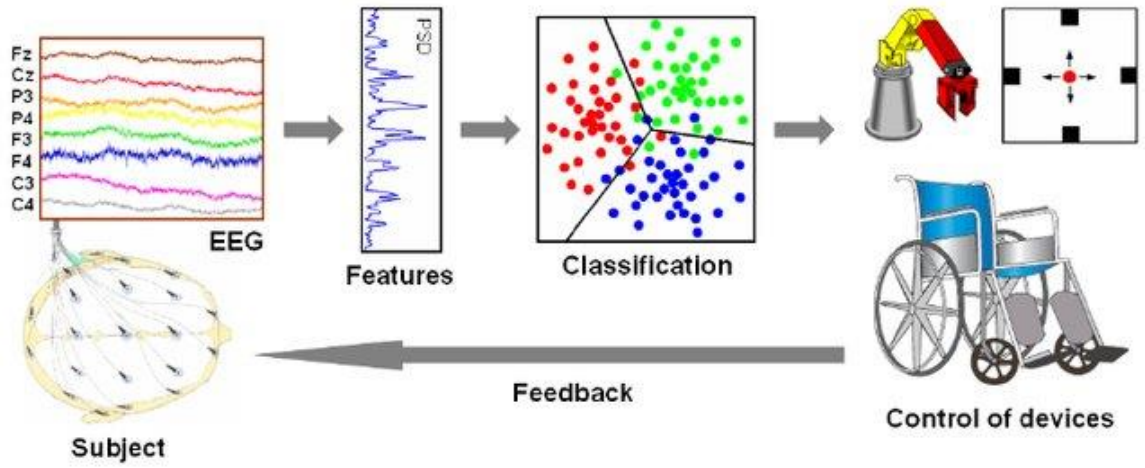

Figure 3.2 - General architecture of a brain-computer interface, showing the different steps of the process: the EEG is measured, features are extracted and then classified into actions that are translated into commands to external devices. – adapted from (Millán et al., 2008).

The applicability of such technology is wide: the game community has early on understood the value of this technology in gaming and some products have already been released that use brain readings as interaction means (using portable and low-cost EEG headsets like Emotiv and NeuroSky, but with poor scientific validation). The military directed the research towards a telepathic communication device, where soldiers could communicate with each other's just by thinking of it (Kotchetkov et al., 2010). But the largest research field has been the neuroscientific one, towards augmenting the capabilities of handicapped people, such as, power muscle implants and restoring partial movement (McFarland and Wolpaw, 2008), or through the widely-known P300 speller, where a user is presented with a matrix of letters and the system identifies the letter he/she wants to communicate, which is a feasible way for patients with locked-in syndrome[2] to communicate (Fazel-rezai and Abhari, 2009; Pires et al., 2011).

Mostly due to its flexibility and easiness to use in domiciliary contexts, EEG has been the neuroimaging modality most explored for the development of BCI systems. Two types of changes can be extracted from the ongoing EEG signals: one change is time and phase-locked (evoked) to an externally or internally-paced event, the other is non-phase-locked (self-induced). Thus, two types of BCI can be differentiated: one corresponding on evoked brain

[2] Locked-in syndrome is a condition in which a patient is conscious and aware but cannot move or communicate verbally due to complete paralysis of nearly all voluntary muscles in the body except for the eyes. *(NORD: National Organization for Rare Diseases - https://rarediseases.org/rare-diseases/locked-in-syndrome/)*

activity by external stimulation (e.g. triggering selective attention) and another based on induced brain activity (e.g. motor imagery).

BCIs based on selective attention require external stimuli provided by the BCI system. The stimuli can be auditory, visual or somatosensory. The most common approaches use visual stimuli. The stimulus most commonly used is some flashing character or image in a computer screen. Commonly, on this type of BCI, each stimulus is associated with a command to the application. On the original BCI speller (Farwell and Donchin, 1988), each stimulus is a character of the alphabet. That way, the user can write by selecting the stimuli's letters. That kind of BCI can be achieved through two different mechanisms, named after the brain patterns they produce: P300 and steady-state visual evoked potentials (SSVEP).

The induced type of BCI usually makes use of the following phenomena: moving or simply contracting a muscle requires brain activity (brain oscillations recorded from the somatosensory and motor areas are known as the sensorimotor rhythms – SMR). Interestingly, the preparation of the movement or its mere imagination change the SMR in a similar way as the movement itself (Pfurtscheller and Neuper, 1997). The decrease of oscillatory activity in a specific frequency band is called event-related desynchronization (ERD). Correspondingly, the increase of oscillatory activity in a specific frequency band is called event-related synchronization (ERS). ERD/ERS patterns can be created by motor imagery, which is the imagination of movement without actually performing it. Since ERD/ERS patterns produced by motor imagery are similar in their topography and spectral behavior to the patterns elicited by actual movements, the mental imagery is a form of inducing brain rhythm changes that can be detected by a BCI system and then transformed into a command (Pfurtscheller et al., 2010). In contrast to BCIs based on selective attention, BCIs based on motor imagery do not depend on external stimuli. Nevertheless, motor imagery is a skill that has to be learned. Some users, however, never get a grip on mental imagery control, which makes this approach invalid for them (it is estimated to be around one third of users) (Kober et al., 2013).

Regarding BCI research on autism, there are very few studies using it. Apart from some initial approaches (Jing Fan et al., 2015), most studies incorporate BCI within a serious game that uses BCI for mental training (for example, reducing the mu rhythm in the sensorimotor cortex) (Friedrich et al., 2014).

We created the first BCI system for training joint-attention in ASD. We optimized it, comparing between three EEG systems which one provided the best setup to use with the ASD participants (Amaral et al., 2017) and worked on the classification algorithms to improve the classification accuracy of the system (Simões et al., 2019b), and conducted a clinical trial on ASD to test its feasibility (Amaral et al., 2018) (ClinicalTrials.gov identifier: NCT02445625). Considering motor imagery, we also conducted an initial study with mental imagery of grasping movements on ASD, which could lead to a BCI intervention (Andrade et al., 2017). Those studies fall out of the primary scope of this thesis and are not fully described in this document. The readers should refer to the papers for further information.

3.2.1.2 Neurofeedback

Neurofeedback can be considered one type of BCI, but it diverges basically in its objective: while in BCI the goal is to control or command an external device, in neurofeedback (NF) the objective is to provide the user with real-time information of a neuronal process, for him to self-regulate it. This way, neurofeedback measures brain activity and provides a visual, auditory or other representation of the measured activity to the participant. With that information, the participant tries to volitionally change his/her neuronal activity, guided by the feedback he is receiving.

Through neuroimaging studies, behavior has been correlated with patterns of brain activity. The concept behind neurofeedback is that if one can train himself/herself to volitionally modulate those patterns of brain activity directly, changes in the associated behavior should be observed. Indeed, some behavioral changes have been observed to result from self-manipulation of neural activation (Shibata et al., 2011), which indicates that the physiological consequences of neurofeedback may be considered to be a form of endogenous neural stimulation.

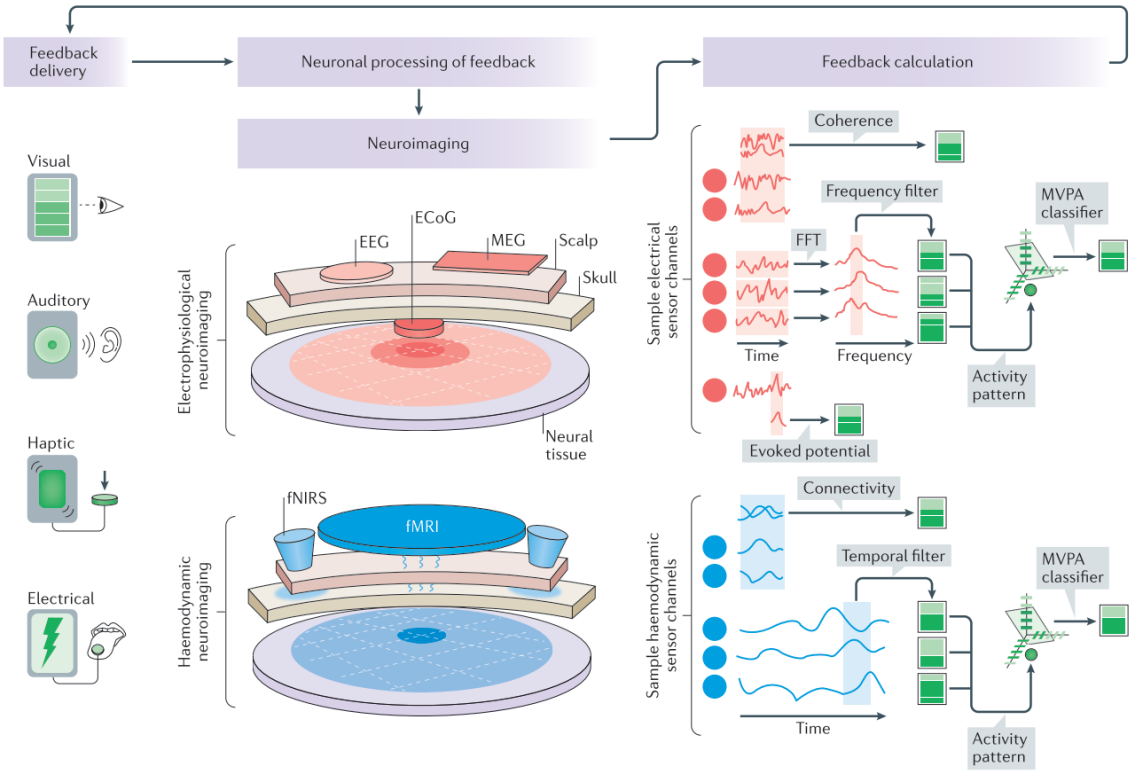

Figure 3.3 - Schematic of the neurofeedback process, considering different feedback delivery means, different neuroimaging types and different forms of extracting indicators from the mental processes to use as feedback – adapted from (Sitaram et al., 2016).

As shown in Figure 3.3, NF implementations can vary in three domains: feedback delivery method, neuroimaging method and feedback calculation method. For the feedback delivery method, the most common approach is to use visual feedback, showing a thermometer with the level corresponding to the activity level. Other approaches change the size of the stimuli in function of the level of activity. Other feedback delivery methods comprise auditory, tactile and even electrical stimuli. Regarding the neuroimaging method, the methods can be subdivided into two major groups: electrophysiological neuroimaging method (EEG, ECoG or MEG) and hemodynamic methods (fMRI or fNIRS). Finally, the feedback calculation process is the greater source of variability between studies, since the idea is to capture a pattern that is representative of a brain process of interest and convert it into a single signal to feedback the participant. At the electrophysiological domain, the most common approach is to filter the signal into frequencies of interest and use ratios between frequency bands (example: alpha /theta ratio) (Imperatori et al., 2017). However, evoked potentials can be used, as well as measures of connectivity between electrodes (like coherence) (Coben, 2007). In the hemodynamic domain, the most common approach is to select a region-of-interest

(ROI) in the brain and extract its level of BOLD signal to use as feedback (Young et al., 2017). Nevertheless, connectivity measures between different ROIs have also been used in the literature (Koush et al., 2013).

EEG-based NF research started in the 1970s and has been widely used in the last decade. However, the level of evidence associated with this technique is still scarce. Micoulaud-Franchi and colleagues (2015) reviewed the level of evidence in the literature for EEG-based neurofeedback applied to mental disorders and concluded that there is some level of efficacy concerning ADHD patients and, for the case of ASD, there are improvements in specific symptoms that are related to the ADHD comorbidity, which is present in 40-50% of ASD patients. Other reviews corroborate this conclusion (Holtmann et al., 2011). Therefore, the level of efficiency of EEG-based NF in ASD is yet to be proven.

fMRI-based NF has the major benefit of providing relatively high spatial resolution access to any brain structure, including deep regions, with millimeter precision. Therefore, fMRI-based NF can target any brain region and use their BOLD activity as feedback signal. However, since it is a technology much more recent than the EEG-based NF (the real-time fMRI was only developed in the mid-90s (Cox et al., 1995)) and, furthermore, much more expensive, fewer studies can be found in the literature using fMRI-based NF. Other consequence is the lower number of sessions per study: since fMRI scans are much more expensive, studies comprise only few training sessions, usually even only one session (mostly in preliminary studies) (Shibata et al., 2011). Nevertheless, its spatial precision granted, in previous studies, interesting behavioral results and several review works highlight its potential application in neuropsychiatric conditions (for a detailed analysis, please refer to (Micoulaud-Franchi et al., 2015; Sitaram et al., 2016; Arns et al., 2017)). Its application on ASD, however, is still very scarce. Despite a project without any public outcome known yet (Caria and de Falco, 2015), no study yet tried to conduct systematic fMRI-based NF training in ASD.

We developed an fMRI-based NF paradigm targeting the pSTS region on ASD using mental imagery of facial expressions as strategy for the BOLD modulation (Direito et al., 2019). With that, we implemented a feasibility clinical trial to test its feasibility on ASD (ClinicalTrials.gov identifier: NCT02440451). The clinical trial showed relevant clinical effects, verified in relevant neuropsychological scales, including emotion recognition. Those differences were present immediately after the intervention and replicated 6 months later (for further details, please refer to Appendix II). These results indicate that the intervention has the potential to

be successful and thus a phase IIb/III clinical trial should be conducted. Therefore, and upon the promising results of this clinical trial, transferring this intervention to an EEG setup would extend its potential application range and scope.

fMRI to EEG neurofeedback transfer

The combination of EEG and fMRI for neurofeedback was made, so far, following two different approaches: one is to explore both techniques as sources for feedback signals (for example, using localized hemodynamic activity and oscillatory electrical activity, as firstly showed by Zotev and colleagues (2014) for the left amygdala BOLD signal and frontal Beta asymmetry from the EEG) and the other is to transfer the fMRI-based NF paradigms to EEG settings (Meir-Hasson et al., 2014). This second approach is motivated by the fact that fMRI-based NF is expensive and inflexible and, therefore, if seeking broader application scopes, the transfer of validated fMRI-based NF paradigms to EEG is a path of utmost importance.

However, this approach faces great challenges: i) the different type of signal measured by both techniques, with dissimilar characteristics, ii) the incapacity of EEG to measure activity from non-cortical (deep) regions, due to the physiological attenuation of the signal, iii) the inter- and intra-subject variability of neuroimaging data. Possibly due to those challenges, literature on NF-transfer from fMRI to EEG is scarce (Perronnet, 2017; Abreu et al., 2018). Despite the works from the Tel-Aviv group (Meir-Hasson et al., 2014, 2016), we are not aware of any other study trying this approach. Nevertheless, these are challenges worth facing, since, as Fovet and colleagues (2015) point out in their critical analysis of the current fMRI-based NF, the major barrier in the translation of fMRI-NF protocols to the clinical practice is the accessibility and cost of the equipment, and the use of less complex devices after a limited number of fMRI-NF sessions (for models calibration, for example) could be a significant step in the translation of fMRI-based NF protocols into clinical practice.

We address these challenges in Chapter 5, where we describe our contribution to transferring the fMRI-based NF protocol previously mentioned (Direito et al., 2019) to an EEG setup.

3.2.2 Virtual rehabilitation interventions

The use of virtual rehabilitation of social deficits in ASD started with computerized or televised interventions. Computerized interventions specific to social skills training appeared in the mid-90s and continued to be developed until nowadays, with studies looking for false belief, facial expressions and feelings (Swettenham, 1996; Silver and Oakes, 2001; Bölte et al., 2002). However, most of those studies found difficulties with generalization of the learned concepts. Through multimedia DVDs, some studies tried to teach emotions to ASD participants (Golan and Baron-Cohen, 2006, 2007; Golan et al., 2010).

With the appearance of the concept of serious games and the development of mobile technologies, the number of applications designed for ASD have exploded. Zakari team (2014) and, more recently, Grossard and colleagues (2017) reviewed the games developed for ASD social skills rehabilitation. An interesting factor identified in the Grossard analysis is a positive correlation between the year of publication and the number of studies, showing a clear trend of the appearance of more applications for social rehabilitation in ASD every year. With them, researchers have been also looking to defining design principles for the development of games adapted for this population (Bartoli et al., 2014; Whyte et al., 2015), which is a fundamental step to develop better and more suitable solutions. The guidelines include

- Strong customizability.
- Increasing levels of complexity of game tasks.
- Clear and easy to understand task goals.
- Multiple means of communicating instructions (e.g. text, voice, visual cues).
- Positive reinforcement with rewards.
- Repeatability and predictability of game play.
- Smooth transitions.
- Minimalistic graphics and sound/music to avoid sensory hyperreactivity.
- Dynamic stimuli.

A factor identified by Liu and colleagues (2017) in their review of technology-facilitated treatments for ASD is the lack of customizable solutions that automatically adapt to the participant. Another point, which limits generalization, is the absence of fully immersive virtual reality interventions (Zakari et al., 2014). Bringing more ecological validity to the training task with immersion should help generalization. Despite the clear advantages of the

use of virtual reality in ASD (that we detailed in section 2.3.1), most of the studies (even the ones claiming to use virtual reality) resort to the use of virtual environments displayed in laptops or tablets (Josman et al., 2008; Parsons and Cobb, 2011; Zakari et al., 2014; Grossard et al., 2017).

We developed a system for virtual rehabilitation training and tested a serious game to train social skills and independent living in ASD. Those contributions are detailed in Chapter 6.

Chapter 4

Processing and imagining dynamic facial expressions

This chapter consists in the paper:

Simões, M., Monteiro, R., Andrade, J., Mouga, S., Franca, F. M., Oliveira, G., Carvalho, P., Castelo-Branco, M. (2018). A novel biomarker of compensatory recruitment of face emotional imagery networks in Autism Spectrum Disorder. ***Frontiers in Neuroscience, 12(November), 1–15. doi: 10.3389/fnins.2018.0079.***

Abstract

Imagery of facial expressions in Autism Spectrum Disorder (ASD) is likely impaired but has been very difficult to capture at a neurophysiological level. We developed an approach that allowed to directly link observation of emotion expressions and imagery in ASD, and to derive biomarkers that are able to classify abnormal imagery in ASD. To provide a handle between perception and action imagery cycles it is important to use visual stimuli exploring the dynamical nature of emotion representation. We conducted a case-control study providing a link between both visualization and mental imagery of dynamic facial expressions and investigated source responses to pure face-expression contrasts. We were able to replicate the same highly group discriminative neural signatures during action observation (dynamical face expressions) and imagery, in the precuneus. Larger activation in regions involved in imagery for the ASD group suggests that this effect is compensatory. We conducted a machine learning procedure to automatically identify these group differences, based on the EEG activity during mental imagery of facial expressions. We compared two classifiers and achieved an accuracy of 81% using 15 features (both linear and nonlinear) of the signal from theta, high-beta and gamma bands extracted from right-parietal locations (matching the precuneus region), further confirming the findings regarding standard statistical analysis. This robust classification of signals resulting from imagery of dynamical expressions in ASD is surprising because it far and significantly exceeds the good classification already achieved with observation of neutral face expressions (74%). This novel neural correlate of emotional imagery in autism could potentially serve as a clinical interventional target for studies designed to improve facial expression recognition, or at least as an intervention biomarker.

4.1 Chapter Introduction

Faces represent a critical source of visual information for social perception, conveying relevant information about identity and emotional states of others (Kanwisher and Yovel, 2006). Since the first months of life, children are capable of understanding and processing facial cues, like facial expressions (Field et al., 1982). The ability to interpret these social signs represents an

essential skill in child development and, therefore, a basic condition for the development of the ability to engage in successful social interactions early in life (Bayless et al., 2011).

Autism Spectrum Disorder (ASD) is a neurodevelopmental disorder characterized by deficits in the social domain which represent hallmark early characteristics (Sperdin et al., 2018). Even for simple visualization of facial expressions (FE), the literature is somewhat inconsistent: while some studies show group differences both in behavioral performance and neural responses, other studies show no identifiable deficits at all (for a compreensive review, see Monteiro et al., 2017).

Importantly, no previous study has considered the role of mental imagery in the FE processing domain, possibly because of the challenges in identifying imagery signatures that mimic neural responses during simple observation. The perceptual strength and spatial frequency of the FE stimuli seem to be relevant to yield ASD group differences during simple visual presentation (Vlamings et al., 2010; Luckhardt et al., 2017), but the large majority of visual perception studies use static frame stimuli, lacking the dynamic characteristics of naturalistic FE (Monteiro et al., 2017). Those dynamics have been shown to play a crucial role on the perception of the respective FE and its emotional valence (Krumhuber et al., 2013) possibly because they allow to generate perception and action imagery cycles.

Another limiting aspect is the notion that specific processing experimental contrasts are needed to isolate effects of interest. For example, the use of blank screen baselines, before the presentation of faces, generates a non-specific contrast of face with expression against a baseline without any stimulus. Therefore, those responses comprise both the processing of low-level core aspects of the face and the specific processing of the FE. In this EEG study we used dynamic FE morphing in a virtual avatar and used its neutral expression as baseline, to ensure a facial expression specific contrast. This way, the neutral FE is already present in the baseline. We believe this stringent contrast provides a response specific to the processing of the FE aspects, isolating it from the simple response to the face static itself. A systematic review of EEG studies regarding facial expression processing in ASD conducted by Monteiro and colleagues (2017) has already identified the need for experimental paradigms targeting the dynamic characteristics of facial expressions. All the studies identified by that review applied non-specific experimental contrasts, using blank screens as baseline of their experimental conditions. To the best of our knowledge, our study is the first one to combine a task-specific contrast for dynamic facial expression stimuli.

Mental imagery (MI) is defined as the simulation or re-creation of perceptual experience (Kosslyn et al., 2001; Pearson et al., 2013). Most of these mental representations are extracted from memory and allow one to mentally revisit the original stimuli or their combination (Pearson et al., 2015). Disturbed MI has been postulated to be present in several psychiatric disorders, from post-traumatic stress disorder (Lanius et al., 2002) to socio-emotional disorders like social phobia or depression (Hirsch et al., 2006). In the specific case of ASD, MI is likely to be impaired, since one of the key deficits included in the ASD diagnosis, in the form of absence or impairment of 'pretend play' (Baron-Cohen et al., 2001; American Psychiatric Association, 2013), which requires preserved action-perception imagery cycles. This deficit is particularly interesting since it spans into the social, imitation and repetitive behavior dimensions (Crespi et al., 2016). Therefore, the study of the neural correlates of MI in ASD gains relevance since it might lead to the understanding of the neural correlates of its core neurodevelopmental limitation and further help into the development of successful therapies.

Here, by providing a critical link between visual observation and subsequent replay imagery, we bound MI to the FE of an avatar, in a task where the participant mentally replays the previously observed dynamic image of the avatar performing a happy or a sad facial expression. We believe this link between visual observation and MI of FE in others addresses both the deficits of FE processing, emotion identification and theory of mind, due to the lack of thinking from the perspective of the other present in ASD. Therefore, the concept of visually imagining others smiling recruits the faculties of expression processing and pretend play, and our experimental design allowed to study such imagery process in ASD, and to use two distinct classification approaches, based on linear and non-linear features describing brain signals, to differentiate between the disease state and normal cognition. Non-linear features consist of quantitative measures that represent in a relatively simple way complex dynamic characteristics of the EEG signals, which the traditional linear methods (amplitude and frequency, for example) are not able to capture. They have been adopted more and more frequently in EEG analysis in general and ASD biomarker research in particular (Bosl et al., 2011, 2017).

4.2 Materials and methods

4.2.1 Participants

Seventeen male teenagers with the diagnosis of idiopathic ASD were recruited from the Unit of Neurodevelopment and Autism from the Pediatrics Unit from the University Hospital of Coimbra and from Portuguese ASD patient associations (Coimbra and Viseu). Since ASD is a disorder far more prevalent in male individuals, with a ratio of four males to every female, and there is accumulated evidence for sex differences in brain connectivity (Alaerts et al., 2016; Irimia et al., 2017; Fu et al., 2018), only male participants were included in the study. The diagnosis of ASD was performed based on the Autism Diagnostic Observation Schedule, the Autism Diagnostic Interview – Revisited and the Diagnostic and Statistical Manual of Mental Disorders – 5th edition criteria, confirmed by an expert multidisciplinary team. Seventeen healthy typically developing (TD) male controls were recruited from our local database of volunteers. Participants from both groups had their Intelligence Quotient (IQ) assessed by the Wechsler Adult Intelligence Scale for participants older than 16 years old, and by the Wechsler Intelligence Scale for Children for younger participants. Groups were matched by chronological age (ASD mean age and standard error (SE): 16.4 ± 0.6 years; TD mean age and SE: 15.5 ± 0.6 years) and performance IQ (ASD mean score and SE: 99.8 ± 3.0; TD mean score and SE: 106.2 ± 4.2). Additional group characterization can be found in Table 4.1.

Table 4.1 – Group characterization: Mean and standard error of the mean (between brackets) of Age, Full Scale IQ (FSIQ), Verbal IQ (VIQ) and Performance IQ (PIQ) (*p > 0.05).

	ASD	TD	
N	17	17	
Age	16.4 (0.6)	15.5 (0.6)	*
FSIQ	92.2 (3.1)	109.2 (4.5)	
VIQ	88.1 (4.2)	110.3 (4.2)	
PIQ	99.8 (3.0)	106.2 (4.2)	*

Written informed consent was obtained from the parents of the participants or, when appropriate, the participants themselves. The study was approved by the ethics committee

from Faculty of Medicine from the University of Coimbra and was conducted in accordance with the declaration of Helsinki.

4.2.2 Experimental tasks

The experiment is divided in two tasks: one of visual stimulation and one of mental imagery requiring "mental replay" of previously observed facial expression, with the goal to identify similar neural signatures. The visual stimulation task and overall experiment were developed in *WorldViz Vizard 5 VR Toolkit* (development edition) using the *male002* virtual avatar from the *Complete Characters HD pack* and its facial expression poses. The total duration of the experiment is about 50 minutes, including 15 minutes for scalp cleaning and placement of the EEG cap, 30 minutes for the experimental tasks and 5 minutes to clean up at the end of the session.

4.2.2.1 Visual stimulation task

This task consists in observing a virtual avatar performing either sad or happy facial expressions (see Figure 4.1a), which represent two antagonistic expressions from the six core expressions (Ekman and Friesen, 1971). The facial expressions were verified in accordance with the action units defined in the Facial Action Coding System (FACS) (Ekman and Friesen, 1978). The happy expression comprises action units 6 (cheek raiser), 12 (lip corner puller) and 25 (lip part), while the sad facial expression uses action units 1 (inner brow raiser), 2 (outer brow raiser), 4 (brow depressor), 15 (lip corner depressor) and 17 (chin raiser).

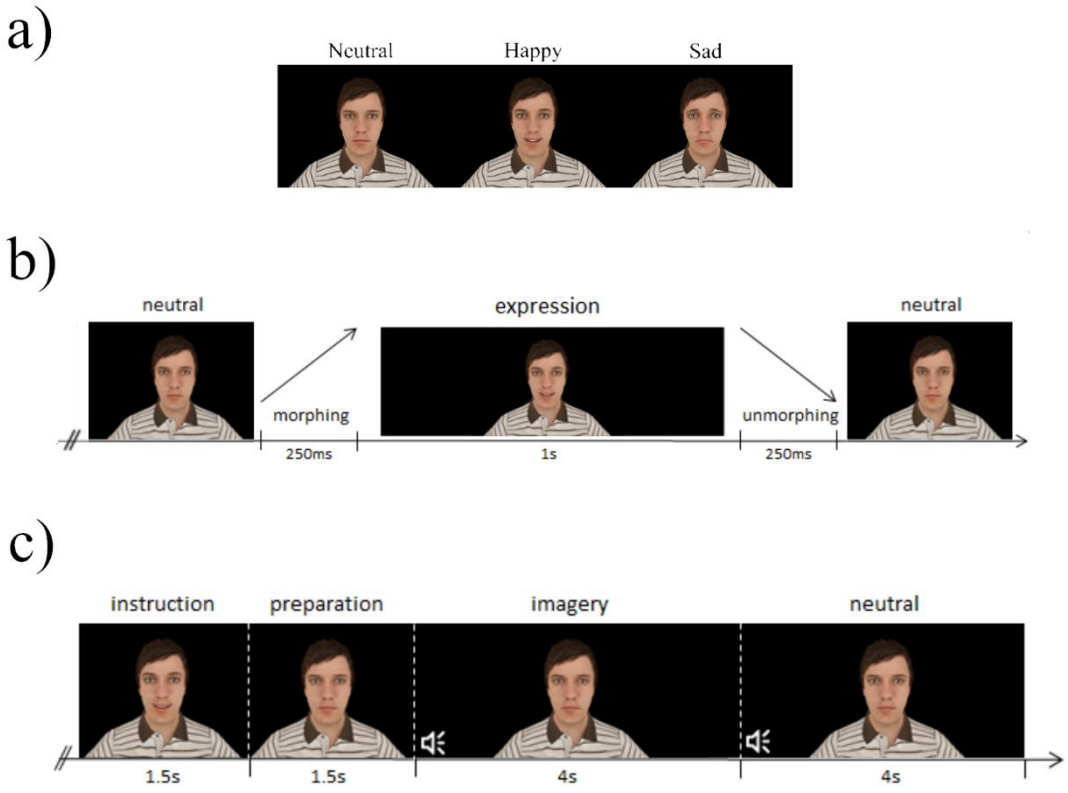

Figure 4.1 – Description of the tasks, both regarding structure and stimuli used. a) Base stimuli used for each expression at their expression endpoint, comprising the neutral, happy and sad facial expressions. b) Structure of the visual stimulation paradigm: each expression lasted 1.5 seconds, divided by facial expression morphing (250 ms), static facial expression (1 s) and facial expression unmorphing (250 ms). c) Structure of the mental imagery paradigm: the instruction is composed by the avatar performing the expression to be imagined, as presented in the visual stimulation task, and to facilitate mental replay. After that, an interval of 1.5 s is left for preparation, and an auditory stimulus (beep) cues the start of the mental imagery process, for 4 seconds, whereas another beep indicates the end of the mental imagery of the expression, and the start of the neutral period.

Each trial is composed by a morphing period of 250 ms where the expression of the avatar gradually changes from neutral to the target expression, followed by a static period where the virtual avatar is displaying the target facial expression for 1000 ms and a final period where the avatar morphs back to the neutral expression, with the duration of 250 ms (see Figure 4.1b). Thus, each stimulus has a duration of 1.5 s and the inter-trial interval consisted in 1s plus a jitter of 500 ms. The neutral face of the avatar is always present during the baseline / inter-trial interval, which creates a stringent contrast with the facial expression since the stimuli

does not come from no stimulus / blank screen, but from the neutral face, as naturally happens in real life.

This part of the experiment is composed by two blocks of 120 randomized trials (60 of each facial expression), for a total of 240 trials. The participants were asked to fixate the face of the avatar in the middle of the eyes and observe the expressions. A rest period was included between blocks to ensure focus and reduce fatigue throughout the experiment. A total of 120 trials per condition were recorded.

4.2.2.2 Mental imagery task

The second part of the experiment consists of a mental imagery paradigm. In this task, the participant is asked to mentally imagine the avatar performing the same types of facial expressions used in the stimulation part (used to facilitate mental replay). The computer screen shows the neutral face of the avatar during the whole period, except for the instruction, when it performs the facial expression the participant is asked to imagine. Then, after a cue, the participant imagines the avatar performing the facial expression, in a period of four seconds, returning to no imagery after that period. The c) section of Figure 4.1 details the structure of the trials. This task is composed by two blocks of 40 randomized trials (20 for each expression), achieving a total of 80 trials for the task.

4.2.3 Experimental setup and data recording

The experiment was conducted in a 22-inch LCD Monitor (frame rate of 60 Hz, 1680x1050 pixel resolution). The participants sat about 60 cm away from the screen (distance measured from the eyes to the center of the screen) and were asked to keep their eyes open and fixed on the face of the avatar. EEG data were recorded using a 64 channel actiCHamp system from Brain Products.

The scalp of the participants was first cleaned using abrasive gel and then the 64 channel actiCAP cap was placed on their head. Data were recorded from 64 Ag/AgCl active electrodes (Brain Products), placed across the head according to the international 10–10 standard system. The ground electrode was placed at AFz position and the reference electrode at the right ear. The impedance of the electrodes was kept under 10 kΩ during the recordings. The electrodes were connected directly to the Brain Products actiCHamp amplifier and sampled at 1000 Hz.

EEG data were recorded using the Brain Products Recorder software. For each paradigm, the individuals were informed about the respective task. The total duration of the experimental procedure (preparation + 2 tasks) was around 50 minutes.

4.2.4 EEG preprocessing

We used MathWorks Matlab 2017b and the EEGLAB toolbox v14.1.1 (Delorme and Makeig, 2004) for EEG signal preprocessing and analysis. EEG data were filtered with a finite impulse response bandpass filter of frequencies 1 and 100Hz and notch filtered with an infinite impulse response filter between 47.5 and 52.5Hz, as implemented in the EEGLAB toolbox. Bad channels were removed, and data were re-referenced for the average reference. Epochs were created locked to the stimulus onsets (please refer to the task-specific analysis for details about the epoch lengths). Bad epochs were removed based on the EEGLAB semi-automatic procedures for extreme values and improbable signal segments. Independent Components Analysis (ICA) was then run on the data using EEGLAB implementation of *infomax* algorithm (Bell and Sejnowski, 1995). Components were used in order to extract noisy components, such as blinks, muscular activity or electrical interference. Components presenting such artifacts were removed and the weights were projected back to the data (Makeig et al., 2004). Bad channels previously removed were then interpolated. Further analysis of EEG data was conducted over these preprocessed signals.

4.2.5 Experimental design and statistical analysis

The analysis focused on identifying group differences for both visualization and mental imagery of the facial expressions. We specify the different analyses performed for each task separately.

4.2.5.1 Visual stimulation task analysis

The visual stimulation epochs comprise one second, starting 100 ms prior to the stimuli onset (baseline) and go to 900 ms after the start of the expression morphing (during the first 250 ms of the epoch, the face of the avatar is continuously morphing the facial expression). Event-related potentials (ERPs) were computed by subtracting each epoch by the mean of its baseline

(from 100 ms pre-stimulus to 0) and then averaging all epochs corresponding to the same stimulus condition.

Source analysis were conducted using the standardized low resolution brain electromagnetic tomography (sLORETA) toolbox (Pascual-Marqui, 2002). The procedure included exporting from EEGLAB the preprocessed single-trial epochs, importing them into sLORETA software, averaging them (per subject and expression) and converting to the source space. Each participant electrode locations were co-registered with the realistic anatomical MR model using landmarks and standard electrode positions. The source space representation consists of a current source density (CSD) map computed with the sLORETA algorithm, a standardized discrete three-dimensional (3D) distributed linear weighted Minimum norm inverse solution that takes several neurophysiologic and anatomical constraints into account and has been shown to yield depth-compensated zero localization error inverse solutions (Pascual-Marqui, 1999; Pascual-Marqui et al., 2002). sLORETA employs the current density estimate given by the minimum norm solution, and localization inference is based on standardized values of the current density estimates (Pascual-Marqui, 2002) and has been shown to outperform its competitor algorithms in terms of localization error and ghost sources (Grech et al., 2008).

For each expression and each group, we identified the peaks of the first and second ERP component for each electrode, and extracted the latencies for both peaks across the scalp. We performed the source localization of the mean activity of around those two ERP components (+- 125ms, see Figure 4.2).

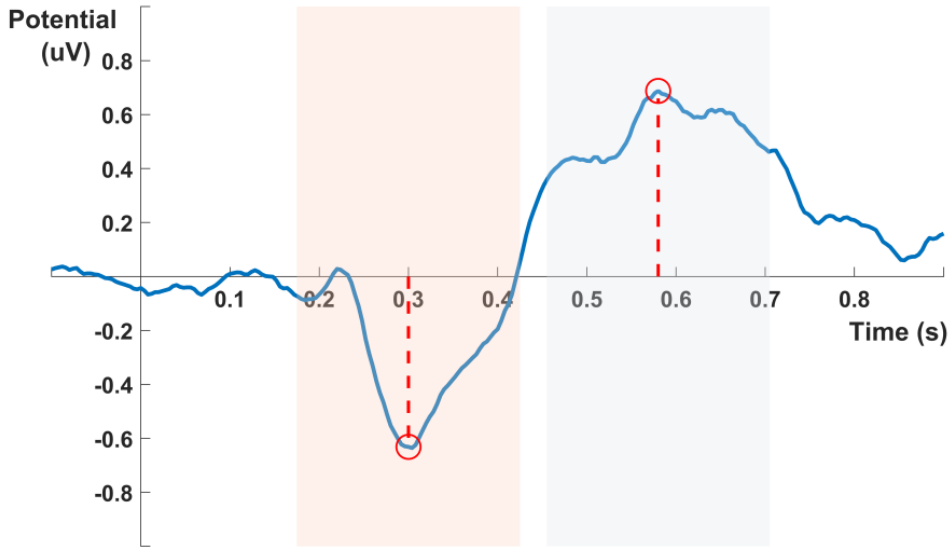

Figure 4.2 – ERP component windows of interest, defined by the minimum and maximum value of the ERP of each electrode.

We conducted a voxel-by-voxel between-group comparison of the mean current source density distribution in those time windows around the ERP peaks, using the sLORETA software implementation of statistical nonparametric mapping (SnPM), employing a log-*F*-ratio statistic for independent groups (for a similar procedure see, for example, Velikova et al., 2011). The SnPM method corrects for multiple comparisons without requiring Gaussian assumptions (Nichols and Holmes, 2001).

4.2.5.2 Mental imagery task analysis

For the mental imagery task, we also performed ERP analysis locked to the sound trigger. For the longer imagery blocks, we performed a spectral source analysis at more distant time windows and investigated the statistical classification of putative neural biomarkers.

Mental imagery ERP source analysis

For the imagery epochs, we investigated the ERP sources originated by the happy and sad imagery triggers. The participant receives the instruction beforehand of which expression to

imagine. We segmented the trials from 100 ms prior to the cue beep and up to 900 ms after it, and subtracted them by the mean of their baseline (-100 ms to 0).

Similarly to the visual stimulation ERPs, for the source analysis we looked for the mean global field power in the window of 0 to 250 ms. The pipeline was analogous to the visual evoked potentials (VEP), as well as the statistical framework.

Mental imagery spectral source analysis

For the mental imagery periods, we investigated frequency bands of the signal during the time window of 500 to 3500 ms, avoiding the contribution of the beep ERP and covering the main period of mental imagery, because mental imagery processes are best captured using time-frequency analysis (Horki et al., 2014). The frequency bands of interest were θ, α, β and δ, as defined in the sLORETA toolbox. This analysis of frequency bands of induced activity comprised the following steps: we export the single trials from EEGLAB and imported them to the sLORETA toolbox. Then we compute the cross-spectrum of each trial and average them per subject and condition. The average cross-spectrum is used to compute the source current density maps used in the second-level analysis.

For both ERP and frequency analysis we conducted voxel-by-voxel between-group comparisons of the current density distribution for each expression, in a way analogous to the VEP procedure.

Mental imagery biomarkers to classify groups

To explore the mental imagery processes through the EEG data, we defined several features from the time, frequency and non-linear domain. We then performed a ranking analysis and selected the best features to train a classifier to discriminate participants between groups. Features were extracted for each channel and trial by trial and averaged across all imagery trials and electrode clusters.

Feature extraction

We follow the procedure of Simoes et al. (2015) for extracting features representative of different EEG characteristics.

Time / frequency domain

For the time and frequency domain, we selected the signal envelope (env), Teager energy operator (teag) and instantaneous power (pow) as features. A detailed description of these features is present in Table 4.2.

Table 4.2 – Time / Frequency domain features and their description

Code	Feature Name	Description
Env	Signal envelope	Envelope of the signal (smooth curve outlining the signal extremes), which corresponds to the magnitude of the analytic signal. The analytic signal is composed by the original waveform and its Hilbert transformation. Hilbert transformation of the signal corresponds to the original waveform with a 90º phase shift. Mathematically, the analytic signal z(t) is defined by $z(t) = x(t) + ix'(t)$ (3.1) in which i represents $\sqrt{-1}$, x'(t) corresponds to the Hilbert transformation of the original signal x(t) (Sadjadi and Hansen, 2015)
Teag	Teager energy operator	An energy estimation operator which uses the sum of the instantaneous energy of the signal divided by the signal length. The instantaneous energy of a signal x at the sample n can be determined using the equation $\Psi[x_n] = x_n^2 - x_{n-1}x_{n+1}$ (3.2) where $\Psi[.]$ denotes the Teager energy operator (Solnik et al., 2010). This operator is sensitive to both amplitude and frequency.
Pow	Instantaneous power	The instantaneous power is achieved by squaring its values $P[x(t)] = x^2(t)$ (3.3) where P[.] denotes the instant power of the signal x at the instant t.

Non-linear domain

To extract signal complexity measures, the EEG signal was transformed to its phase-space. The phase-space is a reconstruction of the chaotic dynamics of the system and, as was proven by Takens (1981), it keeps some of the relevant properties of the state space representation of

the system, such as the topographic properties, Lyaponov exponents and the Kolmogorov-Sinai Entropy. Every possible state of the system can be represented by a point in the multidimensional phase space and time evolution of the system creates a trajectory in the phase space (Kliková and Raidl, 2011). We used the time delay method to reconstruct the phase-space of the signal. Given a time series of a scalar variable it is possible to construct a vector $\mathrm{X}(t_i),\ i = 1, \dots, N$ in phase-space in time t_i as follows:

$$X(t_i) = [x(t_i), x(t_i + \tau), \dots, x(t_i + (m-1)\tau)], \quad i = 1, \dots, N - (m-1)\tau \tag{3.4}$$

where τ is time delay, m is the dimension of reconstructed space and $M = N - (m-1)\tau$ is the number of points (states) in the phase space.

We reconstructed a 2 and 3-dimensional phase-space associated to the EEG data, and the time delay was considered to be the mean of the first local minimum from the signal's autocorrelation (hereafter defined as lag). From the non-linear domain we extracted the spatial filling index (SFI), largest Lyapunov exponent (Lyap), correlation dimension (CorrDim), approximate entropy (ApEn) and sample entropy (SpEn) as features. We provide a detailed description of these features in Table 4.3.

Table 4.3 – Non-linear domain features and their description

Code	Feature Name	Description
SFI	Spatial Filling Index	The states are normalized to the interval [-1, 1]. The phase space area is then divided into small square areas of size $R \times R$, and the number of grids in the normalized phase-space is $n = [2/R]^2$. A new matrix can be obtained with its elements equal to the number of phase space points falling in each grid (Faust et al., 2004). Spatial Filling Index corresponds to the probability of a phase space point falling in a grid.
Lyap	Largest Lyapunov Exponent	Characterizes the rate of separation of infinitesimally close trajectories of the signal in phase space, providing a measure of the degree of the system's instability (Cencini et al., 2010). Mathematically, two

		trajectories in the phase space with initial separation of δZ_0, diverge at a rate given by $$\|\delta Z(t)\| \approx e^{\lambda t}\|\delta Z_0\| \quad (3.5)$$ where λ is the local Lyapunov exponent (local exponential rate of expansion) (Cencini et al., 2010). The rate of separation can be different for different orientations of initial separation vector, leading to a spectrum of Lyapunov exponents – equal in number to the dimensionality of the phase space. The maximum Lyapunov exponent corresponds to the mean exponential rate of divergence, characterizing the trajectory's instability (positive values are associated with a chaotic system).
CorrDim	Correlation Dimension	Chaotic dynamic systems exhibit strange attractors, which tend to be self-similar. The Correlation dimension is a measure of the space fractal dimensionality of the attractor defined in the phase space. Correlation sum is defined as sum the fraction of pairs of points of the phase space whose distance is smaller than r, being r the Lag (defined previously). If this number of points is sufficiently large, the ratio between the logarithm of the correlation sum and logarithm of the time delay is a good estimate of the Correlation Dimension (Cencini et al., 2010).
ApEn	Approximate Entropy	Quantifies the amount of the regularity and unpredictability of fluctuations of the signal. A time series with many repetitive patterns has a small value of ApEn, reflecting its predictability; the opposite happens for less predictable signals (Yentes et al., 2013).
SpEn	Sample Entropy	This feature is a modification of ApEn used for assessing the complexity of a physiological time series data. ApEn depends on the length of the time series and lacks relative consistency. SpEn, similarly to ApEn, quantifies the regularity of the signal but does not have the aforementioned disadvantages (Yentes et al., 2013).

The features were extracted from 3 time windows in each trial: baseline [-500 ms to 0 ms pre instruction], emotion imagery [500 ms to 3500 ms after imagery trigger] and neutral [500 ms to 3500 ms after neutral trigger]. For the emotion and neutral time windows, we used the absolute value for the non-linear features and the normalized values (subtracted by the same feature extracted from the baseline) for the time/frequency domain.

1.1.1.1.1 Frequency bands

All features were extracted from signals filtered at different frequency bands. Band-pass Infinite Impulse Response (IIR) filters were used as implemented in EEGLAB toolbox, for the frequency bands: θ [4-8] Hz, α [8-12] Hz, low β [12-21] Hz, high β [21-30] Hz and γ [30-40] Hz.

1.1.1.1.2 Feature selection

In order to reduce the dimensionality of the feature set, we averaged the features extracted from each electrode in spatial clusters, as defined in Figure 4.3. The clusters were defined by electrode spatial proximity in a way that covers the full scalp, keeps symmetry and lobule divisions (frontal, parietal – subdivided in central and posterior region, occipital and temporal). We then used the *a priori* information provided by the source localization and selected only the clusters closer to the right precuneus region, namely C1, C2, C4 and C5.

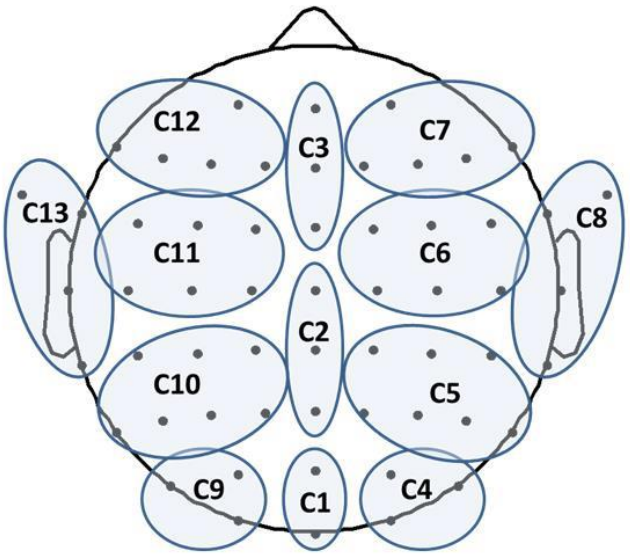

Cluster	Electrodes
C1	POz Oz
C2	Cz CPz Pz
C3	AFz Fz FCz
C4	PO4 PO8 O2
C5	P2 P4 P6 P8 CP2 CP4 CP6
C6	C2 C4 C6 FC2 FC4 FC6
C7	F2 F4 F6 F8 AF4
C8	FT8 FT10 T8 TP8
C9	O1 PO3 PO7
C10	P1 P3 P5 P7 CP1 CP3 CP5
C11	C1 C3 C5 FC1 FC3 FC5
C12	F1 F3 F5 F7 AF3
C13	TP7 T7 FT7 FT9

Figure 4.3 – Clusters defined for the analysis. A full scalp distribution of the clusters was created in order to keep left and right occipital, parietal, central, frontal and temporal areas, and three central clusters for frontal, parietal and occipital lobes. Channel locations are represented with the 10-10 system standard codes.

We ended up with 8 different features x 5 frequency bands x 4 clusters, for a total of 160 different features. We then computed the statistical discriminative value of each feature between groups with two sample T-tests, using only the samples from the training set, and the features were ordered by absolute T value, from the most important to the least.

1.1.1.1.3 Classification

We trained a Support Vector Machine (SVM) with a linear kernel, for being one of the most used classifiers applied to EEG signals (Lotte et al., 2007) and also a Weightless Neural Network (WNN). The WNNs are underused in the literature but present characteristics that generalize well for noisy domains, like the EEG (Simões et al., 2019b). We implemented a variation of the Wilkes, Stonham and Aleksander Recognition Device (WiSARD) combined with a bleaching technique (França et al., 2014) which has been shown to perform at the same level as the SVM in distinct fields and presents fast learning curves, achieving good results even with small datasets of data (Cardoso et al., 2016).

We trained the classifiers to discriminate the group of the participant, based on the feature vector extracted from his EEG data. We divided the participants into train and test sets: 80% of the cases were randomly chosen for training and the remaining 20% for testing. We repeated the procedure more than 30 times, to avoid overfitting, following the guidelines provided by Varoquaux and collegues (2017) regarding the use of machine learning on brain imaging data. Feature selection was performed every time using only training-set data.

To explore the relation between accuracy and the number of features used, the procedure was conducted starting with 5 features and adding 5 more features up to the total of features.

We repeated the full classification procedure using the EEG signal from the neutral part of the mental imagery task, in order to check if the results were specifically improved during over emotion expression imagery.

4.3 Results

4.3.1 Visual stimulation task

This section presents the results of the analysis performed on the ERP responses to the visual stimulation task (observation of happy and sad facial expressions), which was used to identify neural signatures relevant to validate the imagery task.

4.3.1.1 ERP source analysis results

The ERPs obtained from the visual stimulation task present two clear independent components, the first one peaking around 300 ms and the second around 600 ms (Figure 4.4). Since the morphing occurs during the first 250 ms, we expect a delay on the first component, as reported by Graewe and colleagues (2012). The topography of the first component matches the well-known topography of the N170 component, with a negativity around the right and left parietal-occipital regions, but it appears delayed in time, as expected by the morphing animation. The second component has a strong parietal positivity, slightly right lateralized, especially for the ASD group.

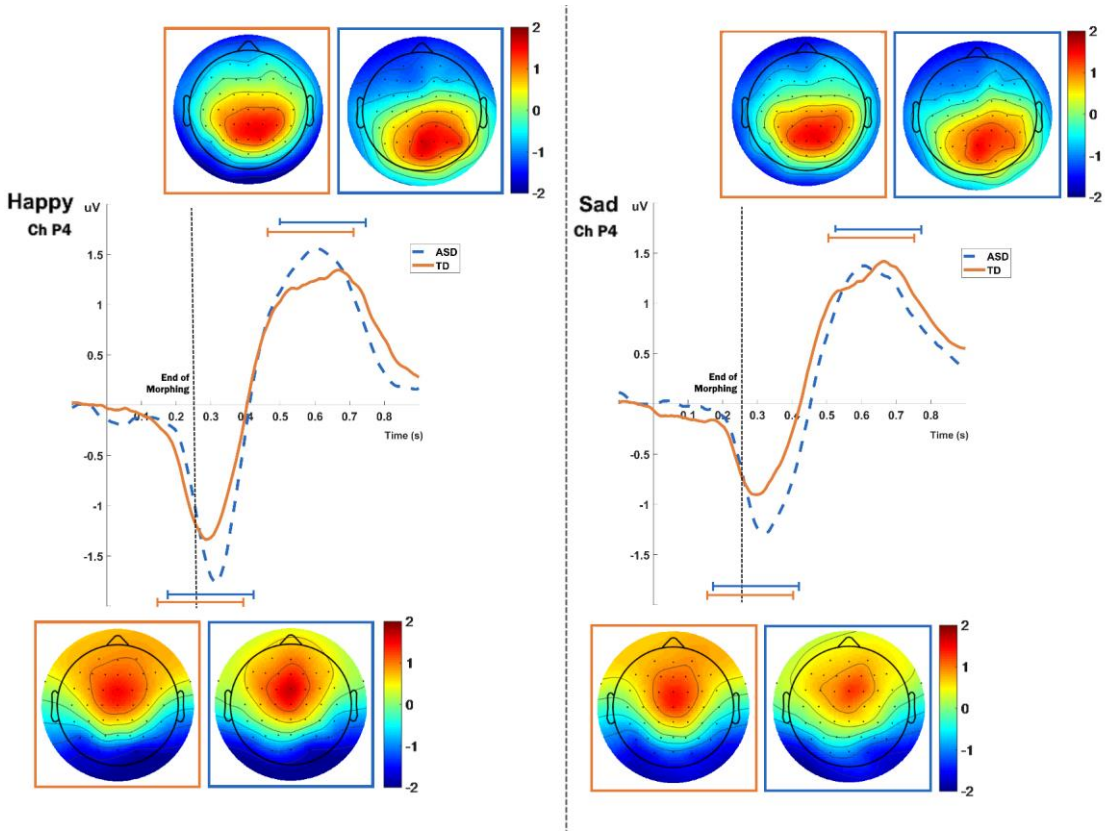

Figure 4.4 – ERPs for both groups and expressions, extracted from the P4 electrode. Topographic maps for each component are present near the ERP plots. Orange marks represent the TD group and blue marks the ASD. Topographic maps show the scalp distribution of the ERP amplitudes extracted from 250 ms windows, centered at the peaks of the components of each expression (refer to Supplementary Table 3 for detailed peak latencies).

For the source analysis of the visual stimulation task ERPs we defined time-windows of 250 ms around the two component peaks of activity in the ERPs. We show the results for the first and the second ERP component, separately. The mean peak latencies used for each expression and each group is detailed in Table 4.4.

Table 4.4 – Latencies of the mean ERP components and respective standard error (in brackets), for each group and facial expression.

GROUP	EXPRESSION	FIRST COMPONENT	SECOND COMPONENT
ASD	Happy	295 (±9) ms	579 (±16) ms
	Sad	299 (±15) ms	585 (±15) ms
TD	Happy	265 (±10) ms	492 (±14) ms
	Sad	285 (±15) ms	576 (±19) ms

The mean current source density of activity in the intervals around the component peaks showed group differences for both expressions in the first component, using voxel-by-voxel independent tests between groups, corrected for multiple comparisons at the 5% level using the SnPM method (two-tailed). Both expressions show the group differences right-lateralized and located at the superior parietal region, in the precuneus area (Figure 4.5). As for the second component, only the sad expression presented statistically significant differences, exactly in the same superior parietal region, which showed also enhanced recruitment for the ASD group, in the right hemisphere.

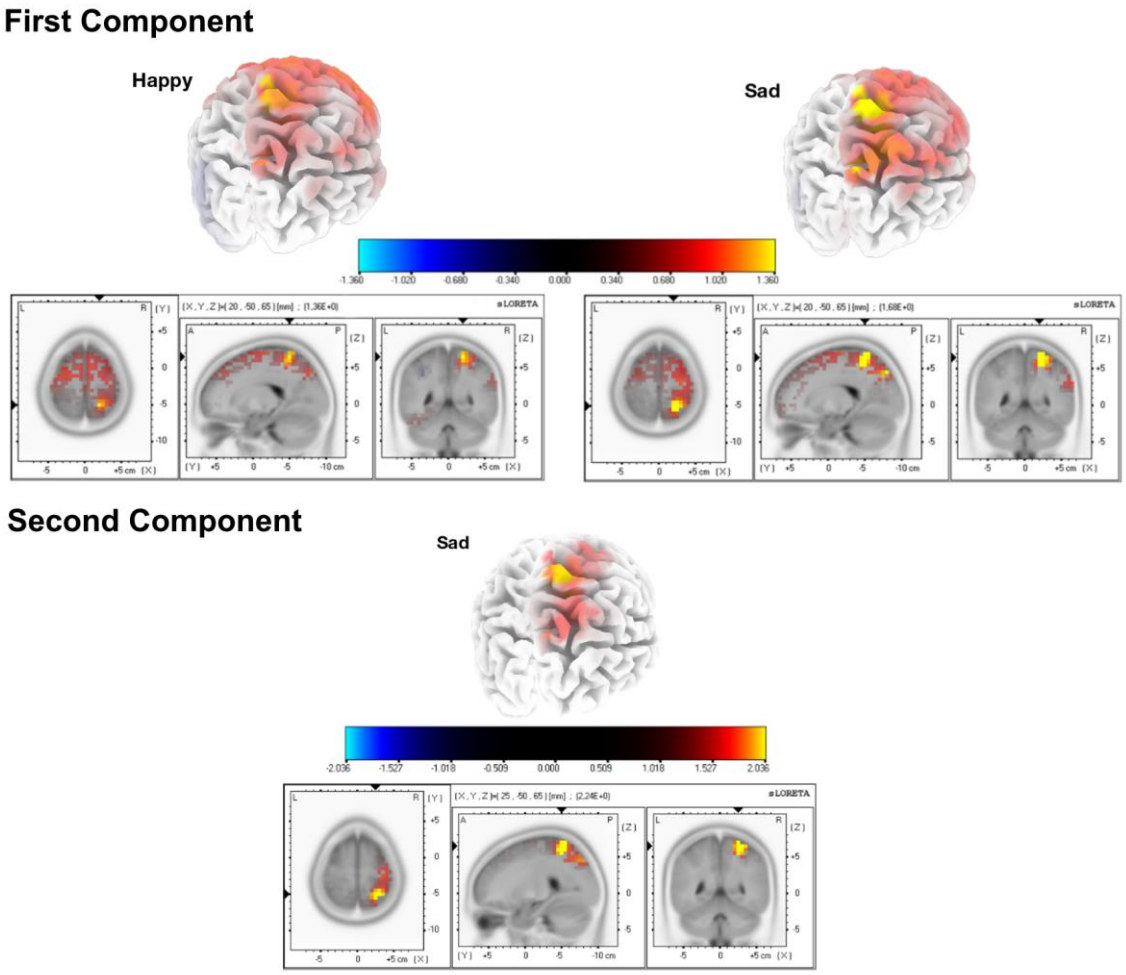

Figure 4.5 – Source group differences for the first and second ERP components, for happy and sad expressions. We found higher activation for the ASD group in the right precuneus using a two tailed alpha level of 5%, corrected with the SnPM method. Regarding the second component, this result was statistically significant specifically for the sad expression.

4.3.2 Mental imagery task

This section presents the results for the mental imagery task. We analyzed the ERP for the initial imagery period and the longer mental imagery blocks through source analysis of the power spectrum and the analysis of several characteristics of the signal using machine learning techniques.

4.3.2.1 Mental imagery ERP source analysis results

After the sound trigger, an initial ERP can be found corresponding to processing the beep and starting the imagery procedure (Figure 4.6). We defined a time window to target at the source level, between 0 and 250ms, in order to investigate specific responses at the source level. The mean current source density in that interval presented group differences for both expressions with $p < 0.01$, using voxel-by-voxel independent tests between groups, corrected for multiple comparisons using the SnPM method. Importantly, the same region identified group differences for both expressions. This was also the same region that was identified during visual stimulation. Accordingly, the ASD group presented higher activation in the superior parietal region (precuneus area – Figure 4.7).

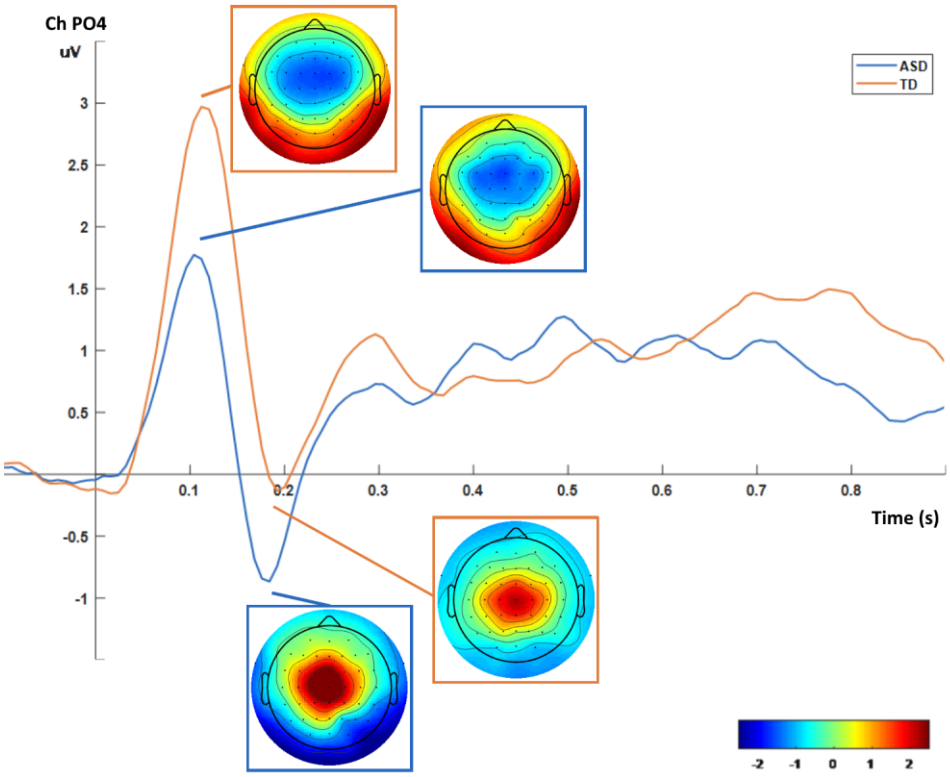

Figure 4.6 – ERP and topographic plots for the mental imagery task (PO4 channel). An initial ERP is visible peaking positively at 100 ms and negatively at 200 ms, with the tonic spectral characteristics overtaking the remaining time period (from 0.5 s onwards).

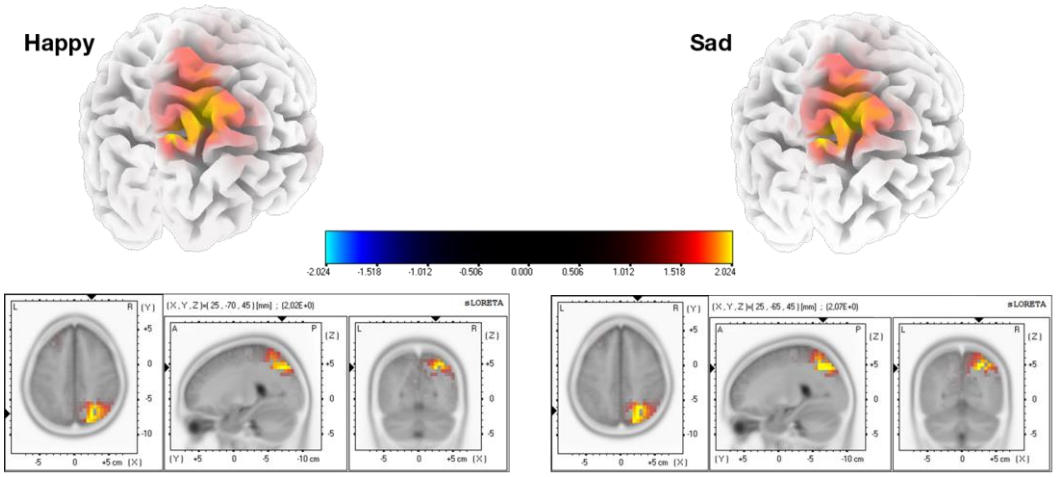

Figure 4.7 – Group differences for the source analysis of the ERPs of mental imagery. Statistical differences (two-tailed $p < 0.01$, SnPM corrected) were found in the region of precuneus, with higher activation for the ASD group.

4.3.2.2 Mental imagery spectral source analysis results

For the longer periods of imagery (500-3500 ms), we conducted a source analysis of the defined frequency bands of the signal. A statistically significant result was found for in the imagery of sad expressions, for the theta band (Figure 4.8). The ASD group shows again higher recruitment of the very same right precuneus area at this frequency.

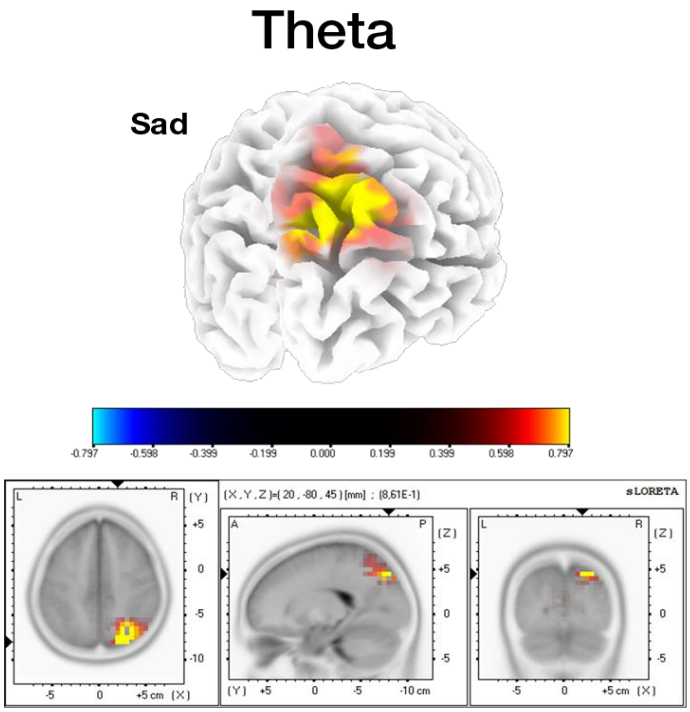

Figure 4.8 – Source analysis for the mental imagery segments, in the theta band. Higher activation for the ASD group in the precuneus area (two tailed $p < 0.05$, SnPM corrected).

4.3.2.3 Statistical classification of mental imagery periods – evidence for a potential biomarker in ASD

We then tested whether the identified neural signatures of imagery of facial expressions could be identified in a data driven manner using statistical classifiers. The linear SVM and the WiSARD classifier were able to achieve high test set accuracies (~77% and ~81% of accuracy, respectively), with the WiSARD yielding the best accuracy of 81% with just 15 features (Figure 4.9). Test set classification accuracy of the neutral face expression segments of the signal were far worse, with ~68% for the SVM and ~74% for the WiSARD, suggesting that important group differences are captured by the features are emotion expression-dependent (for

statistical details see Figure 4.9). We present also a detailed exploration of the performance metrics using the top 15 features. We computed accuracy, specificity, sensitivity/recall, precision and the F1 score for both classifiers using the mental imagery segments and the neutral segments.

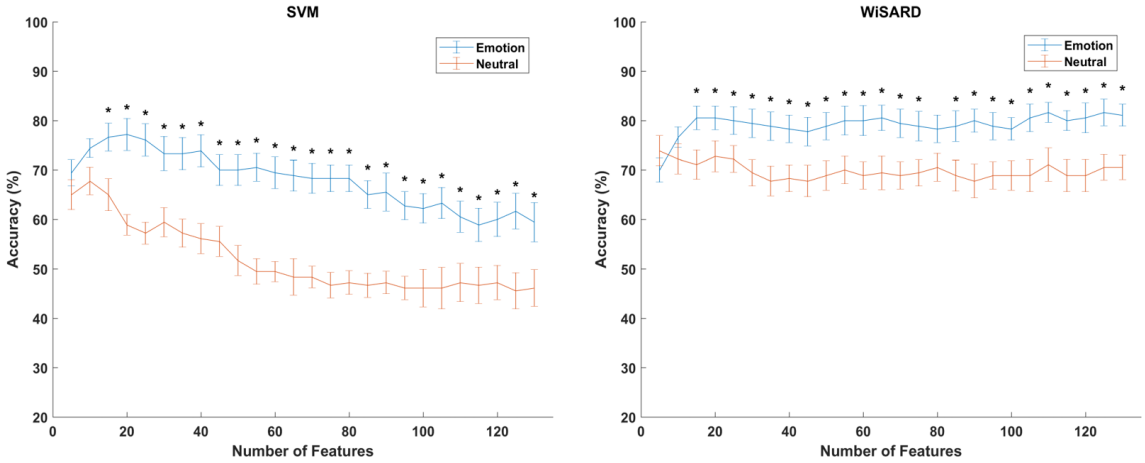

Type	*Classifier*	*Accuracy*	*Specificity*	*Sensitivity*	*Precision*	*F1 Score*
Emotion	**SVM**	76.7% (2.8)	**92.2% (3.1)**	61.1% (5.3)	90.6% (4.1)	71.1% (4.1)
	WiSARD	**80.6% (2.4)**	91.1% (3.2)	**70.0% (4.6)**	**92.5% (2.7)**	**76.2% (3.3)**
Neutral	**SVM**	65.0% (3.2)	68.9% (5.5)	61.1% (6.2)	70.5% (3.9)	69.5% (3.1)
	WiSARD	**71.1% (3.0)**	**72.2% (3.9)**	**70.0% (4.3)**	**73.2% (3.6)**	**69.7% (3.4)**

Figure 4.9 – Accuracy of the classifiers SVM (left) and WiSARD (right) as function of the considered number of features. Mean accuracies are represented with the lines and the error bars show the standard error of the mean. Classification results with the mental imagery part of the EEG signals are represented in blue and the neutral signals in orange. Statistically different accuracies between Emotion and Neutral are marked by * (one-sample T-tests with alpha level of 5% and false discovery rate correction for multiple comparisons). At the bottom we present the performance metrics for both classifiers using the top 25 features. Each cell presents the mean values followed by the standard error of the mean of the respective metric.

We checked the correlation value between the extracted features and the IQ measurements (full-scale, verbal and performance IQ), and no feature was significantly correlated with any of the covariates.

We then focused on the top 15 features that generated the 81% of accuracy. We investigated the most selected frequency bands and clusters of these top features. Figure 4.10 shows the top 15 feature distribution by clusters and frequency bands, showing the specific contribution of theta, high beta and gamma bands for group discrimination. Detailed feature information (Table 4.5) clarifies that the most discriminative features originate from the time-frequency

domain, at the high-beta/gamma bands, and that the non-linear features are mainly from the theta-band.

Table 4.5 – List of the top 15 features used in the classifiers, showing their frequency band, cluster and statistical value. Non-linear features are presented with grey background and time / frequency features with white background. Rank values correspond to the mean order of the feature across training sets, with the respective standard error of the mean. T and P values for each feature are presented, resulting from an independent T-test between the groups. All the 15 features are statistically significant (corrected for multiple comparisons using the false discovery rate algorithm).

FEATURE	FREQ. BAND	CLUSTER	RANK	T	P
ENV	[21 - 30] Hz	4	2.57 (0.41)	4.23	0.0002
TEAG	[21 - 30] Hz	1	4.30 (0.53)	3.84	0.0005
POW	[21 - 30] Hz	1	6.87 (0.77)	3.61	0.0010
ENV	[30-40] Hz	4	7.67 (0.83)	3.67	0.0009
TEAG	[21 - 30] Hz	4	8.73 (0.87)	3.56	0.0012
SPEN	[4 - 8] Hz	4	8.80 (1.16)	3.43	0.0017
LYAP	[4 - 8] Hz	4	9.83 (1.27)	-3.36	0.0020
ENV	[30 - 40] Hz	5	10.03 (0.99)	3.53	0.0013
POW	[21 - 30] Hz	4	11.37 (1.11)	3.41	0.0018
ENV	[21 - 30] Hz	1	12.03 (1.23)	3.22	0.0029
ENV	[30 - 40] Hz	1	13.37 (1.65)	3.24	0.0028
SPI	[4 - 8] Hz	4	13.43 (1.33)	3.25	0.0027
ENV	[21 - 30] Hz	5	13.83 (1.30)	3.37	0.0020
APEN	[4 - 8] Hz	4	14.37 (1.77)	3.15	0.0036
POW	[30 - 40] Hz	1	14.97 (1.14)	3.08	0.0042

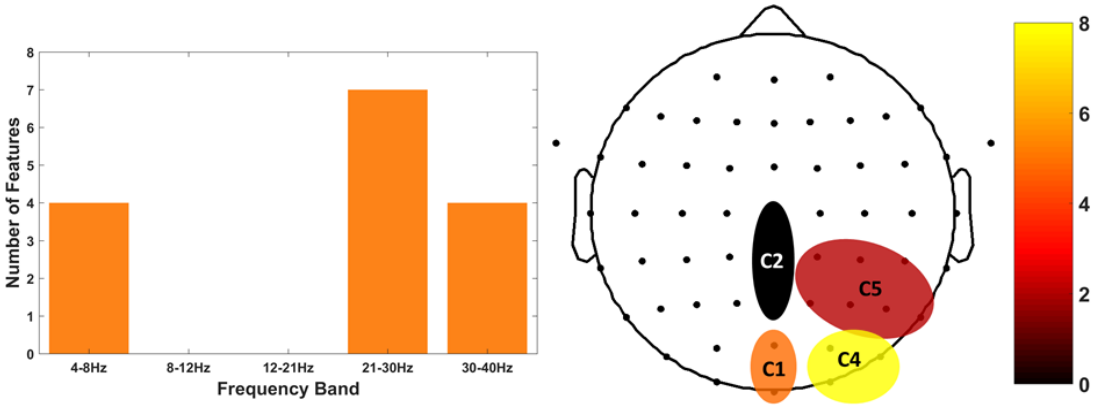

Figure 4.10 – Top 15 features distribution by frequency band (left) and clusters (right). The histogram on the left depicts the exploitability of theta and high-beta / gamma frequency features. The histogram of the right shows the scalp distribution of features within the right parietal-occipital region, showing a preference for the posterior clusters of the region.

4.4 Chapter Discussion

Here we addressed for the first time facial expression (FE) imagery in ASD and identified a common neural correlate of observation and mental imagery of dynamic FEs in this condition, in the precuneus. Robust statistical classification of brain activity patterns using linear and non-linear features could also be achieved, and the identified biomarker of abnormal imagery in ASD can potentially be used as an outcome measure to evaluate clinical interventions addressing cognitive and behavioral improvement in this condition.

We focused on Mental Imagery (MI) of facial expressions in ASD as a major research target in this study. This is a very important cognitive process in the context of this disease, because mental rehearsal is very important for action perception cycles, in particular in the context emotional face recognition. MI is the process of creating a mental representation and corresponding sensory experience of an episode or stimulus without a direct external source (Pearson et al., 2015). In the case of facial expressions, it also involves mental imagery of motor patterns (facial expressions) which requires the involvement of the mirror neuron system. There are indeed several types of MI, namely visual, auditory and motor (for a review, see Kosslyn et al., 2001). Some studies showed the effect of MI on boosting performance in detection tasks (Tartaglia et al., 2009) and on decision making bias (Pearson et al., 2009). In our study, participants were asked to perform visual MI of an avatar performing a FE (mentally replaying previously observed patterns). This task combines MI, perspective taking and theory of mind, since the participant is asked to recreate an expression of another.

A critical aspect that renders the study of imagery difficult in ASD is that it is important to ascertain that imagery really reflects the expected visual content. We could achieve this by showing that similar neural signatures (source localization) can be found by both observation and imagery of facial expressions. The ERP elicited by the imagery cue did indeed reveal that source differences were very similar as compared to the ERP of the FE stimuli, with the precuneus showing higher activation for the ASD group. The right precuneus belongs to task-active networks (Yang et al., 2015) that are also active during imagery (for a review of the relation with the precuneus with visuo-spatial imagery and visuomotor transformations, please refer to (Cavanna and Trimble, 2006)).

One of the common aspects of visualization and mental imagery of the others facial expressions is the need to incorporate the perspective of the other. Because we use a stringent

contrast in the visual stimulation task, we expected the core processing of the face to have less weight than the perspective taking aspects task. The precuneus is one of the core regions present in the perspective taking network, as showed by Healey and Grossman (2018). The authors reviewed the literature and found the precuneus as a key region in both cognitive and affective perspective taking networks (Abu-Akel and Shamay-Tsoory, 2011). Those fMRI studies validate the source we identified in our study.

The link between the precuneus and its role in facial expressions processing has already been demonstrated by some studies (Saarimäki et al., 2016; An et al., 2018), but our study is the first one, to the best of our knowledge, to identify the over-recruitment of this region in the ASD population in a social cognition task. Since visual perspective taking and theory of mind skills are impaired in ASD (Hamilton et al., 2009; David et al., 2010), we believe that ASD participants needed higher recruitment of the right precuneus as a compensatory mechanism for the MI of the other's FE.

Frequency band decomposition of the MI signals showed that theta and high-beta/gamma bands explained the main group differences. The source analysis of the theta band further revealed again a higher activation of the right precuneus for the ASD group (specifically for the sad FE). It was already known that FEs elicited higher theta responses than neutral expressions in healthy participants (for a review, please refer to Güntekin and Başar, 2014). Although theta band activity patterning has been linked to the medial frontal cortex and its role in cognitive control (Cavanagh and Frank, 2014) its source in our study seems to be different. In agreement with our own source, Wang and collegues (2016) demonstrated a relationship between the theta band and activity patterns in the posterior cingulate cortex / precuneus, in a simultaneous EEG-fMRI study. Furthermore, the study from Knyazev et al. (2009) identified the same right parietal source from theta responses to facial expressions. Therefore, we believe the parietal theta band relation with the precuneus to be a core neural correlate of emotional MI processing. Despite using different types of signals (phasic or tonic in relation to the type of mental process) to perform the source localization (ERP and time-frequency decomposition), due to the characteristics of the tasks, it is very interesting to observe the same region involved in both visualization and mental imagery processes.

The precuneus is recruited in several types of imagery, including motor imagery, mental navigation, memory-related imagery, episodic source memory retrieval and emotional state attribution (Cavanna and Trimble, 2006). Specifically regarding attributing emotions to others,

several studies identified the role of the precuneus in Theory of Mind scenarios (Vogeley et al., 2001; Takahashi et al., 2015). Moreover, a connectivity analysis study of resting state fMRI data showed decreased connectivity of the precuneus region with the middle temporal gyrus and the ventromedial frontal cortex in the ASD population, in both hemispheres (Cheng et al., 2015). All these observations pinpoint the precuneus as playing a pivotal role in FE MI. Furthermore, the group difference in the right hemisphere, which is also known to dominate in attention and imagery, suggests that the ASD group processes the FEs of the other in a more effortful, attention-based mechanism than the TD group. This view has been suggested by Harms et al. (2010). Our study is the first one, to our knowledge, to show that the same neural pattern that is observed during FE recognition is replicated for MI of the FEs, in ASD.

Based on the observed group differences, we investigated whether we could extract features that would function as biomarkers (not necessarily as diagnostic, but as intervention targets) of ASD, based on the MI process. The need for diagnostic, prognostic and intervention biomarkers in ASD is well recognized. While ASD biomarkers range from genetics to clinical (for a review, please refer to Ruggeri et al., 2014), the inter-subject variability observed in this disorder justifies the use of machine learning techniques combining multiple features to generate potential biomarkers (Huys et al., 2016). Therefore, we developed two classifiers – a Support Vector Machine (SVM) and a Weightless Neural Network (WNN) to classify each subject (represented by a feature vector extracted from his EEG data) into ASD or TD group. Our purpose is to show that the features used by the classifiers provide exploitable group differences, that can also be used to characterize neural mechanisms underlying ASD (in this case, FE processing) and therefore be used to monitor, for example, rehabilitation efficacy (outcome measure) or aid at subgroup stratification in the ASD population (Castelhano et al., 2018), albeit not for early detection.

We verified that the WNN method achieved around 81% of accuracy using 15 features. When compared to the same classifiers trained with features extracted from EEG of the neutral periods, the accuracy was significantly lower (around 73%).

We then performed a further analysis of the top 15 features selected for classification. The most representative frequency band, when using non-linear features, was the theta band, while the most discriminative features were from the time/frequency domain and high-beta/gamma frequency bands. Those bands and their relation with the precuneus have been explored in the literature by Fomina et al. (2016), which attempted to train the self-regulation of gamma

and theta bands in the precuneus in amyotrophic lateral sclerosis patients. This is consistent with our results, showing that the precuneus activity at the theta and high-beta/gamma bands represent important MI information that can be used for clinical purposes, for instance in BCI based neurofeedback.

The overall use of dynamic FE morphing enabled a more realistic and ecologic approach, because the stimuli featured more realistically the daily life characteristics of social interactions than the commonly used static stimuli. Moreover, we used a specific face expression contrast (emotional expressions vs. neutral expression). As stated by Krumhuber et al. (2013), the dynamic characteristics of FEs are possibly also understudied which is a limitation for the validity of neurocognitive approaches.

Our approach to morph the expression into a virtual avatar makes a potential bridge between dynamic FEs and rehabilitation possibilities using, for instance, virtual reality. Understanding how the FEs are processed in virtual environments opens the door for intervention solutions, where the environment is completely controlled (Miller and Bugnariu, 2016; Simões et al., 2018a). This is important because the neural markers identified in this study could potentially be used as intervention target measures.

A common characteristic of most studies in the literature using EEG and observation of FEs is the use of a black-screen as baseline for the visual stimulus (Monteiro et al., 2017), thus eliciting ERPs that mix the processing of the FE with face and other nonspecific visual features. We argue that the use of a more specific contrast (expressionless/neutral face as baseline) elicits an ERP specific to the dynamic expression characteristics of the face, not the face itself. Moreover, Monteiro et al. (2017) demonstrate disparate findings in the literature when evaluating EEG responses to FEs in ASD. Several studies found expression effects accompanied by group effects. Using a very specific contrast, we were able to identify, even for FE observation, group differences in the right precuneus, with the ASD group showing higher activation in this region. The functional role of precuneus in attentional deployment and imagery is well recognized (Cavanna and Trimble, 2006), with some studies also suggesting a relation to perspective taking (Vogeley et al., 2001; Kircher et al., 2002; Schurz et al., 2015), face familiarity (specifically for the left precuneus) (Lee et al., 2013) and emotional state recognition and attribution (Ochsner et al., 2004; Spies et al., 2017). Our right precuneus group effect for both happy and sad expressions is consistent with several studies using functional Magnetic Resonance Imaging (fMRI) that reported the same effect for ASD in the

right precuneus (see the meta-analysis of Aoki et al., 2015, which found hyperactivation of bilaterate thalamus, caudade and right precuneus for the ASD group). Especially in tasks requiring taking the others perspective, the recruitment of the precuneus is key in both cognitive and affective perspective taking networks (Healey and Grossman, 2018). We hypothesize that the ASD group performs a higher recruitment of the precuneus region to compensate for emotional processing and perspective taking behavioral deficits.

Our study focused only on male subjects to avoid an effect of gender in the analysis. There is evidence for sex differences in brain connectivity in ASD which might influence the EEG analysis we conducted (Alaerts et al., 2016; Irimia et al., 2017; Fu et al., 2018). The replicability of these results in female ASD cohorts lacks further validation. Moreover, in spite of the limitations of our sample size, it paves the way for future replication studies in larger groups.

In conclusion, we found for the first time, a neural correlate of emotion expression imagery in ASD, which was validated as a replication of the neural signatures evoked by visual observation of specific facial expressions. We developed an innovative approach to study FE (facial expression) processing in ASD, combining visualization of dynamic FEs (with a very selective contrast, isolating pure facial expressions from the mere presence of a face) and MI (mental imagery) of FEs in others. Our results emphasize the important role of the precuneus in the ASD facial processing circuit and suggest that its increased recruitment may serve as a compensatory strategy to overcome the natural deficits in their emotional processing. Furthermore, we extracted a set of features and trained a classifier that was able to discriminate between groups with high accuracy. The features were then observed to match topographically and spectrally the group effects, and can therefore be potentially used as intervention targets.

Chapter 5

On the transfer of an fMRI-based neurofeedback intervention to EEG

This chapter describes the exploration of features for transferring the fMRI-based neurofeedback intervention to EEG settings. It combines the following contributions:

Simões, M., Lima, J., Direito, B., Castelhano, J., Ferreira, C., Carvalho, P., Castelo-Branco, M. (2015). Feature analysis for correlation studies of simultaneous EEG-fMRI data: A proof of concept for neurofeedback approaches. in *2015 37th Annual International Conference of the IEEE Engineering in Medicine and Biology Society (EMBC)* (IEEE), 4065–4068. doi:10.1109/EMBC.2015.7319287.

Simões, M., Abreu, R., Direito, B., Sayal, A., Castelhano, J., Carvalho, P., Castelo-Branco, M. How much of the BOLD-fMRI signal can be reconstructed by the EEG data: a comparative simultaneous EEG-fMRI study.

5.1 Chapter Introduction

Our approach for neuroimaging-based rehabilitation of social deficits, an axis of this thesis, was to develop a neurofeedback paradigm that targets the posterior part of the Superior Temporal Sulcus (pSTS). That brain region plays an important role in mechanisms of social information processing in the brain and several studies found it to be abnormally activated in ASD. Our hypothesis was that through the repeated training of neuromodulation of activity on that region, behavioral mechanisms that depend on that region could be restored to a normal functioning. To do so, we developed a task where participants try to modulate the activity on that regions using mental imagery of facial expressions as a mean to achieve it. Our approach included the development of a localization procedure based on dynamic facial expressions contrasted with movement and static faces to identify the parcel of the pSTS region that was specifically responsible for the processing of facial expressions. This stringent contrast guaranteed us that the selected region did not responded merely to faces or to low-level movement features of the stimuli, but to the biological motion of the face. In Appendix I we present the paper that described this approach and validated the mental imagery of facial expressions as a valid mechanism for modulate the BOLD activity in the pSTS region. To validate the possible effectiveness of this NF paradigm in ASD, we conducted a feasibility clinical trial were 15 participants underwent five NF sessions each (ClinicalTrias.gov identifier: NCT02440451). The results showed relevant clinical effects, as documented by improvements in relevant subscale neuropsychological measures, including emotion recognition, which were observed immediately after the intervention and replicated 6 months later (for further details, please refer to Appendix II).

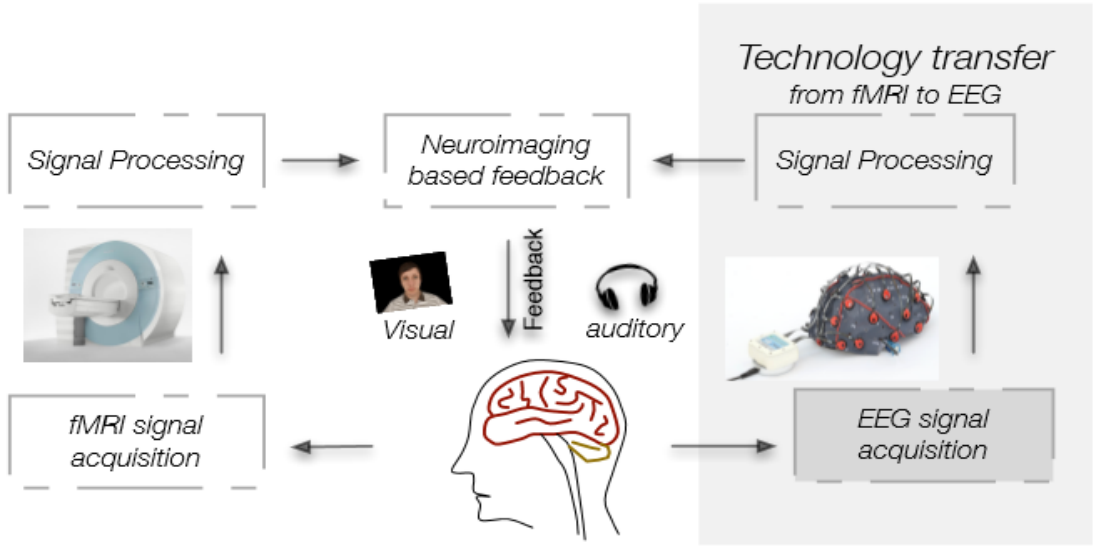

Figure 5.1 – Schematic representation of the transferring approach. We acquire simultaneous EEG-fMRI and use the fMRI to generate neurofeedback for the online task. We then use both EEG and fMRI data to develop a read out mechanism for using EEG as substitute of fMRI in the neurofeedback loop.

However, for an efficient broad application of this NF training approach, the fMRI setup presents a constraint due to its inflexibility and elevated costs of application. In that sense, and following the clinical informatics perspective of this thesis, we focused on the possibility of transferring this NF approach into an EEG solution. For that we acquired a dataset of simultaneous EEG-fMRI of people performing one NF session (Figure 5.1). Using that data, we investigated several features of the EEG signal and evaluated their correlation with the BOLD activity in the pSTS region (section 5.2, published in IEEE EMBC'15 proceedings – *Simões et al., 2015*). Afterwards, after verifying that the base correlations achieved by EEG features with the target BOLD signal, although statistically significant, were judged to be likely too low for being used directly in practical applications as representatives of the BOLD activity in the pSTS activity. We therefore incorporated machine learning algorithms (regressors) to extend the capabilities of relating the EEG features with the BOLD activity, at the scalp and source levels. This final approach is present in section 0.

Furthermore, we tested other approaches, as the one we present in Appendix III, focusing on the relation between the alpha activity with the BOLD signal (Simoes et al., 2017).

5.2 Feature analysis for correlation studies of simultaneous EEG-fMRI data: A proof of concept for neurofeedback approaches

This section is composed by the contents of the following publication:

Simões, M., Lima, J., Direito, B., Castelhano, J., Ferreira, C., Carvalho, P., Castelo-Branco, M. (2015). Feature analysis for correlation studies of simultaneous EEG-fMRI data: A proof of concept for neurofeedback approaches. in *2015 37th Annual International Conference of the IEEE Engineering in Medicine and Biology Society (EMBC)* (IEEE), 4065–4068. doi:10.1109/EMBC.2015.7319287.

Abstract

The identification and interpretation of facial expressions is an important feature of social cognition. This characteristic is often impaired in various neurodevelopmental disorders. Recent therapeutic approaches to intervene in social communication impairments include neurofeedback (NF).

In this study, we present a NF real-time functional Magnetic Resonance Imaging (rt-fMRI), combined with electroencephalography (EEG) to train social communication skills. In this sense, we defined the right Superior Temporal Sulcus as our target region-of-interest. To analyze the correlation between the fMRI regions of interest and the EEG data, we transposed the sources located at the nearest cortical location to the target region. We extracted a set of 75 features from EEG segments and performed a correlation analysis with the brain activations extracted from rt-fMRI in the right pSTS region. The finding of significant correlations of simultaneously measured signals in distinct modalities (EEG and fMRI) is promising. Future studies should address whether the observed correlation levels between local brain activity and scalp measures are enough to implement NF approaches.

5.2.1 Introduction

Neurofeedback (NF) is the general concept of providing the participant real-time information concerning brain activity of a specific brain region, allowing oneself to modulate his own brain activation (LaConte, 2011). The real-time decoding of functional Magnetic Resonance Imaging (fMRI) recordings enables the use of fMRI for NF applications. Along these lines, a subject lying inside an MRI scanner is able to self-regulate blood-oxygenation-level-dependent (BOLD) signal in a target region(s) of his/her own brain, experienced as real time. Several brain regions have been targeted for NF and behavioral improvements were achieved from neuromodulation of specific areas (for a review, see Sulzer et al. - 2013).

fMRI-based NF has the great advantage of spatial resolution, which allows the targeting of specific brain regions. Electroencephalography (EEG), on the opposite, lacks such spatial characteristics, but leverages a very high time resolution. NF studies based on EEG have a longer history, but the approaches are fundamentally different: EEG studies target the modulation of different rhythms, present on different frequency bands, e.g. the sensorimotor rhythms. Applications focus attention deficit/hyperactivity disorders, depression, performance enhancement, etc (Zotev et al., 2014).

Only a few studies use simultaneous EEG-fMRI NF and combine both approaches to provide feedback (Zotev et al., 2014). The analysis of the EEG patterns related with modulation of a specifically mapped (with fMRI) brain area during a NF session has not yet been addressed.

The identification of a signal representative of the modulation of a NF-targeted brain region would make possible to perform that specific NF session with EEG, making it easier and cheaper to perform training sessions. If successful, this approach would allow explicit transfer from a complex technique such as fMRI to more affordable and generalizable NF solutions.

Our study targets the right posterior Superior Temporal Sulcus (pSTS), a region related to the processing of biological motion and facial expressions. Recent studies demonstrated that the development of social cognition abilities is supported in specific brain networks that interpret actions and intentions of others. Functional magnetic resonance imaging studies associated the superior temporal sulcus to important features of social cognition (particularly in the visual analysis of social stimuli/clues)(Pelphrey and Carter, 2008). Along these lines, this region lies in the core of "social brain network" important in tasks such as the interpretation and

prediction of others' actions and intentions based on the analysis of biological motion (Saitovitch et al., 2012).

We present a fMRI-based NF study targeting the right pSTS region. EEG recordings were collected simultaneously, and we analyze different features on the source EEG signal and assess their putative correlation to the modulated BOLD activity in the right pSTS region.

5.2.2 Methods

5.2.2.1 Participants

We performed a simultaneous EEG/fMRI experiment in 13 healthy subjects (mean age: 26 ± 3 years; 12 males). All participants had normal or corrected to normal vision, no history of neurological disorders and were naive regarding the purpose of the study. Eight subjects performed the complete simultaneous EEG/fMRI task (four runs), three did not complete the transfer run (self-driven modulation without NF) and two only performed the localizer and the auditory feedback. This study was approved by the Ethics Commission of the Faculty of Medicine of the University of Coimbra and was conducted in accordance with the declaration of Helsinki. All subjects gave written informed consent to participate in the study.

5.2.2.2 Acquisition Protocol

The acquisition protocol consisted of 4 runs inside of the MRI scanner: localizer, imagery with auditory feedback, imagery with visual feedback and transfer run. The order of auditory and visual feedback was randomized between subjects.

Localizer

The experimental design comprised five different stimulation conditions: i. randomly moving dots, ii. neutral, iii. morphing from neutral to sad, iv. morphing from neutral to happy, v. alternation between sadness and happiness. Each block lasts eight seconds and is repeated eight times during the run. The total duration of the run is approximately 5 minutes. The conditions are ordered randomly. Schematic representation of the face expression. The total

duration of the facial expression presentation is 2000ms. Each expression is repeated four times during a block.

Expression conditions (**iii**, **iv** and **v**) morph from neutral to the endpoint expression during the first 500ms, hold the expression during 1000ms, and then morph back to neutral during 500ms (Figure 5.2). This structure is repeated 4 times during each block (condition **v** alternates expression *happy* and *sad*). Neutral and movement conditions (**i** and **ii**) consisted in presenting the neutral face during the eight seconds of the block and showing random dots moving all over the screen, respectively. These two conditions were used to remove features not related to the facial expressions and movement without biological basis from the activations.

Figure 5.2 – The functional localizer is applied to define the brain networks (i.e., region-of-interest, ROI) related with the processing of facial expressions, particularly the right posterior portion of STS.

Functional MR volumes were recorded consisting of 33 slices (in-plane resolution: 4×4 mm2, field of view (FOV): 256×256 mm^2, slice thickness: 3 mm, flip angle (FA): 90°) yielding a total coverage of the occipital and posterior temporal lobe. Repetition time (TR) was 2000 ms (Echo Time (TE): 30 ms). For each participant, 160 volumes were acquired for the localizer run. Start of each trial was synchronized with the acquisition of the fMRI volumes.

Each scanning session included the acquisition of a high-resolution magnetization-prepared rapid acquisition gradient echo (MPRAGE) sequence for co-registration of functional data (176 slices; TE: 3.42ms; TR: 2530ms; voxel size 1.0×1.0×1.0 mm3.

Neurofeedback runs

The NF runs consisted of two types of feedback and an additional run without feedback (Figure 5.3). The runs were divided in blocks of imagery with duration of 24 seconds,

alternating between baseline and expression blocks. In the baseline blocks, participants were instructed to imagine a neutral face in the avatar, while in the expression blocks they were instructed to imagine repeatedly the morphing of the expression (happy, sad or alternating from happy and sad).

The technical aspects of the functional MR volumes were similarly to the localizer run. Each run had a total duration of 10 minutes, corresponding to a total of 300 volumes.

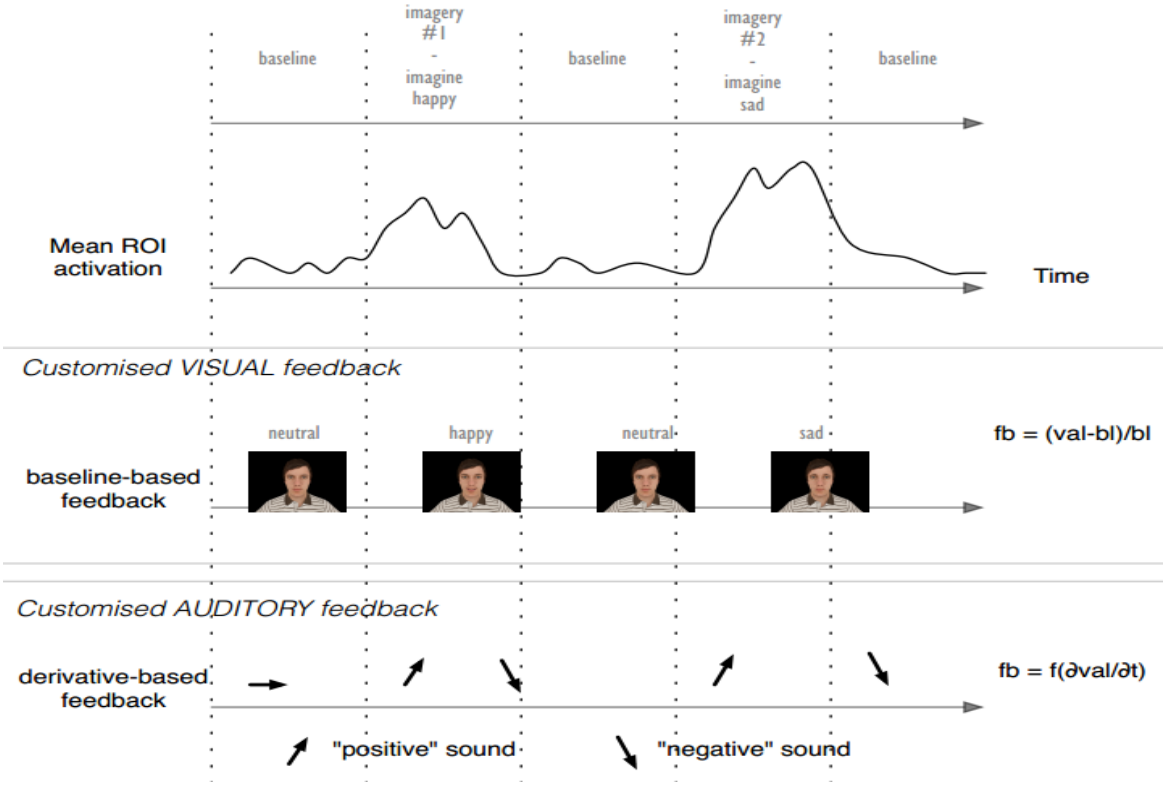

Figure 5.3 – Schematic representation of the face expression. The total duration of the facial expression presentation is 2000 ms. Each expression is repeated four times during a block.

Visual feedback: The avatar's expression was discretized into 15 levels (between neutral and the endpoint expression). The expression level feedback/displayed to the subject was determined based on the level of the signal variation in the mean BOLD activation in the ROI defined in the localizer. To determine the signal variation, we computed the difference between the current activation level and the mean activation obtained in the previous ten baseline instants. The variation percentage was calculated based on a maximum percent signal change (maxPSC) of 2% and truncated to a minimum of 0% and a maximum of 100%, as in

$$fb = \frac{\left[\frac{x - \beta}{\beta}\right]}{maxPSC} \quad (5.1)$$

Auditory feedback: the feedback was given to the participant every six seconds through a positive or negative sound (high or low frequency beep). The polarity of the feedback was based on the derivative of the previous three ROI activations. This approach focused on the local variations of the brain activation, instead of a global variation relative to the baseline, as in visual feedback.

Finally, the transfer run structure was equal to the auditory feedback runs (without the presentation of the avatar), but no feedback was provided to the user.

5.2.2.3 EEG signal recording and processing

For EEG recording, we used an MR compatible EEG system (MagLinkTM, NeuroScan, USA) with a cap providing 64Ag/AgCl nonmagnetic electrodes positioned according to the 10/10 system. The recording reference was set to an electrode close to CZ and EEG and fMRI data were acquired in a continuous way. The electrocardiogram signal (EKG) was also recorded, simultaneously with the EEG. EEG and EKG signals were amplified and recorded at a sampling rate (SR) of 10 kHz.

Signal processing

EEG recordings from simultaneous EEG/fMRI sessions are challenging due to two major interferences: gradient artifacts and ballistocardiogram signals (BCG; which represent physiological cardiac-related artifacts) (Allen et al., 2000).

EEG artifacts related to MR gradient switch were corrected offline using average subtraction gradient correction implemented in Maglink RT Edit software (v4.5, NeuroScan, USA). In brief, an average template of the artifact is created and then subtracted from the recorded EEG (Castelhano et al., 2014). The correction algorithm includes a low-pass filter of 75 Hz.

For the correction of BCG artifacts, an independent component analysis (ICA) approach was followed. Data were high-pass filtered by 1Hz. Bad channels were removed and data were re-referenced to average reference. ICA components were computed using the standard

implementation present in EEGLAB (Matlab toolbox v13_1_1b). The independent components were inspected and the ones with higher correlation with the EKG signal recorded during the acquisition were removed from the signal. Similarly, components related to blinking and eye movements were also removed. We used the scalp topography of the ICA components to identify the ocular component for ocular artifact attenuation. Finally, the signal was divided into two second segments, time-locked to the beginning of each TR from the MR. Noisy segments were excluded.

Standard anatomical MR data were used to create the boundary element model (BEM) of each subject's head, using Curry 7.0 software (NeuroScan, USA). Leadfields were then generated concerning the participant's electrodes position and unconstrained cortex sources. Sources positions were also exported, in Talairach coordinates.

Talairach coordinates of the voxels selected for each subject's ROI (i.e., right pSTS) were identified as well as the nearest sources of the leadfields. EEG signals were then transposed to the source space applying sLORETA method, with a regularization level of 0.1, as presented in (Pascual-Marqui, 2007). From the average of the time courses of the different sources we estimated the source time course for the right pSTS of each subject.

5.2.2.4 Feature extraction

For this study we extracted 75 different features from the source signal segments.

We present the features grouped by category. Each feature was calculated in the original frequency band (1-75Hz) and in two additional frequency bands, targeting the alpha and beta rhythms: [8-11] Hz and [11-13] Hz for alpha, [13-20] Hz and [25-30] Hz for beta.

Time domain

- Hilbert Envelope (Env) – smooth curve outlining the extremes of the signal. Maximum and average values of each segment were extracted.
- Power – the square of the signal. Maximum and average values of each segment were extracted.
- Teager Energy – an energy estimation operator. Maximum and average values were extracted.

Frequency domain

- Power Band Activation (PBA) – absolute spectral power extracted from the different frequency bands.
- Spectral Flux (SF) – Difference between the segment's spectral power and the spectral power present in the baseline.
- Power Spectrum Density peak (PSD) – maximum of the power spectrum density, extracted from the signal filtered at different bands.
- Frequency Roll Off (ROff) – first frequency where the spectrum represented by lower frequencies meets 95% of the power spectrum (only applied in the original frequency band).

Non-linear domain

- Lag – first local minimum from the signal's autocorrelation.
- Detrended Fluctuation Analysis (DFA) – statistical signal self-affinity estimation.
- Largest Lyapunov Exponent (Lyap)- characterization the rate of separation of infinitesimally close trajectories of the signal's phase space.
- Correlation Dimension (CD) – measure of space dimensionality of the signal.
- Approximate Entropy (ApEn) – quantification of the regularity of the signal.
- Sample Entropy – similarly to Approximate Entropy, quantifies the regularity of the signal.

5.2.2.5 Correlation analysis

Features for each subject and each run were normalized based on the mean of the first 20 points of the Neutral expression, the baseline for our conditions. pSTS BOLD activation was also normalized using the same process. Correlations were then calculated between each feature and the BOLD signal. In order to synchronize the EEG features with its corresponding BOLD activation, a hemodynamic delay of six seconds was considered.

5.2.3 Results

For each time segments, a total of 75 features were generated. A Spearman correlation was calculated between the features values and the pSTS BOLD activations. The ten best features

for each expression condition are present in Table 5.1, along with Spearman's rho values and significance levels. Significance levels were corrected for multiple comparisons using the Bonferroni method.

Table 5.1 – Best ten features based on BOLD correlation

Happy		Sad		Alternate	
CD $_{13\text{-}20Hz}$	0,22**	CD $_{13\text{-}20Hz}$	0,20**	CD $_{13\text{-}20Hz}$	0,21**
Teager $_{max}$	0,16**	Teager $_{avg}$	0,20**	ApEn $_{8\text{-}11Hz}$	0,12**
PBA	0,16**	Teager $_{max}$	0,19**	Teager $_{max}$	0,12**
Teager $_{avg}$	0,13**	CD $_{25\text{-}30Hz}$	0,12**	CD $_{25\text{-}30Hz}$	0,11*
Lag $_{8\text{-}11Hz}$	0,12**	Lag $_{25\text{-}30Hz}$	0,12**	SpEn $_{8\text{-}11Hz}$	0,11*
ApEn $_{8\text{-}11Hz}$	0,12**	PBA	0,11**	Teager $_{avg}$	0,11*
CD $_{25\text{-}30Hz}$	0,11*	Env $_{max}$	0,10	Lag $_{8\text{-}11Hz}$	0,10*
Lag $_{25\text{-}30Hz}$	0,11*	Lag $_{8\text{-}11Hz}$	0,08	Lag $_{25\text{-}30Hz}$	0,10*
$SF_{25\text{-}30Hz}$	0,10	SF $_{25\text{-}30Hz}$	0,08	Teager $_{max\ 11\text{-}13Hz}$	0,07
SpEn $_{8\text{-}11Hz}$	0,10	SF $_{11\text{-}13Hz}$	0,08	Power $_{max}$	0,07

The feature Correlation Dimension, when applied on the signal band-pass filtered to the low beta band [13-20]Hz, yields the best correlation levels for all the expression blocks. Although 75 features were tested, only a small subset presented statistically significance, and there is a repetition of most of those features along the different expression conditions.

5.2.4 Discussion

Extraction through the EEG of fMRI activity is very difficult, mostly due to low signal-to-noise ratio (SNR) and difficulties of having good head model representations (Kaiboriboon et al., 2012). The common way to perform source localization of EEG fonts requires the averaging of several trials in order to reduce the SNR. Because our approach focused on getting, in real time, the activation level of a specific brain area, averaging of several trials was not an option. Therefore, correlations of simultaneous measured signals in distinct modalities

(EEG and fMRI) at the single-trial level were not expected to be high, but statistically significant.

We were able to identify a group of features containing a weak yet significant correlation level with right pSTS modulation, for both conditions of happy, sad and alternated imagery. $CD_{[12-20]Hz}$ and $Teager_{max}$ features succeeded it at an alpha level of 0.01 for all conditions. This sheds a promising light of how the energy and phase-space dimensionality of low-beta source EEG signals might relate to real fMRI activity. Additional exploration is still needed to identify the viability of using these techniques for NF approaches.

5.3 How much of the BOLD-fMRI signal can be reconstructed by the EEG data: a comparative simultaneous EEG-fMRI study

This section is composed by the contents of the following publication:

Simões, M., Abreu, R., Direito, B., Sayal, A., Castelhano, J., Carvalho, P., Castelo-Branco, M. How much of the BOLD-fMRI signal can be reconstructed by the EEG data: a comparative simultaneous EEG-fMRI study.

Abstract

The simultaneous acquisition of EEG and fMRI data is motivated by the need to accurately map networks of interest in the brain, exploring their highly complementary properties. The so-called EEG-informed fMRI approach is by far the most commonly used, which relies on extracting a representative time-course of the activity of interest from the EEG, and then identify the brain regions with a BOLD-fMRI signal significantly correlated with it. Conversely, in order to transfer specific fMRI interventions (e.g., neurofeedback) to EEG setups, the BOLD-fMRI signal of specific brain regions and/or networks needs to be reconstructed based only on EEG signals. Because these types of approaches have been poorly explored so far, here we systematically investigated the extent at which the BOLD-fMRI signal recorded from the facial expressions processing network during a neurofeedback task, could be reconstructed from the simultaneously recorded EEG signal. For that purpose, several features from both the scalp and source spaces (the latter estimated using continuous EEG source imaging) were extracted and used as predictors in a regression problem using random forests. When compared with the only approach already proposed in the literature that uses spectral features and considers different time delays, our results show that convolving the features extracted from the scalp with multiple HRF functions peaking at different latencies increase significantly the reconstruction accuracies from 20% (the current literature) to 53%. Importantly, nonlinear features exhibited the highest relevance in the regression problem. At the source level, similar prediction accuracies were obtained when using features extracted from the average source time-courses within brain regions parceled

according to the automated anatomical labeling atlas. Our results highlight the importance of combining different kinds of scalp EEG features (particularly the nonlinear ones) and of addressing the BOLD hemodynamic delay with multiple HRFs, for more accurately reconstruct the BOLD signal, with direct impact in the transfer of fMRI-based neurofeedback interventions to EEG setups.

5.3.1 Introduction

When provided with real-time information about a specific brain process, an individual can attempt to manipulate it through self-regulation, which allows for adjustments in the internal mechanisms used for its manipulation. This process is called neurofeedback (NF) (Kober et al., 2013; Arns et al., 2017). If the brain process under manipulation is dysfunctional, its regularization through NF is expected to result in behavioral changes (Shibata et al., 2011). Therefore, clinical applications of NF interventions have been conducted throughout the last years, namely on patients with Attention Deficit/Hyperactivity Disorder (ADHD), depression, addictions, anxiety disorders and others (Micoulaud-Franchi et al., 2015; Sitaram et al., 2016; Arns et al., 2017).

Electroencephalography (EEG) and functional Magnetic Resonance Imaging (fMRI) are the most commonly used techniques for implementing a NF loop (Sitaram et al., 2016). The different characteristics of each technique led to the development of different approaches for their application in NF studies. In particular, EEG-based NF interventions target mostly attention and relaxation-related EEG rhythms, namely the alpha frequency band, the ratio of theta power over alpha power, or the μ rhythm (Micoulaud-Franchi et al., 2015). Levering its remarkable spatial resolution, NF studies using fMRI target more selective brain regions and/or networks, and therefore represent the hallmark for neuromodulation of localized brain areas (Fovet et al., 2015; Sitaram et al., 2016). In contrast with the low-cost and portability of EEG setups, the economical and logistical constraints of NF interventions using fMRI hamper its widespread application (Sarracanie et al., 2015). In this sense, methods that aim to transfer real-time (rt-)fMRI NF interventions to EEG setups gain considerable relevance.

Considering their complementary properties, the simultaneous acquisition of EEG and fMRI data has been proposed for accurately mapping a given activity of interest in the brain. Although it poses several challenges, recent advances on the improvement of data quality and the integration of the two types of signal, currently allow to exploit the advantages of this

multimodal technique to a fuller extent (de Munck et al., 2009; Zotev et al., 2014; Murta et al., 2015). The most common approach relies on extracting a representative time-course from the EEG, and then identify the brain regions on which the BOLD-fMRI signal recorded is significantly correlated with it (for a comprehensive review, please refer to (Murta et al., 2015) and (Abreu et al., 2018)). However, in order to transfer NF applications from fMRI into EEG, a different approach needs to be carried out, whereby the BOLD-fMRI signal of specific brain regions and/or networks is reconstructed based only on EEG signals. Despite its academic and clinical interest, such methodological strategy has been poorly explored. To the best of our knowledge, only Meir-Hasson and colleagues (Meir-Hasson et al., 2014) have attempted to reconstruct the BOLD-fMRI signal recorded at a specific region (the amygdala) from scalp EEG signals based on a ridge regression of power activity from different frequency bands and several time delays. The authors named this method the EEG Finger-Print (EFP), which is currently the gold standard.

For the purpose of better understanding the extent at which the BOLD-fMRI signal from a specific brain region or network can be accurately reconstructed from the EEG alone in the context of transferring NF interventions from fMRI into EEG, in this paper we systematically explored several EEG features extracted from both the scalp and source spaces, as potential predictors of the BOLD signal recorded from facial expression processing regions during a NF task. We performed the BOLD signal reconstruction based on a regression problem using random forests, and compared the prediction accuracies of the tested features with the EFP method, on simultaneous EEG-fMRI data collected from 10 subjects at 3T.

5.3.2 Methods

5.3.2.1 Participants

Ten healthy participants (mean age: 26 ± 3 years; 9 males) performed a simultaneous EEG-fMRI NF session. All participants had normal or corrected-to-normal vision, and no history of neurological disorders. The study was approved by the Ethics Commission of the Faculty of Medicine of the University of Coimbra and was conducted in accordance with the declaration of Helsinki. All subjects provided written informed consent to participate in the study. The high male/female ratio was purposefully ensured to match the target population (ASD) higher male prevalence.

5.3.2.2 Experimental protocol

The session was performed at the Portuguese Brain Imaging Network (Coimbra, Portugal) and consisted of four fMRI runs: first, a functional localizer specifically developed to identify the facial expressions processing network (anchored on the posterior Superior Temporal Sulcus region; pSTS), followed by three NF runs (of alternated up and down regulation). The first two NF runs used either visual or auditory feedback (random order) and the third had no feedback presented to the participant. The participants were given a mental strategy to follow during the NF runs, but were instructed to adapt it to maximize the modulation outcomes presented by the feedback.

For the localizer run, 8 second blocks of dynamic facial expressions (happy, sad or alternated between happy and sad expressions) morphed into the face of a realistic human virtual character are contrasted with 8 second blocks consisted of the same face with a static neutral expression or motion blocks of moving dots. This rigorous contrast is able to identify regions that respond to the dynamic aspects of the facial expressions but not to the face itself or the movement aspects of the stimuli (Direito et al., 2019). The NF runs consist of 24 second blocks of alternated up and down regulation of the activity extracted in real-time from the pSTS region identified in the localizer run. For the first two NF runs, the participants were presented with visual feedback (materialized in the intensity level of the facial expression displayed by the virtual avatar) or auditory feedback (consisting of high and low pitch beep sounds, corresponding to increasing or decreasing levels of BOLD activity in the pSTS region). The full detailed description of the protocol can be found in our previous paper (Direito et al., 2019), where we assessed the neuroscientific aspects of the fMRI NF sessions.

5.3.2.3 EEG-fMRI data acquisition

Imaging was performed on a 3T Siemens Magnetom Trio MRI scanner (Siemens, Erlangen) using a 12-channel RF receive coil. The functional images were acquired using a 2D multi-slice gradient-echo echo-planar imaging (GE-EPI) sequence, with the following parameters: TR/TE = 2000/30 ms, voxel size = 4.0×4.0×3.0 mm^3, 33 slices, FOV = 256×256 mm^2, FA = 90°, yielding a total coverage of the occipital and posterior temporal lobe. The start of each trial was synchronized with the acquisition of the functional images. A T_1-weighted, magnetization-prepared rapid acquisition gradient-echo (MPRAGE) sequence was used for

the acquisition of structural data (1 mm isotropic, 176 slices, TR/TE = 2530/3.42 ms), for the subsequent co-registration of the functional data. For each participant, 160 fMRI volumes were acquired during the localizer run, yielding approximately 5.33 minutes; the remaining three functional runs consisted of 300 volumes (10 minutes).

The EEG signal was recorded using the MR-compatible 64-channel NeuroScan SynAmps RT Maglink™ system, with a cap of 64 Ag/AgCl non-magnetic electrodes positioned according to the 10/10 coordinate system. The reference electrode was placed close to the Cz position. EEG, electrocardiography (EKG) and fMRI data were acquired simultaneously in a continuous way, and synchronized by means of a Syncbox (NordicNeuroLab, USA) device. EEG and EKG signals were recorded at a sampling rate (SR) of 10 kHz. No filters were applied during the recordings.

Outside the MR scanner and prior to the beginning of the experiment, each subject was submitted to an EEG-only acquisition while performing the localizer stimulation experiment. These data were used for quality checking the EEG recorded inside the MR scanner, after the removal of gradient switching and pulse artifacts.

5.3.2.4 MRI data analysis

Pre-processing steps

The first 10 s of data were discarded to allow the signal to reach steady-state, and non-brain tissue was removed using FSL's tool BET (Smith, 2002). Subsequently, slice timing and motion correction were performed using FSL's tool MCFLIRT (Jenkinson et al., 2002). Then, a high-pass temporal filtering with a cut-off period of 100 s was applied, and spatial smoothing using a Gaussian kernel with full width at half-maximum (FWHM) of 5 mm was performed. Physiological noise was removed by linear regression using the following regressors (Abreu et al., 2017) : 1) quasi-periodic BOLD fluctuations related to cardiac cycles were modeled by a fourth order Fourier series using RETROICOR (Glover et al., 2000) ; 2) aperiodic BOLD fluctuations associated with changes in the heart rate were modeled by convolution with the respective impulsive response function (as described in (Chang et al., 2009) ; 3) the average BOLD fluctuations in white matter (WM) and cerebrospinal fluid (CSF); 4) the six motion parameters (MPs) estimated by MCFLIRT; and 5) scan nulling regressors (motion scrubbing) associated with volumes acquired during periods of large head motion. Because the respiratory

traces were not recorded, the associated physiological fluctuations in the BOLD signal were not removed.

For each participant, WM and CSF masks were obtained from the respective T_1-weighted structural image by segmentation into gray matter, WM and CSF using FSL's tool FAST (Zhang et al., 2001). The functional images were co-registered with the respective T_1-weighted structural images using FSL's tool FLIRT, and subsequently with the Montreal Neurological Institute (MNI) (Collins et al., 1994) template, using FSL's tool FNIRT (Jenkinson et al., 2002; Jenkinson and Smith, 2001) . Both WM and CSF masks were transformed into functional space and were then eroded using a 3 mm spherical kernel in order to minimize partial volume effects (Jo et al., 2010). Additionally, the eroded CSF mask was intersected with a mask of the large ventricles from the MNI space, following the rationale described in (Chang and Glover, 2009).

Mapping of the facial expressions processing network

For the purpose of mapping the regions in the facial expressions processing network (FEPN), a general linear model (GLM) framework was used. For each subject, a GLM comprising five regressors was built (one for each condition), based on boxcar functions with 1s during the respective condition to be modeled, and 0s elsewhere. The regressors were convolved with a canonical, double-gamma hemodynamic response function (HRF) (Friston et al., 1995). The resulting GLMs were then fitted to the pre-processed fMRI data using FSL's improved linear model (FILM) (Woolrich et al., 2001), and voxels exhibiting significant BOLD changes when contrasting the facial expression conditions with the neutral and motion conditions (balanced) were identified by cluster thresholding (voxel $Z > 2.7$, cluster $p < 0.007$). The BOLD signal was averaged across voxels comprising the mapped regions, and subsequently used as target for the reconstruction analysis.

5.3.2.5 EEG data analysis

Here, the pre-processing steps applied to the EEG data are first described, followed by the pipeline used to estimate the temporal dynamics of EEG sources. From these two spaces (scalp and source), the several features extracted for reconstructing the BOLD signal at the FEPN are then described.

Pre-processing steps

EEG datasets from all patients underwent gradient artifact correction on a volume-wise basis using a standard artifact template subtraction (AAS) approach (Allen et al., 2000). Then, bad epochs of 2s (corresponding to one TR) were manually identified and removed from the EEG signal, followed by the visual inspection and interpolation of bad channels. For the removal of the pulse artifact, the method presented in (Abreu et al., 2016) was employed, whereby the EEG data is first decomposed using independent component analysis (ICA), followed by AAS to remove the artifact occurrences from the independent components (ICs) associated with the artifact. The corrected EEG data are then obtained by reconstructing the signal using the artifact-corrected ICs together with the original non-artifact-related ICs. Finally, the EEG data was down-sampled to 250 Hz and band-pass filtered to 1–45 Hz. For the purpose of removing the pulse artifact from the EEG, and the physiological noise from the fMRI, the Pan-Tompkins algorithm (Pan and Tompkins, 1985) was optimized and used for the detection of R peaks on the EKG data (Abreu et al., 2017).

EEG source imaging

The pre-processed EEG data and the subsequent features extracted from it (described next) were then submitted to an EEG source imaging (ESI) procedure. Specifically, the so-called continuous ESI (cESI) was performed, with the purpose of estimating the temporal variations of the EEG sources responsible for generating the electrical potential distributions and EEG features measured at the scalp with a high temporal resolution. This has already been used for the purpose of mapping the epileptic networks on an EEG-correlated fMRI framework (Vulliemoz et al., 2010), and for identifying resting-state networks (RSNs; typically observed on fMRI) with the EEG alone (Liu et al., 2017a, 2018).

A realistic head model was built by first segmenting each subject's structural image into 12 tissue classes (skin, eyes, muscle, fat, spongy bone, compact bone, cortical gray matter, cerebellar gray matter, cortical white matter, cerebellar white matter, cerebrospinal fluid and brain stem), each with a specific electrical conductivity. Because this is not feasible using the currently available segmentation tools (which allow segmentation up to 6 tissues), a state-of-the-art brain tissue model was used (MIDA, available online; Iacono et al., 2015), and co-registered into the structural image. The electrode positions were co-registered to the skin compartment by first considering their standard positions, and then manually adjusting them

to match the distortions clearly observed on the structural images. Finally, the SimBio finite element model (FEM; Wolters et al., 2004) algorithm implemented in FieldTrip (Oostenveld et al., 2011) was then used for numerically approximating the volume conduction model. The source dipoles were placed on a 4-mm 3D grid only spanning the cortical gray matter, followed by the estimation of the leadfield matrix, which maps each possible dipole configuration onto a scalp potential distribution (the forward problem). The inverse problem was solved following a distributed inversion solution approach using the exact low resolution brain electromagnetic tomography (eLORETA; Pascual-Marqui et al., 2011) algorithm, which estimates the strength *j* of each dipole on the source grid at the *x* (j_x), *y* (j_y) and *z* (j_z) directions. For each EEG time sample *t*, the overall strength of a dipole was computed as:

$$p(t) = \sqrt{j_x^2(t) + j_y^2(t) + j_z^2(t)} \quad (1)$$

This was computed for all dipoles, yielding a 4D (3D × *t*) dataset (EEG-cESI). The time-series of dipole strength was then downsampled to 0.5 Hz. These processing steps were selected based on previous studies that comprehensively investigated their impact on detecting RSNs from EEG-cESI data, concluding that this was the optimal processing pipeline (Liu et al., 2017a, 2018).

5.3.2.6 BOLD reconstruction approach

For each subject, we extracted seven EEG features (described next) from seven frequency bands of interest (theta: 4-8 Hz, alpha: 8-13 Hz, beta: 13-30 Hz, low-beta: 13-22 Hz, high-beta: 22-30 Hz, gamma: 30-40 Hz and broadband: 1-45 Hz) from non-overlapping scalp EEG segments of 2 seconds (corresponding to the TR of the fMRI data) at the following electrodes: P4, P6, P8, PO6, PO8, P3, P5, P7, P05 and PO7 (total of ten, five at each hemisphere). Such electrodes were selected based on their proximity to the FEPN. For the source-based models, the abovementioned features were then mapped to the source space and their source time courses extracted from either the FEPN, or from 90 non-overlapping brain regions parceled according to the Automated Automatic Labeling (AAL) atlas.

EEG features extracted

Seven EEG features were considered to build the proposed pool of features (the FeatPool model), three of which extracted from the time-frequency domain; the remaining four were

focused on exploring the nonlinear characteristics of the EEG signal. The latter were motivated by previous studies showing their usefulness on several applications including the characterization of mental imagery processes similar to the ones conveyed by the participants during the NF runs (Bosl et al., 2017, 2018; Simões et al., 2018b). These features were estimated for each frequency band (by previously band-passing the EEG signal across the respective band), and for each 2-second EEG segment.

For the time-frequency domain, we used the power, frequency peak (f-peak) and the Teager energy. The power was computed by squaring the signal and averaging its values. The f-peak was obtained by extracting the maximum values of the frequency spectrum. The Teager energy operator calculates the instantaneous energy of the signal x using

$$\Psi[x(t)] = x(t)^2 - x(t-1)x(t+1) \tag{2}$$

where $\Psi[.]$ denotes the Teager operator (Solnik et al., 2010); the resulting values were then averaged. This operator is sensitive to variations in both amplitude and frequency of the original signal x.

For the nonlinear domain, we transformed each EEG signal into its phase-space, which represents a reconstruction of its chaotic dynamics. As shown by Takens (1981), the phase-space captures the relevant properties of the state space representation of the system, such as the Lyaponov exponents and the Kolmogorov-Sinai Entropy. Every state of the system can be represented by a point in the multidimensional phase space, and the time evolution of the system creates a trajectory in this space (Kliková and Raidl, 2011). We used the time delay embedding method to reconstruct the phase-space of the EEG. Given a time series x, the corresponding vector $\mathrm{X}(t_i), i = 1, \dots, N$ in phase-space at time t_i is given by

$$\begin{aligned} X(t_i) = [x(t_i), x(t_i + \tau), \dots, x(t_i + (m-1)\tau)], i \\ = 1, \dots, N - (m-1)\tau \end{aligned} \tag{3}$$

where τ is the time delay, m is the dimension of reconstructed space and $M = N - (m-1)\tau$ is the number of points (states) in the phase-space. We reconstructed a 2- and 3-dimensional phase-space associated to the EEG data, and the time delay was considered to be the mean of the first local minimum from the autocorrelation of the signal (lag r) (Gao et al., 2012). The evolution of the states of the system in the phase-space creates a trajectory that represents the dynamics of the system. Those dynamics tend to incorporate a bounded subspace referred to

as an attractor. To characterize the attractor and the corresponding dynamics of the system, measures can be taken to estimate its complexity and stability. To estimate complexity, we computed the correlation dimension (CorrDim) of the trajectories, which is the most common approach. For the stability, we used the largest Lyapunov exponent (Lyap) and two entropy measures - approximate entropy (ApEn) and sample entropy (SpEn) – that quantifies the chaos of the attractor (Rodríguez-Bermúdez and García-Laencina, 2015).

The correlation dimension is a measure of the space fractal dimensionality. Correlation sum is defined as the sum of the fraction of pairs of points in the phase-space whose distance is smaller than *r* (the previously defined lag). If this number of points is sufficiently large, the ratio between the logarithm of the correlation sum and the logarithm of the time delay is an accurate estimate of the correlation dimension (Cencini et al., 2010).

The largest Lyapunov exponent characterizes the rate of separation of infinitesimally close trajectories of the signal in phase space, yielding a measure of the degree of the instability of the system (Cencini et al., 2010). Mathematically, two trajectories in the phase space with initial separation of δZ_0, diverge at a rate given by

$$|\delta Z(t)| \approx e^{\lambda t}|\delta Z_0| \quad (4)$$

where λ is the local Lyapunov exponent (local exponential rate of expansion). The maximum Lyapunov exponent corresponds to the mean exponential rate of divergence, characterizing the trajectory's instability.

The approximate (ApEn) and sample (SpEn) entropy quantify the regularity and predictability of signals throughout time. The ApEn is a descriptor of the changing complexity in the embedded space. The SpEn is a variation of the ApEn method which does not depend on the length of the signal and showing usually shows better relative consistency (Yentes et al., 2013). Since ApEn and SpEn present different values for the same characteristic of the signal, we considered both metrics in our analysis.

Addressing the hemodynamic delay of the BOLD signal

In order to tackle the hemodynamic delay of the BOLD signal relative to the EEG signal, the previously proposed EFP method incorporates in the regression problem not only the original spectral power predictors, but also their time-delayed versions up to 12 seconds (Meir-Hasson et al., 2014). Thus, the prediction model associated with this method is described by:

$$y(t) = f\big(x_1(t), x_1(t-1), \dots, x_1(t-n), x_2(t), x_2(t-1), \dots, x_m(t-n)\big) \quad (2)$$

with *y* the BOLD signal to predict at time *t*, x_k the *k*-th EEG feature, considering *m* features and *n* delays; and *f* the prediction function.

However, the most common approach to take into account this delay in conventional EEG-informed fMRI studies is to convolve the EEG time-course of interest with the canonical HRF (Abreu et al., 2018). Therefore, the EEG feature time courses x_k were then convolved with the canonical HRF:

$$x'_k = x_k \otimes HRF \quad (3)$$

yielding the model

$$y(t) = f\big(x'_1(t), x'_2(t), \dots, x'_m(t)\big). \quad (4)$$

Because of the known variability of the HRF across subjects and sessions (Aguirre et al., 1998) and even brain regions (Rangaprakash et al., 2018), the EEG features were also convolved with HRF functions peaking at different latencies (3, 3.5, 4, 4.5, 5, 5.5, 6, 6.5, 7, 8, 10 and 12 seconds):

$$x^l_k = x_k \otimes HRF_l \quad (5)$$

thus resulting in the final model:

$$y(t) = f\left(x^1_1(t), x^2_1(t), \dots, x^l_1(t), x^1_2(t), x^2_2(t), \dots, x^l_m(t)\right). \quad (6)$$

with *l* the number of latencies (in this case, twelve, matching the number of delays considered in the EFP method). These three approaches (delays, canonical HRF and multiple HRFs) were tested on the EEG spectral power features used in the EFP method. Because the multiple HRF convolution approach yielded the highest prediction accuracy (see Results section), it was then considered for the new models proposed here.

Reconstruction approach

Unbiased prediction accuracies were calculated by first concatenating the three NF runs, and then applying a 6-fold cross validation scheme, having so the equivalent of half of a NF run

in the testing sets. For each fold, the minimum redundancy maximum relevance (mRMR) method was used for feature selection, which ranks the features to include in the different models (Peng et al., 2005) In this way, the curse of dimensionality is partially overcome (Keogh and Mueen, 2017), and a fair comparison between the models tested, which have a different number of predictors (see below), can be performed. In order to investigate the impact of model complexity in the reconstruction of the BOLD signal, we varied the number of predictors included in the models according to the mRMR. Specifically, models with 1, 2, 5, 10, 20, 50, 100, 150, 200 and 250 predictors were considered; more complex models were not tested since the reconstruction accuracy reached a plateau for most models.

For the regression step, random forests were used with bootstrap aggregation (bag) of an ensemble of decision trees (number of random predictors per split: number of predictors / 3, minimum number of observations per leaf: 5), as implemented in the MALTAB R2019b's Statistics and Machine Learning toolbox *fitrensemble* function (method: Bag, number of learning cycles: 150). Random forests were selected for their capacity to deal with small sample sizes and large feature sets, outperforming competing machine learning algorithms in several studies (Rodriguez-Galiano et al., 2015; Couronné et al., 2018).

Comparison of reconstruction models

We used as baseline model the state-of-the-art EFP, adapted from Meir-Hasson's work (2014), consisting of the spectral power feature from seven frequency bands and their time-delayed versions, extracted from the scalp EEG signal. In this case, a total of 840 predictors (7 frequency bands × 12 delays × 10 channels) comprise the model used in the EFP method. We then tested the same method using the multiple HRF convolution approach. We named this method improved EFP ($iEFP_{scalp}$), which also consists of 840 predictors (7 frequency bands × 12 latencies × 10 channels). Still at the scalp level, we tested the effect of using all the seven features ($FeatPool_{scalp}$), rather than the spectral power alone, also using the multiple HRF convolution approach. This results in the most complex model, with a total of 5880 predictors (7 features × 7 frequency bands × 12 latencies × 10 channels).

At the source level, we tested firstly the direct source mapping of the EEG signal (EEG_{source}^{ROI} model). This method is particularly interesting due to its simplicity since it avoids the feature extraction step, which could be very efficient for online applications. Furthermore, we tested the source mapping of the iEFP ($iEFP_{source}^{ROI}$) and the FeatPool

($FeatPool_{source}^{ROI}$) models. From the resulting time-courses of source activations, we computed the average across our ROI (the FEPN, mapped according to the localizer run) and submitted to the multiple HRF convolution approach, yielding a total of 12 (number of latencies), 84 (7 frequency bands × 12 latencies) and 588 (7 features × 7 frequency bands × 12 latencies) predictors, for the EEG_{source}^{ROI}, $iEFP_{source}^{ROI}$ and $FeatPool_{source}^{ROI}$ models. In order to consider whole-brain source activations, rather than those from the FEPN alone, the source time-courses were also averaged across 90 non-overlapping brain regions parceled according to the Automated Automatic Labeling (AAL) atlas. In this way, the number of predictors of the previous models increased 90-fold. Figure 5.4 shows the list of models used. Note that despite the high number of predictors of most models, only up to 250 features were considered in the regression step according to the feature ranking approach (mRMR) described above.

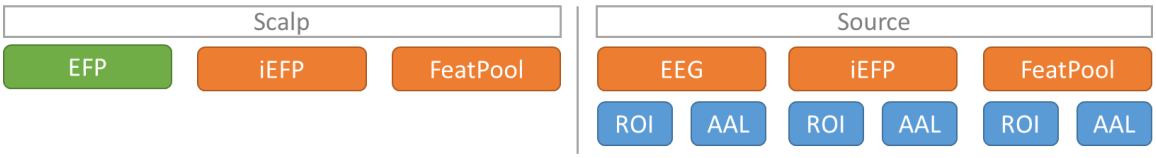

Figure 5.4 – List of the models used on the EEG-based reconstruction of the BOLD signal. The EFP (in green) represents the current state-of-the-art. The scalp methods include also the iEFP and FeatPool, while the source methods include the EEG, iEFP and the FeatPool, each one subdivided into ROI and AAL parcels.

BOLD upsampling effect

The EFP method, as presented in (Meir-Hasson et al., 2014), performs an upsampling of the BOLD signal by a factor of 8 (new sampling frequency of 4 Hz) using spline interpolation. We believe this induces strong linear relations on the target signal that will bias the prediction accuracy of the models. This was verified by investigating the impact of the upsampling step on the EFP model. Otherwise, all the results presented in the paper are conducted in the original BOLD sampling rate of 0.5 Hz.

5.3.2.7 Statistical analysis

In order to compare the performance of the models, we first determined the optimal number of predictors to be included in each model based on their reconstruction accuracy. Then, those

reconstruction accuracy values were submitted to a one-way repeated measures analysis of variance (ANOVA) to assess differences in their means. From that, we conducted post-hoc pairwise comparisons between each pair of models, correcting for multiple comparisons using the Tukey-Kramer method.

We computed correlation maps from the EFP method (the current state-of-the-art, baseline model) and the best model ($FeatPool_{scalp}$). To verify the brain regions related to the reconstructed BOLD signal of the EFP and $FeatPool_{scalp}$ models, we used the reconstructed signals separately as regressors of interest in a GLM analysis of the pre-processed fMRI data using FILM (Woolrich et al., 2001). Voxels exhibiting significant correlations were identified by cluster thresholding (voxel $Z > 2.7$, cluster $p < 0.007$). Group activation maps were then obtained using the FSL's Local Analysis of Mixed Effects (FLAME) (Beckmann et al., 2003). With this analysis, it is possible to assess if the brain regions associated with the reconstructed BOLD signal match those involved in the FEPN.

Afterwards, we investigated the contributions of each feature, frequency band and HRF latency to the reconstruction of the BOLD signal. We averaged the ranks for each feature across participants and cross-validation folds and built histograms for each feature, frequency band and HRF latency whose average rank was below 100. Understanding which frequency bands and features contribute the most for the BOLD reconstruction provide insights on the electrophysiological mechanisms underlying the BOLD signal measured at the FEPN.

5.3.3 Results

The effect of the upsampling step of the BOLD signal on the EFP model is presented in Figure 5.5. While it increases the number of time points by a factor of 8, strong, yet false, linear relationships between neighboring BOLD samples are introduced by the spline interpolation, which in turn inflates the accuracy in an artificial manner, verifiable both in the mean correlation (across folds and participants) and the standard error of the mean. In fact, although the EFP model reached an average prediction accuracy of 90% when considering the upsampled BOLD signal, at the original sampling rate, such accuracy did not go beyond 20%.

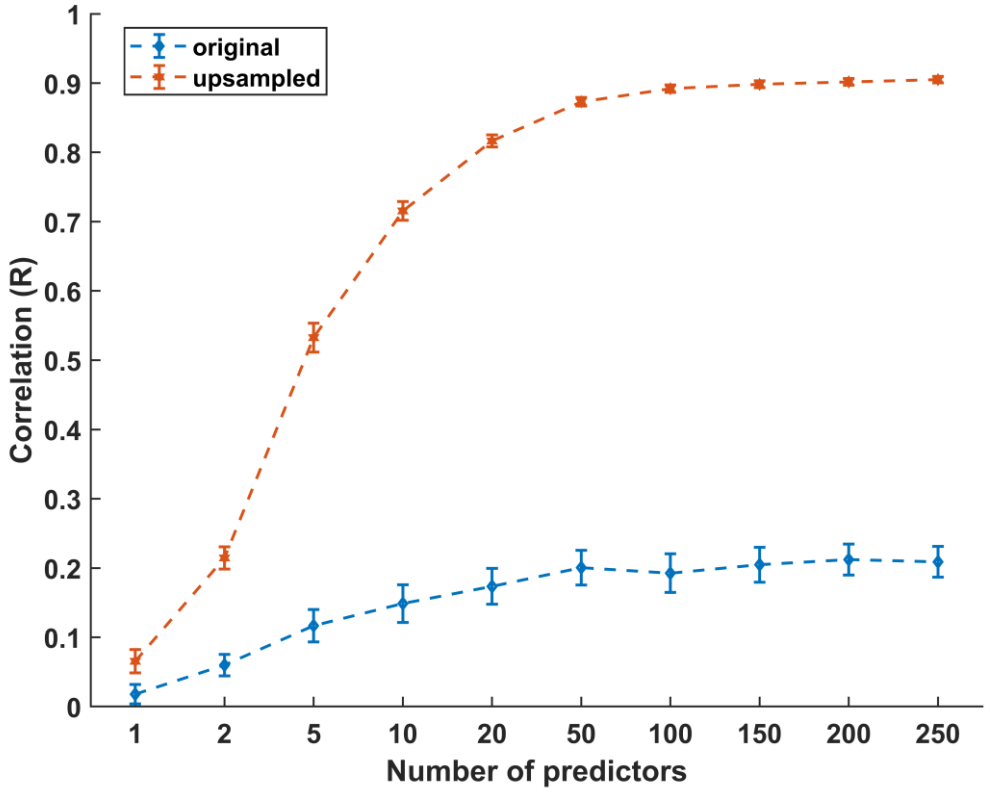

Figure 5.5 – Comparison of the original EFP model with and without upsampling the BOLD signal. The center of each bar corresponds to the mean correlation of all participants between the prediction signal and the BOLD activity of the FEPN, and the error bars present the standard error of the mean. Results are presented in function of the number of predictors included in the models, showing a plateau of the correlations after approximately 50 predictors.

5.3.3.1 Comparison of approaches addressing the BOLD hemodynamic delay

Regarding the approaches considered for dealing with the hemodynamic delay of the BOLD signal, Figure 5.6 shows the effects of using the original approach used in the EFP (delays), the approach used in conventional EEG-fMRI studies (convolution with the canonical HRF), and the new proposed method considering the convolution of multiple HRFs peaking at different latencies. Because it largely outperformed the other two (reconstruction accuracy of approximately 50%, vs. 40% and 20% for the canonical HRF and delays approaches, respectively), only the convolution with multiple HRFs was considered for the remaining models; in particular, the new version of the EFP model using this approach was termed improved EFP (iEFP).

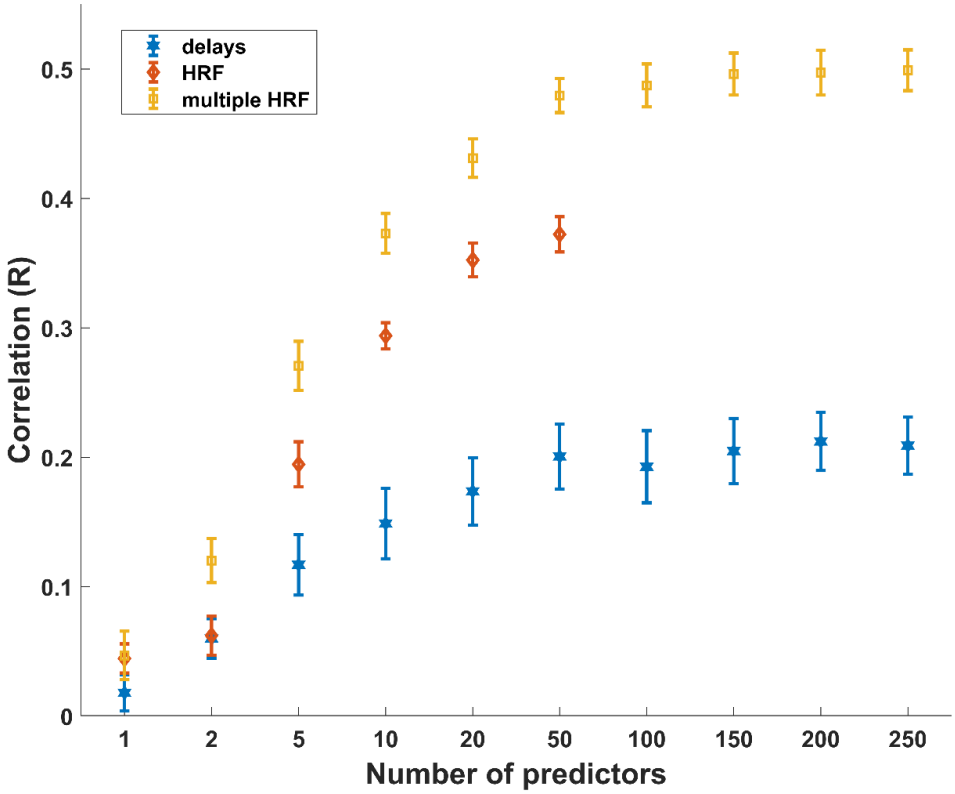

Figure 5.6 – Comparison of the correlations achieved using the EFP method by the three approaches tested to deal with the hemodynamic delay. The HRF method only shows up to 50 predictors because it contains only the power for 7 frequency bands from 10 electrodes (70 predictors), while the other two have the different delays or the multiple convolutions, thus increasing the number of predictors (in this case, 840). Points represent the group mean correlation values and the bars the standard error of the mean.

5.3.3.2 Comparison of the reconstruction accuracy of the models

The analysis for the ideal number of predictors for each model is presented in Table 5.2. For most models, higher correlation values were consistently obtained by increasing the number of predictors (up to 250) included in them; however, we also observed that increasing the number of predictors from 150 to 200, or from 200 to 250, yielded a non-significant increase in the respective correlation values in most cases.

Table 5.2 – Optimal number of predictors included in each model. On the left, the number of features that generated the highest correlation values and, on the right, the last number of features that caused a significant increase in the correlation accuracy.

	Number of Features	
Model	**Max R**	**Last Significant Increase R**
EFP_{scalp}	200	150

$iEFP_{scalp}$	200	50
$FeatPool_{scalp}$	250	150
EEG_{source}^{ROI}	5	5
EEG_{source}^{AAL}	250	250
$iEFP_{source}^{ROI}$	50	20
$iEFP_{source}^{AAL}$	250	100
$FeatPool_{source}^{ROI}$	200	100
$FeatPool_{source}^{AAL}$	250	250

Considering for each model the number of predictors with maximum R, Figure 5.7 shows the post-hoc pairwise comparisons between the R values achieved by each model. Comparing with the state-of-the-art model (EFP), only the $\mathbf{EEG_{source}^{ROI}}$ model did not surpass its correlation; in contrast, all the BOLD reconstructions from the other proposed models obtained statistically significantly higher correlations. At the scalp level, the FeatPool outperformed the iEFP model, showing that the pool of features is able to capture additional task-specific brain processes that are not fully identified using only the EEG power. At the source level, the same pattern was observed, with the FeatPool exhibiting better results than the iEFP (both for ROI and AAL versions). As expected, using the information from several brain regions parcelled according to the AAL, rather than the pSTS region alone, higher correlation values were obtained. correlation values were obtained.

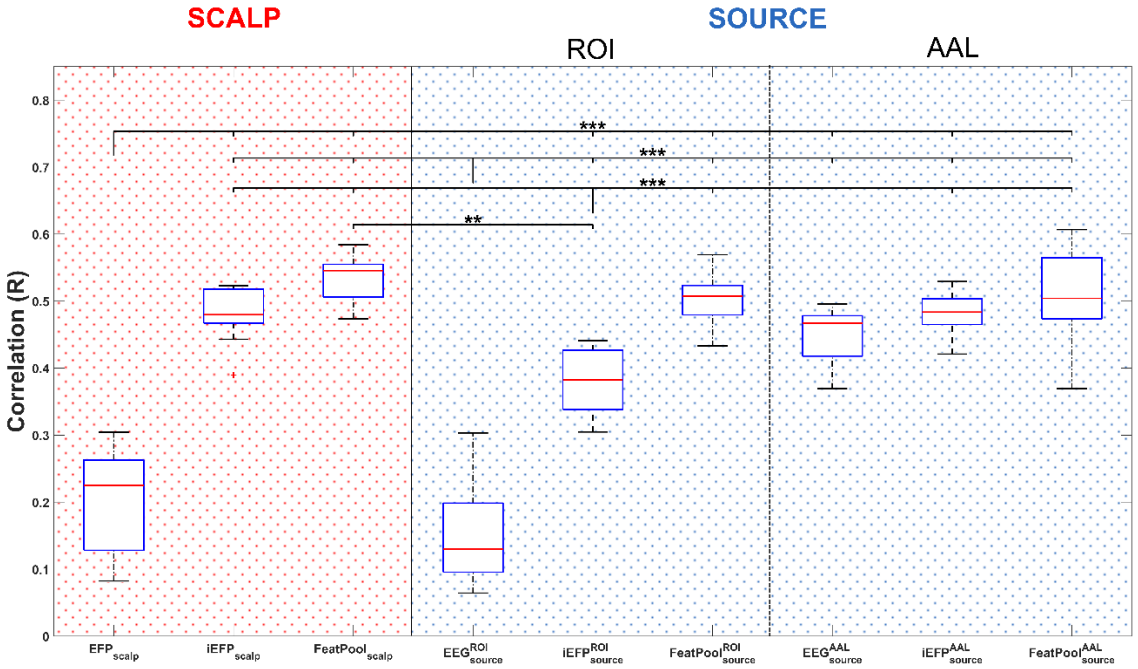

Figure 5.7 - Comparison of the correlation achieved by the BOLD reconstructions of each model. Significance bars on top show statistical significance between the model with the longer tick and the remainder signaled models (* p < 0.05, ** p < 0.01, *** p < 0.001).

Based on the group correlation maps shown in Figure 5.8, it is possible to observe that by using the proposed *FeatPool*$_{scalp}$ model, the brain regions associated with the reconstructed BOLD signal match those involved in the FEPN (mapped from the Localizer run at the group level), which is not observed when considering the EFP model.

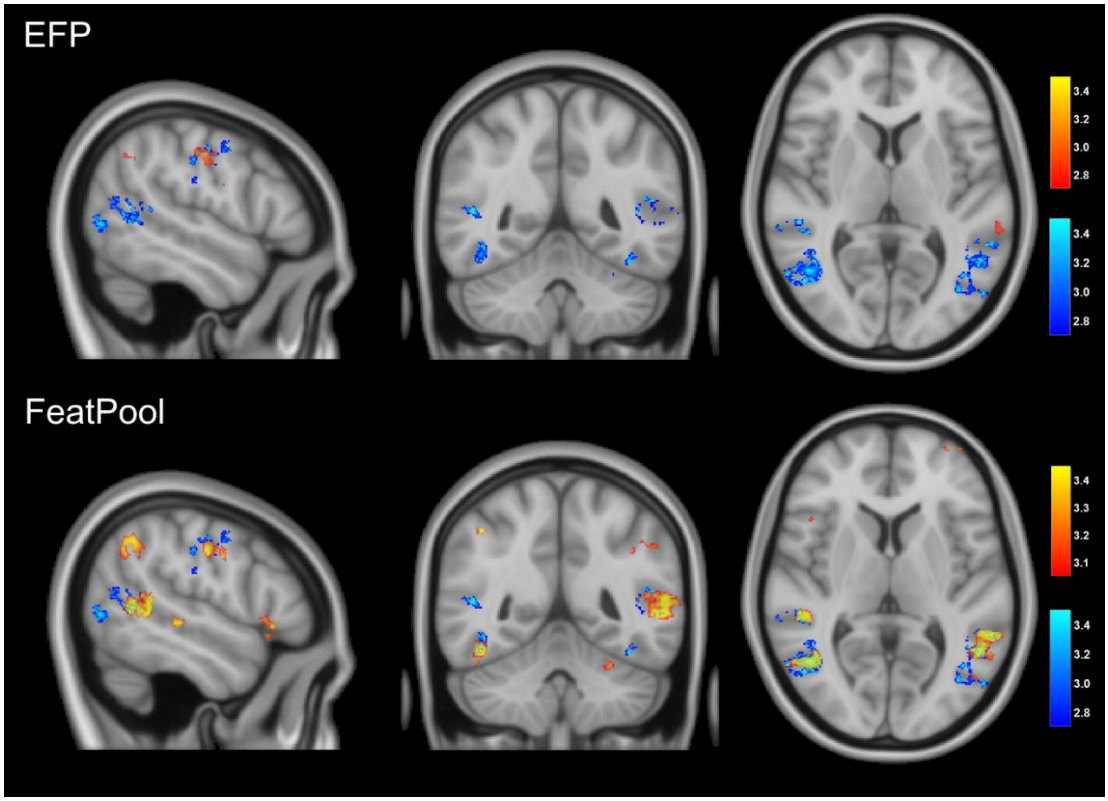

Figure 5.8 – Group correlation maps for the EFP method (top) and the FeatPool method (bottom) (MNI coordinates: x = -52, y = -48, z = 6). The FeatPool method recovers most of the FEPN identified by the localizer (in blue) while the EFP method fails to reconstruct even its main locations. The maps are cluster thresholded for Z > 2.7 (top) and Z > 3.1 (bottom).

5.3.3.3 Features, frequency bands and HRFs importance to the model

Considering the $FeatPool_{scalp}$ as the best model to reconstruct the BOLD signal from the pSTS region, we then investigated which features, frequency bands and HRF functions (among the top ranked predictors according to the mRMR) contributed the most for the reconstruction (Figure 5.9). We verified a strong contribution from the largest Lyaponov exponent and the sample entropy features. For the frequency bands, the theta band was the most used, followed by the beta sub-bands (low-beta and high-beta) and only after those the alpha band, along with the broadband. Finally, we observed that the most used HRF functions were those close to the canonical HRF, prevailing the peak latencies around 5.5 seconds. However, two uncommon clusters are also discernible, one for the short response functions (3.5 seconds) and another one for the long response functions (10 seconds). The morphologies captured by the HRF functions peaking at those clusters are never captured by the canonical HRF nor the linear delays function, which clarifies the usefulness of using a set of HRF functions with variable peak latencies.

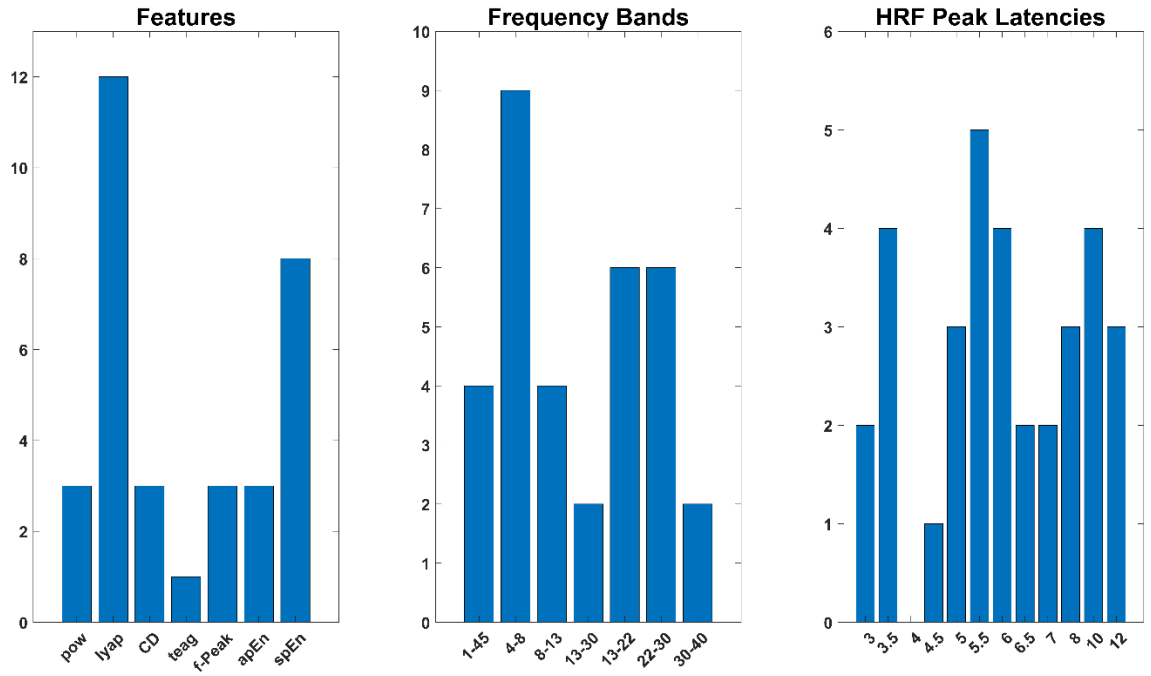

Figure 5.9 – Histograms for the top ranked features, frequency bands and HRF functions (average rank < 100).

5.3.4 Discussion

In this study, we systematically investigated the extent at which the BOLD-fMRI signal recorded from the facial expressions processing network (FEPN) during a neurofeedback task could be reconstructed from the simultaneously recorded EEG signal. We proposed novel features potentially predictive of the BOLD signal, as well as new approaches to tackle its hemodynamic delay. Using random forests for the regression, we compared our novel contributions with the EFP (the current state-of-the-art) and found that combining our newly proposed features with the convolution of multiple HRFs peaking at different latencies yielded the best model ($FeatPool_{scalp}$), achieving an accuracy of 53%. This represented an improvement of 33 percentage points relative to the EFP_{scalp}.

The $FeatPool_{scalp}$ model outperformed the $iEFP_{scalp}$, showing that only spectral characteristics of the EEG are not sufficient to capture the BOLD signal up to its full extent, since the exploration of other characteristics of the EEG signal increased the correlations achieved. Furthermore, we verified that the nonlinear features provided a strong contribution to the $FeatPool_{scalp}$ model, especially the ones that characterize the stability of the phase-space

attractors, namely the largest Lyaponov exponent and the sample entropy. We also verified a strong contribution of features extracted from the theta band, which is in line with our previous study where nonlinear features in the theta band discriminated the mental imagery of facial expressions processes from autism spectrum disorder patients and controls (Simões et al., 2018b). Importantly, other studies have already shown the pivotal role of nonlinear aspects of the EEG signal in mental imagery tasks, especially in the brain-computer interfaces domain (Solhjoo et al., 2005; Montri and Masahiro, 2008; Banitalebi et al., 2009; Wang et al., 2011). However, to the best of our knowledge, no study has yet addressed the use of nonlinear features for the characterization, and more importantly reconstruction, of the BOLD signal.

The preponderance of the theta and beta sub-bands over the alpha band is surprising, since most studies focus on the relationship of the EEG alpha rhythm with the BOLD signal (Laufs et al., 2003; Gonçalves et al., 2006; de Munck et al., 2009; Jann et al., 2009). However, EEG power over the theta and beta bands has been shown to exhibit significant correlations with the BOLD signal in the prefrontal cortex during memory tasks (Bäuml et al., 2010; Hanslmayr et al., 2011). Nevertheless, our results reinforce the relationship between EEG power over the theta band and facial emotion processing (Balconi and Lucchiari, 2006; Balconi et al., 2015; Simões et al., 2018b), given the observed strong contribution of this frequency band for the reconstruction of the BOLD signal at the FEPN.

Regarding the hemodynamic delay between the BOLD and EEG signals, the EFP_{scalp} method does not include any *a priori* knowledge of the BOLD hemodynamic response, letting the regression procedure weight each delay according to its contribution to the final reconstruction. This is different from conventional EEG-correlated fMRI studies, whereby the predictors are typically convolved with the canonical HRF (with a fixed delay of 5s), thus including the expected behavior of the BOLD response (Abreu et al., 2018). We verified that, for the same number of predictors, convolving the predictors with the canonical HRF outperformed the delays approach used in the EFP method in terms of the reconstruction accuracy of the BOLD signal. In (Meir-Hasson et al., 2014), a similar comparison is also presented; however, the "delays" approach surprisingly outperforms the canonical HRF convolution in this case. These contradictory results may result from unfairly comparing models with different complexities, with the original EFP model comprising twelve times more (the number of delays) predictors than those used when considering the convolution with the canonical HRF. Motivated by the known variability of the HRF (Aguirre et al., 1998;

Rangaprakash et al., 2018), Sato and colleagues (2010) followed an approach similar to the "delays" approach used in the EFP model to estimate the transfer function between the EEG and the BOLD signal measured at the visual cortex. Despite their promising results, only two pilot subjects were considered, which limits the generalization of the results. The morphology of the estimated transfer functions varied significantly across participants and experiments, thus supporting the convolution of the proposed EEG features with multiple HRF functions peaking at different latencies. For the same number of predictors, this approach outperformed the other two, possibly because it not only incorporates the hemodynamic response behavior in the predictor time course, but also addresses the variability of the HRF function, which has already been found across subjects, sessions and brain regions (Aguirre et al., 1998; Rangaprakash et al., 2018).

Some insights can also be derived from the analysis of the higher ranked (according to the mRMR) HRF latencies used in the best model (the $FeatPool_{scalp}$). While the canonical HRF and its smaller variations were the most frequently used in the higher ranked predictors, the $FeatPool_{scalp}$ model also exploited HRF functions deviating from the canonical HRF. The relevance of such shorter and larger latency peaks has also been previously reported (Jacobs et al., 2008; Feige et al., 2017), but never in the context of task-specific studies. Our results are in agreement with those of Feige and colleagues (2017) who observed that, depending on the EEG spectral band or network/region of interest, the lag between the EEG phenomenon and the corresponding deconvolved BOLD signal representative of different resting-state networks varied from 0 to 10.5 seconds. This highlights the importance of exploring different HRF modulation approaches, especially when integrating different imaging modalities.

The source-based models also provided different results: the $\mathbf{EEG}_{\mathbf{source}}^{\mathbf{ROI}}$ model, which comprises the average source time-course across the FEPN from the direct mapping of the EEG signal was not better than the original EFP method. Despite the expected gain in sensitivity by considering the more informative 3D space of the source, rather than the 2D space of the scalp, volume conduction induces redundancy between adjacent brain regions, which may compromise this source model extracted from such small regions as the FEPN (Tenke and Kayser, 2012). However, when considering the source model comprising the parcel-averaged source time-courses ($\mathbf{EEG}_{\mathbf{source}}^{\mathbf{AAL}}$) the reconstruction accuracy improves significantly, suggesting that despite the volume conduction problem, whole-brain source activations convey crucial information for the reconstruction of the BOLD signal at the

FEPN. Consistently, the source models considering the AAL atlas outperformed the equivalent ROI versions of the source methods. Exploring EEG source activations over time itself represents a new contribution to this field, as only a number of studies has explored this approach and its relationship with the BOLD signal in the context of disease (epilepsy) or resting-state. Specifically, the average source time-course across an epilepsy-related ROI has been shown to improve the epileptic network mapping with simultaneous EEG-fMRI, when compared with the typically used unitary regressors to model the BOLD signal (Vulliemoz et al., 2010). More recently, resting-state networks, which are typically observed in fMRI, were shown to be also present on continuous EEG source data (Pascual-Marqui et al., 2014; Custo et al., 2017; Liu et al., 2017a, 2018). To the best of our knowledge, our work is the first to conduct it in a task-based paradigm and to use the continuous source time courses of features extracted at the scalp, instead of the source mapping of the EEG signal or its spectral characteristics directly.

The fact that the best reconstruction was achieved by the $FeatPool_{scalp}$ model suggests that the combination of different kinds of features (linear and nonlinear) with the convolution of multiple HRF functions peaking at different latencies, together with the use of random forests for the regression was pivotal. As shown in (Simoes et al., 2015), the isolated use of features is unable to perform a direct mapping of the BOLD modulation in the FEPN. It is the convolution of the features extracted with different HRF functions that creates a feature set that sufficiently captures the variance of the BOLD signal of interest. We were able to clarify the isolated effects of the feature set and delay approach, and this dissociation should help future studies to target both domains (features and delays) of EEG-fMRI transfer functions.

Concluding, the exploration of nonlinear EEG features as the largest Lyapunov exponent or the sample entropy extracted from different frequency bands is crucial for more accurately reconstructing the BOLD signal at the facial expression processing network. Furthermore, we show that convolving EEG the features with multiple HRF functions peaking at different latencies best captures the variability of the hemodynamic delay of the BOLD signal, yielding robust improvements on the overall localized BOLD signal reconstruction from the EEG data, with direct impact in the transfer of fMRI-based neurofeedback interventions to EEG setups. Future studies should address how these models generalize across subjects and sessions.

5.4 Chapter Discussion

Transferring an fMRI-based neurofeedback intervention approach to EEG poses several challenges. Firstly, the two neuroimaging techniques record signals of intrinsically different origins, and spatiotemporal resolutions, with fMRI measuring hemodynamic changes and EEG measuring electrical activity. Furthermore, the indirect nature of the BOLD signal creates a delay of several seconds between the mental activity and the variation detected in the signal, whilst the EEG measures brain activity directly, thus capturing processes at (almost) real time. Moreover, since our region-of-interest is located in a sulcus, cancelation processes can occur (Ahlfors et al., 2009; Irimia et al., 2012), which limits the activity measurable at the scalp. Considering the inter-subject variability, the problem is, undoubtedly, challenging.

Nevertheless, the difficulty of the problem is countered by the benefits of a successful outcome. Since there is evidence of positive behavioral effects as consequence of the NF intervention (Appendix II), achieving a successful transfer of this intervention would widespread its application range and prevalence. Not only it would be possible to include more patients in interventional approaches, but also to perform more interventional sessions per participant. There could be the case that greater benefits would only appear after more training sessions, which are not possible to convey on the MR machine due to its high costs and setup inflexibility (Fovet et al., 2015). Therefore, we addressed this problem framing it as identifying a framework that, based simply on EEG activity, can generate a read-out signal that correlates with the fMRI activity in our target regions, the facial expression processing network.

Our first step was to extract several features from the EEG that cover time/frequency and non-linear domains and check their direct correlation with the target signal. Since the correlation levels were too low to be used in practice, we explored the addition of a regressor to combine several features as predictors of the BOLD activity of interest. We were able to improve the correlation levels achieved by the state-of-the-art method, the EEG finger print, showing that the exploration of nonlinear features captures more brain dynamics than the EEG signal power by itself. Furthermore, we proposed an improvement in the method for dealing with the hemodynamic delay of the BOLD signal: to convolve the predictors with a set of HRF functions peaking at different time latencies, thus addressing inter and intra-subject variability of the HRF. We showed this method significantly improves the prediction accuracy of the models. Those contributions helped to highlight the relations between EEG and fMRI

signal measures, and we propose new methodologies for addressing the transferring of fMRI NF interventions into EEG.

Still, to fully transfer the NF intervention from imaging modalities, the models must be tested between independent runs and sessions. We addressed this by training the models with two neurofeedback runs and testing on the third, thus providing a first independent evaluation of the model generalization capacities (the first generalization level, since we were still using data from the same session but different runs). The results, however, did not surpass a performance level above 25%, showing that further steps are still needed to make the transfer viable.

Chapter 6

Virtual Rehabilitation for ASD

This chapter describes the exploration of virtual reality for evaluate and rehabilitate ASD deficits. It combines the following two contributions:

Simoes, M., Mouga, S., Pereira, A., Gonçalves, H., Oliveira, G., Carvalho, P., Castelo-Branco, M. 6.2 Assessing immersive virtual reality feasibility for studying personal space regulation in Autism spectrum disorder**.**

Simões, M.*, Bernardes, M.*, Barros, F., & Castelo-Branco, M. (2018). Virtual Travel Training for Autism Spectrum Disorder: Proof-of-Concept Interventional Study. *JMIR Serious Games*, *6*(1), e5. https://doi.org/10.2196/games.8428.

6.1 Chapter Introduction

For the virtual rehabilitation part of the thesis, we studied the use of virtual reality for rehabilitating social deficits or daily living tasks. The literature presents the general idea of using virtual reality for the study and training social skills in ASD, advocating several arguments such as the control it provides to repeat the same task under different scenarios to help the generalization of the concept, the safety or the preference ASD patients usually manifest regarding computerized and technological setups (for a more detailed description, please refer to section 2.3.1 – Virtual rehabilitation). However, there is no study, to the best of our knowledge, to show that behavioral metrics can be replicated in the virtual environments, comparing them to the same behavioral metrics measured in the real environments. Therefore, we created a virtual reality environment that fully replicates the same real environment, providing the perfect set for a feasibility assessment. We used the preferred interpersonal distance measured in both environments as metric of comparison, since it represents a simple behavioral social metric that can easily be measured in both environments with high levels of accuracy. We present this study in section 6.2.

We then created an immersive virtual reality serious game to train participants in performing a challenging daily living task, such as taking a bus. This task represents several challenges to an individual with ASD, since it presents several subtasks with some levels of unpredictability, which cause anxiety and are difficult to handle. We implemented in the game a biofeedback system that automatically adjusted some disturbing factors of the game (like the noise inside the bus or dogs barking in the streets) based on the anxiety level of the user (measured through electrodermal activity), and performed a pilot one-arm intervention study with three training sessions of increasing complexity. This work is described in 6.3.

To accompany and support this and other serious games, we created a platform for managing the games, users, training plans, progress of the players as well as providing gamification strategies such as awards and badges to keep players engaged in the rehabilitation. This work is presented in Appendix IV.

6.2 Virtual reality immersion rescales regulation of interpersonal distance in controls but not in Autism Spectrum Disorder

This section is composed by the contents of the following publication:

Simões, M., Mouga, S., Pereira, A., Gonçalves, H., Oliveira, G., Carvalho, P., Castelo-Branco, M. Virtual reality immersion rescales regulation of interpersonal distance in controls but not in Autism Spectrum Disorder.

Abstract

Interpersonal distance (IPD) is a simple social regulation metric which is altered in autism. We performed a stop-distance paradigm to evaluate IPD regulation in ASD and control groups in a real versus a virtual environment mimicking in detail the real one. We found a bimodal pattern of IPDs only in ASD. Both groups showed high IPD correlations between real and virtual environments, but the significantly larger slope in the control group suggests rescaling, which was absent in ASD. We argue that loss of nuances of non-verbal communication, such as perception of subtle body gestures in the virtual environment, lead to changed regulation of IPD in controls, whilst ASD participants show similar deficits in perceiving such subtle cues in both environments.

6.2.1 Introduction

Virtual reality (VR) has been repeatedly referred as a suitable tool for performing virtual rehabilitation in autism spectrum disorder (ASD) patients (Strickland, 1997; Blascovich et al., 2002; Goodwin, 2008; Bellani et al., 2011; Parsons and Cobb, 2011; Kandalaft et al., 2013; Didehbani et al., 2016; Simões et al., 2018a). According to those authors, several reasons account for this match, including the level of control virtual stimulations provide regarding the amount of stimuli and clutter in the environments, allowing for simplifications that are tolerable by the patients; the possibility of repeating the same task in different environments, helping the generalization of the trained concepts; the safety of virtual settings, enabling the

training of possibly dangerous tasks without the danger of harming the participant (like crossing a busy street or driving a car); and the frequently observed adherence of ASD participants to computerized setups, mostly due to their structure and predictability. However, despite this apparently perfect match, very few studies addressed the use of fully-immersive VR simulations in ASD. Most virtual rehabilitation interventions categorize themselves as VR interventions, but the large majority of them consists solely on computerized interventions (Lorenzo et al., 2016).

The review by Miller and Bugnariu (2016) shows that the level of immersion of experimental settings directly impacts the assessment and teaching of social skills in ASD. However, most studies identified by that review only present low to moderate immersion levels. Furthermore, there was no study, to the best of our knowledge, performing a fair comparison between real and fully-immersive environments assessing a social skill in ASD. Therefore, the advantage of virtual settings in the training or assessment of social skills for this disorder still lacks supporting evidence.

In this paper, we compare and evaluate the feasibility of a fully-immersive VR setup to measure a simple social skill: the interpersonal space social regulation. We developed a virtual environment that is a detailed and realistic replica of the real environment where the experiment is conducted, thus reducing the variability between experimental settings, enabling a fairer comparison of results.

Interpersonal space social regulation is the way one adjusts the distance maintained between himself/herself and other people (Gessaroli et al., 2013; Perry et al., 2015a). That distance is called interpersonal distance (IPD), and has been used as a measure of extent of social personal space (Candini et al., 2017). People spontaneously monitor and closely adjust their IPD in order to maintain a comfortable distance of interaction with others. IPD varies with the social context, both in animals and humans. It increases in situations of threat, but is also sensitive to friendship, attraction or intimacy in others (Delevoye-Turrell et al., 2011; Perry et al., 2015a). Nevertheless, apart from cultural and situational differences, IPD seems to be stable within each individual throughout his/her lifespan (Perry et al., 2015b). Thus, individually-measured IPD can be used as a metric of human social interaction.

There is evidence for abnormal IPD in several neuropsychiatric or neuropsychological disorders, like early child abuse (Vranic, 2003), post-traumatic stress disorder (Bogovic et al., 2014) and social anxiety (Perry et al., 2013), among others. Since social deficits represent the

core characteristic of ASD, some studies have addressed the personal space regulation in this neurodevelopmental disorder. However, the results are controversial: while some studies show a preference for wider distances (Gessaroli et al., 2013; Candini et al., 2017), other authors found that participants would choose very close distances without feeling any discomfort (Parsons et al., 2004; Kennedy and Adolphs, 2014; Perry et al., 2015a). This variability suggests that other factors might be responsible for the IPD preference, like sensory sensitivity levels or severity of social impairments (Perry et al., 2015b).

Immersive virtual environments have been used to study personal space. Some works compared behavior in virtual settings and concluded they follow the expected patterns observed in real ones (Blascovich, 2002; Bailenson et al., 2003), but no direct quantitative measure was performed between real and virtual settings. Another study compared the IPD preference between different types of virtual agents, but with no direct validation against real environments (Iachini et al., 2014). Regarding ASD studies of personal space using virtual environments, Parsons and colleagues (2004) conducted an experiment where participants were evaluated on whether they would disrupt the personal space of virtual avatars engaged on a social interaction. Once again, no direct test against a real environment was conducted and, furthermore, the virtual setting was rendered in a non-immersive setup (laptop).

Our approach consisted on the use of a modified version of the stop-distance paradigm (Gessaroli et al., 2013) applied both in a real environment and in an immersive virtual replica of the same setting. A group of ASD participants and a group of typically-developing (TD) youngsters underwent the experiment. Our goal was to compare regulation of interpersonal distance in the real and virtual environments in the two groups and, through that comparison, to investigate how immersive virtual and environments compare across groups and if they can provide reliable measures of a social interaction action metric.

6.2.2 Methods

6.2.2.1 Participants

The study comprised two groups of participants: the experimental group, composed by individuals with confirmed ASD diagnosis; and the control group, composed by individuals with typical neurodevelopment. A total of 48 participants were enrolled in the study, 25 for

the ASD group and 23 for the control group. Groups were matched by age and performance intelligence quotient (PIQ). Further characterization details can be found in Table 6.1.

ASD participants were recruited from the Autism Unit, Child Developmental Center, Pediatrics Hospital from the University Hospital of Coimbra and from Portuguese ASD patient associations (Coimbra and Viseu). The diagnosis of ASD was performed based on the *Autism Diagnostic Observation Schedule*, the *Autism Diagnostic Interview – revisited* and the *Diagnostic and Statistical Manual of Mental Disorders – 5th edition* criteria, confirmed by an experienced multidisciplinary team coordinated by neurodevelomental Pediatricians. Participants from both groups had their intelligence quotient (IQ) assessed with the *Wechsler Intelligence Scale for Children* for younger participants, and with the Wechsler Adult Intelligence Scale for participants older than 16 years old, by a trained neurodevelopmental psychologist.

Table 6.1 – Characterization of Groups: Mean and standard error of the mean – within parenthesis – of age, full scale IQ (FSIQ), verbal IQ (VIQ) and performance IQ (PIQ) (* p > 0.05).

	ASD	**TD**	
N	25	23	
M/F	23/2	22/1	
Age	12.8 (0.6)	13.0 (0.6)	*
FSIQ	99.4 (3.0)	115.8 (4.1)	
VIQ	96.6 (2.4)	116.3 (4.4)	
PIQ	102.7 (4.0)	110.0 (3.5)	*

Written informed consent was obtained from the parents of the participants or, when appropriate, the participants themselves. The study was approved by the ethics committee from Faculty of Medicine from the University of Coimbra and was conducted in accordance with the declaration of Helsinki.

6.2.2.2 Experimental setup

The experiment was conducted in our VR lab, established at the Centro de Investigação e Formação Clínica of Hospital Pediátrico, Centro Hospitalar e Universitário de Coimbra, Coimbra, Portugal. The lab consists in a rectangular room with approximate dimensions of 4 x 5.5 x 2.5 meters. The lab is equipped with 3-D Vizard Virtual Reality Toolkit Devices for

Integrated VR Setups and a Position Tracking System. Virtual stimuli were presented through the Oculus Rift (Oculus, USA) head mounted display (HMD), with a low persistence OLED display with 960×1080 resolution per eye, refreshed at 60 Hz. Head orientation was tracked using the Oculus internal Adjacent Reality Tracker and head position was tracked using a passive optical tracking system (Precision Position Tracker, PPT-H2; WorldViz, USA), with an infrared emitter attached to the HMD. Graphics displayed in the HMD were updated on the basis of the position and orientation of participant's head. A long cable connected the HMD to the desktop computer on the corner of the room, allowing for the participant to move freely inside the room.

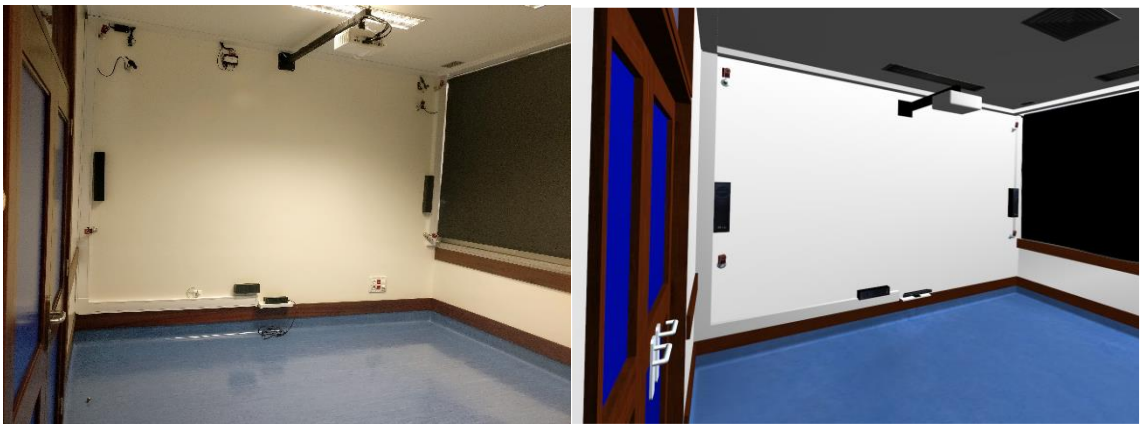

Figure 6.1 - Images of the VR lab (photography, left) and its 3D representation used as virtual environment (3D rendering, right).

The virtual environment experiment was developed using the Vizard software, and for the virtual avatars we used the male m002 and female f008 from the Complete Characters HD Pack (Worldviz, USA). Due to the position tracking system and having the exact same environment, the virtual walls are in the exact same positions as the real ones, so the participants can touch and feel the virtual walls (while touching the real ones). Figure 6.1 shows photographic captures of both environments.

Stop-distance paradigm

We applied an adapted version of the stop-distance paradigm used by Gessaroli and colleagues (2013). All subjects met the experimenters for the first time. All subjects were tested in the same room and virtual environment, against real and virtual experimenters of similar appearance. For each environment, 16 trials were conducted, corresponding to every possible

combination of the 4 binary factors tested: gender of the experimenter (male or female), experimenter's gaze direction (direct or averted), mode (starting from far away – 3 meters – and walking towards the other or starting very close – 30 cm – and walking away from the other) and actor (the experimenter or the participant is the one who walks). Figure 6.2 shows the different combinations of these last two modes. Trials were presented in random order in both environments, to avoid adaptation effects.

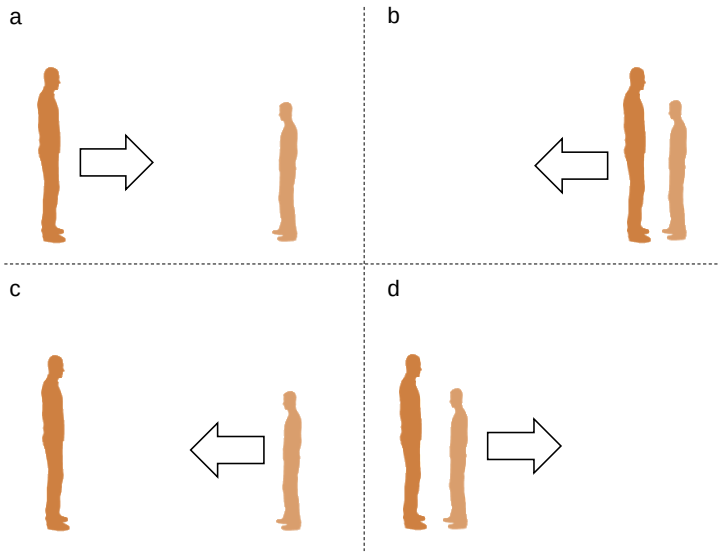

Figure 6.2 – Example showing four different conditions, regarding who is walking and the walking person. A) The experimenter approaches the participant. B) The experimenter recedes from the participant. C) The participant approaches the experimenter. D) The participant recedes from the experimenter.

In the trials in which the participant is the one moving, he/she simply stops at the distance he/she feels more comfortable. For the other trials, the experimenter walks in a steady pace towards or away from the participant, who was instructed to say the word "stop" whenever they feel the distance is appropriate. They could then fine-tune that distance by asking the experimenter to move slightly closer of farther away. Afterwards, the distance between the waists of the experimenter and the participant were measured with a digital laser measurer (model DLR165K; Bosch; error ±0.003 m).

Two marks in the room floor, 3 meters from each other, marked the starting positions for the participant and the experimenter, so between each trial the experimenter and the participant reset their positions. Inside the virtual environment the avatars (male or female) playing as experimenters appeared in the beginning of each trial in the same place as the starting position

of the real environment and were programmed to walk towards or away from the participant. The avatar's gaze was directed or averted to the participant, depending on the trial condition. The participants had to act as in the real environment: saying "stop" at the distance they felt more comfortable, or simply stop in the trials they were the ones walking. Afterwards, they could adjust the distance asking the avatar to come a bit closer or farther away. Stopping the avatars and the final adjustments to the position were controlled by one of the experimenters. Figure 6.3 shows a participant performing the same trial in the real environment and immersed in the virtual one.

Figure 6.3 – Capture of a user performing the task in both environments: the real environment, on the left, and the user using the VR setup, on the right. On the projection wall we display the same content that is presented to the user through the HMD.

6.2.2.3 Statistical Analysis

Since IPD relates to a social face-to-face contact, we converted the waist-to-waist distance into a face-to-face distance, based on the height of each participant and the experimenters applying the Pythagoras theorem

$$F_{dist} = \sqrt{D^2 + \left|Experimenter_{height} - Participant_{height}\right|^2} \quad (6.1)$$

using the measured distance (*D*) and the height difference between the experimenter and the participant.

For the first level analysis, we computed a generalized linear model (GLM) for each participant's measures under each environment to find explained variance introduced by each factor. The model goes as

$$D_k = D_m + \beta_1 * ExpGender_k + \beta_2 * ExpGaze_k + \beta_3 * ProxMode_k + \beta_4 * WhoWalks_k + \varepsilon_k \quad (6.2)$$

with D_k as the measured distance at trial *k*, the D_m the mean distance for that participant (intercept of the model) and $\beta_i, i \in [1,4]$ as the weights of each factor *i*. Each factor (ExpGender, ExpGaze, ProxMode and WhoWalks) assumes the value 0 or 1 depending on the respective trial *k*. Figure 6.4 shows the design matrix for this model. The models were computed through the *glmfit* function of the Statistics and Machine Learning Toolbox from the Mathworks Matlab r2019b software.

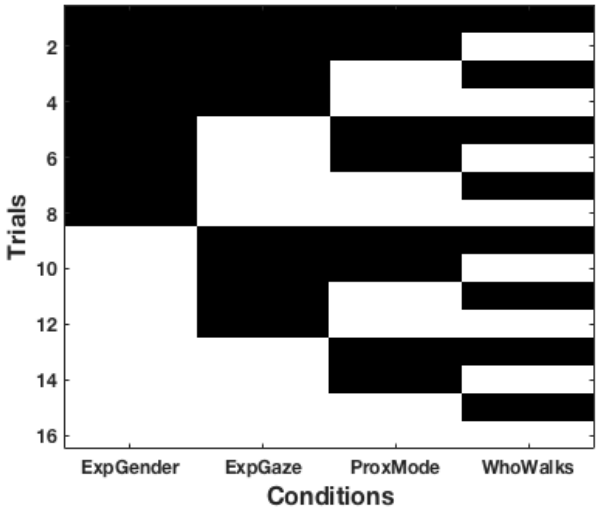

Figure 6.4 - Design matrix for the GLM models computed at the first level analysis.

The D_m and β values were carried to the second level analysis. Non-parametric tests were used since data normality was not verified for all the distributions (verified through the Kolmogorov-Smirnoff test). β values were tested against 0 to see if they had influence in the distances observed, using the Wilcoxon signed rank test. Between group comparisons were performed for median (Wilcoxon rank sum test) and variance (Brown–Forsythe test). The relation across environments was compared through Pearson correlations of the distances of each participant for both environments, and between groups through the analysis of the slopes of each group's least-squares fit (Brame et al., 1998). Additionally, to rule out influence of age

or IQ, we verified the correlations between the participant IPDs and their age, full-scale IQ, verbal IQ and performance IQ. Tests were conducted considering the statistical α threshold of 5%.

6.2.3 Results

From the IPD histograms obtained for each group in the environment (Figure 6.5) we verify that the TD group (orange) shows a sharper distribution around the mean, while the ASD group manifests a twofold distribution, with a sub-group choosing closer IPDs and another subgroup wider ones.

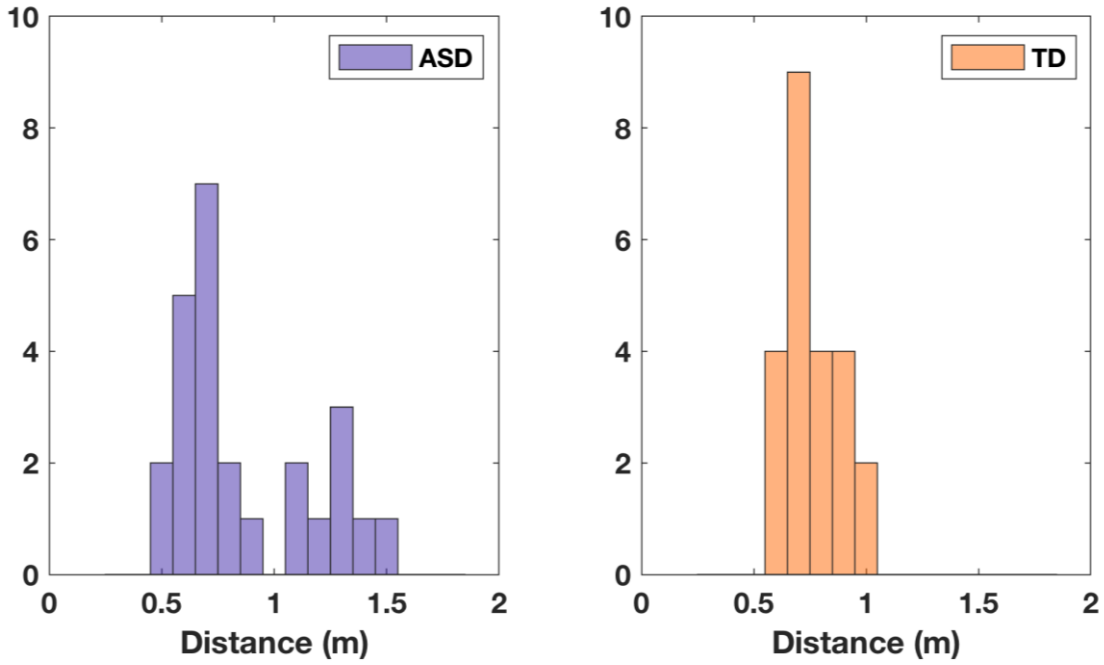

Figure 6.5 - Histogram of interpersonal distance measures for both groups, in the real environment. At the left we present the histogram for the ASD group, in blue, and at the right the histogram for the TD group.

The Kolmogorov-Smirnoff test for normality showed that, while the TD group presented a normal distribution (K-S(22) = 0.1208, p = 0.16), the IPDs for the ASD group did not (K-S(24) = 0.2018, p < 0.01). We found no median difference between the groups (Z=-0.1445, p = 0.89) but, when tested for difference in variance, the Brown–Forsythe test confirmed the difference perceivable from Figure 6.5 histograms (F(1,46) = 9.6865, p < 0.005), where a

bimodal pattern can also be identified. This bimodal pattern suggests that the ASD can be divided in two strata.

Factor effects were not found to affect the distance, since none of the factors tested for statistically significantly different than 0 (

Table 6.2). Additionally, we found no effect of age, IQ or height covariates in the observed distances, for neither group (Table 6.3).

Table 6.2 - Wilcoxon signed rank test results for the factors within each group. Z and respective *p* values are presented.

	ASD		TD	
	Z	***p***	**Z**	***P***
ExpGender	-1.2243	0.2209	-0.2737	0.7843
ExpGaze	0.1480	0.8824	1.5207	0.1283
ProxMode	0.3902	0.6964	1.9466	0.0516
WhoWalks	-0.2825	0.7775	-0.7604	0.4470

Table 6.3 - Pearson correlations between the age, full-scale IQ, verbal IQ, performance IQ and height covariates and the interpersonal distance preferences of participants, for both groups. We present the R value and respective *p* value.

	ASD		TD	
	R	***p***	**R**	***P***
Age	-0.2910	0.1582	-0.3680	0. 0840
FSIQ	-0.1666	0.4261	0. 3016	0. 1620
VIQ	-0.1835	0.3799	0.3520	0. 0995
PIQ	-0.2022	0.3323	0.1679	0. 4438
Height	-0.0177	0.9331	-0.1536	0.4840

When considering the IPDs measured in the virtual environment, the ASD group maintained the wide range verified in the real environment, with a range from 0.4 to 1.7 meters compared to the real environment range from 0.5 to 1.5 meters (see Figure 6.6). The TD group, however, increased the variation of the IPDs observed. While in the real environment the distances measured vary from 0.6 to 1.0 meter, in the virtual environment the range starts also at 0.6 meters but goes to 1.6 meters. When comparing the variances between real and virtual environments there was no difference for the ASD group ($F(1,46) = 0.1639$, $p = 0.69$), but

for the TD group we found a tendency for a significant effect ($F(1,46) = 3.4437$, $p = 0.07$), which corroborates the differences between the IPD histograms of this group.

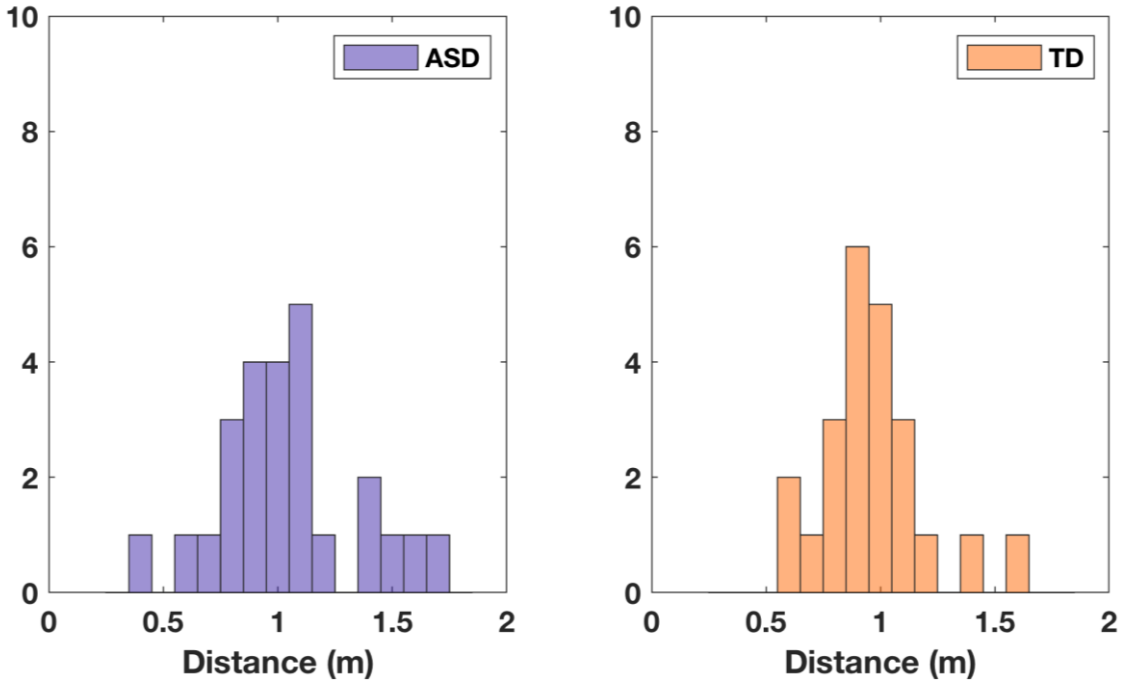

Figure 6.6 - Histogram of interpersonal distance measures for both groups, in the virtual environment. At the left we present the histogram for the ASD group, in blue, and at the right the histogram for the TD group. The bimodal pattern is still discernible in the ASD group.

For a more direct comparison between environments, we computed the Pearson correlation between the distances measured in both environments (see Figure 6.7). We found statistically significant correlations for both groups, with a similar, albeit higher correlation for the ASD group ($R = 0.85$, $p < 0.001$) than the TD group ($R = 0.82$, $p < 0.001$). To investigate scaling effects, we tested the difference of the slopes of the least squares fit lines for each group (ASD: 0.81, TD: 1.68) and found it statistically significant ($Z = 3.11$, $p = 0.003$). The slopes for ASD were 0.81 whereas for TD, 1.68; meaning that for each step in the real world the TD group does a step twice as large in the virtual world than does the ASD group.

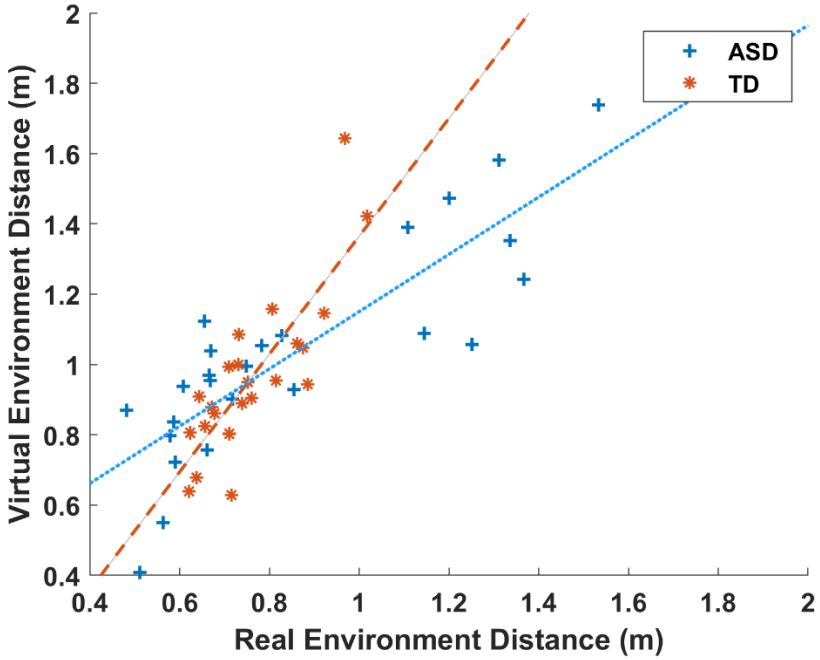

Figure 6.7 - Scatter plot comparing the measures in the real and virtual environments, for the ASD group (in blue) and the TD group (in orange). The slopes of the least squares fit lines for each group (ASD: 0.81, TD: 1.68) show that the virtual disruption is grater for the controls, since a small difference in the real environment distances manifests a high increase in the distance observed in the virtual environment (Z = -3.11, p = 0.003).

6.2.4 Discussion

The use of VR for studying and rehabilitating social deficits of ASD has been repeatedly advocated in the literature (Strickland, 1997; Blascovich et al., 2002; Goodwin, 2008; Bellani et al., 2011; Parsons and Cobb, 2011; Kandalaft et al., 2013; Didehbani et al., 2016; Simões et al., 2018a). However, there is no study, to the best of our knowledge, comparing the same social regulation behavior in the exact same real and virtual environment. In this paper, we created a VR setup that mimics a real environment (which it overlays), thus providing a very accurate setting for VR validation, since it provides the same exact visual input to the participant whichever its position and orientation are inside the environment, both real and virtual. This type of immersive setup is frequently used in the literature (Blascovich, 2002; Bailenson et al., 2003; Iachini et al., 2014). However, to the best of our knowledge, no study emulated the exact same environment as the one the immersion is performed in.

To validate the use of virtual environments for tasks that study social abilities in ASD, we selected a simple quantitative metric that could be similarly measured in the real environment and inside the virtual environment: the IPD. We implemented a well-established protocol for

the identification of the IPD of a person – the stop-distance paradigm – and performed it in the real and virtual environments.

The results for the real environment showed different patterns for the ASD group and the TD group, not in terms of average distance, but in terms of the type of distribution (near normal in TD and bimodal in ASD) and, in particular, the type of dispersion of the observed distances. While the TD group showed a more compact distribution around the median, the ASD group had some participants opting for closer distances and others to much wider distances (half a meter more that the wider distance for the TD group). This statistically significant difference between groups may help reconcile previous studies in the literature showing disparate results, with some studies reporting preference for wider distances (Gessaroli et al., 2013; Candini et al., 2017), while other authors found that ASD participants would choose very close distances (Parsons et al., 2004; Kennedy and Adolphs, 2014; Perry et al., 2015a). Our data show that both behaviors occurred in our sample. Since regulation of IPD is quite important in social interactions, these results identify a stratum within ASD whereby patients might benefit from an intervention to improve such regulation, for the cases whose distances become socially disruptive. The possibility to manipulate the distance of virtual avatars in a controlled way allows the systematic study of neurobehavioral and physiological responses of the patients to different IPDs, an aspect that future studies should address. The combination of this simulation with biosensors like electrodermal activity, heart rate frequency or electroencephalography would help to understand indirect factors that could influence the IPD, like stress-related aspects (Perry et al., 2015a; Simões et al., 2018a).

We tested whether the IPD depended on other factors like age or IQ. Furthermore, since the height of participants was used to convert the waist-to-waist distance to the face-to-face one, we also tested its influence on the results. However, no covariate showed to be statistically significant, which points towards a social-specific deficit in young adolescents.

We found no effect of gender, gaze, starting point mode or who walks. While this is consistent with some studies (Gessaroli et al., 2013), other studies found that who walks affects the IPD (Asada et al., 2016; Candini et al., 2017). Further studies need to be conducted to clarify the reasons behind this discrepancy. Importantly, cultural effects cannot not be discarded since no multi-centric international study was yet conducted.

Considering the comparison between real and virtual environments, our results showed a slope of IPDs closer to 1 for the ASD group than the TD group (which departed largely from

an isometric slope of 1). This critically suggests that ASD patients interact in similar and replicable ways (similar scale) in virtual and real worlds, in contrast with TD, who seem to show large rescaling, departing from an isometric slope of 1. Interestingly, the TD group showed greater variability inside the virtual environment, but not the bimodal pattern that was seen in ASD both in real and virtual environments.

In sum, between environment correlations were high both for the ASD and TD groups, but the later showed significantly different and large rescaling. We believe this is due to two factors: 1. Patients interact with the real world as if they were in a VR world, without processing the social nuances, like subtle body gestures and micro-expressions; 2. Control participants are affected by the absence of those social nuances in the virtual environment, in a phenomenon similar to the "uncanny valley" effect. The uncanny valley effect is a negative feeling reported for interaction with artificially human-like stimuli that have high levels of realism but can still be perceived as artificial (Kätsyri et al., 2015, 2017; Macdorman, 2017). Our perception of the other comprises a holistic evaluation, which includes several subconscious features like micro facial expressions, pupil dilations, odors and several non-verbal communication aspects (Mundy et al., 1986), which are very difficult to recreate in full by virtual avatars. We argue that the ASD group performs the task in the real world ignoring those nuances – due to their core deficits in social interactions –, and thus perform similarly in the two environments, while the TD group finds the virtual environment more artificial, more disruptive, showing a distinct behavioral pattern in this setting, with large rescaling, as shown by the slope analysis.

Our results validate the use of VR for ASD social evaluation and its potentially helpfulness to conduct specific social rehabilitation programs, since the behavioral metrics recorded inside the virtual environment matched the ones in the real environment. These results support the body of literature theory advocating the use of VR in ASD. On the light of this evidence, future studies can expand the range of virtual environments used for studying IPD and possibly adapt it into a training task, where ASD participants with extreme abnormal IPDs which undermine their social interactions can learn to regulate their personal space, in the format of a serious game.

6.3 Virtual Travel Training for Autism Spectrum Disorder: Proof-of-Concept Interventional Study

This section is composed by the contents of the following publication:

Simões M, Bernardes M, Barros F, Castelo-Branco M (2018) Virtual Travel Training for Autism Spectrum Disorder: Proof-of-Concept Interventional Study. JMIR serious games 6:e5. doi: 10.2196/games.8428.

Abstract

Background: Autism Spectrum Disorder (ASD) is a neurodevelopmental disorder characterized by impairments in social interaction and repetitive patterns of behavior, which can lead to deficits in adaptive behavior. In this study, a serious game was developed to train individuals with ASD for an important type of outdoor activity, which is the use of buses as a means of transportation.

Objective: To develop a serious game that defines a "safe environment" where the players became familiar with the process of taking a bus and to validate if it could be used effectively to teach bus-taking routines and adaptive procedures to individuals with ASD.

Methods: In the game, players were placed in a three-dimensional city and were submitted to a set of tasks that involved taking buses to reach specific destinations. Participants with ASD (n=10) underwent between 1 and 3 training sessions. Participants with typical development (n=10) were also included in this study for comparison purposes and received one control session.

Results: We found a statistically significant increase in the measures of knowledge of the process of riding a bus and a reduction in the electrodermal activity (a metric of anxiety) measured inside the bus environments with a high success rate of their application within the game (93.8%).

Conclusions: The developed game proved to be potentially useful in the context of emerging immersive virtual reality technologies, of which use in therapies and serious games is still in its infancy. Our findings suggest that serious games, using these technologies, can be used effectively in helping people with ASD become more independent in outdoor activities, specifically regarding the use of buses for transportation.

6.3.1 Introduction

Autism Spectrum Disorder (ASD) is a neurodevelopmental disorder responsible for impairments in social communication and interaction and restricted repetitive patterns of behavior, interests, or activities. Current ASD prevalence is estimated to be around 1% of the population, worldwide (American Psychiatric Association, 2013). Given that a cure is yet to be found, individuals rely on interventional approaches to improve and overcome their impairments. Further increasing the relevance of rehabilitation driven strategies is the fact that still only a minority of individuals with ASD are able to live independently in adulthood (American Psychiatric Association, 2013).

Virtual reality (VR) consists of artificial, 3D, computer-generated environments which the user can explore and interact with (Gutiérrez A. et al., 2008). VR usually takes advantage of different types of devices such as head-mounted displays and controllers to deliver the stimulation and provide means of interaction that lead to immersive experiences (Kim, 2005). The immersiveness of an experience is measured by the level of fidelity, concerning all sensory modalities, that a VR system can provide. Thus, immersion is objective, measurable, and depends only on the technology used by the VR system. Presence, on the other hand, is the human reaction to immersion, the feeling of actually being in the virtual environment and behaving as such (Slater and Wilbur, 1997; Slater, 2003; Sanchez-Vives and Slater, 2005). In fact, the immersive VR technologies available nowadays are able to present users with experiences realistic enough to trick the mind and create a feeling of presence within the environment (Bimber, 2014). These technologies have already been used and proven effective in therapies for posttraumatic stress disorder (Rizzo et al., 2014), phobias (Emmelkamp et al., 2001), as well as ASD (Strickland and Marcus, 1996). There are several reasons that justify the use of VR in those approaches. Its capacity to provide safe, realistic, and controlled environments (Parsons and Cobb, 2011) make therapy possible for people who, due to

physical (e.g. paralysis) or psychological (e.g. anxiety) reasons, cannot undergo exposure in real life situations. Moreover, this creates the possibility of applying therapies at ease without the need to go to a specific location where real exposure occurs. Finally, even when using low-budget hardware and software, it has been proven that VR therapies can be as effective as exposure in real life (Emmelkamp et al., 2001).

Serious games have also been proven effective in ASD therapies, not only for including game design techniques to keep the players motivated, but also because individuals with ASD are often interested in computer-based activities (Chen and Bernard-Opitz, 1993). However, according to Zakari et al (2014), most of the serious games developed for ASD rehabilitation between 2004 and 2014 are delivered through nonimmersive VR (e.g., desktops, tablets) and focus mainly on communication and social skill development. This highlights both the importance of focusing on other relevant ASD impairments, including executive function in outdoor situations, as well as exploring the potential of these new immersive technologies.

The aim of this study was to develop and validate a serious game which uses a VR headset (Oculus Rift) as a proof of concept for rehabilitation of individuals with ASD. Teaching a person with ASD to use public transportation requires parents or therapists to practice with them until they are ready and comfortable enough to perform this task alone (basically, the same process used with people with typical development, but with all the obstacles set by ASD particularities). In fact, being able to engage in outdoor activities such as the efficient use of public transport can be particularly challenging for people with ASD due to deficits in adaptive behavior (Mouga et al., 2015) and anxiety (White et al., 2009). This project intended to ease this process by creating and validating a game that prepares the players to use, in this case, buses for transportation. This included not only teaching the required skills, but also making them comfortable with the involved procedures and environments. To our knowledge, this is the first study to use VR training for teaching the process of bus-taking for people with ASD.

6.3.2 Methods

In this section, we describe the game, the experimental setup, the participants, and the validation procedure.

6.3.2.1 Game Description

The game was developed in-house with the aim of preparing individuals with ASD to use buses for transportation. To achieve that, it places the user in a three-dimensional city and sets a task that is completed by riding buses to reach a specific destination. Figure 6.8 shows different screenshots of the city and the buses.

Figure 6.8 – Screenshot from the virtual environment, showing two views from the bus stop perspective on the top, and two views from inside the bus. On the top left corner, we can see one bus stop, with other people waiting for the bus, and the map to be used by the participant on the wall. On the top right, we see a bus with its designated number signaled in red, and some traffic on the street. The bottom images show two perspectives from inside of the bus.

There are several different buses driving in 4 pre-defined routes within the city. Figure 6.9 shows the map of the city with the 4 bus lines available. The player can enter any of these buses, validate his/her ticket, choose a place to sit, and press the STOP button, requesting the bus to stop, and leave the bus. Before starting the game, it is possible to choose from 7 different tasks, 4 of them labelled by complexity as simple (the player only needs to take one bus to reach the destination) and 3 labelled as complex (the player needs to take 2 buses to reach the destination). Each task has 2 levels of difficulty: an easy and a hard mode. The easy mode leads the player, step by step, to the destination, while in the hard mode, the player is only told the place he/she must go to. At the end of each task, a scoring system evaluates the performance of the player on 2 different components: "Actions" (the capacity of the player to

memorize and execute bus norms, eg, validating the ticket or sitting on unreserved seats) and "Route" (the capacity of the player to plan a route to the destination, eg, if the player took the right buses in the right bus stops).

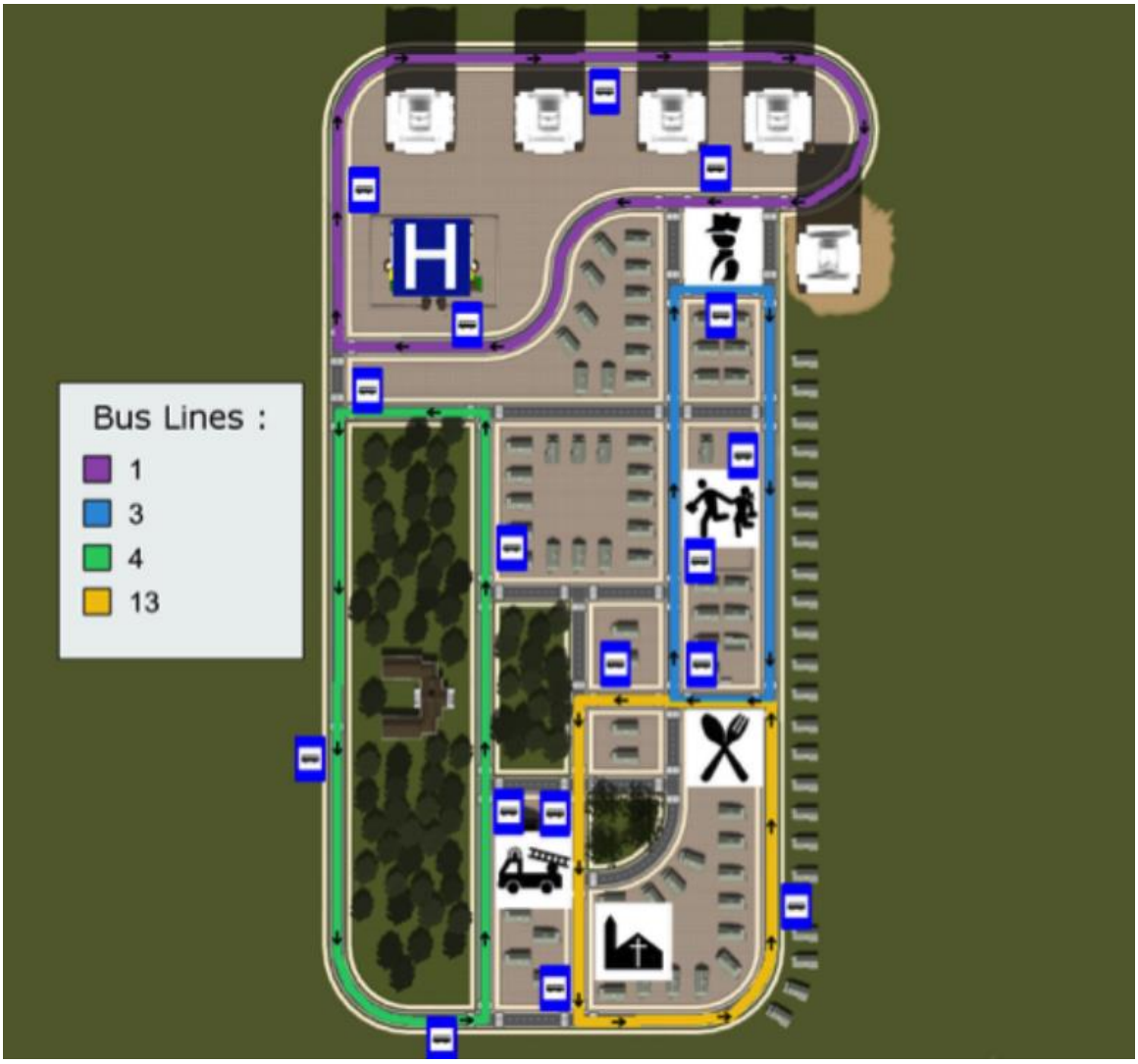

Figure 6.9 – City map showing the bus lines, stops and important places like the hospital, church, restaurant, and others.

The game includes several objects/elements, such as people, traffic, and dogs, which might cause anxiety, depending on the player. For that reason, a biofeedback system was implemented to ensure that, while the player becomes familiarized with the environment, it never becomes hostile to him/her. This is achieved by assessing the anxiety felt by the player through the analysis of the electrodermal activity (EDA) and reducing the stimulus clutter the player is exposed to, in real time, in case high anxiety levels are reached (eg, reducing the amount of noise in the environment). Figure 6.10 schematizes the biofeedback loop.

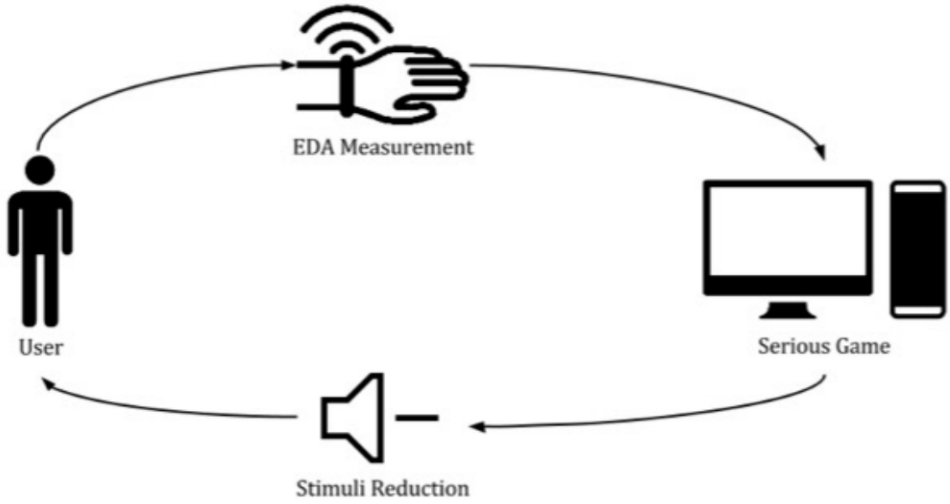

Figure 6.10 – Biofeedback loop diagram. The level of electrodermal activity is measured from the participant by the game. If it detects a peak of activity, it decreases the level of stimuli and noise in the scene.

6.3.2.2 Recruitment

For this project, 2 groups were selected: a clinical and a control group. For the clinical group, 10 participants with ASD, whose diagnosis followed the criteria established on the Diagnostic and Statistical Manual of Mental Disorders, 5th Edition (American Psychiatric Association, 2013), were recruited from Associação Portuguesa para as Perturbações do Desenvolvimento e Autismo de Viseu (APPDA-Viseu). For the clinical group, 9 males and 1 female were recruited, with a mean age of 18.8 (SD 4.5) years. In the same group, 8 were without intellectual disability (IQ equal to 70 or higher) and 2 were with mild intellectual disability (IQ between 50 and 69 (World Health Organization, 1993)). For the control group, 10 individuals with typical development (TD) were also recruited; 4 males and 6 females, with a mean age of 21.9 (SD 3.56) years. The groups were matched by age ($t(18)=-1.633$, $P=.12$). Participants gave oral consent, and a written informed consent was obtained from their parents/guardians or themselves if they were adults with sufficient autonomy.

6.3.2.3 Intervention Protocol

The ASD group underwent an intervention of 3 sessions of increasing complexity and difficulty (see Table 6.4), with a duration between 20 and 40 minutes each. Of the 10 participants recruited with ASD, only 6 performed all the intervention sessions of the study

due to scheduling issues. During the recruitment, participants completed a questionnaire to assess their experience in using buses for transportation. With an exception for 1 of the participants, all the participants were unable to take buses autonomously at the beginning of the study.

Table 6.4 – Task complexity and difficulty per session.

Metric	Session 1	Session 2	Session 3
Difficulty	Easy	Hard	Hard
Complexity	Simple	Simple	Complex

The control group was submitted to a single session (corresponding to the first of the patients). This group was used to provide a task baseline and to assess the capacity of the serious game to identify differences between groups.

The sessions took place in APPDA-Viseu for the ASD participants and in the Institute of Biomedical Imaging and Life Sciences for the TD participants. In all of them, the same research staff was present. This study and all the procedures were reviewed and approved by the Ethics Commission of our Faculty of Medicine from University of Coimbra and were conducted in accordance with the declaration of Helsinki.

6.3.2.4 Session Procedure

In each session, the players received a tutorial (to learn or review the game controls) and a task. The task difficulty and complexity changed from session to session, as shown in Table 6.4. At the end of every session, participants were asked to describe the process of riding a bus, from the moment they arrived at the bus stop, until they reached their destination, but never received feedback on the answer given. Their responses were recorded in a checklist containing all the steps existing in a bus trip (Textbox 6.1).

Textbox 6.1 - Checklist with steps existing in a bus trip.

- Wait for the bus
- Enter in the bus
- Validate ticket
- Avoid reserved seats
- Sit

- Wait until getting close to the destination
- Press stop button
- Leave the bus

6.3.2.5 Acquisition Setup

In every session, players sat on a swivel chair and wore a bracelet for wireless EDA recording (Biopac Bionomadix BN-PPGED and MP150 amplifier). All tasks were run on a laptop computer (Windows 8.1, 16.0 GB RAM and an IntelCore i7 2.50 GHz processor). The head-mounted display used was Oculus Rift Development Kit 2, firmware version 2.12, and a gamepad was used for input. Three participants with ASD and one with TD received the tasks without the Oculus Rift, due to vision impairments. Figure 6.11 illustrates the setup used.

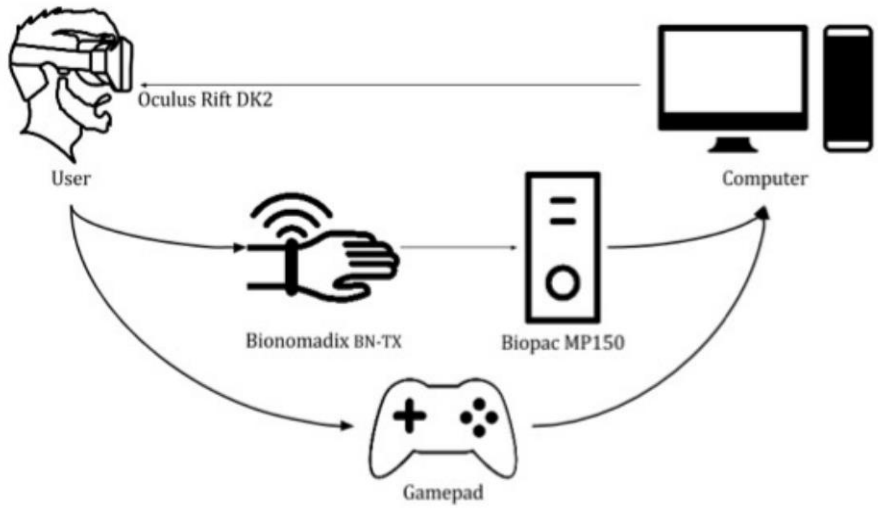

Figure 6.11 – Diagram of the setup used during the sessions, including the VR headset, game controller, biosignal recorder, and the main computer.

6.3.2.6 Metrics and Outcome Measures

Because the main objective of the serious game was to teach how to use a bus, we defined two main outcome measures to evaluate the knowledge of the process of riding the bus. One is measured automatically by the game and the other is measured using the debriefing. Both consist of the percentage of the checklist (Textbox 6.1) performed correctly.

Actions Accuracy

The game identified every action of the participant (entering the bus, ticket validation, etc) and calculated the actions accuracy based on the equation: number of correct actions/number of expected actions (Textbox 6.1).

Debriefing Accuracy

After the game, we asked the participants to describe the step-by-step process of riding a bus and calculated an accuracy based on the same equation of the actions accuracy.

Additional Metrics

Task Duration

Duration, in minutes, of the time taken to complete the task in each session. Since the tasks changes in complexity and difficulty, this metric is not directly comparable between sessions. Nevertheless, it is useful to analyze intersubject variability and to perform intergroup comparisons for the first session.

Anxiety Level

The variation of EDA values during the session was used as a measure of anxiety. To calculate it, we detrended the signal, subtracting it to its best fit to a straight-line (for details, see detrend implementation in MathWorks Matlab), then calculated the standard deviations of the detrended EDA values. We then created heat maps of anxiety peaks in the "virtual city", where it is possible to highlight the game locations where EDA peaks occurred, corresponding to anxiety events felt by the players. If the locations of anxiety peaks are the same between subjects and sessions, those locations will become red, but if they are sparse, their representations are green and blue. The heat maps were created using heatmap.js (Wied, n.d.), an open source heat map visualization library for JavaScript. Since the game has two major different situations (the city streets and the inside of the buses), two different conditions were defined: one representing the anxiety felt on the streets of the city and another with the anxiety felt inside the buses.

6.3.2.7 Statistical Analysis

For every metric, normality was assessed using histograms, Q-Q plots and the Kolmogorov-Smirnov test. Normality test results were used to choose between parametric and nonparametric test, accordingly.

Clinical vs Control Group Analysis:

The metrics actions accuracy, debriefing accuracy, and task duration were not normally distributed. Therefore, we used the Mann-Whitney U test for the between-group comparison of those metrics. Anxiety Level data was nevertheless normally distributed. Thus, we used two-sample T test for those between-groups comparisons.

Intervention Analysis (Intragroup Analysis for the Clinical Group):

As expected from the intergroup analysis, Actions Accuracy, Debriefing Accuracy, and Task Duration were not normally distributed. Paired data for last and first session were therefore compared using a Wilcoxon Sign-rank test. Regarding Anxiety Level, a one-sample T test was used for the paired data (last and first session). Additionally, we generated heat maps of locations where consistent peaks of anxiety where identified.

6.3.3 Results

The results are organized in two sections, one for the intergroup analysis and another for the within-subject analysis of the clinical group. In the figures presented, the error bars always represent the standard error of the mean, and the horizontal bar represents the median when considering nonparametric data (actions and debriefing accuracies, as well as task durations) and the mean when considering parametric data (EDA measures).

6.3.3.1 Clinical vs control group results

Regarding the actions accuracy (percentage of correct actions performed during the task), we found a statistically significant difference between groups. The Mann-Whitney U test indicated that the actions accuracy of the control group (median=100%) was greater than for the clinical

group (median=88%), U=75.0, *P*=.01. When analyzing the knowledge retained by the debriefing, the control group (median=100%) has greater accuracy than the clinical group (median=62.5%), as shown by the Mann-Whitney U test, U=80.5, *P*=.02 (Figure 6.12).

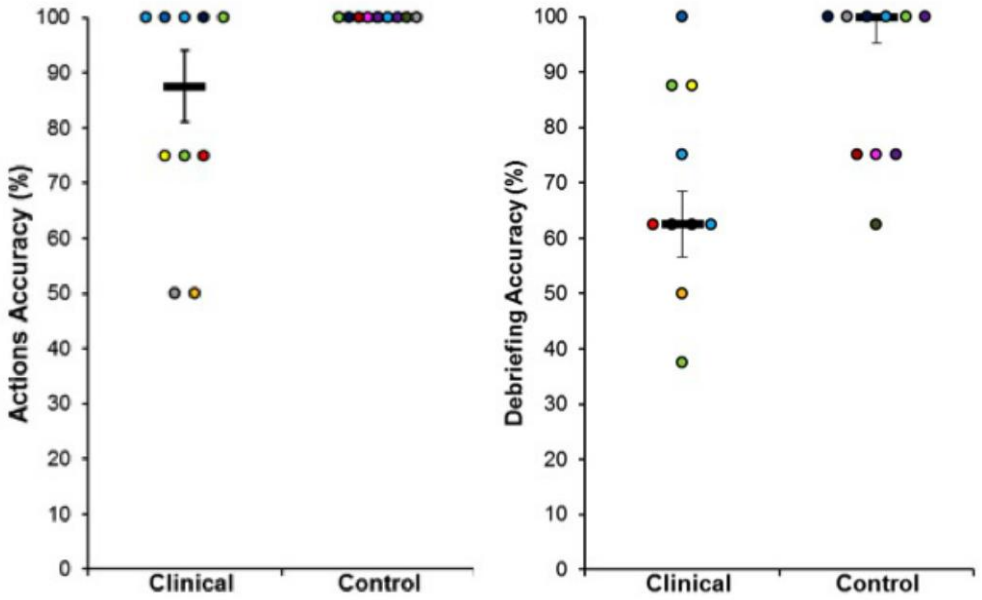

Figure 6.12 – *Left:* Actions accuracy for both groups in the first session. The control group (typical development) had a perfect performance, while participants in the clinical group missed some actions. *Right:* Debriefing accuracy for both groups. Higher, but not perfect, accuracy was found in the control group.

In terms of Task Duration, Figure 6.13 shows the between-group differences. A Mann-Whitney U test showed that the task duration of the ASD group (median=3.76) was statistically significant higher than for the control group (median=3.19), U=18.0, *P*=.02.

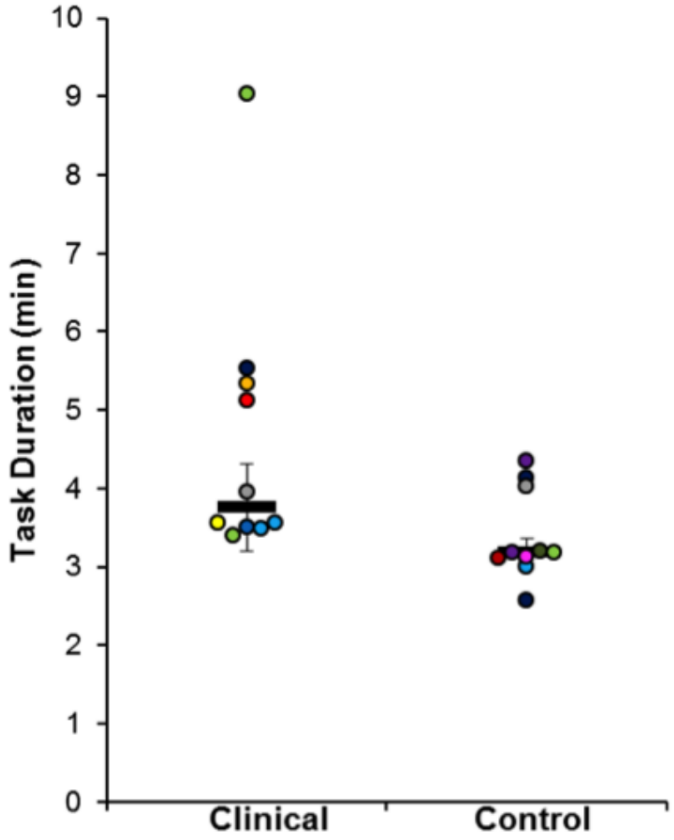

Figure 6.13 – Task duration for session 1 from each group.

Regarding the anxiety level of each group, we see a trend for higher values for the clinical group for all the scenarios (global EDA, inside the bus and outdoors, in the street). Figure 6.14 shows the mean EDA fluctuations of each group in each condition. However, two-sample T tests showed no statistically significant differences (possibly because of the biofeedback implementation) for either of the conditions (global EDA: $t(18)=-0.60$, $P=.56$; bus condition: $t(18)=-0.99$, $P=.33$; streets condition: $t(18)=-0.48$, $P=.63$).

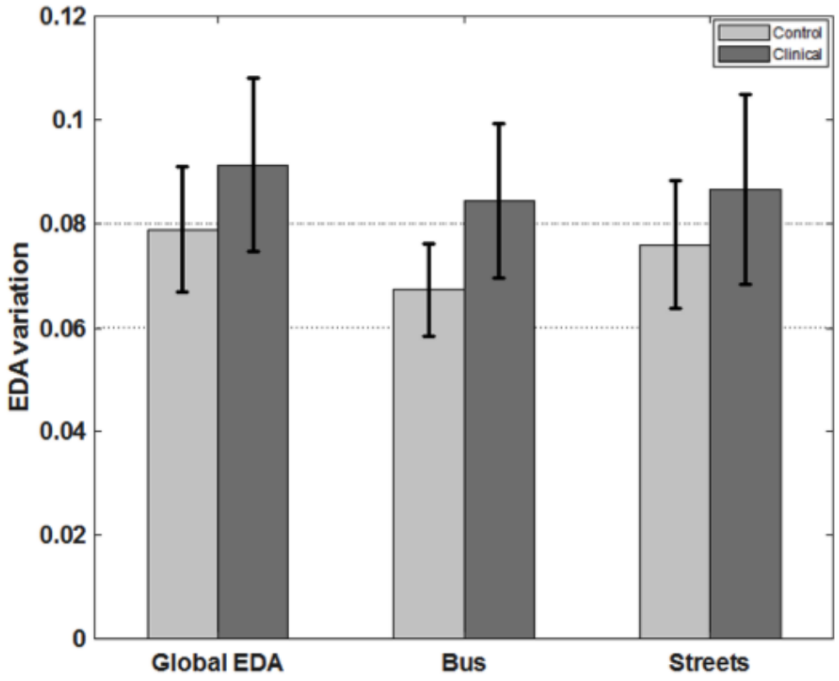

Figure 6.14 – Anxiety levels for each group (mean and standard error) for the overall task and two subconditions: inside the bus and outside (streets). The clinical group presents higher values for all the settings, although without statistical significance.

6.3.3.2 Intervention Results

We then compared the main outcome measures pre- and postintervention for the 6 participants who completed the 3 sessions. The in-game measure (actions accuracy) evolved positively throughout the sessions (preintervention median accuracy=75.0%, postintervention median accuracy=93.8%; see Figure 6.15), with a Wilcoxon signed-rank test showing a small trend for significant differences ($Z=1.63$, $P=.10$). Even though the differences were not statistically significant when using "in-game" measures, the same test applied to the Debriefing Accuracy show a significant increase ($Z=2.22$, $P=.03$) from session 1 (median=68.8%) to session 3 (median=100.0%). Figure 6.16 illustrates the evolution of the debriefing checklist accuracy throughout the sessions.

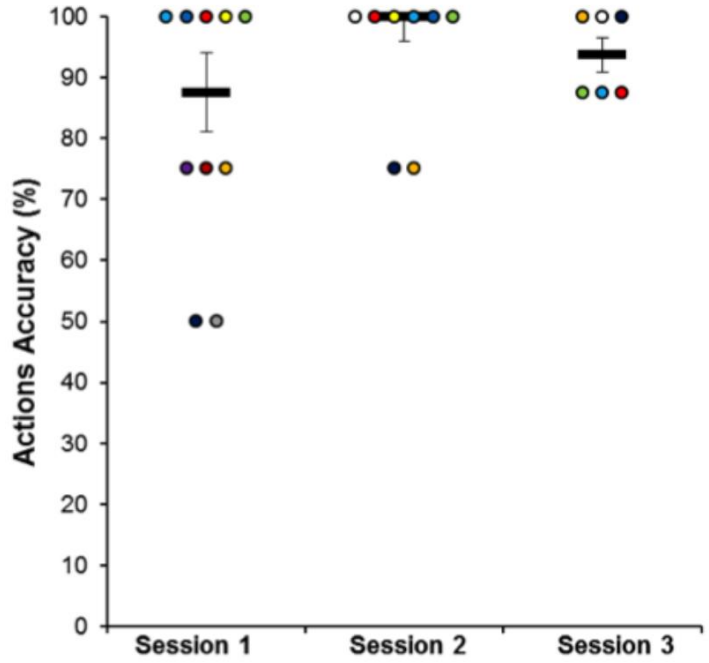

Figure 6.15 – Actions accuracy for the clinical group, measured "inside the game" throughout the intervention sessions.

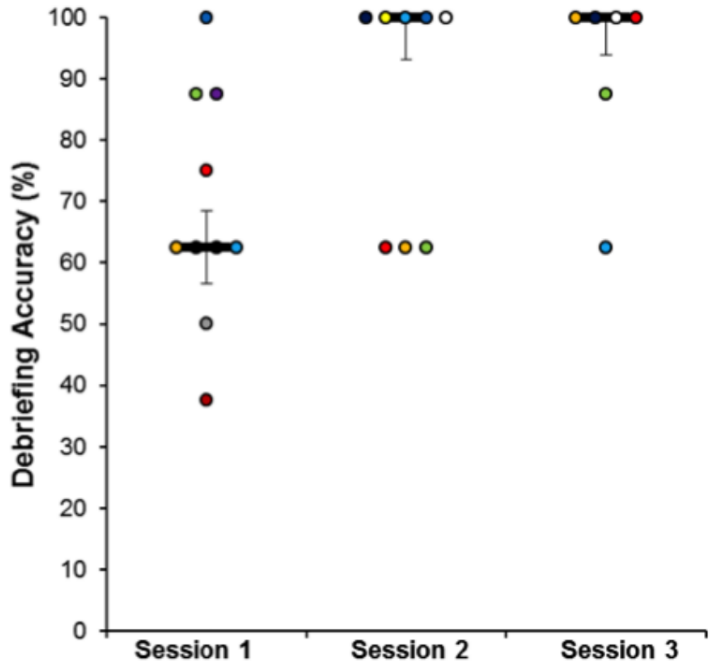

Figure 6.16 – Debriefing accuracy of the intervention group for each session.

Regarding the task duration, since the tasks increased in complexity and difficulty along the intervention, the task duration is not directly comparable. However, it is important to verify that the time to successfully complete the task did not statistically increase, even with exposure to harder levels (Figure 6.17). In session 1, the task was performed in the "easy" mode, in which players are guided step by step, from the starting position until the final location. Tasks in "easy" mode do not require as much planning as the ones in "hard" mode, but slowly introduce the player to this concept and demonstrate how buses can be used to travel between bus stations. The "hard" mode tasks, on the other hand, only tell the player where they must go to complete the task (eg, "go to the hospital"). In these tasks, players have to analyze the map to discover which bus or buses they can take to reach the final destination. Furthermore, the tasks received in sessions 1 and 2 required the player to take 1 bus, while the task from session 3 required the player to take 2 buses. A Wilcoxon signed-rank test show no difference between the easiest and simpler (first session) task and the most complex and difficult task (last session), Z=0.105, *P*=.92.

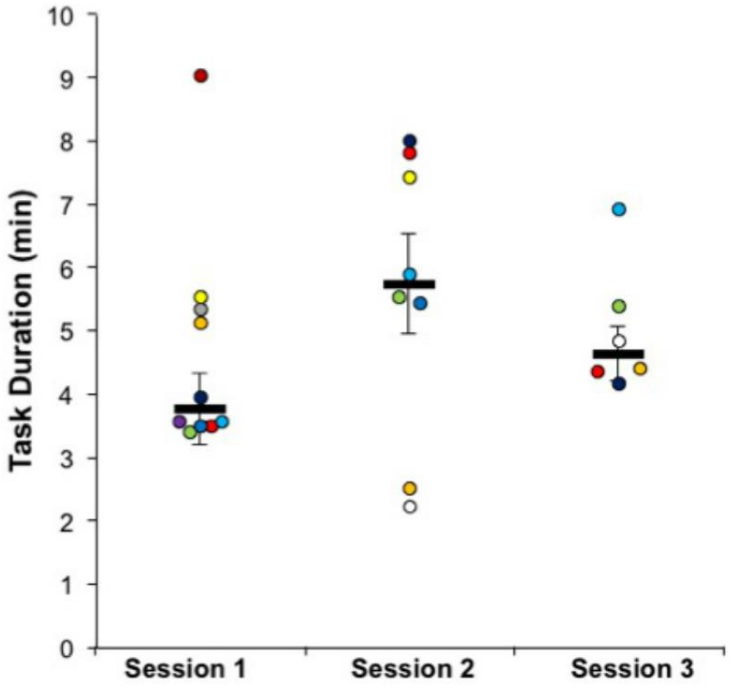

Figure 6.17 – Time taken by each participant in the clinical group to complete the task in each intervention session.

The anxiety levels decreased from the first to the last session, for both overall EDA and for the bus and streets conditions. Figure 6.18 shows the mean differences and their error. However, only the bus condition shows a strong tendency to significance ($t(5)=-2.36$, $P=.07$). The general EDA values showed a weak tendency towards an effect ($t(5)=-1.93$, $P=.11$) and the EDA values on the streets had the smaller decrease with the intervention ($t(5)=-1.48$, $P=.20$).

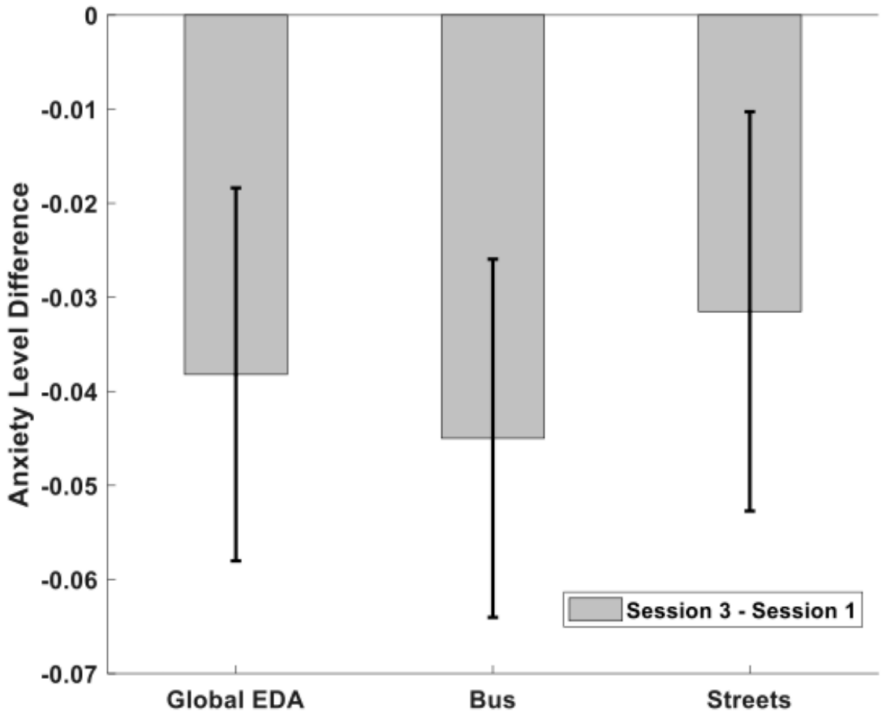

Figure 6.18 – Decrease observed in anxiety levels, measured by electrodermal activity variability, between the last session and the first.

We created heatmaps using the peaks of anxiety of each participant and separated the conditions inside the bus and outside. Figure 6.19 shows the streets scenario for each of the sessions, and Figure 6.20 shows the same metrics but for the inside the bus condition.

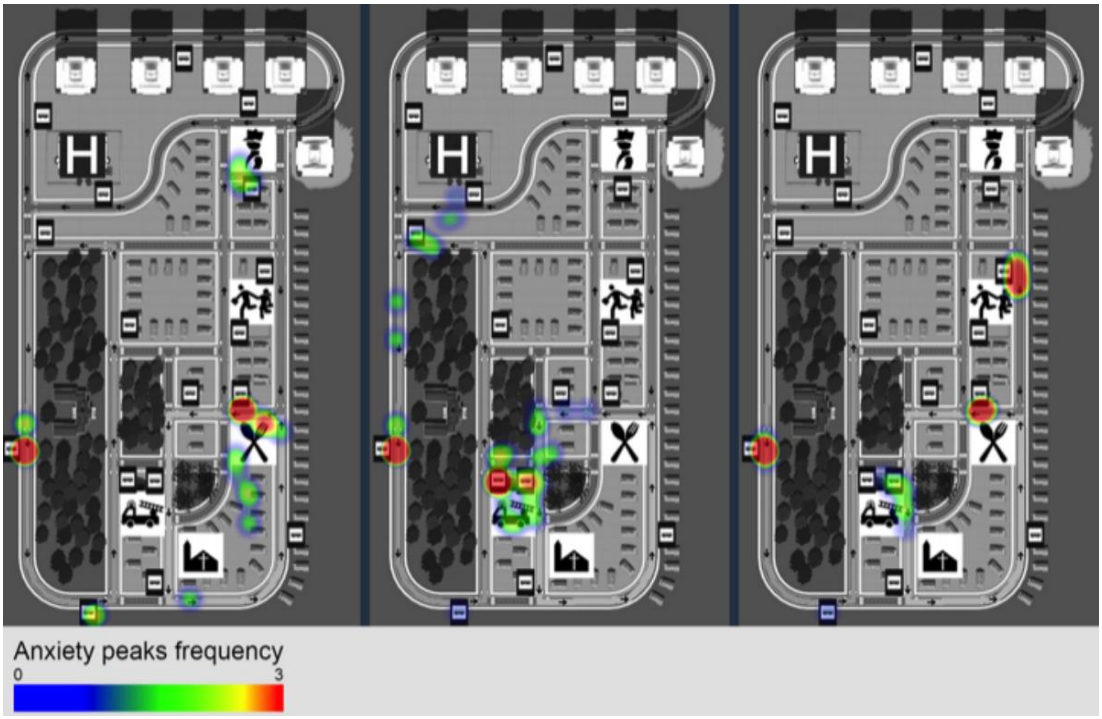

Figure 6.19 – Anxiety peaks heat map from session 1 (left) to session 3 (right), for the times the participant was not inside of the bus environment. Most of the locations represent bus stops, where participants need to make the decision of what bus to take and wait for it to arrive.

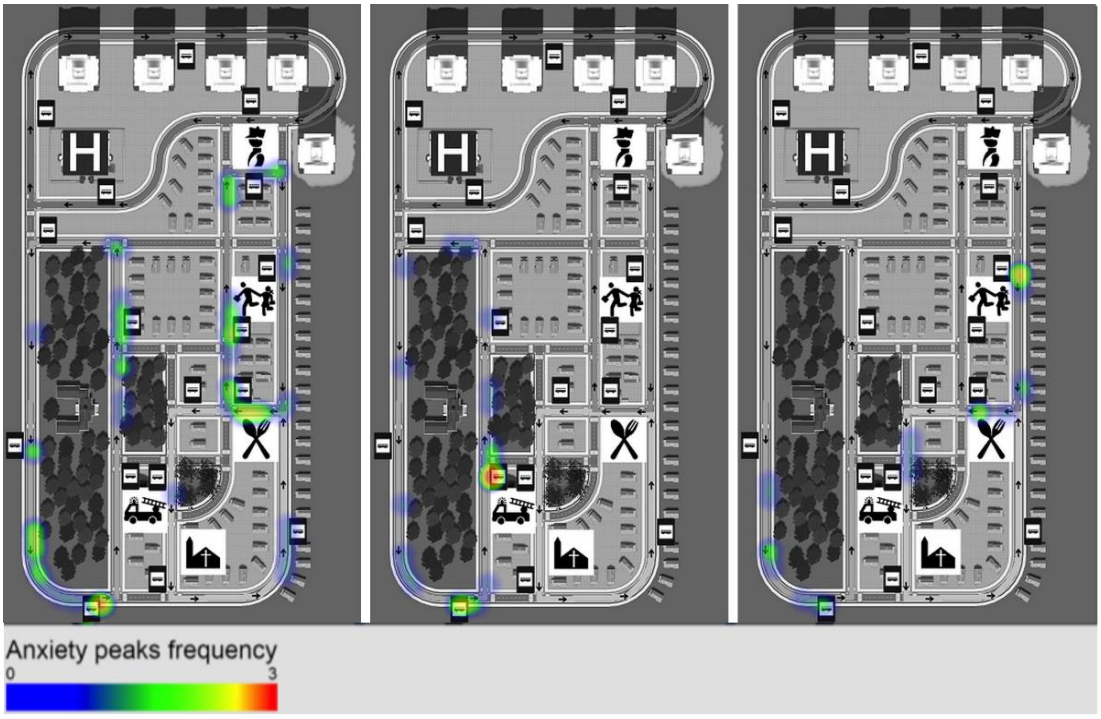

Figure 6.20 – Anxiety peaks heat map from session 1 (left) to session 3 (right), for the times the participant was inside of the bus environment. The locations are much more dispersed through the route than in the outside the bus scenario. There is a visible decrease in frequency of anxiety peaks from the first to the last session.

According to Figure 6.19, players felt most anxious in 3 different situations (Textbox 6.2).

Textbox 6.2 – Situations in which players felt anxious.

- When waiting for the bus at the bus stops (red areas near the bus stop signs)
- When planning the trip or looking for the correct bus stop in the starting areas (ie, green areas near the restaurant in session 1, the fire station in stage 2, one of the bus stops in session 3)
- When reaching or looking for the destination in the finishing areas (ie, green areas near the police station in session 1, the hospital in session 2, and the fire station in session 3).

6.3.4 Discussion

This project aimed to assess the potential of the developed serious game and here presents it as a tool for rehabilitation. The game is, to our knowledge, the first application specifically developed to teach ASD individuals to use public transportation systems. In addition, we were able to measure psychophysiological markers of anxiety, paving the way for future biofeedback applications. With only three sessions, it was possible to improve the knowledge of the participants regarding the norms of the bus-taking process and to reduce the anxiety levels felt by the participants during that process.

The impacts of a learning tool with this purpose are broad since it trains executive functions and might increase the autonomy of the users, providing them with a new way of moving through a city. It is also a way to make cities more inclusive, providing people with special needs ways to successfully use this type of public service.

Some studies have been conducted using VR training for ASD, usually focusing on training other skills. Most interventional approaches target social performance training (Kandalaft et al., 2013; Stichter et al., 2014) or job interviewing (Smith et al., 2014). Gaming platforms (Simões et al., 2014b) and brain-computer interfaces (Simões et al., 2012) were also suggested in the literature for autism training, but without validation with patients. Although these are important targets of intervention, our work focuses on a more specific task of executive function that is relevant for the needs of daily life. Our pilot validation study aimed to assess

not only the efficacy of the application, but also the acceptance of the solution with this specific clinical population. Few studies perform fully immersive interventions, and the difficulties of combining them with biofeedback create a technology apparatus that could potentially be disruptive to the participants. The 4 drop-outs during the intervention occurred exclusively due to scheduling issues. No patient dropped the study due to discomfort or raised any difficulty in using the setup. There were specific cases where the Oculus device was not used, but all of those were related to vision impairments, not to lack of tolerance from the user.

The baseline comparison with the control group was clear in identifying the impairments in the clinical group. Both the debriefing of the procedure for taking the bus and the in-game actions showed statistically different results between groups, proving the validity of the rehabilitation target and confirming the capacity of the game to, by itself, identify the deficits of target participants in the process of taking the bus. Additionally, the time needed to complete the task was increased for the clinical group. Despite having mean anxiety levels above the control group, this difference was not significant, perhaps due to the small statistical power resulting from a small group of participants, as well as the implementation of biofeedback, which decreases differences between groups.

The intervention was successful in increasing the accuracy of the process description during the debriefing, showing a statistically significant improvement in the theoretical knowledge of the process, which was the main outcome measure. When evaluated inside the game by the user actions, the increase was not statistically significant, but showed a tendency that we believe additional sessions or a larger intervention group would further confirm. It was also successful in decreasing the anxiety felt by participants, especially inside the bus. By using heat maps to represent the anxiety peaks recorded, it was possible to understand that participants with ASD felt more anxious in bus stops and near the starting and finishing areas. This led to the conclusion that, when outside the buses, players felt most anxious when planning the trip, when looking for the bus stop, when waiting for the bus, and when looking for the final destination. Inside the bus, we observed a desensitization to stress throughout the sessions, with a final session showing fewer peaks of EDA activity.

Despite the increase of task complexity and difficulty across sessions, the time duration to complete the task did not increase, suggesting a learning effect and adaptation to the serious game.

By using the game as a therapeutic intervention tool, in just three sessions it was possible to improve the general efficiency of participants and expose them to peculiar scenarios in which they could train their planning skills. More importantly, it was possible to nearly extinguish the anxiety felt in bus environments and teach the bus-taking norms necessary for the autonomous use of buses for transportation, both in theoretical and practical contexts. Future studies should conduct randomized controlled trials, with larger intervention groups, to replicate the findings and extend them to other clinical populations with executive function deficits and lack of autonomy.

6.4 Chapter Discussion

For the virtual rehabilitation part of this thesis, we created a virtual reality lab for performing fully-immersive virtual reality experiments with ASD patients. We verified that, in the literature, despite the consensus that virtual reality is a suitable and promising setting for studying and training social skills in ASD, no study conducted a fair comparison between real and virtual environments. So, we created a 3D representation of the lab and tested a simple social measure in a real environment and in its virtual replica. The results confirmed that we are able to reproduce, with high levels of accuracy, the social behavior observed in the real world inside the VR environment. This is a basilar study to support the applicability of VR studies in ASD.

Furthermore, and despite some evidence showing that higher levels of immersion produce better outcomes in for computerized ASD interventions (Miller and Bugnariu, 2016), most studies claim the use of "virtual reality" when performing simple computerized tasks on tablets or computers (Lorenzo et al., 2016). With our intervention game to training ASD individuals to use the bus, we were able to improve participants' knowledge on the rules to use the bus, verified inside the game (by automatically analyzing the actions of the players) and outside the game, through debriefing. Furthermore, we were able to reduce the anxiety levels manifested by the participants during the task throughout the sessions, with some participants (and parents) reporting in the end of the intervention sessions that would then be willing to use the bus autonomously. We confirmed through an informal follow up that at least one case actually started to use buses as a consequence of the training sessions with the serious game.

The variability of symptomatology and specificities of each ASD patient poses several challenges on the development of such interventions. One way to deal with it is letting the game adapt to the patient needs and skills (Bartoli et al., 2014; Whyte et al., 2015). To provide that kind of adaptation, the implemented biofeedback system played an important role. The seemingly change in game noise and disturbing elements based on the stress level felt by the participants provided a smoother interaction without disrupting the experience. Furthermore, the customization of the game with several levels with different difficulty and complexity allows the users to incrementally progress based on their skills at the time. The integration with the **neurohab** platform (Simões et al., 2014b - Appendix IV) provides progress

monitoring for the therapists and caregivers, as well as an automatic adjustment of the difficulty levels or the implementation of pre-defined training plans.

We believe that this integrative view of patients, caregivers, therapists and technology in the tackling of the deficits of the patient might significantly improve the quality of interventions offered to this population. The costs of intensive training are too expensive for several families to support and is, most of the times, only available in large urban centers. Remote families struggle to provide the patients at their care intensive therapeutic training. For such families, platforms like **neurohab** can be a solution that provide them access to therapies that would be, otherwise, impossible to have. Future studies will need to further validate the efficacy of these interventions, through phase II and III clinical trials.

Chapter 7

General Discussion and Future Work

This thesis aimed at the understanding of social deficits in ASD and their rehabilitation, from a clinical informatics perspective. Our approach for tackling ASD social deficits is supported on an integrative solution between knowledge derived from neuroimaging and the development of virtual rehabilitation techniques, where virtual reality technology is used to mimic social scenarios and interactive situations and the neuroscience inspired neuroimaging technology provides real-time information about the ongoing brain activity, allowing the patient to endogenously manipulate his/her brain activity in that social context.

Firstly, we investigated the known social deficits of ASD. One of the major difficulties recognized in the literature is the identification of the direct neural underpinnings of processing of facial expressions in others. Our systematic review (Monteiro et al., 2017) showed that the state-of-the-art regarding EEG studies on facial expression processing in ASD present inconsistent findings, with most studies using static images of facial expressions, contrasted with neutral expressions. We argue that most social nuances are anchored on the dynamism of facial expressions, which is lost in the experimental paradigms based on static pictures. Hence, we implemented a dynamic facial expression morphing paradigm using virtual avatars, in which we contrasted the morphing of the facial expression with the neutral expression (Simões et al., 2018b). This stringent contrast enabled us to better recreate social interaction situations and separate the processing of the facial expression from the processing of the face itself. Most studies in the literature are not able to isolate these two processes because the contrasts are usually made against a blank baseline. We previously had conducted a pilot study with EEG and virtual reality that showed the feasibility of such an approach (Simões et al., 2014a).

The ecology introduced in the experimental design, along with the restrictive and focused experimental contrast, allowed us to identify two event-related components that responded specifically to the expression-related features of the face, the first around 300 ms after the stimulus onset and the second around 600 ms. Sources analysis of those two components identified a group difference in the right Precuneus, with the ASD group showing a higher

recruitment of the mentioned region. Because we used a stringent contrast in the visual stimulation task, we expected the core processing of the face (irrespective of emotional aspects) to have less weight than the emotional perspective-taking aspects task. The precuneus is one of the core regions present in the perspective taking network (Healey and Grossman, 2018), for both cognitive and affective perspective taking networks (Abu-Akel and Shamay-Tsoory, 2011). Although the link between the precuneus and its role in facial expressions processing had already been shown by some studies (Saarimäki et al., 2016; An et al., 2018), ours was the first one, to the best of our knowledge, to identify its over-recruitment by the ASD population in a social cognition task.

From the standpoint of the analysis of the visual perception of facial expressions, we then studied the mental imagery of facial expressions in ASD. Mental rehearsal is very important for action perception cycles, in particular in the context emotional face recognition. Our task combined mental imagery, perspective taking and theory of mind, since the participant is asked to recreate an expression of another. We found that the ERP elicited by the imagery cue did indeed reveal that source differences were very similar as compared to the ERP of the FE stimuli, with the precuneus showing higher activation for the ASD group. Moreover, the source analysis conducted on the sub-bands of the frequency spectrum showed that, for the theta band, the same region presented a higher activation pattern for the ASD group. The right Precuneus belongs to task-active networks (Yang et al., 2015) that are also active during imagery (Cavanna and Trimble, 2006). Since visual perspective taking and theory of mind skills are impaired in ASD (Hamilton et al., 2009; David et al., 2010), we believe that ASD participants needed higher recruitment of the right precuneus as a compensatory mechanism for the mental imagery of the other's facial expressions.

We assessed the feasibility of exploring the over-recruitment shown in this region as a biomarker linked to the facial expression deficit. We extracted a group of features (from the time-frequency domain and from the non-linear domain) from the right center-parietal EEG electrodes (overlapping the right Precuneus region) that we used to train two classifiers to distinguish between ASD individuals and controls. We verified that we were able to distinguish the groups with an accuracy of 81% using only 15 features from the mental imagery time segments. When trained the same classifiers using features extracted from EEG of the neutral periods, the accuracy was significantly lower (around 73%), which reinforced the facial expression related specificity of the differences extracted by the EEG features. Furthermore, we found that non-linear features captured particularly well the differences for the theta band,

while time-frequency features took better advantage of the differences for the high-beta and gamma bands. This result confirmed that nonlinear characteristics of EEG signals contain information that can be explored for ASD characterization, especially if combined with machine learning algorithms (Bosl et al., 2017, 2018).

The potential applicability range of quantifiable measures associated with specific social processing deficits is wide. One of the main challenges encountered by current clinical trials of innovative solutions is the difficulty to quantify its effects, relying most of the times on neuropsychological evaluation scales, which have high variability, low sensitivity and are often biased (Casaletto and Heaton, 2017; Fernández and Abe, 2018). Therefore, the discovery of quantifiable neurophysiological measures associated with specific symptomatology of ASD could be explored to aid diagnosis, predict developmental trajectories of monitor treatment outcomes (Jeste et al., 2015). The biomarker we identified associated with this compensatory neural correlate in ASD could possibly be explored for monitoring treatment outcomes that target facial expression processing deficits, after further validation studies to ascertain its level of specificity and reproducibility.

We then advanced to the rehabilitation arm of our objectives. With the focus on the facial expression deficits, we implemented a real-time fMRI neurofeedback intervention based on the same mental imagery of facial expressions mechanism, targeting the posterior Superior Temporal Sulcus for its core role in the social interaction network (Fox et al., 2009) and its reported impairment in ASD (Saitovitch et al., 2012; Alaerts et al., 2013; Cheng et al., 2015). Our primary results showed the BOLD activity in the pSTS region is successfully manipulated through the mental imagery strategy (Direito et al., 2019). With that, we implemented a phase IIa clinical trial consisting of 5 neurofeedback sessions, where we were able to observe improvements in several neuropsychological measures, including emotion recognition, immediately after the intervention. These improvements were retained after 6 months (Appendix II).

Despite the need for phase III clinical trials to fully assess the behavioral outcomes of this intervention, the phase IIa trial showed promising indicators regarding the success of this strategy. Therefore, with the goal of increasing the application range of this intervention, we focused our attention in transferring the intervention to an EEG setting, which would enable

the creation of a system for personalized domiciliary training, without the cost and inflexibility constraints imposed by an fMRI setup (Sarracanie et al., 2015).

We explored several features extracted from the EEG signal and tested their direct correlation with the BOLD signal of interest (Simoes et al., 2015). The obtained correlations were statistically significant for some features but still insufficient to provide a reliable signature of the pSTS BOLD signal that could be used in a practical application. Hence, we explored the addition of machine learning algorithms to predict the BOLD activity based on the EEG features. We followed and extended the approach of the only existing study in the literature (Meir-Hasson et al., 2014) – to the best of our knowledge – and analyzed the effect of adding different features (at the scalp and source level) and considered different approaches for dealing with the HRF delay. Our results showed that the approach followed in literature overestimated the prediction accuracy by adding a linear dependence in the upsampling of the BOLD signal, which generates a dependency (autocorrelation) between timepoints exploited by the regressors. We show that our proposed features (especially the nonlinear ones) improve the prediction accuracy of the models and the convolution of the predictors with multiple HRFs with variable peak latencies provide a more robust way to deal with the BOLD hemodynamic delay, since it explores the inter and intra-subject HRF variability. Furthermore, we explored several approaches of converting the signal into the source space, which also showed promising results and confirmed the benefits of the exploration of more features beyond the power of the signal to increase the models' accuracy.

When looking for the generalization of the models to different runs or sessions, the obtained prediction accuracies were not high enough to allow the transfer of the intervention protocol from fMRI to an EEG application. As we verified, the challenge of transferring fMRI to EEG is high, due to the intrinsic different characteristics of both signals. One may argue that the source approach is valid even without high but significant correlations with the BOLD signal, because of those intrinsic differences. Manipulating a signal localized at the target region will necessarily affect the neural activity of that region, notwithstanding the consequential BOLD variation. Future studies should focus on the integration of data from multiple sessions and multiple subjects in the trained models to increase the diversity of the extracted patterns and, hopefully, help the generalization process. To do so, larger EEG-fMRI datasets will be needed, which will also allow to address this problem with different approaches, like the use of deep learning methods.

Finally, following the logic of clinical informatics approaches, we investigated the application of virtual reality for rehabilitation in parallel with the neurofeedback approach. Our objective was to validate that both approaches are useful independently, so that we can, in the future, merge them into one final solution that incorporates neurofeedback training inside a serious game for virtual rehabilitation.

We created a virtual reality lab in the Pediatrics' Hospital of Coimbra and a 3D version of the same lab, producing the ideal setup to assess virtual reality feasibility with real vs virtual environment comparisons. With that, we defined the interpersonal distance as metric for performing a quantitative comparison because it represents a validated metric for social interaction that has been shown impaired in ASD (Gessaroli et al., 2013; Lough et al., 2015; Perry et al., 2015a; Asada et al., 2016) and it could be easily measured in both environments with high levels of accuracy. We first verify the abnormal distance pattern for the ASD group, with a dual characteristic: some individuals chose closer distances, while others opted for distances much higher than the control group. This pattern was replicated in the virtual environment, with high correlation levels, thus showing the VR setup can be effectively used for assessment and rehabilitation of social skills in ASD.

Interestingly, we found lack of isometry between environments for the control group, with a regression slope much above 1, suggesting rescaling. The social nuances are difficult to reproduce in full or to be perceived in the virtual environment, leading to a break in isometry. Virtual avatars are realistic but limited in their expressiveness and overall non-verbal communication. We believe this rigidity influenced the behavior of the control group, but not the ASD group, whose regression slope was closer to 1, evidencing that individuals from the ASD group also do not use the above mentioned social nuances in their social space regulation in the real world (Pellicano, 2013). The dissociation between the scales of virtual and real world in control participants may be due to the so-called "uncanny valley effect". This may lead to the observation that a step in the real world is almost doubled in virtual environments, as observed by the control group anisometric pattern.

Our findings in this study supported the idea of using virtual reality systems to study and rehabilitate social deficits in ASD (Strickland, 1997; Goodwin, 2008; Bellani et al., 2011; Parsons and Cobb, 2011; Kandalaft et al., 2013; Didehbani et al., 2016). Thus, we implemented our own virtual reality rehabilitation serious game to train ASD patients to perform a daily

activity they found very challenging: taking a bus. This type of task, if successful, aids the patients in their autonomous living. Moreover, it includes several social interaction steps in the process (buy bus tickets, validate them in the bus, picking a place to sit, among others). We combined the virtual reality game with a biofeedback system, providing the automatic adjustment of the environment noise to the level of stress measured in the patient. Our results showed that in just three sessions it was possible to improve the general efficiency of participants and expose them to peculiar scenarios in which they could train their planning skills. Moreover, we were able to nearly extinguish the anxiety felt in bus environments and teach the bus-taking norms necessary for the autonomous use of buses for transportation, both in theoretical and practical contexts.

In our view, one must approach rehabilitation in ASD with individualized and integrative clinical informatics solutions. We developed the **Neurohab** platform (Simões et al., 2014b and Appendix IV) with the flexibility to provide such a kind of solution, and performed feasibility studies on the independent neurorehabilitation branches (neurofeedback and virtual rehabilitation). In future work we will integrate this vision, with systems combining task-related neurofeedback training within virtual rehabilitation serious games for combined neuro-behavioral training, in both home-based and clinical settings. The search for neuroscientific validity before dissemination is of utmost importance in this area. As mentioned in the State of the art chapter, several EEG-based neurofeedback interventions have been used in the past for a few decades, but without supporting scientific evidence (Holtmann et al., 2011; Micoulaud-Franchi et al., 2015). Therefore, we believe other interventions should follow the same process as ours: start from an initial scientific neuroimaging probe and validate it with clinical trials before performing its broad dissemination. We also follow this approach in other studies, where we integrated a BCI joint-attention task with a virtual reality environment and performed a clinical trial to test its feasibility (Amaral et al., 2018). To do so, we first looked into the basic neural signature used by the system (Amaral et al., 2015) and tested the best setup to conduct the trial (Amaral et al., 2017) as well as the improvement of the machine learning algorithms behind the BCI system (Simões et al., 2019b). Despite its relation to this work and topic, this study falls out the scope of this doctoral thesis and is not detailed here.

The integration of neurofeedback tasks within serious games increases the level of engagement and entertainment during the interventions – due to gamification strategies –, which potentiates acceptance and adherence (Kapp, 2012; Lieberoth, 2015). The domiciliary and remote aspects of those solutions will improve accessibility for patients with difficult access

to urban areas, where most specialized rehabilitation treatments are conducted. Furthermore, by providing a way for patients conducting individualized training on their own as complement of rehabilitation sessions, we reduce the number of specialized human labor hours needed for intensive rehabilitation training, thus reducing the costs for these interventions, which currently are extremely high (Ganz, 2007; Amendah et al., 2011; Buescher et al., 2014). The reduction of intervention costs makes virtual rehabilitation an important response to the societal change we face with the growing prevalence of this disorder. Furthermore, this kind of serious games can be extended and adapted to other disorders, as we did for the Huntington disease (Júlio et al., 2019), or even healthy or cognitively impaired ageing (Pinto et al., 2019; Simões et al., 2019c, 2019a). This thesis paves the way for the neuroscientific-based clinical informatics systems for rehabilitation of ASD social deficits and promotion of independent living.

REFERENCES

Abrahams BS, Geschwind DH (2008) Advances in autism genetics: On the threshold of a new neurobiology. Nat Rev Genet 9:341–355. doi: 10.1038/nrg2346.

Abreu R, Leal A, Figueiredo P (2018) EEG-Informed fMRI: A Review of Data Analysis Methods. Front Hum Neurosci 12:1–23. doi: 10.3389/fnhum.2018.00029.

Abreu R, Leite M, Jorge J, Grouiller F, van der Zwaag W, Leal A, Figueiredo P (2016) Ballistocardiogram artifact correction taking into account physiological signal preservation in simultaneous EEG-fMRI. Neuroimage 135:45–63. doi: 10.1016/j.neuroimage.2016.03.034.

Abreu R, Nunes S, Leal A, Figueiredo P (2017) Physiological noise correction using ECG-derived respiratory signals for enhanced mapping of spontaneous neuronal activity with simultaneous EEG-fMRI. Neuroimage 154:115–127. doi: 10.1016/J.NEUROIMAGE.2016.08.008.

Abtahi F (2011) Feasibility of fetal EEG recording.

Abu-Akel A, Shamay-Tsoory S (2011) Neuroanatomical and neurochemical bases of theory of mind. Neuropsychologia 49:2971–2984. doi: 10.1016/j.neuropsychologia.2011.07.012.

Adamson LB, Bakeman R, Suma K, Robins DL (2019) An Expanded View of Joint Attention: Skill, Engagement, and Language in Typical Development and Autism. Child Dev 90:e1–e18. doi: 10.1111/cdev.12973.

Aguirre GK, Zarahn E, D'Esposito M (1998) The variability of human, BOLD hemodynamic responses. Neuroimage 8:360–369. doi: 10.1006/nimg.1998.0369.

Ahlfors SP, Han J, Lin F-H, Witzel T, Belliveau JW, Hämäläinen MS, Halgren E (2009) Cancellation of EEG and MEG signals generated by extended and distributed sources. Hum Brain Mapp 71:NA-NA. doi: 10.1002/hbm.20851.

Akechi H, Senju A, Kikuchi Y, Tojo Y, Osanai H, Hasegawa T (2010) The effect of gaze direction on the processing of facial expressions in children with autism spectrum disorder: An ERP study. Neuropsychologia 48:2841–2851. doi: 10.1016/j.neuropsychologia.2010.05.026.

Alaerts K, Swinnen SP, Wenderoth N (2016) Sex differences in autism: A resting-state fMRI investigation of functional brain connectivity in males and females. Soc Cogn Affect Neurosci 11:1002–1016. doi: 10.1093/scan/nsw027.

Alaerts K, Woolley DG, Steyaert J, Di Martino A, Swinnen SP, Wenderoth N (2013) Underconnectivity of the superior temporal sulcus predicts emotion recognition deficits in autism. Soc Cogn Affect Neurosci 9:1589–1600. doi: 10.1093/scan/nst156.

Allen PJ, Josephs O, Turner R (2000) A method for removing imaging artifact from continuous EEG recorded during functional MRI. Neuroimage 12:230–239. doi: 10.1006/nimg.2000.0599.

Amaral C, Mouga S, Simões M, Pereira HC, Bernardino I, Quental H, Playle R, McNamara R, Oliveira G, Castelo-Branco M (2018) A feasibility clinical trial to improve social attention in Autistic Spectrum Disorder (ASD) using a brain computer interface. Front Neurosci 12:1–13. doi: 10.3389/fnins.2018.00477.

Amaral C, Simões M, Souga S, Andrade J, Castelo-Branco M (2017) A novel Brain Computer Interface for classification of social joint attention in autism and comparison of 3 experimental setups: A feasibility study. J Neurosci Methods 290:105–115. doi: 10.1016/j.jneumeth.2017.07.029.

Amaral CP, Simões M a., Castelo-Branco MS (2015) Neural Signals Evoked by Stimuli of Increasing Social Scene Complexity Are Detectable at the Single-Trial Level and Right Lateralized. PLoS One 10:e0121970. doi: 10.1371/journal.pone.0121970.

Amendah D, Grosse SD, Peacock G, Mandell DS (2011) The economic costs of autism: A review. In: Autism Spectrum Disorders (Amaral D, Geschwind D, Dawson G, eds), pp 1347–1360. Oxford: Oxford University Press.

American Psychiatric Association (2013) Autism Spectrum Disorder. In: Diagnostic and Statistical Manual of Mental Disorders. Washington, DC: American Psychiatric Association.

An S, Han X, Wu B, Shi Z, Marks M, Wang S, Wu X, Han S (2018) Neural activation in response to the two sides of emotion. Neurosci Lett 684:140–144. doi: 10.1016/j.neulet.2018.07.011.

Anagnostou E, Taylor MJ (2011) Review of neuroimaging in autism spectrum disorders: What have we learned and where we go from here. Mol Autism 2:4. doi: 10.1186/2040-2392-2-4.

Andrade J, Cecílio J, Simões M, Sales F, Castelo-Branco M (2017) Separability of motor imagery of the self from interpretation of motor intentions of others at the single trial level: an EEG study. J Neuroeng Rehabil 14:63. doi: 10.1186/s12984-017-0276-4.

Aoki Y, Cortese S, Tansella M (2015) Neural bases of atypical emotional face processing in autism: A meta-analysis of fMRI studies. World J Biol Psychiatry 16:291–300. doi: 10.3109/15622975.2014.957719.

Apicella F, Sicca F, Federico RR, Campatelli G, Muratori F (2013) Fusiform Gyrus responses to neutral and emotional faces in children with Autism Spectrum Disorders: A High Density ERP study. Behav Brain Res 251:155–162. doi: 10.1016/j.bbr.2012.10.040.

Arns M, Batail J-M, Bioulac S, Congedo M, Daudet C, Drapier D, Fovet T, Jardri R, Le-Van-Quyen M, Lotte F, Mehler D, Micoulaud-Franchi J -a., Purper-Ouakil D, Vialatte F (2017) Neurofeedback: One of today's techniques in psychiatry? Encephale 43:135–145. doi: 10.1016/j.encep.2016.11.003.

Asada K, Tojo Y, Osanai H, Saito A, Hasegawa T, Kumagaya S (2016) Reduced personal space in individuals with Autism spectrum disorder. PLoS One 11:1–11. doi: 10.1371/journal.pone.0146306.

Assecondi S, Hallez H, Staelens S, Bianchi AM, Huiskamp GM, Lemahieu I (2009) Removal of the ballistocardiographic artifact from EEG–fMRI data: a canonical correlation approach. Phys Med Biol 54:1673–1689. doi: 10.1088/0031-9155/54/6/018.

Awan FG, Saleem O, Kiran A (2018) Recent trends and advances in solving the inverse problem for EEG source localization. Inverse Probl Sci Eng 0:1–16. doi: 10.1080/17415977.2018.1490279.

Bai X, He B (2005) On the estimation of the number of dipole sources in EEG source

localization. Clin Neurophysiol 116:2037–2043. doi: 10.1016/j.clinph.2005.06.001.

Bailenson JN, Blascovich J, Beall AC, Loomis JM (2003) Interpersonal distance in immersive virtual environments. Pers Soc Psychol Bull 29:819–833. doi: 10.1177/0146167203029007002.

Baio J et al. (2018) Prevalence of Autism Spectrum Disorder Among Children Aged 8 Years — Autism and Developmental Disabilities Monitoring Network, 11 Sites, United States, 2014. MMWR Surveill Summ 67:1–23. doi: 10.15585/mmwr.ss6706a1.

Balconi M, Grippa E, Vanutelli ME (2015) What hemodynamic (fNIRS), electrophysiological (EEG) and autonomic integrated measures can tell us about emotional processing. Brain Cogn 95:67–76. doi: 10.1016/j.bandc.2015.02.001.

Balconi M, Lucchiari C (2006) EEG correlates (event-related desynchronization) of emotional face elaboration: A temporal analysis. Neurosci Lett 392:118–123. doi: 10.1016/j.neulet.2005.09.004.

Bandettini PA, Wong EC, Hinks RS, Tikofsky RS, Hyde JS (1992) Time course EPI during task activation. Magn Res Med 25:390–397.

Banitalebi A, Setarehdan SK, Hossein-Zadeh GA (2009) A technique based on chaos for brain computer interfacing. In: 2009 14th International CSI Computer Conference, pp 464–469. IEEE. doi: 10.1109/CSICC.2009.5349623.

Barak B, Feng G (2016) Neurobiology of social behavior abnormalities in autism and Williams syndrome. Nat Neurosci 19:647–655. doi: 10.1038/nn.4276.

Baron-Cohen S, Wheelwright S, Skinner R, Martin J, Clubley E (2001) The Autism Spectrum Quotient : Evidence from Asperger syndrome/high functioning autism, males and females, scientists and mathematicians. J Autism Dev Disord 31:5–17. doi: 10.1023/A:1005653411471.

Bartoli L, Garzotto F, Gelsomini M, Oliveto L, Valoriani M (2014) Designing and evaluating touchless playful interaction for ASD children. In: Proceedings of the 2014 conference on Interaction design and children - IDC '14, pp 17–26. New York, New York, USA: ACM Press. doi: 10.1145/2593968.2593976.

Batty M, Meaux E, Wittemeyer K, Rogé B, Taylor MJ (2011) Early processing of emotional

faces in children with autism: An event-related potential study. J Exp Child Psychol 109:430–444. doi: 10.1016/j.jecp.2011.02.001.

Batty M, Taylor MJ (2003) Early processing of the six basic facial emotional expressions. Cogn Brain Res 17:613–620. doi: 10.1016/S0926-6410(03)00174-5.

Bauer EP, Paz R, Pare D (2007) Gamma Oscillations Coordinate Amygdalo-Rhinal Interactions during Learning. J Neurosci 27:9369–9379. doi: 10.1523/JNEUROSCI.2153-07.2007.

Bauman ML (2010) Medical comorbidities in autism: Challenges to diagnosis and treatment. Neurotherapeutics 7:320–327. doi: 10.1016/j.nurt.2010.06.001.

Bäuml KH, Pastötter B, Hanslmayr S (2010) Binding and inhibition in episodic memory-Cognitive, emotional, and neural processes. Neurosci Biobehav Rev 34:1047–1054. doi: 10.1016/j.neubiorev.2009.04.005.

Bayless SJ, Glover M, Taylor MJ, Itier RJ (2011) Is it in the eyes? Dissociating the role of emotion and perceptual features of emotionally expressive faces in modulating orienting to eye gaze. Vis cogn 19:483–510. doi: 10.1080/13506285.2011.552895.

Beckmann CF, Jenkinson M, Smith SM (2003) General multilevel linear modeling for group analysis in FMRI. Neuroimage 20:1052–1063. doi: 10.1016/S1053-8119(03)00435-X.

Belaoucha B (2017) Using diffusion MR information to reconstruct networks of brain activations from MEG and EEG measurements.

Bell AJ, Sejnowski TJ (1995) An Information-Maximization Approach to Blind Separation and Blind Deconvolution. Neural Comput 7:1129–1159. doi: 10.1162/neco.1995.7.6.1129.

Bellani M, Fornasari L, Chittaro L, Brambilla P (2011) Virtual reality in autism: state of the art. Epidemiol Psychiatr Sci 20:235–238.

Belliveau J, Kennedy D, McKinstry R, Buchbinder B, Weisskoff R, Cohen M, Vevea J, Brady T, Rosen B (1991) Functional mapping of the human visual cortex by magnetic resonance imaging. Science (80-) 254:716–719. doi: 10.1126/science.1948051.

Benbow AA, Anderson PL (2018) A meta-analytic examination of attrition in virtual reality

exposure therapy for anxiety disorders. J Anxiety Disord:0–1. doi: 10.1016/j.janxdis.2018.06.006.

Benuzzi F, Pugnaghi M, Meletti S, Lui F, Serafini M, Baraldi P, Nichelli P (2007) Processing the socially relevant parts of faces. Brain Res Bull 74:344–356. doi: 10.1016/j.brainresbull.2007.07.010.

Berger A (2002) Magnetic Resonance Scanner: How does it work? Magn Reson Imaging Clin N Am 10:303–324. doi: 10.1016/S1064-9689(01)00004-6.

Berger H (1929) Über das Elektrenkephalogramm des Menschen. Arch Psychiatr Nervenkr 87:527–570. doi: 10.1007/BF01797193.

Biessmann F, Plis S, Meinecke FC, Eichele T, Muller K-R (2011) Analysis of Multimodal Neuroimaging Data. IEEE Rev Biomed Eng 4:26–58. doi: 10.1109/RBME.2011.2170675.

Billeci L, Narzisi A, Tonacci A, Sbriscia-Fioretti B, Serasini L, Fulceri F, Apicella F, Sicca F, Calderoni S, Muratori F (2017) An integrated EEG and eye-tracking approach for the study of responding and initiating joint attention in Autism Spectrum Disorders. Sci Rep 7:1–13. doi: 10.1038/s41598-017-13053-4.

Bimber O (2014) Thinking Virtual. Computer (Long Beach Calif) 47:22–23. doi: 10.1109/MC.2014.196.

Bishop-Fitzpatrick L, Mazefsky CA, Eack SM, Minshew NJ (2017) Correlates of social functioning in autism spectrum disorder: The role of social cognition. Res Autism Spectr Disord 35:25–34. doi: 10.1016/j.rasd.2016.11.013.

Blascovich J (2002) Social Influence within Immersive Virtual Environments. In, pp 127–145. doi: 10.1007/978-1-4471-0277-9_8.

Blascovich J, Loomis J, Beall AC, Swinth KR, Hoyt CL, Bailenson JN (2002) TARGET ARTICLE: Immersive Virtual Environment Technology as a Methodological Tool for Social Psychology. Psychol Inq 13:103–124. doi: 10.1207/S15327965PLI1302_01.

Blau VC, Maurer U, Tottenham N, McCandliss BD (2007) The face-specific N170 component is modulated by emotional facial expression. Behav Brain Funct 3:7. doi: 10.1186/1744-9081-3-7.

Bogovic A, Mihanovic M, Jokic-Begic N, Svagelj A (2014) Personal Space of Male War Veterans With Posttraumatic Stress Disorder. Environ Behav 46:929–945. doi: 10.1177/0013916513477653.

Bohlander AJ, Orlich F, Varley CK (2012) Social skills training for children with autism. Pediatr Clin North Am 59:165–174. doi: 10.1016/j.pcl.2011.10.001.

Bölte S, Feineis-Matthews S, Leber S, Dierks T, Hubl D, Poustka F (2002) The development and evaluation of a computer-based program to test and to teach the recognition of facial affect. Int J Circumpolar Health 61 Suppl 2:61–68.

Bosl W, Tierney A, Tager-Flusberg H, Nelson C (2011) EEG complexity as a biomarker for autism spectrum disorder risk. BMC Med 9. doi: 10.1186/1741-7015-9-18.

Bosl WJ, Loddenkemper T, Nelson CA (2017) Nonlinear EEG biomarker profiles for autism and absence epilepsy. Neuropsychiatr Electrophysiol 3:1. doi: 10.1186/s40810-017-0023-x.

Bosl WJ, Tager-Flusberg H, Nelson CA (2018) EEG Analytics for Early Detection of Autism Spectrum Disorder: A data-driven approach. Sci Rep 8:1–20. doi: 10.1038/s41598-018-24318-x.

Brame R, Mazerolle P, Piquero A, Paternoster R (1998) Using the Correct Statistical Test for the Equality of Regression Coefficients. Criminology 36:859–866. doi: 10.1111/j.1745-9125.1998.tb01268.x.

Brammer M (2009) The role of neuroimaging in diagnosis and personalized medicine--current position and likely future directions. Dialogues Clin Neurosci 11:389–396.

Brandeis D, Michel CM, Amzica F (2010) From neuronal activity to scalp potential fields. In: Electrical Neuroimaging (Michel CM, Koenig T, Brandeis D, Gianotti LRR, Wackermann J, eds), pp 1–24. Cambridge: Cambridge University Press. doi: 10.1017/CBO9780511596889.002.

Brewer N, Young RL, Barnett E (2017) Measuring Theory of Mind in Adults with Autism Spectrum Disorder. J Autism Dev Disord 47:1927–1941. doi: 10.1007/s10803-017-3080-x.

Buescher AVS, Cidav Z, Knapp M, Mandell DS (2014) Costs of autism spectrum disorders in

the United Kingdom and the United States. JAMA Pediatr 168:721–728. doi: 10.1001/jamapediatrics.2014.210.

Bunge SA, Kahn I (2010) Cognition: An Overview of Neuroimaging Techniques. Encycl Neurosci 2:1063–1067. doi: 10.1016/B978-008045046-9.00298-9.

Burdea GC, Weiss PLT, Thalmann D (2007) Guest editorial: Special theme on virtual rehabilitation. IEEE Trans Neural Syst Rehabil Eng 15:1. doi: 10.1109/TNSRE.2007.891367.

Buxton RB, Frank LR (1997) A model for the coupling between cerebral blood flow and oxygen metabolism during neural stimulation. J Cereb Blood Flow Metab 17:64–72. doi: 10.1097/00004647-199701000-00009.

Buxton RB, Wong EC, Frank LR (1998) Dynamics of blood flow and oxygenation changes during brain activation: The balloon model. Magn Reson Med 39:855–864. doi: 10.1002/mrm.1910390602.

Buzsáki G, Anastassiou CA, Koch C (2012) The origin of extracellular fields and currents — EEG, ECoG, LFP and spikes. Nat Rev Neurosci 13:407–420. doi: 10.1038/nrn3241.

Candini M, Giuberti V, Manattini A, Grittani S, di Pellegrino G, Frassinetti F (2017) Personal space regulation in childhood autism: Effects of social interaction and person's perspective. Autism Res 10:144–154. doi: 10.1002/aur.1637.

Canton R (1875) Electrical Currents of the Brain. In: Forty-Third Annual Meeting of the British Medical Association, pp 257–279. doi: 10.1136/bmj.2.765.257.

Cardoso DO, Carvalho DS, Alves DSF, Souza DFP, Carneiro HCC, Pedreira CE, Lima PMV, França FMG (2016) Financial credit analysis via a clustering weightless neural classifier. Neurocomputing 183:70–78. doi: 10.1016/j.neucom.2015.06.105.

Caria A, de Falco S (2015) Anterior insular cortex regulation in autism spectrum disorders. Front Behav Neurosci 9:1–9. doi: 10.3389/fnbeh.2015.00038.

Casaletto KB, Heaton RK (2017) Neuropsychological Assessment: Past and Future. J Int Neuropsychol Soc 23:778–790. doi: 10.1017/s1355617717001060.

Castelhano J, Duarte IC, Abuhaiba SI, Rito M, Sales F, Castelo-Branco M (2017) Cortical

functional topography of high-frequency gamma activity relates to perceptual decision: An Intracranial study. PLoS One 12:1–15. doi: 10.1371/journal.pone.0186428.

Castelhano J, Duarte IC, Wibral M, Rodriguez E, Castelo-Branco M (2014) The dual facet of gamma oscillations: Separate visual and decision making circuits as revealed by simultaneous EEG/fMRI. Hum Brain Mapp 00:1–17. doi: 10.1002/hbm.22545.

Castelhano J, Tavares P, Mouga S, Oliveira G, Castelo-Branco M (2018) Stimulus dependent neural oscillatory patterns show reliable statistical identification of autism spectrum disorder in a face perceptual decision task. Clin Neurophysiol 129:981–989. doi: 10.1016/j.clinph.2018.01.072.

Castelli F (2005) Understanding emotions from standardized facial expressions in autism and normal development. Autism 9:428–449. doi: 10.1177/1362361305056082.

Cavanagh JF, Frank MJ (2014) Frontal theta as a mechanism for cognitive control. Trends Cogn Sci 18:414–421. doi: 10.1016/j.tics.2014.04.012.

Cavanna AE, Trimble MR (2006) The precuneus: A review of its functional anatomy and behavioural correlates. Brain 129:564–583. doi: 10.1093/brain/awl004.

Cencini M, Cecconi F, Vulpiani A (2010) Chaos: From Simple Models to Complex Systems. Singapore: World Scientific. ISBN 9789814277655.

Chang C, Cunningham JP, Glover GH (2009) Influence of heart rate on the BOLD signal: The cardiac response function. Neuroimage 44:857–869. doi: 10.1016/j.neuroimage.2008.09.029.

Chang C, Glover GH (2009) Effects of model-based physiological noise correction on default mode network anti-correlations and correlations. Neuroimage 47:1448–1459. doi: 10.1016/j.neuroimage.2009.05.012.

Charman T (2003) Why is joint attention a pivotal skill in autism? Philos Trans R Soc Lond B Biol Sci 358:315–324. doi: 10.1098/rstb.2002.1199.

Chawarska K, Klin A, Paul R, Volkmar F (2007) Autism spectrum disorder in the second year: stability and change in syndrome expression. J Child Psychol Psychiatry 48:128–138. doi: 10.1111/j.1469-7610.2006.01685.x.

Chen SH, Bernard-Opitz V (1993) Comparison of personal and computer-assisted instruction for children with autism. Ment Retard 31:368–376.

Cheng W, Rolls ET, Gu H, Zhang J, Feng J (2015) Autism: Reduced connectivity between cortical areas involved in face expression, theory of mind, and the sense of self. Brain 138:1382–1393. doi: 10.1093/brain/awv051.

Chevallier C, Kohls G, Troiani V, Brodkin ES, Schultz RT (2012) The Social Motivation Theory of Autism Introduction: Social motivation and social cognition, two competing. Trends Cogn Sci 16:231–239. doi: 10.1016/j.tics.2012.02.007.

Chowdhury MEH, Mullinger KJ, Glover P, Bowtell R (2014) Reference layer artefact subtraction (RLAS): A novel method of minimizing EEG artefacts during simultaneous fMRI. Neuroimage 84:307–319. doi: 10.1016/j.neuroimage.2013.08.039.

Clayton MS, Yeung N, Cohen Kadosh R (2018) The many characters of visual alpha oscillations. Eur J Neurosci 48:2498–2508. doi: 10.1111/ejn.13747.

Coben R (2007) Connectivity-guided neurofeedback for autistic spectrum disorder. Biofeedback 35:131–135. doi: 10.1300/J184v11n01.

Coben R, Clarke AR, Hudspeth W, Barry RJ (2008) EEG power and coherence in autistic spectrum disorder. Clin Neurophysiol 119:1002–1009. doi: 10.1016/j.clinph.2008.01.013.

Collins DL, Neelin P, Peters TM, Evans AC (1994) Automatic 3D intersubject registration of MR volumetric data in standardized Talairach space. J Comput Assist Tomogr 18:192–205.

Corbett BA, Carmean V, Ravizza S, Wendelken C, Henry ML, Carter C, Rivera SM (2009) A functional and structural study of emotion and face processing in children with autism. Psychiatry Res Neuroimaging 173:196–205. doi: 10.1016/j.pscychresns.2008.08.005.

Couronné R, Probst P, Boulesteix AL (2018) Random forest versus logistic regression: A large-scale benchmark experiment. BMC Bioinformatics 19:1–14. doi: 10.1186/s12859-018-2264-5.

Cox RW, Jesmanowicz A, Hyde JS (1995) Real-Time Functional Magnetic Resonance Imaging. Magn Reson Med 33:230–236. doi: 10.1002/mrm.1910330213.

Coyle H, Traynor V, Solowij N (2015) Computerized and virtual reality cognitive training for individuals at high risk of cognitive decline: Systematic review of the literature. Am J Geriatr Psychiatry 23:335–359. doi: 10.1016/j.jagp.2014.04.009.

Craig A, Sherman WR, Will JD (2009) Developing Virtual Reality Applications: Foundations of Effective Design. Morgan Kaufmann. ISBN 0123749433.

Crespi B, Leach E, Dinsdale N, Mokkonen M, Hurd P (2016) Imagination in human social cognition, autism, and psychotic-affective conditions. Cognition 150:181–199. doi: 10.1016/j.cognition.2016.02.001.

Cruz-Neira C, Sandin DJ, DeFanti TA, Kenyon R V., Hart JC (1992) The CAVE: audio visual experience automatic virtual environment. Commun ACM 35:64–72. doi: 10.1145/129888.129892.

Cukor J, Gerardi M, Alley S, Reist C, Roy M, Rothbaum BO, Difede J, Rizzo A (2015) Virtual Reality Exposure Therapy for Combat-Related PTSD. In: Posttraumatic Stress Disorder and Related Diseases in Combat Veterans, pp 69–83. Cham: Springer International Publishing. doi: 10.1007/978-3-319-22985-0_7.

Currie S, Hoggard N, Craven IJ, Hadjivassiliou M, Wilkinson ID (2013) Understanding MRI: Basic MR physics for physicians. Postgrad Med J 89:209–223. doi: 10.1136/postgradmedj-2012-131342.

Custo A, Van De Ville D, Wells WM, Tomescu MI, Brunet D, Michel CM (2017) Electroencephalographic Resting-State Networks: Source Localization of Microstates. Brain Connect 7:671–682. doi: 10.1089/brain.2016.0476.

da Silva FL (2009) EEG: Origin and Measurement. In: EEG - fMRI: Physiological Basis, Technique and Applications (Mulert C, Lemieux L, eds), pp 19–38. Berlin, Heidelberg: Springer Berlin Heidelberg. doi: 10.1007/978-3-540-87919-0_2.

Dalton KM, Nacewicz BM, Johnstone T, Schaefer HS, Gernsbacher MA, Goldsmith HH, Alexander AL, Davidson RJ (2005) Gaze fixation and the neural circuitry of face processing in autism. Nat Neurosci 8:519–526. doi: 10.1038/nn1421.

David N, Aumann C, Bewernick BH, Santos NS, Lehnhardt FG, Vogeley K (2010) Investigation of mentalizing and visuospatial perspective taking for self and other in

asperger syndrome. J Autism Dev Disord 40:290–299. doi: 10.1007/s10803-009-0867-4.

Davies MS, Dapretto M, Sigman M, Sepeta L, Bookheimer SY (2011) Neural bases of gaze and emotion processing in children with autism spectrum disorders. Brain Behav 1:1–11. doi: 10.1002/brb3.6.

Dawson G, Carver L, Meltzoff AN, Panagiotides H, McPartland J, Webb SJ (2002) Neural correlates of face and object recognition in young children with autism spectrum disorder, developmental delay, and typical development. Child Dev 73:700–717. doi: 10.1111/1467-8624.00433.

Dawson G, Toth K, Abbott R, Osterling J, Munson J, Estes A, Liaw J (2004) Early social attention impairments in autism: social orienting, joint attention, and attention to distress. Dev Psychol 40:271–283. doi: 10.1037/0012-1649.40.2.271.

Dawson G, Webb SJ, McPartland J (2005) Understanding the nature of face processing impairment in autism: insights from behavioral and electrophysiological studies. Dev Neuropsychol 27:403–424. doi: 10.1207/s15326942dn2703_6.

de Haan M, Nelson CA, Gunnar MR, Tout KA (1998) Hemispheric differences in brain activity related to the recognition of emotional expressions by 5-year-old children. Dev Neuropsychol 14:495–518. doi: 10.1080/87565649809540725.

de Jong MC, van England H, Kemner C (2008) Attentional Effects of Gaze Shifts Are Influenced by Emotion and Spatial Frequency, but Not in Autism. J Am Acad Child Adolesc Psychiatry 47:443–454. doi: 10.1097/CHI.0b013e31816429a6.

de Munck JCC, Gonçalves SII, Mammoliti R, Heethaar RMM, Lopes da Silva FHH (2009) Interactions between different EEG frequency bands and their effect on alpha-fMRI correlations. Neuroimage 47:69–76. doi: 10.1016/j.neuroimage.2009.04.029.

De Taeye L, Pourtois G, Meurs A, Boon P, Vonck K, Carrette E, Raedt R (2015) Event-related potentials reveal preserved attention allocation but impaired emotion regulation in patients with epilepsy and comorbid negative affect. PLoS One 10:1–16. doi: 10.1371/journal.pone.0116817.

Debener S, Mullinger KJ, Niazy RK, Bowtell RW (2008) Properties of the ballistocardiogram artefact as revealed by EEG recordings at 1.5, 3 and 7 T static magnetic field strength.

Int J Psychophysiol 67:189–199. doi: 10.1016/j.ijpsycho.2007.05.015.

Delevoye-Turrell Y, Vienne C, Coello Y (2011) Space boundaries in schizophrenia voluntary action for improved judgments of social distances. Soc Psychol (Gott) 42:193–204. doi: 10.1027/1864-9335/a000063.

Delmonte S, Balsters JH, McGrath J, Fitzgerald J, Brennan S, Fagan AJ, Gallagher L (2012) Social and monetary reward processing in autism spectrum disorders. Mol Autism 3:1. doi: 10.1186/2040-2392-3-7.

Delorme A, Makeig S (2004) EEGLAB: an open sorce toolbox for analysis of single-trail EEG dynamics including independent component anlaysis. J Neurosci Methods 134:9–21. doi: 10.1016/j.jneumeth.2003.10.009.

Delorme A, Miyakoshi M, Jung T, Makeig S (2015) Grand average ERP-image plotting and statistics: A method for comparing variability in event-related single-trial EEG activities across subjects and conditions. J Neurosci Methods 250:3–6. doi: 10.1016/j.jneumeth.2014.10.003.

Didehbani N, Allen T, Kandalaft M, Krawczyk D, Chapman S (2016) Virtual Reality Social Cognition Training for children with high functioning autism. Comput Human Behav 62:703–711. doi: 10.1016/j.chb.2016.04.033.

Direito B, Lima J, Simões M, Sayal A, Sousa T, Luehrs M, Ferreira C, Castelo-Branco M (2019) Targeting dynamic facial processing mechanisms in superior temporal sulcus using a novel fMRI neurofeedback target. Neuroscience 406:97–108. doi: 10.1016/j.neuroscience.2019.02.024.

Duffy FH, Als H (2012) A stable pattern of EEG spectral coherence distinguishes children with autism from neuro-typical controls - a large case control study. BMC Med 10:64. doi: 10.1186/1741-7015-10-64.

Edmans J a, Gladman JRF, Cobb S, Sunderland A, Pridmore T, Hilton D, Walker MF (2006) Validity of a virtual environment for stroke rehabilitation. Stroke 37:2770–2775. doi: 10.1161/01.STR.0000245133.50935.65.

Eichele T, Moosmann M, Wu L, Gutberlet I, Debener S (2010) Removal of MRI Artifacts from EEG Recordings. In: Simultaneous EEG and fMRI, pp 95–106. Oxford University

Press. doi: 10.1093/acprof:oso/9780195372731.003.0006.

Eimer M, Holmes A (2001) An ERP study on the time course of emotional face processing. Cogn Neurosci Neuropsychol 13:427–431.

Eimer M, Holmes A, McGlone FP (2003) The role of spatial attention in the processing of facial expression: an ERP study of rapid brain responses to six basic emotions. Cogn Affect Behav Neurosci 3:97–110.

Ekman P, Friesen W V. (1971) Constants across cultures in the face and emotion. J Pers Soc Psychol 17:124–129. doi: 10.1037/h0030377.

Ekman P, Friesen W V. (1978) Facial Action Coding System: A Technique for the Measurement of Facial Movement. Palo Alto: Consulting Psychologists Press.

Ellingson M., Liebenthal E, Spanaki M., Prieto T., Binder J., Ropella K. (2004) Ballistocardiogram artifact reduction in the simultaneous acquisition of auditory ERPS and fMRI. Neuroimage 22:1534–1542. doi: 10.1016/j.neuroimage.2004.03.033.

Eloyan A, Li S, Muschelli J, Pekar JJ, Mostofsky SH, Caffo BS (2014) Analytic programming with fMRI data: A quick-start guide for statisticians using R. PLoS One 9. doi: 10.1371/journal.pone.0089470.

Emmelkamp PMG, Bruynzeel M, Drost L, van der Mast CAPG (2001) Virtual Reality Treatment in Acrophobia: A Comparison with Exposure in Vivo. CyberPsychology Behav 4:335–339. doi: 10.1089/109493101300210222.

Eschmann K, Bader R, Mecklinger A (2018) Topographical differences of frontal-midline theta activity reflect functional differences in cognitive control abilities. Brain Cogn 123:57–64. doi: 10.1016/j.bandc.2018.02.002.

Farwell L, Donchin E (1988) Talking off the top of your head: toward a mental prosthesis utilizing event-related brain potentials. Electr Clin Neurophysiol 70:510–523.

Faust O, Acharya U R, Krishnan SM, Min LC (2004) Analysis of cardiac signals using spatial filling index and time-frequency domain. Biomed Eng Online 3:1–11. doi: 10.1186/1475-925X-3-30.

Fazel-rezai R, Abhari K (2009) A region-based P300 speller for brain-computer interface. Can

J Elect Comput Eng, 34:81–85.

Feige B, Spiegelhalder K, Kiemen A, Bosch OG, Tebartz van Elst L, Hennig J, Seifritz E, Riemann D (2017) Distinctive time-lagged resting-state networks revealed by simultaneous EEG-fMRI. Neuroimage 145:1–10. doi: 10.1016/j.neuroimage.2016.09.027.

Felblinger J, Slotboom J, Kreis R, Jung B, Boesch C (1999) Restoration of electrophysiological signals distorted by inductive effects of magnetic field gradients during MR sequences. Magn Reson Med 41:715–721. doi: 10.1002/(SICI)1522-2594(199904)41:4<715::AID-MRM9>3.0.CO;2-7.

Fernández AL, Abe J (2018) Bias in cross-cultural neuropsychological testing: problems and possible solutions. Cult Brain 6:1–35. doi: 10.1007/s40167-017-0050-2.

Ferreira JL, Wu Y, Besseling RMH, Lamerichs R, Aarts RM (2016) Gradient Artefact Correction and Evaluation of the EEG Recorded Simultaneously with fMRI Data Using Optimised Moving-Average. J Med Eng 2016:1–17. doi: 10.1155/2016/9614323.

Field T, Woodson R, Greenberg R, Cohen D (1982) Discrimination and imitation of facial expression by neonates. Science (80-) 218:179–181. doi: 10.1126/science.7123230.

Fomina T, Lohmann G, Erb M, Ethofer T, Schölkopf B, Grosse-Wentrup M (2016) Self-regulation of brain rhythms in the precuneus: A novel BCI paradigm for patients with ALS. J Neural Eng 13. doi: 10.1088/1741-2560/13/6/066021.

Formaggio E, Storti SF, Cerini R, Fiaschi A, Manganotti P (2010) Brain oscillatory activity during motor imagery in EEG-fMRI coregistration. Magn Reson Imaging 28:1403–1412. doi: 10.1016/j.mri.2010.06.030.

Fovet T, Jardri R, Linden D (2015) Current Issues in the Use of fMRI-Based Neurofeedback to Relieve Psychiatric Symptoms. Curr Pharm Des 21:3384–3394. doi: 10.2174/1381612821666150619092540.

Fox CJ, Iaria G, Barton JJSS (2009) Defining the face processing network: Optimization of the functional localizer in fMRI. Hum Brain Mapp 30:1637–1651. doi: 10.1002/hbm.20630.

França FMG, de Gregorio M, Lima PM V., de Oliveira WR (2014) Advances in Weightless

Neural Systems. 22th Eur Symp Artif Neural Networks:497–504. doi: 10.13140/2.1.2688.6403.

Freitag CM, Luders E, Hulst HE, Narr KL, Thompson PM, Toga AW, Krick C, Konrad C (2009) Total Brain Volume and Corpus Callosum Size in Medication-Naïve Adolescents and Young Adults with Autism Spectrum Disorder. Biol Psychiatry 66:316–319. doi: 10.1016/j.biopsych.2009.03.011.

Friedrich EVC, Suttie N, Sivanathan A, Lim T, Louchart S, Pineda JA (2014) Brain-computer interface game applications for combined neurofeedback and biofeedback treatment for children on the autism spectrum. Front Neuroeng 7:1–7. doi: 10.3389/fneng.2014.00021.

Friston KJJ, Holmes APP, Poline J-BB, Grasby PJJ, Williams SCRC, Frackowiak RSJS, Turner R (1995) Analysis of fMRI time-series revisited. ISBN 1053-8119 (Print)n1053-8119 (Linking). doi: 10.1006/nimg.1995.1007.

Fu Z, Tu Y, Di X, Du Y, Sui J, Biswal BB, Zhang Z, de Lacy N, Calhoun VD (2018) Transient increased thalamic-sensory connectivity and decreased whole-brain dynamism in autism. Neuroimage:1–14. doi: 10.1016/j.neuroimage.2018.06.003.

Ganz ML (2007) The lifetime distribution of the incremental societal costs of autism. Arch Pediatr Adolesc Med 161:343–349. doi: 10.1001/archpedi.161.4.343.

Gao J, Hu J, Tung WW (2012) Entropy measures for biological signal analyses. Nonlinear Dyn 68:431–444. doi: 10.1007/s11071-011-0281-2.

Gessaroli E, Santelli E, di Pellegrino G, Frassinetti F (2013) Personal Space Regulation in Childhood Autism Spectrum Disorders. PLoS One 8:1–8. doi: 10.1371/journal.pone.0074959.

Glover GH (2011) Overview of Functional Magnetic Resonance Imaging. Neurosurg Clin N Am 22:133–139. doi: 10.1016/j.nec.2010.11.001.

Glover GH, Li TQ, Ress D (2000) Image-based method for retrospective correction of physiological motion effects in fMRI: RETROICOR. Magn Reson Med 44:162–167. doi: 10.1002/1522-2594(200007)44:1<162::AID-MRM23>3.0.CO;2-E.

Golan O, Ashwin E, Granader Y, McClintock S, Day K, Leggett V, Baron-Cohen S (2010)

Enhancing Emotion Recognition in Children with Autism Spectrum Conditions: An Intervention Using Animated Vehicles with Real Emotional Faces. J Autism Dev Disord 40:269–279. doi: 10.1007/s10803-009-0862-9.

Golan O, Baron-Cohen S (2006) Systemizing empathy: teaching adults with Asperger syndrome or high-functioning autism to recognize complex emotions using interactive multimedia. Dev Psychopathol 18:591–617. doi: 10.1017/S0954579406060305.

Golan O, Baron-Cohen S (2007) Teaching adults with autism spectrum conditions to recognize emotions: sys- tematic training for empathizing difficulties. In: Autism: An Integrated View from Neurocognitive, Clinical, and Intervention Research (McGregor E, Nunez N, Cebula K, Gomez JC, eds), pp 236–259. Oxford, U.K.: Blackwell Publishing.

Goldani AAS, Downs SR, Widjaja F, Lawton B, Hendren RL (2014) Biomarkers in Autism. Front Psychiatry 5:1281–1289. doi: 10.3389/fpsyt.2014.00100.

Goldman RI, Stern JM, Engel J, Cohen MS (2000) Acquiring simultaneous EEG and functional MRI. Clin Neurophysiol 111:1974–1980. doi: 10.1016/S1388-2457(00)00456-9.

Gonçalves SI et al. (2006) Correlating the alpha rhythm to BOLD using simultaneous EEG/fMRI: Inter-subject variability. Neuroimage 30:203–213. doi: 10.1016/j.neuroimage.2005.09.062.

Goodwin MS (2008) Enhancing and Accelerating the Pace of Autism Research and Treatment. Focus Autism Other Dev Disabl 23:125–128. doi: 10.1177/1088357608316678.

Graewe B, de Weerd P, Farivar R, Castelo-Branco M (2012) Stimulus dependency of object-evoked responses in human visual cortex: An inverse problem for category specificity. PLoS One 7. doi: 10.1371/journal.pone.0030727.

Grech R, Cassar T, Muscat J, Camilleri KP, Fabri SG, Zervakis M, Xanthopoulos P, Sakkalis V, Vanrumste B (2008) Review on solving the inverse problem in EEG source analysis. J Neuroeng Rehabil 5:25. doi: 10.1186/1743-0003-5-25.

Grossard C, Grynspan O, Serret S, Jouen AL, Bailly K, Cohen D (2017) Serious games to

teach social interactions and emotions to individuals with autism spectrum disorders (ASD). Comput Educ 113:195–211. doi: 10.1016/j.compedu.2017.05.002.

Guivarch J, Murdymootoo V, Elissalde S-N, Salle-Collemiche X, Tardieu S, Jouve E, Poinso F (2017) Impact of an implicit social skills training group in children with autism spectrum disorder without intellectual disability: A before-and-after study. PLoS One 12:e0181159. doi: 10.1371/journal.pone.0181159.

Güllmar D, Haueisen J, Reichenbach JR (2010) Influence of anisotropic electrical conductivity in white matter tissue on the EEG/MEG forward and inverse solution. A high-resolution whole head simulation study. Neuroimage 51:145–163. doi: 10.1016/j.neuroimage.2010.02.014.

Gulrajani RM, Roberge FA, Savard P (1984) Moving Dipole Inverse ECG and EEG Solutions. IEEE Trans Biomed Eng BME-31:903–910. doi: 10.1109/TBME.1984.325257.

Güntekin B, Başar E (2014) A review of brain oscillations in perception of faces and emotional pictures. Neuropsychologia 58:33–51. doi: 10.1016/j.neuropsychologia.2014.03.014.

Gutiérrez A. MA, Vexo F, Thalmann D (2008) Stepping into virtual reality. ISBN 9781848001169. doi: 10.1007/978-1-84800-117-6.

Hall EH (1879) On a New Action of the Magnet on Electric Currents. Am J Math 2:287. doi: 10.2307/2369245.

Hallez H, Vanrumste B, Grech R, Muscat J, De Clercq W, Vergult A, D'Asseler Y, Camilleri KP, Fabri SG, Van Huffel S, Lemahieu I (2007) Review on solving the forward problem in EEG source analysis. J Neuroeng Rehabil 4:46. doi: 10.1186/1743-0003-4-46.

Hamilton AF d. C, Brindley R, Frith U (2009) Visual perspective taking impairment in children with autistic spectrum disorder. Cognition 113:37–44. doi: 10.1016/j.cognition.2009.07.007.

Hammon PS, de Sa VR (2007) Preprocessing and meta-classification for brain-computer interfaces. IEEE Trans Biomed Eng 54:518–525. doi: 10.1109/TBME.2006.888833.

Handwerker DA, Ollinger JM, D'Esposito M (2004) Variation of BOLD hemodynamic responses across subjects and brain regions and their effects on statistical analyses.

Neuroimage 21:1639–1651. doi: 10.1016/j.neuroimage.2003.11.029.

Hanlon FM, Shaff NA, Dodd AB, Ling JM, Bustillo JR, Abbott CC, Stromberg SF, Abrams S, Lin DS, Mayer AR (2016) Hemodynamic response function abnormalities in schizophrenia during a multisensory detection task. Hum Brain Mapp 37:745–755. doi: 10.1002/hbm.23063.

Hansen SN, Schendel DE, Parner ET (2015) Explaining the increase in the prevalence of autism spectrum disorders: The proportion attributable to changes in reporting practices. JAMA Pediatr 169:56–62. doi: 10.1001/jamapediatrics.2014.1893.

Hanslmayr S, Volberg G, Wimber M, Raabe M, Greenlee MW, Bauml K-HTHT (2011) The Relationship between Brain Oscillations and BOLD Signal during Memory Formation: A Combined EEG-fMRI Study. J Neurosci 31:15674–15680. doi: 10.1523/JNEUROSCI.3140-11.2011.

Happe F (1999) Autism: cognitive deficit or cogntive style? Trends Cogntive Sci 3:216–222. doi: 10.1016/S1364-6613(99)01318-2.

Hardy C, Ogden J, Newman J, Cooper S (2002) Autism and ICT: A Guide for Teachers and Parents (Fulton D, ed). London: David Fulton Publishers This. ISBN 9781134140862.

Harms MB, Martin A, Wallace GL (2010) Facial Emotion Recognition in Autism Spectrum Disorders: A Review of Behavioral and Neuroimaging Studies. Neuropsychol Rev 20:290–322. doi: 10.1007/s11065-010-9138-6.

Haxby J V., Hoffman EA, Gobbini MI (2000) The distributed human neural system for face perception. Trends Cogn Sci 4:223–233. doi: 10.1016/S1364-6613(00)01482-0.

He BJ (2014) Scale-free brain activity: Past, present, and future. Trends Cogn Sci 18:480–487. doi: 10.1016/j.tics.2014.04.003.

Healey ML, Grossman M (2018) Cognitive and affective perspective-taking: Evidence for shared and dissociable anatomical substrates. Front Neurol 9:1–8. doi: 10.3389/fneur.2018.00491.

Hernandez LM, Rudie JD, Green SA, Bookheimer S, Dapretto M (2015) Neural signatures of autism spectrum disorders: Insights into brain network dynamics. Neuropsychopharmacology 40:171–189. doi: 10.1038/npp.2014.172.

Herrington JD, Nymberg C, Schultz RT (2011) Biological motion task performance predicts superior temporal sulcus activity. Brain Cogn 77:372–381. doi: 10.1016/j.bandc.2011.09.001.

Hirsch CR, Clark DM, Mathews A (2006) Imagery and Interpretations in Social Phobia: Support for the Combined Cognitive Biases Hypothesis. Behav Ther 37:223–236. doi: 10.1016/j.beth.2006.02.001.

Hollander E, Anagnostou E, Chaplin W, Esposito K, Haznedar MM, Licalzi E, Wasserman S, Soorya L, Buchsbaum M (2005) Striatal volume on magnetic resonance imaging and repetitive behaviors in autism. Biol Psychiatry 58:226–232. doi: 10.1016/j.biopsych.2005.03.040.

Holtmann M, Steiner S, Hohmann S, Poustka L, Banaschewski T, Bölte S, B??lte S (2011) Neurofeedback in autism spectrum disorders. Dev Med Child Neurol 53:986–993. doi: 10.1111/j.1469-8749.2011.04043.x.

Horki P, Bauernfeind G, Klobassa DS, Pokorny C, Pichler G, Schippinger W, MÃ¼ller-Putz GR (2014) Detection of mental imagery and attempted movements in patients with disorders of consciousness using EEG. Front Hum Neurosci 8:1–9. doi: 10.3389/fnhum.2014.01009.

Hotier S et al. (2017) Social cognition in autism is associated with the neurodevelopment of the posterior superior temporal sulcus. Acta Psychiatr Scand 136:517–525. doi: 10.1111/acps.12814.

Huettel S, Song A, McCarthy G (2004) Fuctional Magnetic Resonance Imaging, 3rd ed. OUP USA. ISBN 0878932887.

Huys QJM, Maia T V., Frank MJ (2016) Computational psychiatry as a bridge from neuroscience to clinical applications. Nat Neurosci 19:404–413. doi: 10.1038/nn.4238.

Iachini T, Coello Y, Frassinetti F, Ruggiero G (2014) Body space in social interactions: A comparison of reaching and comfort distance in immersive virtual reality. PLoS One 9:25–27. doi: 10.1371/journal.pone.0111511.

Iacono MI, Neufeld E, Akinnagbe E, Bower K, Wolf J, Vogiatzis Oikonomidis I, Sharma D, Lloyd B, Wilm BJ, Wyss M, Pruessmann KP, Jakab A, Makris N, Cohen ED, Kuster N,

Kainz W, Angelone LM (2015) MIDA: A Multimodal Imaging-Based Detailed Anatomical Model of the Human Head and Neck Jespersen SN, ed. PLoS One 10:e0124126. doi: 10.1371/journal.pone.0124126.

IFSECN (1974) A glossary of terms most commonly used by clinical electroencephalographers. Electroencephalogr Clin Neurophysiol 37:538–548. doi: 10.1016/0013-4694(74)90099-6.

Imperatori C, Della Marca G, Amoroso N, Maestoso G, Valenti EM, Massullo C, Carbone GA, Contardi A, Farina B (2017) Alpha/Theta Neurofeedback Increases Mentalization and Default Mode Network Connectivity in a Non-Clinical Sample. Brain Topogr 30:822–831. doi: 10.1007/s10548-017-0593-8.

Irimia A, Torgerson CM, Jacokes ZJ, Van Horn JD (2017) The connectomes of males and females with autism spectrum disorder have significantly different white matter connectivity densities. Sci Rep 7:1–10. doi: 10.1038/srep46401.

Irimia A, Van Horn JD, Halgren E (2012) Source cancellation profiles of electroencephalography and magnetoencephalography. Neuroimage 59:2464–2474. doi: 10.1016/j.neuroimage.2011.08.104.

Ives J, Warach S, Schmitt F, Edelman R, Schomer D (1993) Monitoring the Short communication patient's EEG during echo planar MRI. Electroencephalogr Clin Neurophysiol 87:417–420. doi: 10.1016/j.jped.2016.12.008.

J. E, A.E. L, M. B, S. D (2014) Robust features for the automatic identification of autism spectrum disorder in children. J Neurodev Disord 6:1–12. doi: 10.1186/1866-1955-6-12.

Jacobs J, Hawco C, Kobayashi E, Boor R, LeVan P, Stephani U, Siniatchkin M, Gotman J (2008) Variability of the hemodynamic response as a function of age and frequency of epileptic discharge in children with epilepsy. Neuroimage 40:601–614. doi: 10.1016/j.neuroimage.2007.11.056.

Jann K, Dierks T, Boesch C, Kottlow M, Strik W, Koenig T (2009) BOLD correlates of EEG alpha phase-locking and the fMRI default mode network. Neuroimage 45:903–916. doi: 10.1016/j.neuroimage.2009.01.001.

Jenkinson M, Bannister P, Brady M, Smith S (2002) Improved Optimization for the Robust

and Accurate Linear Registration and Motion Correction of Brain Images. Neuroimage 17:825–841. doi: 10.1006/nimg.2002.1132.

Jenkinson M, Smith S (2001) A global optimisation method for robust affine registration of brain images. Med Image Anal 5:143–156. doi: 10.1016/S1361-8415(01)00036-6.

Jeste SS, Frohlich J, Loo SK (2015) Electrophysiological biomarkers of diagnosis and outcome in neurodevelopmental disorders. Curr Opin Neurol 28:110–116. doi: 10.1097/WCO.0000000000000181.

Jia X, Kohn A (2011) Gamma rhythms in the brain. PLoS Biol 9:2–5. doi: 10.1371/journal.pbio.1001045.

Jing Fan, Wade JW, Dayi Bian, Key AP, Warren ZE, Mion LC, Sarkar N (2015) A Step towards EEG-based brain computer interface for autism intervention. In: 2015 37th Annual International Conference of the IEEE Engineering in Medicine and Biology Society (EMBC), pp 3767–3770. IEEE. doi: 10.1109/EMBC.2015.7319213.

Jo HJ, Saad ZS, Simmons WK, Milbury L a., Cox RW (2010) Mapping sources of correlation in resting state FMRI, with artifact detection and removal. Neuroimage 52:571–582. doi: 10.1016/j.neuroimage.2010.04.246.

Jobski K, Höfer J, Hoffmann F, Bachmann C (2017) Use of psychotropic drugs in patients with autism spectrum disorders: a systematic review. Acta Psychiatr Scand 135:8–28. doi: 10.1111/acps.12644.

Jones CRG, Pickles A, Falcaro M, Marsden AJS, Happé F, Scott SK, Sauter D, Tregay J, Phillips RJ, Baird G, Simonoff E, Charman T (2011) A multimodal approach to emotion recognition ability in autism spectrum disorders. J Child Psychol Psychiatry Allied Discip 52:275–285. doi: 10.1111/j.1469-7610.2010.02328.x.

Josman N, Ben-Chaim HM, Friedrich S, Weiss PL (2008) Effectiveness of virtual reality for teaching street-crossing skills to children and adolescents with autism. Int J Disabil Hum Dev 7:657–658. doi: 10.1515/IJDHD.2008.7.1.49.

Júlio F, Ribeiro MJ, Patrício M, Malhão A, Pedrosa F, Gonçalves H, Simões M, van Asselen M, Simões MR, Castelo-Branco M, Januário C (2019) A Novel Ecological Approach reveals Early Executive Function Impairments in Huntington's Disease. Front Psychol

10:585. doi: 10.3389/FPSYG.2019.00585.

Kaiboriboon K, Lüders HO, Hamaneh M, Turnbull J, Lhatoo SD (2012) EEG source imaging in epilepsy—practicalities and pitfalls. Nat Rev Neurol 8:498–507. doi: 10.1038/nrneurol.2012.150.

Kaiser MD, Hudac CM, Shultz S, Lee SM, Cheung C, Berken AM, Deen B, Pitskel NB, Sugrue DR, Voos AC, Saulnier CA, Ventola P, Wolf JM, Klin A, Vander Wyk BC, Pelphrey KA (2010) Neural signatures of autism. Proc Natl Acad Sci 107:21223–21228. doi: 10.1073/pnas.1010412107.

Kamiya J (1969) Operant control of the EEG alpha rhythm and some of its reported effects on consciousness. In: Altered states of consciousness., pp 489–501. New York: Wiley.

Kandalaft MR, Didehbani N, Krawczyk DC, Allen TT, Chapman SB (2013) Virtual reality social cognition training for young adults with high-functioning autism. J Autism Dev Disord 43:34–44. doi: 10.1007/s10803-012-1544-6.

Kanner L (1943) Autistic disturbances of affective contact. Nerv Child 2:217–250.

Kanwisher N, Yovel G (2006) The fusiform face area: a cortical region specialized for the perception of faces. Philos Trans R Soc B Biol Sci 361:2109–2128. doi: 10.1098/rstb.2006.1934.

Kapp KM (2012) The Gamification of Learning and Instruction: Game-based Methods and Strategies for Training and Education. Pfeiffer. ISBN 978-1-118-09634-5.

Kätsyri J, Förger K, Mäkäräinen M, Takala T (2015) A review of empirical evidence on different uncanny valley hypotheses: Support for perceptual mismatch as one road to the valley of eeriness. Front Psychol 6:1–16. doi: 10.3389/fpsyg.2015.00390.

Kätsyri J, Mäkäräinen M, Takala T (2017) Testing the 'uncanny valley' hypothesis in semirealistic computer-animated film characters: An empirical evaluation of natural film stimuli. Int J Hum Comput Stud 97:149–161. doi: 10.1016/j.ijhcs.2016.09.010.

Kennedy DP, Adolphs R (2014) Violations of personal space by individuals with autism spectrum disorder. PLoS One 9. doi: 10.1371/journal.pone.0103369.

Keogh E, Mueen A (2017) Curse of Dimensionality. In: Encyclopedia of Machine Learning

and Data Mining (Sammut C, Webb GI, eds), pp 314–315. Boston, MA: Springer US. doi: 10.1007/978-1-4899-7687-1_192.

Keynan JN, Cohen A, Jackont G, Green N, Goldway N, Davidov A, Meir-Hasson Y, Raz G, Intrator N, Fruchter E, Ginat K, Laska E, Cavazza M, Hendler T (2019) Electrical fingerprint of the amygdala guides neurofeedback training for stress resilience. Nat Hum Behav 3:63–73. doi: 10.1038/s41562-018-0484-3.

Kilavik BE, Zaepffel M, Brovelli A, MacKay WA, Riehle A (2013) The ups and downs of beta oscillations in sensorimotor cortex. Exp Neurol 245:15–26. doi: 10.1016/j.expneurol.2012.09.014.

Kim G (2005) Designing Virtual Reality Systems The Structured Approach. London: Springer London. ISBN 978-1-85233-958-6. doi: 10.1007/978-1-84628-230-0.

Kim KH, Yoon HW, Park HW (2004) Improved ballistocardiac artifact removal from the electroencephalogram recorded in fMRI. J Neurosci Methods 135:193–203. doi: 10.1016/j.jneumeth.2003.12.016.

Kircher TTJ, Brammer M, Bullmore E, Simmons A, Bartels M, David AS (2002) The neural correlates of intentional and incidental self processing. Neuropsychologia 40:683–692. doi: 10.1016/S0028-3932(01)00138-5.

Kleinhans NM, Richards T, Johnson LC, Weaver KE, Greenson J, Dawson G, Aylward E (2011) fMRI evidence of neural abnormalities in the subcortical face processing system in ASD. Neuroimage 54:697–704. doi: 10.1016/j.neuroimage.2010.07.037.

Kliková B, Raidl A (2011) Reconstruction of Phase Space of Dynamical Systems Using Method of Time Delay. Proc 20th Annu Conf Dr Students - WDS 2011:83–87.

Klin A, Shultz S, Jones W (2015) Social visual engagement in infants and toddlers with autism: Early developmental transitions and a model of pathogenesis. Neurosci Biobehav Rev 50:189–203. doi: 10.1016/j.neubiorev.2014.10.006.

Knyazev GG, Slobodskoj-Plusnin JY, Bocharov A V. (2009) Event-related delta and theta synchronization during explicit and implicit emotion processing. Neuroscience 164:1588–1600. doi: 10.1016/j.neuroscience.2009.09.057.

Kober SE, Witte M, Ninaus M, Neuper C, Wood G (2013) Learning to modulate one's own

brain activity: the effect of spontaneous mental strategies. Front Hum Neurosci 7:1–12. doi: 10.3389/fnhum.2013.00695.

Kohls G, Schulte-Rüther M, Nehrkorn B, Müller K, Fink GR, Kamp-Becker I, Herpertz-Dahlmann B, Schultz RT, Konrad K (2013) Reward system dysfunction in autism spectrum disorders. Soc Cogn Affect Neurosci 8:565–572. doi: 10.1093/scan/nss033.

Kosslyn SM, Ganis G, Thompson WL (2001) Neural Foundations of Imagery. Nat Rev Neurosci 2:635–642. doi: 10.1038/35090055.

Kotchetkov IS, Hwang BY, Appelboom G, Kellner CP, Connolly ES (2010) Brain-computer interfaces: military, neurosurgical, and ethical perspective. Neurosurg Focus 28:E25. doi: 10.3171/2010.2.FOCUS1027.

Koush Y, Rosa MJ, Robineau F, Heinen K, W. Rieger S, Weiskopf N, Vuilleumier P, Van De Ville D, Scharnowski F (2013) Connectivity-based neurofeedback: Dynamic causal modeling for real-time fMRI. Neuroimage 81:422–430. doi: 10.1016/j.neuroimage.2013.05.010.

Krishnaswamy P, Bonmassar G, Poulsen C, Pierce ET, Purdon PL, Brown EN (2016) Reference-free removal of EEG-fMRI ballistocardiogram artifacts with harmonic regression. Neuroimage 128:398–412. doi: 10.1016/j.neuroimage.2015.06.088.

Krumhuber EG, Kappas A, Manstead ASR (2013) Effects of dynamic aspects of facial expressions: A review. Emot Rev 5:41–46. doi: 10.1177/1754073912451349.

Kwong KK, Belliveau JW, Chesler DA, Goldberg IE, Weisskoff RM, Poncelet BP, Kennedy DN, Hoppel BE, Cohen MS, Turner R (1992) Dynamic magnetic resonance imaging of human brain activity during primary sensory stimulation. Proc Natl Acad Sci 89:5675–5679. doi: 10.1073/pnas.89.12.5675.

LaConte SM (2011) Decoding fMRI brain states in real-time. Neuroimage 56:440–454. doi: 10.1016/j.neuroimage.2010.06.052.

Lanius RA, Williamson PC, Boksman K, Densmore M, Gupta M, Neufeld RWJ, Gati JS, Menon RS (2002) Brain activation during script-driven imagery induced dissociative responses in PTSD: A functional magnetic resonance imaging investigation. Biol Psychiatry 52:305–311. doi: 10.1016/S0006-3223(02)01367-7.

Lau HM, Smit JH, Fleming TM, Riper H (2017) Serious games for mental health: Are they accessible, feasible, and effective? A systematic review and meta-analysis. Front Psychiatry 7. doi: 10.3389/fpsyt.2016.00209.

Laufs H, Kleinschmidt A, Beyerle A, Eger E, Salek-Haddadi A, Preibisch C, Krakow K (2003) EEG-correlated fMRI of human alpha activity. Neuroimage 19:1463–1476. doi: 10.1016/S1053-8119(03)00286-6.

Lee TMC, Leung MK, Lee TMY, Raine A, Chan CCH (2013) I want to lie about not knowing you, but my precuneus refuses to cooperate. Sci Rep 3:1–5. doi: 10.1038/srep01636.

Lei X, Valdes-Sosa PA, Yao D (2012) EEG/fMRI fusion based on independent component analysis: Integration of data-driven and model-driven methods. J Integr Neurosci 11:313–337. doi: 10.1142/s0219635212500203.

Lemm S, Curio G, Hlushchuk Y, Müller K-R (2006) Enhancing the signal-to-noise ratio of ICA-based extracted ERPs. IEEE Trans Biomed Eng 53:601–607. doi: 10.1109/TBME.2006.870258.

Lerner MD, McPartland JC, Morris JP (2013) Multimodal emotion processing in autism spectrum disorders: An event-related potential study. Dev Cogn Neurosci 3:11–21. doi: 10.1016/j.dcn.2012.08.005.

Leuthardt EC, Schalk G, Roland J, Rouse A, Moran DW (2009) Evolution of brain-computer interfaces: going beyond classic motor physiology. Neurosurg Focus 27:E4. doi: 10.3171/2009.4.FOCUS0979.

Li D, Karnath HO, Xu X (2017) Candidate Biomarkers in Children with Autism Spectrum Disorder: A Review of MRI Studies. Neurosci Bull 33:219–237. doi: 10.1007/s12264-017-0118-1.

Lieberoth A (2015) Shallow Gamification. Games Cult 10:229–248. doi: 10.1177/1555412014559978.

Liu EY, Haist F, Dubowitz DJ, Buxton RB (2019) Cerebral blood volume changes during the BOLD post-stimulus undershoot measured with a combined normoxia/hyperoxia method. Neuroimage 185:154–163. doi: 10.1016/j.neuroimage.2018.10.032.

Liu Q, Farahibozorg S, Porcaro C, Wenderoth N, Mantini D (2017a) Detecting large-scale

networks in the human brain using high-density electroencephalography. Hum Brain Mapp 38:4631–4643. doi: 10.1002/hbm.23688.

Liu Q, Ganzetti M, Wenderoth N, Mantini D (2018) Detecting Large-Scale Brain Networks Using EEG: Impact of Electrode Density, Head Modeling and Source Localization. Front Neuroinform 12:1–11. doi: 10.3389/fninf.2018.00004.

Liu X, Wu Q, Zhao W, Luo X (2017b) Technology-Facilitated Diagnosis and Treatment of Individuals with Autism Spectrum Disorder: An Engineering Perspective. Appl Sci 7:1051. doi: 10.3390/app7101051.

Liu Y, Waterton JC (2017) Imaging Biomarkers in Clinical Trials. In: Imaging Biomarkers, pp 295–306. Cham: Springer International Publishing. doi: 10.1007/978-3-319-43504-6_21.

Lopes Da Silva FH, Pijn JP, Velis D, Nijssen PCG (1997) Alpha rhythms: Noise, dynamics and models. Int J Psychophysiol 26:237–249. doi: 10.1016/S0167-8760(97)00767-8.

Lopes Da Silva FH, Storm Van Leeuwen W (1977) The cortical source of the alpha rhythm. Neurosci Lett 6:237–241. doi: 10.1016/0304-3940(77)90024-6.

Lorenzo G, Lledó A, Pomares J, Roig R (2016) Design and application of an immersive virtual reality system to enhance emotional skills for children with autism spectrum disorders. Comput Educ 98:192–205. doi: 10.1016/j.compedu.2016.03.018.

Lotte F, Congedo M, Lécuyer A, Lamarche F, Arnaldi B (2007) A review of classification algorithms for EEG-based brain-computer interfaces. J Neural Eng 4:R1–R13.

Lough E, Hanley M, Rodgers J, South M, Kirk H, Kennedy DP, Riby DM (2015) Violations of Personal Space in Young People with Autism Spectrum Disorders and Williams Syndrome: Insights from the Social Responsiveness Scale. J Autism Dev Disord 45:4101–4108. doi: 10.1007/s10803-015-2536-0.

Luckhardt C, Jarczok TA, Bender S (2014) Elucidating the neurophysiological underpinnings of autism spectrum disorder: New developments. J Neural Transm 121:1129–1144. doi: 10.1007/s00702-014-1265-4.

Luckhardt C, Kröger A, Cholemkery H, Bender S, Freitag CM (2017) Neural Correlates of Explicit Versus Implicit Facial Emotion Processing in ASD. J Autism Dev Disord 47:1944–1955. doi: 10.1007/s10803-017-3141-1.

Luo W, Feng W, He W, Wang NY, Luo YJ (2010) Three stages of facial expression processing: ERP study with rapid serial visual presentation. Neuroimage 49:1857–1867. doi: 10.1016/j.neuroimage.2009.09.018.

Macdorman KF (2017) Familiar faces rendered strange : Why inconsistent realism drives characters into the uncanny valley Debaleena Chattopadhyay. 16:1–25. doi: 10.1167/16.11.7.doi.

Makeig S, Debener S, Onton J, Delorme A (2004) Mining event-related brain dynamics. Trends Cogn Sci 8:204–210. doi: 10.1016/j.tics.2004.03.008.

Mandelkow H, Halder P, Boesiger P, Brandeis D (2006) Synchronization facilitates removal of MRI artefacts from concurrent EEG recordings and increases usable bandwidth. Neuroimage 32:1120–1126. doi: 10.1016/j.neuroimage.2006.04.231.

Marino M, Liu Q, Koudelka V, Porcaro C, Hlinka J, Wenderoth N, Mantini D (2018) Adaptive optimal basis set for BCG artifact removal in simultaneous. Sci Rep:1–11. doi: 10.1038/s41598-018-27187-6.

Marzbani H, Marateb HR, Mansourian M, Neuroscience C, Sciences M, Marzbani H, Marateb HR, Mansourian M (2016) Methodological Note: Neurofeedback: A Comprehensive Review on System Design, Methodology and Clinical Applications. Basic Clin Neurosci J 7:143–158. doi: 10.15412/J.BCN.03070208.

Maurer U, Brem S, Liechti M, Maurizio S, Michels L, Brandeis D (2014) Frontal Midline Theta Reflects Individual Task Performance in a Working Memory Task. Brain Topogr 28:127–134. doi: 10.1007/s10548-014-0361-y.

McFarland DJ, Miner LA, Vaughan TM, Wolpaw JR (2000) Mu and beta rhythm topographies during motor imagery and actual movements. Brain Topogr 12:177–186. doi: 10.1023/A:1023437823106.

McFarland DJ, Wolpaw JR (2008) Brain-Computer Interface Operation of Robotic and Prosthetic Devices. Computer (Long Beach Calif) 41:52–56. doi: 10.1109/MC.2008.409.

McPartland J, Dawson G, Webb SJ, Panagiotides H, Carver LJ (2004) Event-related brain potentials reveal anomalies in temporal processing of faces in autism spectrum disorder. J Child Psychol Psychiatry 45:1235–1245. doi: 10.1111/j.1469-7610.2004.00318.x.

McPheeters ML, Warren Z, Sathe N, Bruzek JL, Krishnaswami S, Jerome RN, Veenstra-VanderWeele J (2011) A Systematic Review of Medical Treatments for Children With Autism Spectrum Disorders. Pediatrics 127:e1312–e1321. doi: 10.1542/peds.2011-0427.

Meir-Hasson Y, Keynan JN, Kinreich S, Jackont G, Cohen A, Podlipsky-Klovatch I, Hendler T, Intrator N (2016) One-class FMRI-inspired EEG model for self-regulation training Schmahl C, ed. PLoS One 11:e0154968. doi: 10.1371/journal.pone.0154968.

Meir-Hasson Y, Kinreich S, Podlipsky I, Hendler T, Intrator N (2014) An EEG Finger-Print of fMRI deep regional activation. Neuroimage 102:128–141. doi: 10.1016/j.neuroimage.2013.11.004.

Michel CM, Brandeis D (2010) The Sources and Temporal Dynamics of Scalp Electric Fields. In: Simultaneous EEG and fMRI, pp 3–20. Oxford University Press. doi: 10.1093/acprof:oso/9780195372731.003.0001.

Micoulaud-Franchi J-A, McGonigal A, Lopez R, Daudet C, Kotwas I, Bartolomei F (2015) Electroencephalographic neurofeedback: Level of evidence in mental and brain disorders and suggestions for good clinical practice. Neurophysiol Clin Neurophysiol 45:423–433. doi: 10.1016/j.neucli.2015.10.077.

Millán J, Ferrez P, Galán F, Lew Ei, Chavarriaga R (2008) Non-Invasive Brain-Machine Interaction. Int J Pattern Recognit Artif Intell 22:959–972. doi: 10.1142/S0218001408006600.

Miller HL, Bugnariu NL (2016) Level of Immersion in Virtual Environments Impacts the Ability to Assess and Teach Social Skills in Autism Spectrum Disorder. Cyberpsychology, Behav Soc Netw 19:246–256. doi: 10.1089/cyber.2014.0682.

Mishkind MC, Norr AM, Katz AC, Reger GM (2017) Review of Virtual Reality Treatment in Psychiatry: Evidence Versus Current Diffusion and Use. Curr Psychiatry Rep 19. doi: 10.1007/s11920-017-0836-0.

Moher D, Liberati A, Tetzlaff J, Altman DG, Grp P (2009) Preferred Reporting Items for Systematic Reviews and Meta-Analyses: The PRISMA Statement (Reprinted from Annals of Internal Medicine). Phys Ther 89:873–880. doi: 10.1371/journal.pmed.1000097.

Monteiro R, Simões M, Andrade J, Castelo Branco M (2017) Processing of Facial Expressions in Autism: a Systematic Review of EEG/ERP Evidence. Rev J Autism Dev Disord 4:255–276. doi: 10.1007/s40489-017-0112-6.

Montri P, Masahiro N (2008) EEG-based classification of motor imagery tasks using fractal dimension and neural network for brain-computer interface. IEICE Trans Inf Syst E91-D:44–53. doi: 10.1093/ietisy/e91-d.1.44.

Mouga S, Almeida J, Café C, Duque F, Oliveira G (2015) Adaptive Profiles in Autism and Other Neurodevelopmental Disorders. J Autism Dev Disord 45:1001–1012. doi: 10.1007/s10803-014-2256-x.

Mulert C, Jäger L, Schmitt R, Bussfeld P, Pogarell O, Möller H-J, Juckel G, Hegerl U (2004) Integration of fMRI and simultaneous EEG: towards a comprehensive understanding of localization and time-course of brain activity in target detection. Neuroimage 22:83–94. doi: 10.1016/j.neuroimage.2003.10.051.

Mullinger K, Bowtell R (2011) Combining EEG and fMRI. In: Magnetic Resonance Neuroimaging (Modo M, Bulte JWM, eds), pp 303–326 Methods in Molecular Biology. Totowa, NJ: Humana Press. doi: 10.1007/978-1-61737-992-5_15.

Mullinger KJ, Chowdhury MEH, Bowtell R (2014) Investigating the effect of modifying the EEG cap lead configuration on the gradient artifact in simultaneous EEG-fMRI. Front Neurosci 8:1–10. doi: 10.3389/fnins.2014.00226.

Mullinger KJ, Havenhand J, Bowtell R (2013) Identifying the sources of the pulse artefact in EEG recordings made inside an MR scanner. Neuroimage 71:75–83. doi: 10.1016/j.neuroimage.2012.12.070.

Mullinger KJ, Yan WX, Bowtell R (2011) Reducing the gradient artefact in simultaneous EEG-fMRI by adjusting the subject's axial position. Neuroimage 54:1942–1950. doi: 10.1016/j.neuroimage.2010.09.079.

Mundy P, Sigman M, Ungerer J, Sherman T (1986) Defining the Social Deficits of Autism: the Contribution of Non-verbal Communication Measures of Child Psychology and Psychiatry. J Child Psychol Psychiatry 27:657–669. doi: 10.1111/j.1469-7610.1986.tb00190.x.

Murta T, Leite M, Carmichael DW, Figueiredo P, Lemieux L (2015) Electrophysiological correlates of the BOLD signal for EEG-informed fMRI. Hum Brain Mapp 36:391–414. doi: 10.1002/hbm.22623.

Neuper C, Scherer R, Wriessnegger S, Pfurtscheller G (2009) Motor imagery and action observation: Modulation of sensorimotor brain rhythms during mental control of a brain-computer interface. Clin Neurophysiol 120:239–247. doi: 10.1016/j.clinph.2008.11.015.

Nguyen VT, Cunnington R (2014) The superior temporal sulcus and the N170 during face processing: Single trial analysis of concurrent EEG–fMRI. Neuroimage 86:492–502. doi: 10.1016/j.neuroimage.2013.10.047.

Niazy RK, Beckmann CF, Iannetti GD, Brady JM, Smith SM (2005) Removal of FMRI environment artifacts from EEG data using optimal basis sets. Neuroimage 28:720–737. doi: 10.1016/j.neuroimage.2005.06.067.

Nichols TE, Holmes AP (2001) Nonparametric Permutation Tests for {PET} functional Neuroimaging Experiments: A Primer with examples. Hum Brain Mapp 15:1–25. doi: 10.1002/hbm.1058.

Noam G, Jacob A, Eti B-S, Libat W, Marc C, Talma H, Haggai S (2016) EEG-Neurofeedback targeting amygdala activity reduces disease impact and improves sleep in Patients with Fibromyalgia. Front Hum Neurosci 10. doi: 10.3389/conf.fnhum.2016.220.00112.

O'Connor K, Hamm JP, Kirk IJ (2005) The neurophysiological correlates of face processing in adults and children with Asperger's syndrome. Brain Cogn 59:82–95. doi: 10.1016/j.bandc.2005.05.004.

Oberman LM, Hubbard EM, McCleery JP, Altschuler EL, Ramachandran VS, Pineda J a (2005) EEG evidence for mirror neuron dysfunction in autism spectrum disorders. Brain Res Cogn Brain Res 24:190–198. doi: 10.1016/j.cogbrainres.2005.01.014.

Ochsner KN, Knierim K, Ludlow DH, Hanelin J, Ramachandran T, Glover G, Mackey SC (2004) Reflecting upon Feelings: An fMRI Study of Neural Systems Supporting the Attribution of Emotion to Self and Other. J Cogn Neurosci 16:1746–1772. doi: 10.1162/0898929042947829.

Ogawa S, D.W. T, R.S. RM, J.M. E, G. KS, H. M, K. U (1992) Intrinsic Signal Changes Accompanying Sensory Stimulation: Functional Brain Mapping with Magnetic Resonance Imaging. Proc Natl Acad Sci 89:5951–5955. doi: 10.1073/pnas.89.13.5951.

Ogawa S, Lee TM, Kay AR, Tank DW (1990) Brain magnetic resonance imaging with contrast dependent on blood oxygenation. Proc Natl Acad Sci U S A 87:9868–9872. doi: 10.7566/JPSJ.84.064704.

Oliveira G, Ataíde A, Marques C, Miguel TS, Coutinho AM, Mota-Vieira L, Gonçalves E, Lopes NM, Rodrigues V, Carmona da Mota H, Vicente AM (2007) Epidemiology of autism spectrum disorder in Portugal: prevalence, clinical characterization, and medical conditions. Dev Med Child Neurol 49:726–733. doi: 10.1111/j.1469-8749.2007.00726.x.

Oostenveld R, Fries P, Maris E, Schoffelen JM (2011) FieldTrip: Open source software for advanced analysis of MEG, EEG, and invasive electrophysiological data. Comput Intell Neurosci 2011. doi: 10.1155/2011/156869.

Pan J, Tompkins WJ (1985) A real-time QRS detection algorithm. IEEE Trans Biomed Eng 32:230–236. doi: 10.1109/TBME.1985.325532.

Parsons S, Cobb S (2011) State-of-the-art of virtual reality technologies for children on the autism spectrum. Eur J Spec Needs Educ 26:355–366. doi: 10.1080/08856257.2011.593831.

Parsons S, Mitchell P, Leonard A (2004) The use and understanding of virtual environments by adolescents with autistic spectrum disorders. J Autism Dev Disord 34:449–466. doi: 10.1023/B:JADD.0000037421.98517.8d.

Parsons TD, Rizzo AA, Rogers S, York P (2009) Virtual reality in paediatric rehabilitation: a review. Dev Neurorehabil 12:224–238.

Pascual-Marqui R (1999) Review of methods for solving the EEG inverse problem. Int J Bioelectromagn 1:75–86.

Pascual-Marqui RD (2002) Standardized low-resolution brain electromagnetic tomography (sLORETA): technical details. Methods Find Exp Clin Pharmacol 24 Suppl D:5–12.

Pascual-Marqui RD (2007) Instantaneous and lagged measurements of linear and nonlinear dependence between groups of multivariate time series: frequency decomposition. :1–

18.

Pascual-Marqui RD, Esslen M, Kochi K, Lehmann D (2002) Functional imaging with low-resolution brain electromagnetic tomography (LORETA): a review. Methods Find Exp Clin Pharmacol 24 Suppl C:91–95.

Pascual-Marqui RD, Lehmann D, Faber P, Milz P, Kochi K, Yoshimura M, Nishida K, Isotani T, Kinoshita T (2014) The resting microstate networks (RMN): cortical distributions, dynamics, and frequency specific information flow. :1–14.

Pascual-Marqui RD, Lehmann D, Koukkou M, Kochi K, Anderer P, Saletu B, Tanaka H, Hirata K, John ER, Prichep L, Biscay-Lirio R, Kinoshita T (2011) Assessing interactions in the brain with exact low-resolution electromagnetic tomography. Philos Trans R Soc A Math Phys Eng Sci 369:3768–3784. doi: 10.1098/rsta.2011.0081.

Paul R, Chawarska K, Fowler C, Cicchetti D, Volkmar F (2007) "Listen My Children and You Shall Hear": Auditory Preferences in Toddlers With Autism Spectrum Disorders. J Speech, Lang Hear Res 50:1350–1364. doi: 10.1044/1092-4388(2007/094).

Pearson DG, Deeprose C, Wallace-Hadrill SMA, Heyes SB, Holmes EA (2013) Assessing mental imagery in clinical psychology: A review of imagery measures and a guiding framework. Clin Psychol Rev 33:1–23. doi: 10.1016/j.cpr.2012.09.001.

Pearson J, Clifford C, Tong F (2009) The functional impact of mental imagery on conscious perception. Curr Biol 18:982–986. doi: 10.1016/j.cub.2008.05.048.The.

Pearson J, Naselaris T, Holmes EA, Kosslyn SM (2015) Mental Imagery: Functional Mechanisms and Clinical Applications. Trends Cogn Sci 19:590–602. doi: 10.1016/j.tics.2015.08.003.

Pellicano E (2013) Sensory symptoms in autism: A blooming, buzzing confusion? Child Dev Perspect 7:143–148. doi: 10.1111/cdep.12031.

Pelphrey KA, Carter EJ (2008) Brain mechanisms for social perception: Lessons from autism and typical development. Ann N Y Acad Sci 1145:283–299. doi: 10.1196/annals.1416.007.

Peng H, Long F, Ding C (2005) Feature selection based on mutual information criteria of max-dependency, max-relevance, and min-redundancy. IEEE Trans Pattern Anal Mach

Intell 27:1226–1238. doi: 10.1109/TPAMI.2005.159.

Perronnet L (2017) Combinaison de l ' électroencéphalo- graphie et de l ' imagerie par résonance magnétique fonctionnelle pour le neurofeedback Thèse soutenue à Rennes.

Perry A, Levy-Gigi E, Richter-Levin G, Shamay-Tsoory SG (2015a) Interpersonal distance and social anxiety in autistic spectrum disorders: A behavioral and ERP study. Soc Neurosci 10:354–365. doi: 10.1080/17470919.2015.1010740.

Perry A, Nichiporuk N, Knight RT (2015b) Where does one stand: A biological account of preferred interpersonal distance. Soc Cogn Affect Neurosci 11:317–326. doi: 10.1093/scan/nsv115.

Perry A, Rubinsten O, Peled L, Shamay-Tsoory SG (2013) Don't stand so close to me: A behavioral and ERP study of preferred interpersonal distance. Neuroimage 83:761–769. doi: 10.1016/j.neuroimage.2013.07.042.

Pesaran B, Pezaris JS, Sahani M, Mitra PP, Andersen RA (2002) Temporal structure in neuronal activity during working memory in macaque parietal cortex. Nat Neurosci 5:805–811. doi: 10.1038/nn890.

Pfurtscheller G, Allison BZ, Brunner C, Bauernfeind G, Solis-Escalante T, Scherer R, Zander TO, Mueller-Putz G, Neuper C, Birbaumer N (2010) The hybrid BCI. Front Neurosci 4:30. doi: 10.3389/fnpro.2010.00003.

Pfurtscheller G, Neuper C (1997) Motor imagery activates primary sensorimotor area in humans. Neurosci Lett 239:65–68. doi: 10.1016/S0304-3940(97)00889-6.

Pinto M, Pereira M, Raposo D, Simoes M, Castelo-Branco M (2019) GameAAL - an AAL solution based on Gamification and Machine Learning Techniques. In: 2019 IEEE Conference on Computational Intelligence in Bioinformatics and Computational Biology (CIBCB), pp 1–4. Siena: IEEE. doi: 10.1109/CIBCB.2019.8791454.

Piquepaille R (2010) Virtual reality used for stroke rehabilitation. zdnet - Emerg Tech:8–9.

Pires G, Castelo-Branco M, Nunes U (2008) Visual P300-based BCI to steer a wheelchair: a Bayesian approach. Conf Proc IEEE Eng Med Biol Soc 2008:658–661. doi: 10.1109/IEMBS.2008.4649238.

Pires G, Nunes U, Castelo-Branco M (2011) Statistical spatial filtering for a P300-based BCI: tests in able-bodied, and patients with cerebral palsy and amyotrophic lateral sclerosis. J Neurosci Methods 195:270–281. doi: 10.1016/j.jneumeth.2010.11.016.

Powers MBB, Rothbaum BOO (2019) Recent advances in virtual reality therapy for anxiety and related disorders: Introduction to the special issue. J Anxiety Disord 61:1–2. doi: 10.1016/j.janxdis.2018.08.007.

R. Michael D, L. Chen S (2006) Serious Games: Games That Educate, Train, and Inform. Boston: Thomson Course Technology. ISBN 1592006221.

Rajan A, Siegel SN, Liu Y, Bengson J, Mangun GR, Ding M (2018) Theta Oscillations Index Frontal Decision-Making and Mediate Reciprocal Frontal–Parietal Interactions in Willed Attention. Cereb Cortex:1–12. doi: 10.1093/cercor/bhy149.

Rangaprakash D, Wu GR, Marinazzo D, Hu X, Deshpande G (2018) Hemodynamic response function (HRF) variability confounds resting-state fMRI functional connectivity. Magn Reson Med 80:1697–1713. doi: 10.1002/mrm.27146.

Rao, Shaila M, Gagie B (2006) Learning Through Seeing and Doing : Visual Supports for Children With Autism. Teach Except Child:26–33. doi: 10.1007/s11257-011-9099-3.

Rellecke J, Sommer W, Schacht A (2013) Emotion effects on the N170: A question of reference? Brain Topogr 26:62–71. doi: 10.1007/s10548-012-0261-y.

Ridgway JP (2010) Cardiovascular magnetic resonance physics for clinicians: part I. J Cardiovasc Magn Reson 12:71. doi: 10.1186/1532-429X-12-71.

Ritter P, Villringer A (2006) Simultaneous EEG-fMRI. Neurosci Biobehav Rev 30:823–838. doi: 10.1016/j.neubiorev.2006.06.008.

Ritterfeld U, Cody M, Vorderer P (2009) Serious Games: Mechanisms and Effects. ISBN 9780415993692.

Rizzo a., Wiederhold BK (n.d.) Virtual Reality Technology for Psychological/Neuropsychological/Motor Assessment and Rehabilitation: Applications and Issues. IEEE Virtual Real Conf (VR 2006):308–308. doi: 10.1109/VR.2006.144.

Rizzo A, Hartholt A, Grimani M, Leeds A, Liewer M (2014) Virtual reality exposure therapy

for combat-related posttraumatic stress disorder. Computer (Long Beach Calif) 47:31–37. doi: 10.1109/MC.2014.199.

Rizzo AS, Kim GJ (2005) A SWOT Analysis of the Field of Virtual Reality Rehabilitation and Therapy. Presence Teleoperators Virtual Environ 14:119–146. doi: 10.1162/1054746053967094.

Roane HS, Fisher WW, Carr JE (2016) Applied Behavior Analysis as Treatment for Autism Spectrum Disorder. J Pediatr 175:27–32. doi: 10.1016/j.jpeds.2016.04.023.

Rodríguez-Bermúdez G, García-Laencina PJ (2015) Analysis of EEG signals using nonlinear dynamics and chaos: A review. Appl Math Inf Sci 9:2309–2321. doi: 10.12785/amis/090512.

Rodriguez-Galiano V, Sanchez-Castillo M, Chica-Olmo M, Chica-Rivas M (2015) Machine learning predictive models for mineral prospectivity: An evaluation of neural networks, random forest, regression trees and support vector machines. Ore Geol Rev 71:804–818. doi: 10.1016/j.oregeorev.2015.01.001.

Rothbaum BO, Hodges LF (1999) The Use of Virtual Reality Exposure in the Treatment of Anxiety Disorders. Behav Modif 23:507–525. doi: 10.1177/0145445599234001.

Ruggeri B, Sarkans U, Schumann G, Persico AM (2014) Biomarkers in autism spectrum disorder: The old and the new. Psychopharmacology (Berl) 231:1201–1216. doi: 10.1007/s00213-013-3290-7.

Rump KM, Giovannelli JL, Minshew NJ, Strauss MS (2009) The development of emotion recognition in individuals with autism. Child Dev 80:1434–1447. doi: 10.1111/j.1467-8624.2009.01343.x.

Saarimäki H, Gotsopoulos A, Jääskeläinen IP, Lampinen J, Vuilleumier P, Hari R, Sams M, Nummenmaa L (2016) Discrete Neural Signatures of Basic Emotions. Cereb Cortex 26:2563–2573. doi: 10.1093/cercor/bhv086.

Sadjadi SO, Hansen JHL (2015) Mean Hilbert envelope coefficients (MHEC) for robust speaker and language identification. Speech Commun 72:138–148. doi: 10.1016/j.specom.2015.04.005.

Saitovitch A, Bargiacchi A, Chabane N, Brunelle F, Samson Y, Boddaert N, Zilbovicius M

(2012) Social cognition and the superior temporal sulcus: Implications in autism. Rev Neurol (Paris) 168:762–770. doi: 10.1016/j.neurol.2012.07.017.

Sanchez-Vives M V., Slater M (2005) From presence to consciousness through virtual reality. Nat Rev Neurosci 6:332–339. doi: 10.1038/nrn1651.

Sarracanie M, Lapierre CD, Salameh N, Waddington DEJ, Witzel T, Rosen MS (2015) Low-Cost High-Performance MRI. Sci Rep 5:1–9. doi: 10.1038/srep15177.

Sato JR, Rondinoni C, Sturzbecher M, de Araujo DB, Amaro E (2010) From EEG to BOLD: Brain mapping and estimating transfer functions in simultaneous EEG-fMRI acquisitions. Neuroimage 50:1416–1426. doi: 10.1016/j.neuroimage.2010.01.075.

Schultz RT (2005) Developmental deficits in social perception in autism: the role of the amygdala and fusiform face area. Int J Dev Neurosci 23:125–141. doi: 10.1016/j.ijdevneu.2004.12.012.

Schurz M, Kronbichler M, Weissengruber S, Surtees A, Samson D, Perner J (2015) Clarifying the role of theory of mind areas during visual perspective taking: Issues of spontaneity and domain-specificity. Neuroimage 117:386–396. doi: 10.1016/j.neuroimage.2015.04.031.

Schwab S, Koenig T, Morishima Y, Dierks T, Federspiel A, Jann K (2015) Discovering frequency sensitive thalamic nuclei from EEG microstate informed resting state fMRI. Neuroimage 118:368–375. doi: 10.1016/j.neuroimage.2015.06.001.

Schwartz S, Kessler R, Gaughan T, Buckley AW (2017) Electroencephalogram Coherence Patterns in Autism: An Updated Review. Pediatr Neurol 67:7–22. doi: 10.1016/j.pediatrneurol.2016.10.018.

Scott-Van Zeeland AA, Dapretto M, Ghahremani DG, Poldrack RA, Bookheimer SY (2010) Reward processing in autism. Autism Res 3:n/a-n/a. doi: 10.1002/aur.122.

Sel A, Calvo-Merino B, Tuettenberg S, Forster B (2015) When you smile, the world smiles at you: ERP evidence for self-expression effects on face processing. Soc Cogn Affect Neurosci 10:1316–1322. doi: 10.1093/scan/nsv009.

Shibata K, Watanabe T, Sasaki Y, Kawato M (2011) Perceptual Learning Incepted by Decoded fMRI Neurofeedback Without Stimulus Presentation. Science (80-) 334:1413–1415. doi:

10.1126/science.1212003.

Shih P, Keehn B, Oram JK, Leyden KM, Keown CL, Müller R-A (2011) Functional Differentiation of Posterior Superior Temporal Sulcus in Autism: A Functional Connectivity Magnetic Resonance Imaging Study. Biol Psychiatry 70:270–277. doi: 10.1016/j.biopsych.2011.03.040.

Shim M, Kim D-W, Yoon S, Park G, Im C-H, Lee S-H (2016) Influence of spatial frequency and emotion expression on face processing in patients with panic disorder. J Affect Disord 197:159–166. doi: http://dx.doi.org/10.1016/j.jad.2016.02.063.

Silver M, Oakes P (2001) Evaluation of a new computer intervention to teach people with autism or Asperger syndrome to recognize and predict emotions in others. Autism 5:299–316.

Simões M, Abreu R, Gonçalves H, Rodrigues A, Bernardino I, Castelo-Branco M (2019a) Serious games for ageing : a pilot interventional study in a cohort of heterogeneous cognitive impairment. In: 2019 IEEE International Conference on Serious Games and Applications for Health (SeGAH). Kyoto: IEEE.

Simões M, Amaral C, Carvalho P, Castelo-Branco M (2014a) Specific EEG/ERP Responses to Dynamic Facial Expressions in Virtual Reality Environments. In: The International Conference on Health Informatics. IFMBE Proceedings (Zhang Y, ed), pp 331–334 IFMBE Proceedings. Cham: Springer. doi: 10.1007/978-3-319-03005-0_84.

Simões M, Amaral C, França F, Carvalho P, Castelo-Branco M (2019b) Applying Weightless Neural Networks to a P300-Based Brain-Computer Interface. In: World Congress on Medical Physics and Biomedical Engineering 2018. IFMBE Proceedings (Lhotska L, Sukupova L, Lacković I, Ibbott G, eds), pp 113–117. Singapore: Springer. doi: 10.1007/978-981-10-9023-3_20.

Simões M, Bernardes M, Barros F, Castelo-Branco M (2018a) Virtual Travel Training for Autism Spectrum Disorder: Proof-of-Concept Interventional Study. JMIR serious games 6:e5. doi: 10.2196/games.8428.

Simões M, Carvalho P, Castelo-Branco M (2012) Virtual reality and brain-computer interface for joint-attention training in autism. Proc 9th Intl Conf Disabil Virtual Real Assoc Technol:507–510.

Simoes M, Direito B, Lima J, Castelhano J, Ferreira C, Couceiro R, Carvalho P, Castelo-Branco M (2017) Correlated alpha activity with the facial expression processing network in a simultaneous EEG-fMRI experiment. In: 2017 39th Annual International Conference of the IEEE Engineering in Medicine and Biology Society (EMBC), pp 2562–2565. IEEE. doi: 10.1109/EMBC.2017.8037380.

Simões M, Gonçalves H, Abreu R, Pinto M, Pereira M, Castelo-Branco M (2019c) GameAAL – Gamification applied to ambient assisted living. In: 2019 IEEE International Conference on Serious Games and Applications for Health (SeGAH). Kyoto: IEEE.

Simoes M, Lima J, Direito B, Castelhano J, Ferreira C, Carvalho P, Castelo-Branco M (2015) Feature analysis for correlation studies of simultaneous EEG-fMRI data: A proof of concept for neurofeedback approaches. In: 2015 37th Annual International Conference of the IEEE Engineering in Medicine and Biology Society (EMBC), pp 4065–4068. IEEE. doi: 10.1109/EMBC.2015.7319287.

Simões M, Monteiro R, Andrade J, Mouga S, França F, Oliveira G, Carvalho P, Castelo-Branco M (2018b) A novel biomarker of compensatory recruitment of face emotional imagery networks in autism spectrum disorder. Front Neurosci 12:1–15. doi: 10.3389/fnins.2018.00791.

Simões M, Mouga S, Pedrosa F, Carvalho P, Oliveira G, Branco MC (2014b) Neurohab: A Platform for Virtual Training of Daily Living Skills in Autism Spectrum Disorder. In: Procedia Technology (João Varajão, Manuela Cunha, Niels Bjørn-Andersen, Rodney Turner, Duminda Wijesekera, Ricardo Martinho RR, ed), pp 1417–1423. Procedia Technology. doi: 10.1016/j.protcy.2014.10.161.

Simonoff E, Pickles A, Charman T, Chandler S, Loucas T, Baird G (2008) Psychiatric Disorders in Children With Autism Spectrum Disorders: Prevalence, Comorbidity, and Associated Factors in a Population-Derived Sample. J Am Acad Child Adolesc Psychiatry 47:921–929. doi: 10.1097/CHI.0b013e318179964f.

Sitaram R, Ros T, Stoeckel L, Haller S, Scharnowski F, Lewis-Peacock J, Weiskopf N, Blefari ML, Rana M, Oblak E, Birbaumer N, Sulzer J (2016) Closed-loop brain training: the science of neurofeedback. Nat Rev Neurosci 18:86–100. doi: 10.1038/nrn.2016.164.

Slater M (2003) A note on presence terminology. Presence Connect 3:1–5.

Slater M, Wilbur S (1997) A Framework for Immersive Virtual Environments (FIVE): Speculations on the Role of Presence in Virtual Environments. Presence Teleoperators Virtual Environ 6:603–616. doi: 10.1162/pres.1997.6.6.603.

Slocum TA, Detrich R, Wilczynski SM, Spencer TD, Lewis T, Wolfe K (2014) The evidence-based practice of applied behavior analysis. Behav Anal 37:41–56. doi: 10.1007/s40614-014-0005-2.

Smith MJ, Ginger EJ, Wright K, Wright MA, Taylor JL, Humm LB, Olsen DE, Bell MD, Fleming MF (2014) Virtual reality job interview training in adults with autism spectrum disorder. J Autism Dev Disord 44:2450–2463. doi: 10.1007/s10803-014-2113-y.

Smith SM (2002) Fast robust automated brain extraction. Hum Brain Mapp 17:143–155. doi: 10.1002/hbm.10062.

Solhjoo S, Nasrabadi AM, Golpayegani MRH (2005) Classification of chaotic signals using HMM classifiers: EEG-based mental task classification. 13th Eur Signal Process Conf EUSIPCO 2005:257–260.

Solnik S, Rider P, Steinweg K, Devita P, Hortobágyi T (2010) Teager-Kaiser energy operator signal conditioning improves EMG onset detection. Eur J Appl Physiol 110:489–498. doi: 10.1007/s00421-010-1521-8.

Sperdin HF, Coito A, Kojovic N, Rihs TA, Jan RK, Franchini M, Plomp G, Vulliemoz S, Eliez S, Michel CM, Schaer M (2018) Early alterations of social brain networks in young children with autism. Elife 7:1–18. doi: 10.7554/eLife.31670.

Spies M, Kraus C, Geissberger N, Auer B, Klöbl M, Tik M, Störkat IL, Hahn A, Woletz M, Pfabigan DM, Kasper S, Lamm C, Windischberger C, Lanzenberger R (2017) Default mode network deactivation during emotion processing predicts early antidepressant response. Transl Psychiatry 7:e1008-9. doi: 10.1038/tp.2016.265.

Spruston N (2008) Pyramidal neurons: dendritic structure and synaptic integration. Nat Rev Neurosci 9:206–221. doi: 10.1038/nrn2286.

Stichter JP, Laffey J, Galyen K, Herzog M (2014) iSocial: Delivering the Social Competence Intervention for Adolescents (SCI-A) in a 3D virtual learning environment for youth with high functioning autism. J Autism Dev Disord 44:417–430. doi: 10.1007/s10803-

013-1881-0.

Strickland D (1997) Virtual reality for the treatment of autism. Stud Health Technol Inform 44:81–86.

Strickland D, Marcus LM (1996) Brief report: Two case studies using virtual reality as a learning tool for autistic children. 26:651–659.

Sulzer J, Haller S, Scharnowski F, Weiskopf N, Birbaumer N, Blefari ML, Bruehl AB, Cohen LG, DeCharms RC, Gassert R, Goebel R, Herwig U, LaConte S, Linden D, Luft A, Seifritz E, Sitaram R (2013) Real-time fMRI neurofeedback: progress and challenges. Neuroimage 76:386–399. doi: 10.1016/j.neuroimage.2013.03.033.

Sutherland IE (1965) The Ultimate Display. Proc IFIPS Congr 2:506–508. doi: 10.1109/MC.2005.274.

Swettenham J (1996) Can children with autism be taught to understand false belief using computers? J Child Psychol Psychiatry Allied Discip 37:157–165. doi: 10.1111/j.1469-7610.1996.tb01387.x.

Tagliazucchi E, Laufs H (2015) Multimodal Imaging of Dynamic Functional Connectivity. Front Neurol 6:1–9. doi: 10.3389/fneur.2015.00010.

Takahashi HK, Kitada R, Sasaki AT, Kawamichi H, Okazaki S, Kochiyama T, Sadato N (2015) Brain networks of affective mentalizing revealed by the tear effect: The integrative role of the medial prefrontal cortex and precuneus. Neurosci Res 101:32–43. doi: 10.1016/j.neures.2015.07.005.

Takens F (1981) Detecting strange attractors in turbulence. In: Dynamical Systems and Turbulence (Rand DA, Young LS, eds), pp 366–381 Lecture Notes in Mathematics (Dynamical Systems and Turbulence, Warwick 1980). Springer. doi: 10.1007/BFb0091924.

Tanaka JW, Sung A (2016) The "Eye Avoidance" Hypothesis of Autism Face Processing. J Autism Dev Disord 46:1538–1552. doi: 10.1007/s10803-013-1976-7.

Tartaglia EM, Bamert L, Mast FW, Herzog MH (2009) Human Perceptual Learning by Mental Imagery. Curr Biol 19:2081–2085. doi: 10.1016/j.cub.2009.10.060.

Tavares PP, Mouga SS, Oliveira GG, Castelo-Branco M (2016) Preserved face inversion effects in adults with autism spectrum disorder. Neuroreport 27:587–592. doi: 10.1097/wnr.0000000000000576.

Tenke CE, Kayser J (2012) Generator localization by current source density (CSD): Implications of volume conduction and field closure at intracranial and scalp resolutions. Clin Neurophysiol 123:2328–2345. doi: 10.1016/j.clinph.2012.06.005.

Thal LJ, Kantarci K, Reiman EM, Klunk WE, Weiner MW, Zetterberg H, Galasko D, Pratic?? D, Griffin S, Schenk D, Siemers E (2006) The Role of Biomarkers in Clinical Trials for Alzheimer Disease. Alzheimer Dis Assoc Disord 20:6–15. doi: 10.1097/01.wad.0000191420.61260.a8.

Thornton RC, Rodionov R, Laufs H, Vulliemoz S, Vaudano A, Carmichael D, Cannadathu S, Guye M, McEvoy A, Lhatoo S, Bartolomei F, Chauvel P, Diehl B, De Martino F, Elwes RDC, Walker MC, Duncan JS, Lemieux L (2010) Imaging haemodynamic changes related to seizures: Comparison of EEG-based general linear model, independent component analysis of fMRI and intracranial EEG. Neuroimage 53:196–205. doi: 10.1016/j.neuroimage.2010.05.064.

Threapleton K, Drummond A, Standen P (2016) Virtual rehabilitation: What are the practical barriers for home-based research? Digit Heal 2:205520761664130. doi: 10.1177/2055207616641302.

Tye C, Battaglia M, Bertoletti E, Ashwood KL, Azadi B, Asherson P, Bolton P, McLoughlin G (2014) Altered neurophysiological responses to emotional faces discriminate children with ASD, ADHD and ASD+ADHD. Biol Psychol 103:125–134. doi: 10.1016/j.biopsycho.2014.08.013.

van Diepen RM, Mazaheri A (2017) Cross-sensory modulation of alpha oscillatory activity: suppression, idling, and default resource allocation. Eur J Neurosci 45:1431–1438. doi: 10.1111/ejn.13570.

Van Heijst BFC, Geurts HM (2015) Quality of life in autism across the lifespan: A meta-analysis. Autism 19:158–167. doi: 10.1177/1362361313517053.

van Zijl PCM, Hua J, Lu H (2012) The BOLD post-stimulus undershoot, one of the most debated issues in fMRI. Neuroimage 62:1092–1102. doi:

10.1016/j.neuroimage.2012.01.029.

Vanderperren K, De Vos M, Ramautar JR, Novitskiy N, Mennes M, Assecondi S, Vanrumste B, Stiers P, Van den Bergh BRH, Wagemans J, Lagae L, Sunaert S, Van Huffel S (2010) Removal of BCG artifacts from EEG recordings inside the MR scanner: A comparison of methodological and validation-related aspects. Neuroimage 50:920–934. doi: 10.1016/j.neuroimage.2010.01.010.

Varoquaux G, Raamana PR, Engemann DA, Hoyos-Idrobo A, Schwartz Y, Thirion B (2017) Assessing and tuning brain decoders: Cross-validation, caveats, and guidelines. Neuroimage 145:166–179. doi: 10.1016/j.neuroimage.2016.10.038.

Velikova S, Magnani G, Arcari C, Falautano M, Franceschi M, Comi G, Leocani L (2011) Cognitive impairment and EEG background activity in adults with Down's syndrome: A topographic study. Hum Brain Mapp 32:716–729. doi: 10.1002/hbm.21061.

Vivanti G, Fanning PAJ, Hocking DR, Sievers S, Dissanayake C (2017) Social attention, joint attention and sustained attention in autism spectrum disorder and williams syndrome: Convergences and divergences. J Autism Dev Disord 47:1866–1877. doi: 10.1007/s10803-017-3106-4.

Vlamings P, Jonkman L, Van Daalen E, Van Der Gaag RJ, Kemner C (2010) Basic abnormalities in visual processing affect face processing at an early age in autism spectrum disorder. Biol Psychiatry 68:1107–1113. doi: 10.1016/j.biopsych.2010.06.024.

Vogeley K, Bussfeld P, Newen A, Herrmann S, Happé F, Falkai P, Maier W, Shah NJ, Fink GR, Zilles K (2001) Mind reading: Neural mechanisms of theory of mind and self-perspective. Neuroimage 14:170–181. doi: 10.1006/nimg.2001.0789.

Vorwerk J, Clerc M, Burger M, Wolters CH (2012) Comparison of boundary element and finite element approaches to the EEG forward problem. Biomed Tech 57:795–798. doi: 10.1515/bmt-2012-4152.

Vranic A (2003) Personal Space in Physically Abused Children. Environ Behav 35:550–565. doi: 10.1177/0013916503035004006.

Vulliemoz S, Rodionov R, Carmichael DW, Thornton R, Guye M, Lhatoo SD, Michel CM, Duncan JS, Lemieux L (2010) Continuous EEG source imaging enhances analysis of

EEG-fMRI in focal epilepsy. Neuroimage 49:3219–3229. doi: 10.1016/j.neuroimage.2009.11.055.

Wagner JB, Hirsch SB, Vogel-Farley VK, Redcay E, Nelson CA (2013) Eye-tracking, autonomic, and electrophysiological correlates of emotional face processing in adolescents with autism spectrum disorder. J Autism Dev Disord 43:188–199. doi: 10.1007/s10803-012-1565-1.

Walden K, Pornpattananangkul N, Curlee A, McAdams DP, Nusslock R (2014) Posterior versus frontal theta activity indexes approach motivation during affective autobiographical memories. Cogn Affect Behav Neurosci 15:132–144. doi: 10.3758/s13415-014-0322-7.

Wan X, Sekiguchi A, Yokoyama S, Riera J, Kawashima R (2008) Electromagnetic source imaging: Backus–Gilbert resolution spread function-constrained and functional MRI-guided spatial filtering. Hum Brain Mapp 29:627–643. doi: 10.1002/hbm.20424.

Wang Q, Sourina O, Nguyen MK (2011) Fractal dimension based neurofeedback in serious games. Vis Comput 27:299–309. doi: 10.1007/s00371-011-0551-5.

Wang W, Viswanathan S, Lee T, Grafton ST (2016) Coupling between theta oscillations and cognitive control network during cross-modal visual and auditory attention: Supramodal vs modality-specific mechanisms. PLoS One 11:1–16. doi: 10.1371/journal.pone.0158465.

Webb SJ, Dawson G, Bernier R, Panagiotides H (2006) ERP evidence of atypical face processing in young children with autism. J Autism Dev Disord 36:881–890. doi: 10.1007/s10803-006-0126-x.

Weiskopf N, Scharnowski F, Veit R, Goebel R, Birbaumer N, Mathiak K (2004) Self-regulation of local brain activity using real-time functional magnetic resonance imaging (fMRI). J Physiol 98:357–373. doi: 10.1016/j.jphysparis.2005.09.019.

White SW, Oswald D, Ollendick T, Scahill L (2009) Anxiety in children and adolescents with autism spectrum disorders. Clin Psychol Rev 29:216–229. doi: 10.1016/j.cpr.2009.01.003.

Whyte EM, Smyth JM, Scherf KS (2015) Designing Serious Game Interventions for

Individuals with Autism. J Autism Dev Disord 45:3820–3831. doi: 10.1007/s10803-014-2333-1.

Wied P (n.d.) heatmap.js - Dynamic Heatmaps for the Web.

Wolters CH, Grasedyck L, Hackbusch W (2004) Efficient computation of lead field bases and influence matrix for the FEM-based EEG and MEG inverse problem. Inverse Probl 20:1099–1116. doi: 10.1088/0266-5611/20/4/007.

Won H, Mah W, Kim E (2013) Autism spectrum disorder causes, mechanisms, and treatments: focus on neuronal synapses. Front Mol Neurosci 6:1–26. doi: 10.3389/fnmol.2013.00019.

Wong TKW, Fung PCW, Chua SE, McAlonan GM (2008) Abnormal spatiotemporal processing of emotional facial expressions in childhood autism: dipole source analysis of event-related potentials. Eur J Neurosci 28:407–416. doi: 10.1111/j.1460-9568.2008.06328.x.

Woolrich MW, Ripley BD, Brady M, Smith SM (2001) Temporal autocorrelation in univariate linear modeling of FMRI data. Neuroimage 14:1370–1386. doi: 10.1006/nimg.2001.0931.

World Health Organization (1993) The ICD-10 Classification of Mental and Behavioural Disorders. Nonserial Publ WHO 10:1–267.

Yang YL, Deng HX, Xing GY, Xia XL, Li HF (2015) Brain functional network connectivity based on a visual task: Visual information processing-related brain regions are significantly activated in the task state. Neural Regen Res 10:298–307. doi: 10.4103/1673-5374.152386.

Yentes JM, Hunt N, Schmid KK, Kaipust JP, McGrath D, Stergiou N (2013) The appropriate use of approximate entropy and sample entropy with short data sets. Ann Biomed Eng 41:349–365. doi: 10.1007/s10439-012-0668-3.

Young KD, Siegle GJ, Zotev V, Phillips R, Misaki M, Yuan H, Drevets WC, Bodurka J (2017) Randomized clinical trial of real-time fMRI amygdala neurofeedbackfor major depressive disorder: Effects on symptoms and autobiographical memory recall. Am J Psychiatry 174:748–755. doi: 10.1176/appi.ajp.2017.16060637.

Yuan H, Zotev V, Phillips R, Drevets WC, Bodurka J (2012) Spatiotemporal dynamics of the brain at rest — Exploring EEG microstates as electrophysiological signatures of BOLD resting state networks. Neuroimage 60:2062–2072. doi: 10.1016/j.neuroimage.2012.02.031.

Zakari HM, Ma M, Simmons D (2014) A Review of Serious Games for Children with Autism Spectrum Disorders (ASD). In: Lecture Notes in Computer Science: Serious Games Development and Applications (Ma M, Oliveira MF, Baalsrud Hauge J, eds), pp 93–106 Lecture Notes in Computer Science. Cham: Springer International Publishing. doi: 10.1007/978-3-319-11623-5_9.

Zhang Y, Brady M, Smith S (2001) Segmentation of brain MR images through a hidden Markov random field model and the expectation-maximization algorithm. IEEE Trans Med Imaging 20:45–57. doi: 10.1109/42.906424.

Zheng C, Colgin LL (2015) Beta and Gamma Rhythms Go with the Flow. Neuron 85:236–237. doi: 10.1016/j.neuron.2014.12.067.

Zotev V, Phillips R, Yuan H, Misaki M, Bodurka J (2014) Self-regulation of human brain activity using simultaneous real-time fMRI and EEG neurofeedback. Neuroimage 85:985–995. doi: 10.1016/j.neuroimage.2013.04.126.

Appendix I

Targeting dynamic facial processing mechanisms in superior temporal sulcus using a novel fMRI neurofeedback target

This appendix is composed by the contents of the following publication:

Direito B, Lima J, Simões M, Sayal A, Sousa T, Luehrs M, Ferreira C, Castelo-Branco M (2019) Targeting dynamic facial processing mechanisms in superior temporal sulcus using a novel fMRI neurofeedback target. Neuroscience 406:97–108. doi: 10.1016/j.neuroscience.2019.02.024.

Abstract

The superior temporal sulcus (STS) encompasses a complex set of regions involved in a wide range of cognitive functions. To understand its functional properties, neuromodulation approaches such brain stimulation or neurofeedback can be used. We investigated whether the posterior STS (pSTS), a core region in the face perception and imagery network, could be specifically identified based on the presence of dynamic facial expressions (and not just on simple motion or static face signals), and probed with neurofeedback. Recognition of facial expressions is critically impaired in autism spectrum disorder, making this region a relevant target for future clinical neurofeedback studies. We used a stringent localizer approach based on the contrast of dynamic facial expressions against static neutral faces plus moving dots. The target region had to be specifically responsive to dynamic facial expressions instead of mere motion and/or the presence of a static face. The localizer was successful in selecting this region across subjects. Neurofeedback was then performed, using this region as a target, with two novel feedback rules (mean or derivative-based, using visual or auditory interfaces). Our results provide evidence that a facial expression-selective cluster in pSTS can be identified and may represent a suitable target for neurofeedback approaches, aiming at social and emotional cognition. These findings highlight the presence of a highly selective region in STS encoding

dynamic aspects of facial expressions. Future studies should elucidate its role as a mechanistic target for neurofeedback strategies in clinical disorders of social cognition such as autism.

1. Introduction

The organization of the superior temporal sulcus (STS) comprises distinct functional sub-regions that have been previously associated to various features of social perception and cognition. These include the perception and imagery of facial expressions, as well as understanding others' actions or mental states (Allison et al., 2000; Hein and Knight, 2008; Pitcher et al., 2011; Deen et al., 2015).

In terms of the organization of STS, Deen et al. (2015) proposed a structured set of domain-specific regions along a posterior-to-anterior axis. According to the study, this rich spatial organization is compatible with the existence of sub- regions that integrate information from several neighboring sources.

One of the most relevant sub-regions in terms of social cognition is the posterior region of the STS (pSTS). Ishai et al. (2002) found small subsets of face-selective regions (in the face perception network, including STS) which activated during visual imagery of famous faces. Kim et al. (2007) examined brain activity during imagery of emotional facial expressions and compared to the imagery of neutral facial expressions. The authors report the activation of the amygdala, dorsolateral prefrontal cortex, ventral premotor cortex, STS, parahippocampal gyrus, lingual gyrus and the midbrain. Rebola and Castelo-Branco (2014) reported a direct link between pSTS and the social face cognition net- works. Most of these studies use relatively liberal functional contrast criteria, which is not optimal to isolate processing of specific features, although this enables higher statistical power at the cost of specificity. Nevertheless, the studies support the notion that there are common neural correlates involved in visual perception and imagery in the pSTS. Taking this into account, we hypothesize that the brain activity of functional subdomains within the pSTS can be volitionally modulated using imagery strategies, paving the way to neurofeedback approaches targeting this region. Here we aimed to isolate the functional subdomain related specifically to dynamic facial expressions, irrespective of simple motion signals or the presence of a static face.

1.1 A neuroscientific approach based on neurofeedback to study facial expression of emotions

Determining whether individuals are able to volitionally control the pSTS subdomain activity using neurofeedback strategies is relevant given the association between impaired functional activation patterns in pSTS and social cognition disorders such as autism spectrum disorder (ASD) (Saitovitch et al., 2012; Alaerts et al., 2014; Cheng et al., 2015). ASD is characterized by a range of clinical features that include deficits in the identification and interpretation of the emotional and mental state of others (Baron-Cohen et al., 2001). Neurobiological theories on the mechanisms underlying this condition commonly emphasize impaired neuroactivation in regions such as the amygdala (involved in emotional processing), the STS and the fusiform gyrus (important in face recognition) (Silver and Rapin, 2012). Additionally, neuroimaging studies suggest widespread abnormalities affecting these and other regions and connections over distributed networks (Muller, 2007).

Neuroscientific and technological advances in functional magnetic resonance imaging (fMRI) combined with multi- variate supervised learning methods have made possible to decode brain states in real time. Such states can be assessed noninvasively, by measures of the blood oxygenation level-dependent (BOLD) signal, which is a delayed, indirect measure of neural activity (Logothetis, 2008). These advances led to the recognition of real-time fMRI (rt-fMRI) as a potentially useful tool in a broad range of basic and clinical applications that include diagnosis, disease monitoring, or even therapeutic approaches based on neurofeedback (Weiskopf et al., 2007; Subramanian et al., 2011).

In neurofeedback studies, the decoded brain states are presented to the participants, who are instructed to control their own brain activity in real time (LaConte, 2011; Weiskopf, 2012). This closed-loop approach combined with the human inherent adaptability and flexibility to volitionally up- and down-regulate attention and engagement (Mishra and Gazzaley, 2015), facilitates specific changes in brain function and may ultimately optimize system-level neuroplasticity (Ros et al., 2010; Sagi et al., 2012).

Neurofeedback in therapeutic applications features the enablement of the control of physiological targets to be trained (based on skill learning), producing changes in specific neural networks that might be clinically useful by restoring impaired cognition and/or behavior (Stoeckel et al., 2014). Moreover, there is increasing evidence that self-regulation through fMRI neurofeedback is achievable in both healthy individuals and psychiatric patients (Ruiz et al., 2013b).

1.1.1 Functional properties of neurofeedback target regions: challenges and the need for a mechanistic approach

Various target areas (regions of interest, ROIs) have been previously chosen for neurofeedback-guided modulation such as the somatosensory cortex (deCharms et al., 2004; Bray et al., 2007), motor areas (Weiskopf et al., 2004; LaConteetal.,2007; Sitarametal.,2012), the amygdala (Posse et al., 2003; Johnston et al., 2010), the anterior cingulate cortex (ACC) (Weiskopf et al., 2003; deCharms et al., 2005; Hamilton et al., 2011; Mathiak et al., 2015) and visual areas (Sousa et al., 2016).

Considering electroencephalography-based brain–computer interfaces (BCI) / neurofeedback applications, only about one third of participants can immediately achieve brain control (Friedrich et al., 2014). Another third would only gain rough control after training, while the rest of the participants are unable to achieve control using BCI or neuro- feedback setups. In this sense, different aspects may contribute to the participants' engagement and success in BCI and neurofeedback technologies, such as the type of training protocol (including task, instructions and feedback type) and psychological traits such as motivation (Reiner et al., 2018).

In recent years, an emerging trend in neurofeedback research is the pairing of stimulus and feedback presentation with more explicit rewards directly related to the goals of the intervention. In a classic approach, the feedback is presented as a thermometer with a discrete color bar changing its level based on the brain activity in the target area selected; the instructions given to the participants are to increase or decrease the colored bar level. The participants' own reward is achieved by successfully con- trolling the thermometer display. Novel approaches use task-related stimuli, namely images with dynamically changing properties (e.g. size) which are adjusted as a function of brain activity. deCharms et al. (2005)

used a continuous video display depicting a larger or smaller virtual fire to learn to control activation in the rostral ACC (a region involved in pain perception and regulation). Sokunbi et al. (2014) introduced a presentation framework that uses food pictures to evoke responses in areas related to food craving: the brain activity mediated gradual changes in picture size. Mathiak et al. (2015) introduced "social reward" in their feedback paradigm. A positive feedback, for the successful control in the dorsal ACC, is provided through a facial expression (avatar smiling). Recently, Krause et al. (2017) successfully tested 2 alternatives to the thermometer display, demonstrating the feasibility of multiple visual feedback presentations.

Given the importance of face perception in normal human cognition and social interaction, the pivotal role of pSTS in this process, and the ability shown by healthy subjects to self-regulate BOLD activity of specific ROIs, it is pertinent to investigate the ability to self-regulate BOLD activity derived from functionally defined subdomains in pSTS, and thereby test their physiological selectivity.

The current study explores the definition of a functional sub-domain in pSTS based on a very selective localizer approach specifically isolating the processing of facial expressions. Moreover, we aimed to probe it by designing new neuro- feedback interfaces, and to determine if such combination (rt-fMRI neurofeedback technique, mental imagery strategies and novel neurofeedback target) is feasible.

To this end, we investigated the following research questions: (1) Is it possible to reliably define a functional subdomain in pSTS that selectively encodes dynamic facial expressions, irrespective of the simple presence of motion and/or static faces? (2) Can one probe this pSTS domain as a mechanistic neurofeedback target based on mental imagery strategies?

We addressed these questions based on 2 groups: an active and an alternative ROI group. Both performed neuro- feedback training using two interfaces: a visual and an auditory one. The feedback indicated variations in the activation level of a pSTS ROI in the active neurofeedback group (NF group). To control for non-specific effects of the neurofeedback procedure, the participants of the alternative ROI – control group (alt-roi group) attempted to up-regulate their brain activity based on an ROI selected with a set of voxels non-related to the task. The ability to voluntarily modulate pSTS in an identical paradigm with no feedback served as a measure for within-subject control.

2. Methods

2.1 Participants

Twenty healthy participants were recruited for a single-blind neurofeedback experiment and assigned to 1 of 2 groups. One group received feedback from the pSTS target region — NF group, and the other received feedback from an alternative ROI – alt-roi group. All participants remained unaware of the group assignment and successfully completed the protocol.

Hence, 10 participants were assigned to the NF group (9 male; mean age: 25.70 ± 3.65 years) and the other 10 to the alt-roi group (8 male; mean age 26.60 ± 3.02 years). None of the participants had a history of neurological disorders, based on their medical and psychiatric history. Most of the participants in this study are male which is in line with a future application in autism research where males dominate.

This study was approved by the Ethics Commission of the Faculty of Medicine of the University of Coimbra and was conducted in accordance with the declaration of Helsinki. All subjects provided written informed consent to participate in the study.

2.2 System architecture and stimuli presentation

The data-flow implemented in the rt-fMRI neurofeedback system includes a closed-loop setup composed of 3 major subsystems responsible for successfully accomplishing 3 tasks: A) fMRI image acquisition, B) signal processing and C) neuroimaging-based feedback. The three subsystems are connected using a Local Area Network.

Subsystem A is the MRI scanner/acquisition equipment (3-T Siemens Magnetom Trio scanner with a 12-channel head coil, at the Portuguese Brain Imaging Network) that is connected to the image processing subsystem (B). The data are collected and saved in a network shared folder.

Subsystem B accesses the data and performs data preprocessing and real-time statistical analysis using Turbo BrainVoyager 3.2 (TBV) (Brain Innovation, Maastricht, The

Netherlands). The mean BOLD values computed in real- time are based on an ROI defined with a functional localizer run of pSTS performed prior to the neurofeedback task.

Subsystem C performs the computation of the neuroimaging-based feedback and is connected to the monitor placed inside the MRI scanner room (the routines were programmed using the Psychophysics toolbox (Brainard, 1997)). At the beginning of each run, a new randomized protocol is created and shared with subsystem B for the creation of the appropriate general linear model (GLM). During the neurofeedback run, subsystem C receives the average BOLD values and computes the feedback values, presenting visual (or auditory) stimuli. The feedback presentation strategy considers the delays inherent to the signal acquisition, signal processing and feedback calculation processes (we further detail the computational aspects of the feedback calculation in the following sections).

The visual stimuli were designed with an 800 × 600–pixel resolution and presented on a 70 × 39.5–cm LCD monitor, with a resolution of 1920 × 1080 pixels (refresh rate of 60 Hz), that the participant observes through a mirror The LCD was placed at an effective distance of 156 cm from the participant's eyes resulting on a vertical visual angle of approximately 8°.

2.3 Experimental protocol

Each scanning session started with a high-resolution magnetization-prepared rapid acquisition gradient echo sequence for co-registration of functional data [176 slices; echo time (TE): 3.42 ms; repetition time (TR): 2530 ms; voxel size 1mm3 isotropic, flip angle (FA): 7°; matrix size: 256 × 256].

Participants from both groups were briefed on the experimental goals and were given the same instructions. An experienced MRI technician accompanied the participants to the scanner and placed them on the table. Foam cushions were placed to minimize head movements throughout the experiments.

After the structural image sequence, 4 functional sequences were acquired: 1 functional localizer and 3 imagery runs. To cover the occipital and posterior temporal lobes, 33 slices of 3 mm thickness were selected, with in-plane resolution: 4mm2, matrix size: 64 × 64, FA: 90°, TR: 2000 ms and TE: 30 ms. The protocol duration was approximately 40 min.

2.3.1 Localizer run

The pSTS region was functionally localized using a block-based design with 40 blocks of 8 s and 5 different conditions (160 volumes in total). Each condition was repeated 8 times during the localizer run. The subjects were instructed to attentively look at the screen. This localizer was very selective for the processing of facial expressions, as explained below in terms of the chosen statistical contrasts.

The functional localizer comprised 5 conditions: i. Neutral – static neutral face to help subtract static aspects of face processing; ii. Happy – morphing face from neutral to happy; iii. Sad – morphing face from neutral to sad; iv. Alternate expressions – alternating between sad and happy; v. Moving dots – randomly moving dots, to help subtract motion processing.

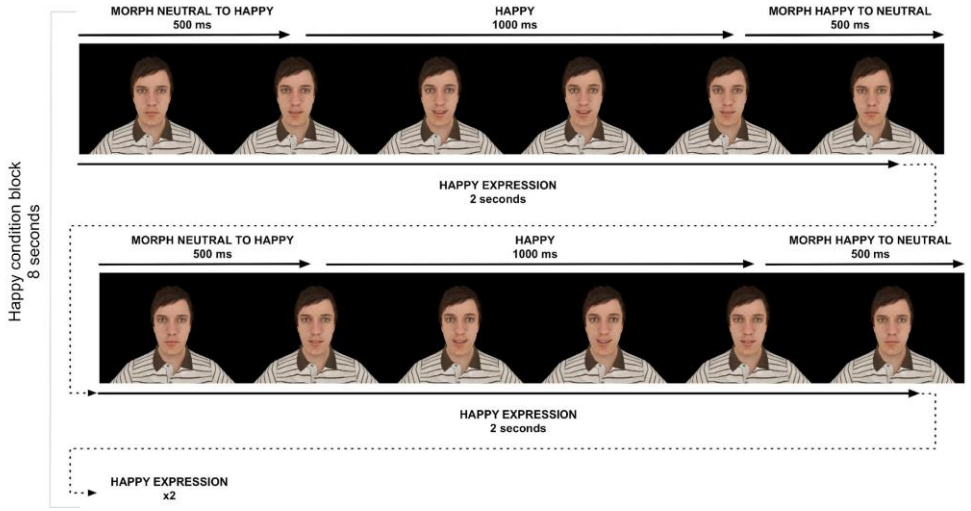

Figure 1 – The localizer includes 5 different conditions: i. Neutral; ii. Happy; iii. Sad; iv. Alternate expressions; v. Moving dots. The figure presents a scheme of condition ii. Happy. The avatar starts in the neutral position and morphs from neutral to happy inthe first 500 ms, holds the expression during 1000ms, and thenmorphs back to neutral during the last 500 ms. The expression is repeated 4 times during each block.

Video clips of an avatar performing a facial expression (Vizard Virtual Reality Software Toolkit, Worldviz) were used as stimuli for conditions ii. Happy, iii. Sad and iv. Alternate expressions. The video clips were composed of 60 frames, presented at a frame rate of 30 images per second (total duration of 2 s). Expression conditions (ii. Happy, iii. Sad, iv. Alternate expressions) were morphed from neutral to the endpoint expression during the first 500 ms; the expression was held during 1000 ms, and then morphed back to neutral during

500 ms (Fig. 1 exemplifies the process for condition ii. Happy). This process is repeated 4 times in each block.

According to Furl et al. (2013), contrasting between dynamic and static faces versus static objects, dynamic objects and random-dot patterns allows for the identification of the face-selective areas (including face and biological motion perception, and social content of the dynamical facial expressions). To isolate a functional subdomain in the posterior portion of STS (closely related to face perception (Deen et al., 2015)), we introduced as control stimuli the conditions v. Moving and i. Neutral. Note that this localizer approach is quite stringent, since the regions processing static facial features will be elicited by the non-dynamic face stimuli. With this contrast, we aim to capture the brain areas responsible for the specific processing of dynamic facial expressions.

The data were analyzed in real-time as implemented in TBV. The design matrix contained a separate predictor for each of the 5 conditions. The real-time setup allowed continuous monitoring of the BOLD signal time-course.

2.3.1.1 Regions of interest selection

The NF group target area was selected according to the contrast (i. Neutral, v. Moving dots) < (ii. Happy, iii. Sad, iv. Alternate expressions), balanced. A 3-dimensional box was visually selected in TBV over the cluster displaying the strongest response in the statistical activation map around the posterior portion of the STS, on either the left or right hemisphere. The voxels significantly activated in this 3-dimensional box defined our target region of interest for neurofeedback.

Despite previous studies associating the right pSTS region to the processing of information with social content (e.g. gaze and voice (Pelphrey and Carter, 2008; Saitovitch et al., 2012)), in this study we aimed to explore the best placement for a neurofeedback target specifically related with facial expression processing. To this end, we selected the neuro- feedback target in the hemisphere presenting the strongest response in the pSTS region.

The functional approach to select the ROI takes into account inter-subject variability. This decision was based on the observation that the functional domain of interest (and the focus of our study) does not necessarily follow precise anatomical landmarks, and to ensure optimal selection of voxels for calculating a stable neurofeedback signal for each participant.

The alt-roi group ROI was based on a scattered set of white matter voxels that presented nonsignificant statistical values for the contrast of interest. The selection of the ROI was determined by the need to select a set of voxels uncorrelated with the task proposed and stimuli presented throughout the procedure, i.e. the alternative brain signal must be functionally and neuroanatomically as independent as possible (Alino et al., 2016).

2.3.2 Imagery runs

After the definition of the neurofeedback target region, the participants from both groups performed 2 rt-fMRI- neurofeedback runs.

Each run presented 25 blocks (12 up-regulation blocks alternating with 13 down-regulation blocks), each one with the duration of 24 s, totaling a length of 600 s (300 volumes). At the beginning of each block, an auditory instruction was given to the participant presenting the condition, while at the end a beep informed them of the end of each block.

Each run consisted of 4 conditions. The up-regulation blocks included three randomly presented conditions: ii. Happy — imagery of a happy facial expression, iii. Sad — imagery of a sad facial expression, iv. Alternate — alternated imagery of happy and sad facial expressions. The down-regulation condition is the i. Neutral — imagery of a static neutral facial expression. Participants from both groups were instructed to upregulate mean ROI activation during conditions ii. Happy, iii. Sad and iv. Alternate and to downregulate during condition i. Neutral. Feedback would inform them of the activation pattern during the run.

The participants were informed about the hemodynamic delay (approximately 6 s between any change in brain activity and its effect in the BOLD activation pattern). We tested 2 different neurofeedback modalities: visual and auditory. One of the neurofeedback runs was performed with a task-tailored visual feedback while the other was performed with auditory feedback based on the derivative of the BOLD activity. The starting order was randomized.

2.3.3 Visual feedback

During visual feedback runs (Fig. 2), the expression of the avatar in the screen was updated based on the mean ROI activation of the neurofeedback target. The expression of the avatar

was discretized into 15 levels (between neutral and the endpoint expression). The expression level displayed is determined considering the level of the mean ROI activation signal variation.

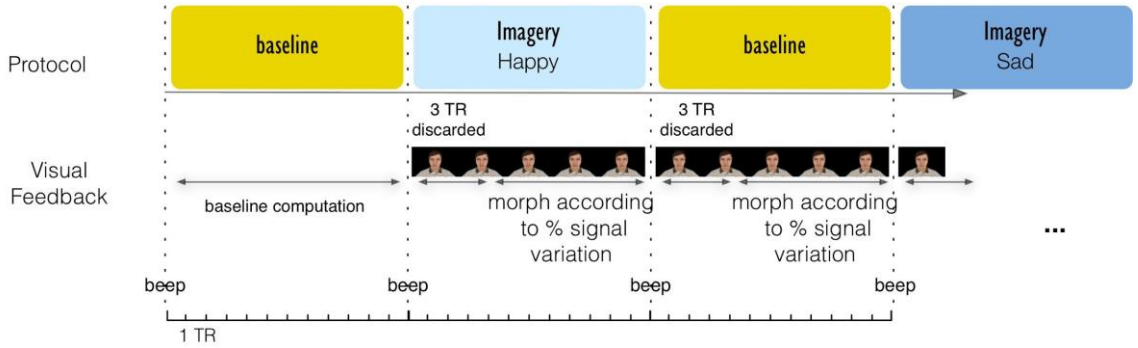

Figure 2 - Block design of the visual neurofeedback runs.

Flow-chart in Fig. 3 presents the visual feedback algorithm.

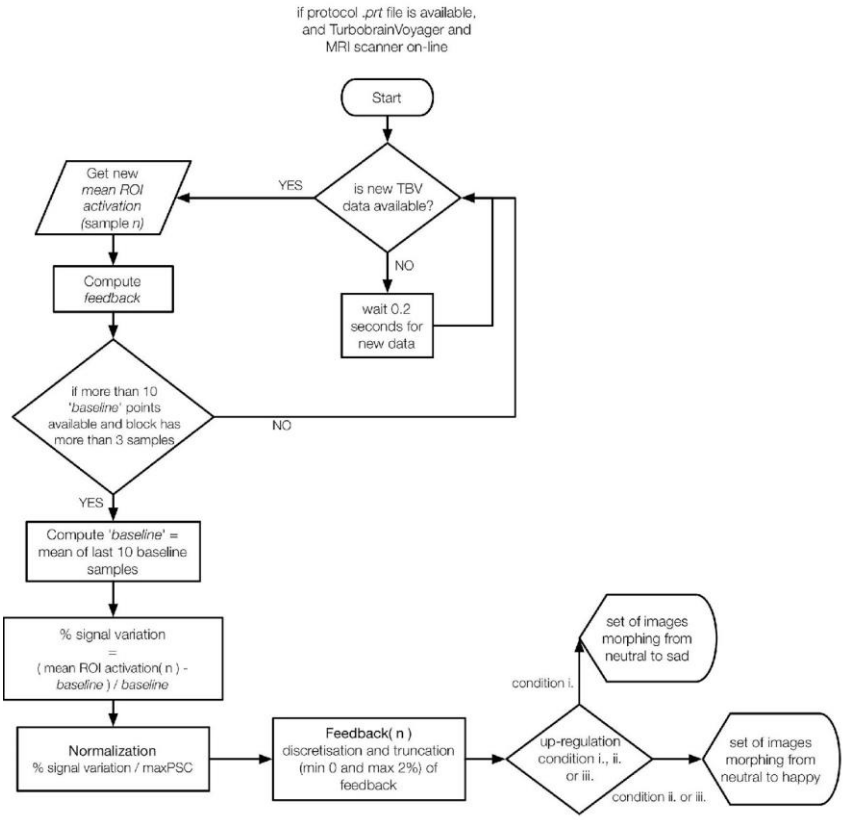

Figure 3 - Algorithm for visual feedback.

First, the protocol is created. The acquisition starts with a baseline block which allows the computation of the baseline variable b (BOLD activity in the ROI - mean over the ROI voxels for the last 10 samples of condition i. Neutral). Computing the baseline considering points from the i. Neutral condition block just before the up-regulation blocks mitigates the impact of low frequency drifts on the baseline and feedback values.

When new samples become available, the feedback is computed after 3 points have been received. The waiting period is due to the delay inherent to the process (e.g. hemodynamic delay). If these rules apply, the signal variation is computed for every new sample and according to Eq. 1:

$$\% \text{ signal variation } (n) = (x(n) - b) / b \qquad \text{(Eq. 1)}$$

where x(n) represents ROI activation (mean over the voxels) in sample n and b the baseline. The baseline variable is calculated (and updated at every time point throughout the run) based on a data buffer containing the last 10 samples of the down-regulation condition i. Neutral. The signal variation value is then normalized and discretized (considering 15 levels). The avatar morphs to the endpoint expression when level 15 is achieved (happy for conditions ii. Happy. and iv. Alternate, and sad for condition iii. Sad).

2.3.4 Auditory feedback

The rationale supporting the auditory algorithm is the control of the brain activity based on the feedback of the short-term trend of the mean ROI activity.

The short-term (three samples, i.e. 6 s) positive or negative trend is translated into a "positive" or "negative" sound, respectively. To help the participant in the imagery task, we briefly (2 s) present the avatar's neutral expression before the instruction (Fig. 4).

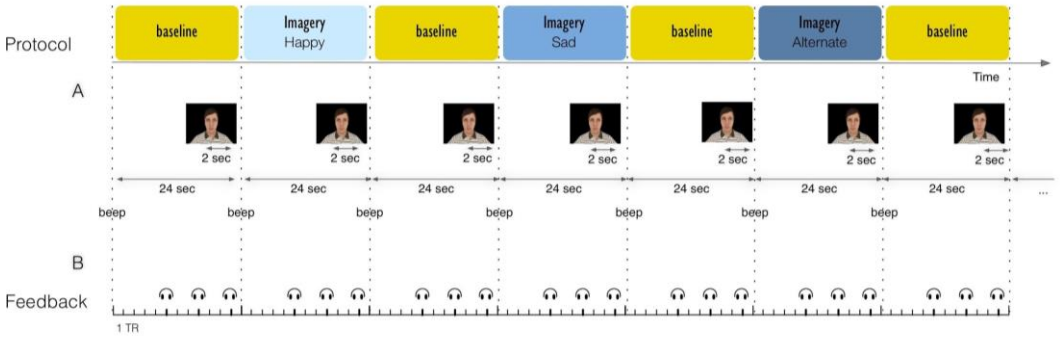

Figure 4 - Block design of the auditory neurofeedback runs.

Flow-chart in Fig. 5 presents the auditory feedback algorithm.

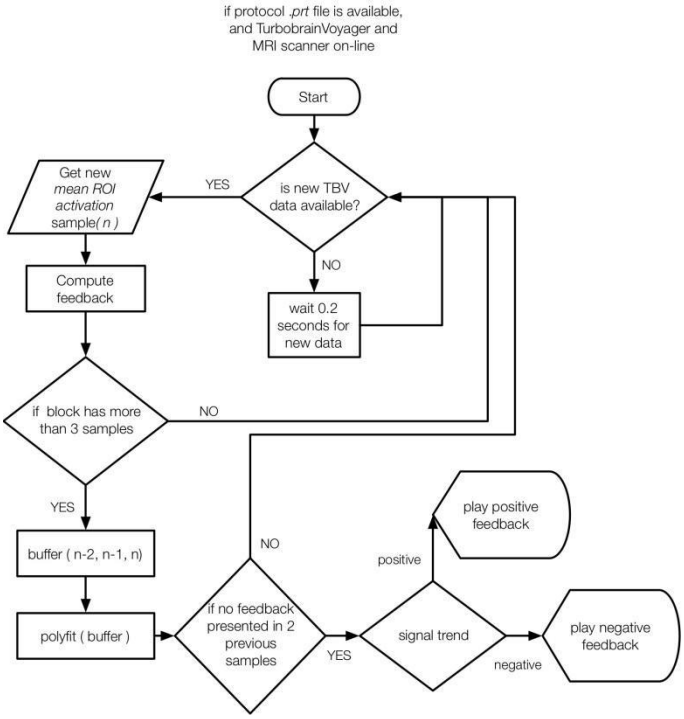

Figure 5 - Algorithm for auditory feedback.

Similarly to the visual feedback algorithm, the protocol is created in subsystem C and shared with subsystem B.

We calculate the feedback (positive or negative) based on the short-term trend, determined as the first-degree polynomial curve fitting (MATLAB 2013b, Mathworks) of the last three data samples. To avoid confusing the participants with information from previous blocks (while also considering the delay inherent to the neurofeedback process), we discarded the first three points of each block. In this sense, the feed- back is presented to the participants in volumes 5 (buffer with samples number 3, 4 and 5), 8 (6, 7, and 8) and 11 (9, 10 and 11) of each block. The time between two consecutive updates is 6 seconds.

The feedback for a positive or negative signal change was a high or low frequency beep, respectively, determined according to the polarity of the short-term data trend. The sounds were previously presented to the participants.

2.3.5 No feedback run

After the 2 neurofeedback runs, the participants performed a run without feedback, with a block design similar to the neurofeedback runs. The participants were instructed to maintain the imagery strategy as in the previous neurofeedback runs but without the visual or auditory feedback information. This run is performed to assess the ability to maintain the modulation without feedback.

2.4 Offline fMRI data analysis

The fMRI data were analyzed using Brain- Voyager QX 2.8 (Brain Innovation, Maastricht, Netherlands).

Pre-processing of single-subject fMRI data included slice-time correction, realignment to the first image to compensate for head motion and temporal high-pass filtering to remove low-frequency drifts. Co-registration of the functional data with the anatomical scan and normalization into Talairach coordinate space (Talairach and Tournoux, 1988) was also performed.

In the first-level analysis of the functional runs, we used a standard GLM analysis for each run. Predictors were modeled as a boxcar function with the length of each condition (24 s), convolved with the canonical hemodynamic response function. Six motion parameters (three translational and three rotational) and predictors based on spikes (outliers in the BOLD time course) were also included into the GLM as covariates.

Our main goal was to analyze the statistical significance of activation achieved within the pSTS ROI, for facial expressions. In this sense, we used an ROI-GLM and assessed the contrast (i. Neutral) vs. (ii. Happy, iii. Sad and iv. Alternate), balanced. The alternative ROI in the alt-roi group was defined as a set of white matter voxels with minimal statistical value considering the contrast of interest. The rationale for the definition of an alternative ROI based on a set of voxels from white matter regions was to have a truly negative control to fully prevent the possibility of participants to gain control over the feedback signal as compared to the experimental group (negative control) (Sulzer et al., 2013; Sorger et al., 2019). In addition to the negative control, we also considered a grey matter area (positive control) for both groups — a target region in the left anterior frontal cortex (BA 10).

To analyze differences between NF group and alt-roi group, 3D spatial smoothing was performed 8 mm full-width at half maximum Gaussian kernel. Then we performed a random effects (RFX) analysis considering each group individually. Finally, we compared the brain activation patterns between groups based on a two-sample t-test.

3. Results

3.1 Online definition of the ROI based on the functional localizer

The localizer run allowed the real-time definition of subject-specific ROIs selective for facial expression perception for the NF group (we present the probability map for the ROI positions in Fig. 6 and an overview of the neurofeedback targets/ROIs in Table 1). The ROI was selected in the right hemisphere in seven subjects, while in the other three the ROI was defined in the left (based on statistical criteria).

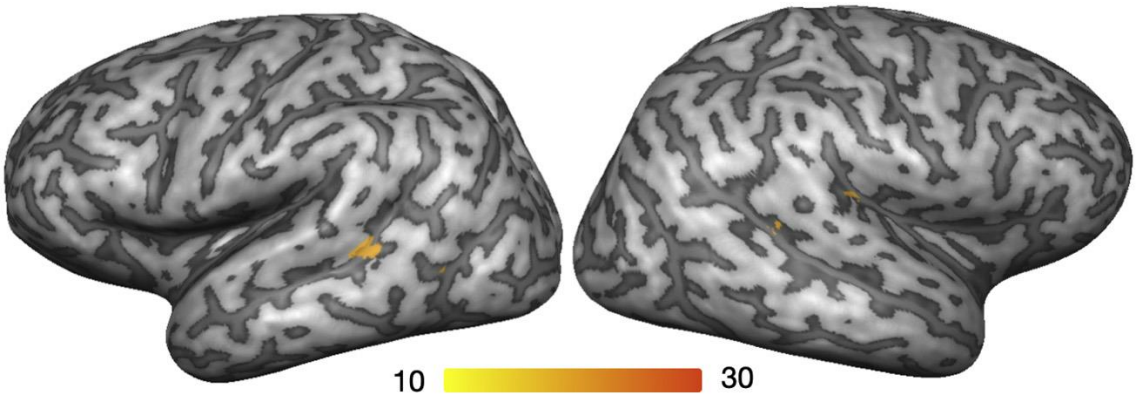

Figure 6 – Probability map of the ROIs selected online in the NF-group. Clusters in right and left pSTS represent the overlapping of the neurofeedback target of each participant.

Table 1 – ROIs selected using the functional localizer run for the active NF group. The functional data presented are based on the Talairach-normalized brain to enable between-participant comparison. The t-statistic corresponds to the ROI-GLM with contrast (i. Neutral, v. Moving dots) < (ii. Happy, iii. Sad, iv. Alternate).

Part.	Mean Talairach coordinates (x, y, z)	Cluster size (voxels)	t-statistic of contrast (i, ii < iii, iv, v)
NF-S01	(51, -35,11)	725	4.171
NF-S02	(43, -61,4)	1200	9.560
NF-S03	(-49, -57,5)	1408	8.048
NF-S04	(-53,-49,10)	540	6.849
NF-S05	(45,-40,15)	983	5.254
NF-S06	(-51,-52,7)	1468	12.774
NF-S07	(54,-25,21)	1295	9.356
NF-S08	(60,-25,18)	721	8.912
NF-S09	(56,-36,12)	1172	7.826
NF-S10	(54,-47,15)	1270	10.092
		1078.2 (319.583)	8.284 (2.462)

3.2 Offline analysis of the localizer run

The functional localizer revealed significant activation within the pSTS, fusiform gyrus, occipital inferior gyrus and preCentral Gyrus (Fig. 7, RFX-GLM, FDR corrected, t(19), $p<0.0081$). All these regions are involved in the extended system of the face perception network (Fox et al., 2009) or associated to neural responses to specific components of face expressions (Radua et al., 2010).

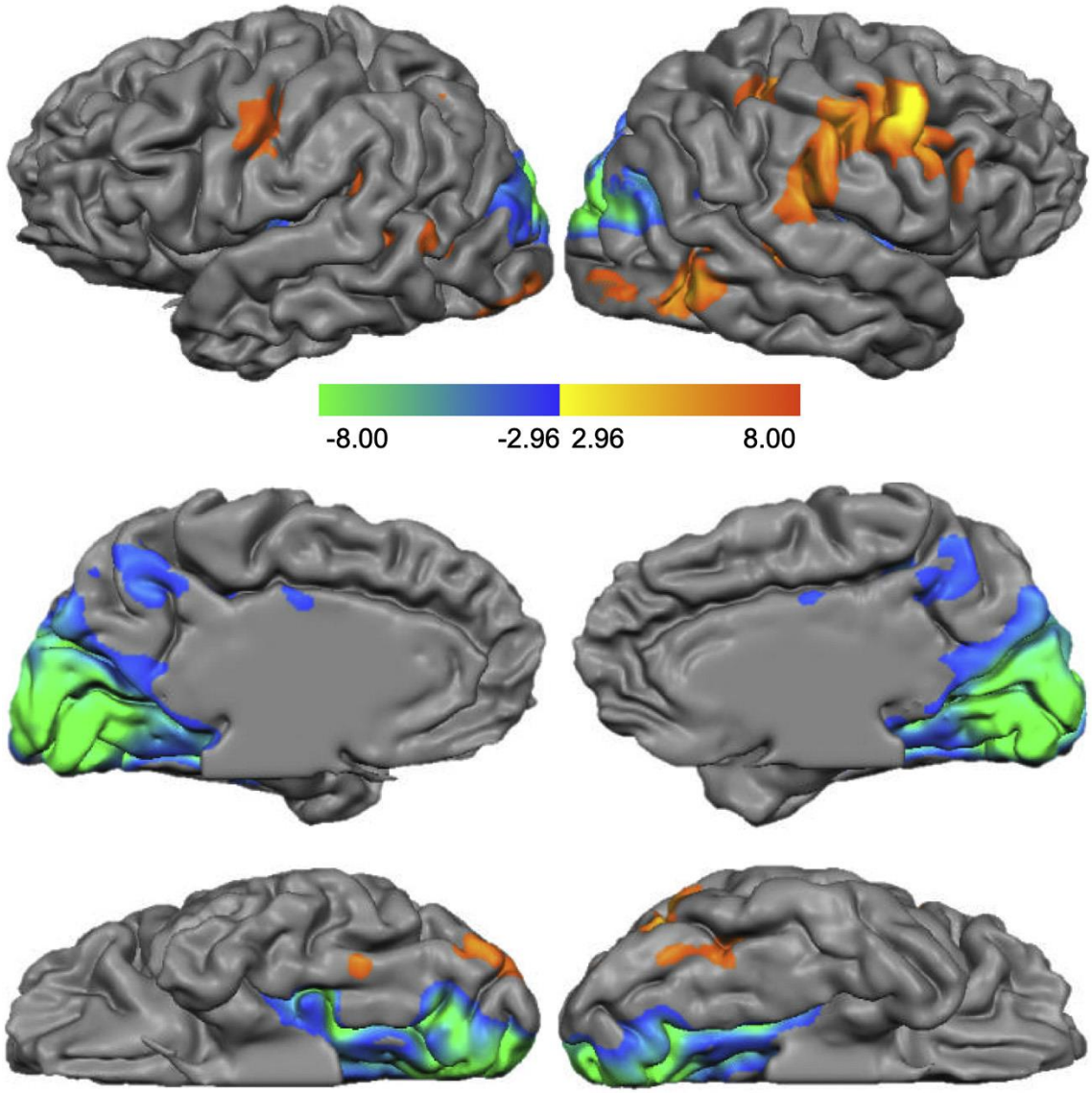

Figure 7 – Statistical map of the localizer run. The clusters represent sets of statistically significant voxels during the localizer run (RFX-GLM, FDR corrected, t(19), p<0.0081). Most of the highlighted regions are associated to specific components of the facial expression network, such as the pSTS, fusiform gyrus, occipital inferior gyrus and preCentral Gyrus. Note that this contrast truly highlights high level visual processing of dynamical facial expressions as compared to early level (de)activations.

3.3 Imagery runs analysis

In the visual neurofeedback runs, the participants were asked to control the facial expression of the avatar by up- and down-regulating the BOLD activation in the subject-specific ROI. In the auditory modality, the feedback information was provided in the form of 'positive' and 'negative' sounds.

Based on the ROI-GLM, we computed t-statistic for each participant of the NF group, corresponding to the contrast of interest (i. Neutral) < (ii. Happy, iii. Sad, and iv. Alternate), balanced — i.e. down- vs. up-regulation conditions. The results suggest that self-regulation of pSTS using a mental imagery strategy is possible. According to the statistical criteria defined, ROI-GLM balanced contrast (i. Neutral) vs. (ii. Happy, iii. Sad and iv. Alternate) (FDR corrected, $p<0.05$), 9 out of 10 subjects were able to successfully regulate BOLD activity in at least 1 of the neurofeedback runs. The t-statistic value averaged 1.943 (± 1.533 standard deviation) for the auditory feedback run, for the visual feedback run the t-statistic averaged 3.244 (± 2.563), and for the run without feedback the t-statistic averaged 1.688 (± 1.617) (see Table 2 for details). Seven out of the 10 participants presented statistically significant results for the visual feedback run, 4 for the auditory feedback run and 4 for the run without feedback (suggesting that these were able to modulate activity even without a closed loop, reinforcing the importance of the mental imagery strategy, that if effective may work irrespective of the feedback).

Table 2 – The t-values correspond to the ROI-GLM with contrast (i. Neutral) < (ii. Happy, iii. Sad, and iv. Alternate) (* indicates p<0.05), (indicates p<0.001).**

Part.	Auditory Feedback	Visual Feedback	No feedback
	pSTS-based ROI-GLM t-statistic		
NF-S01	2.021*	3.410	1.222
NF-S02	1.624	0.511	1.778
NF-S03	2.852*	0.420	1.383
NF-S04	1.054	8.761**	0.528
NF-S05	1.419	3.799**	-1.542
NF-S06	2.912*	5.263**	4.041**
NF-S07	0.135	3.108*	0.850
NF-S08	4.712**	3.361*	3.684**
NF-S09	3.167*	0.292	2.516*
NF-S10	-0.460	3.513*	2.426*
mean	***1.943***	***3.244***	***1.688***

3.4 Offline analysis of the pSTS ROI activation across groups

To compare NF group and alt-roi group and assess the specificity of the target region, we also selected a pSTS ROI in the alt-roi group (following the same strategy used in the NF group). The effect size between the t-statistic from the pSTS ROI of the 2 groups, measured as the Hedge's g, was relatively small (the visual feedback run presented an effect size of 0.263, 0.279 for the auditory feedback run and 0.323 for the run without feedback).

For the alt-roi group, we also determined ROI-GLM t statistic for the contrast of interest in the alternative ROI (used online). The effect size between the target regions used in each group (pSTS ROI on the NF group vs. WM ROI on the alt-roi group) presented an effect size of 0.519, 0.545, 0.669 for the visual feedback, auditory feedback and run without feedback, respectively. One-sample t-tests assessed the significance of the BOLD % change within each ROI. The alternative ROI in no case reached statistical significance, unlike the pSTS-based ROIs in both groups (NF group and alt-roi group) (for details see Fig. 8).

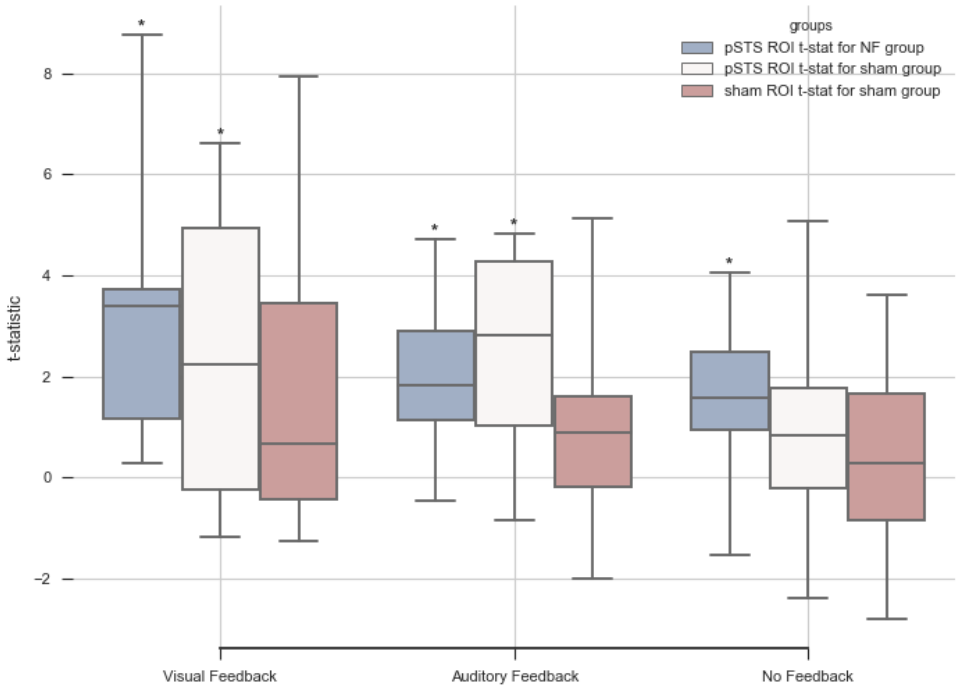

Figure 8 – Box plots, depicting performance for each rt-fMRI neurofeedback and transfer runs per groups and ROI (* indicates statistical significance according to a One-sample t-test).

In order to evaluate the neural correlates of the neurofeedback runs based on a pSTS-ROI, we assessed the pattern of brain activation of the two different groups in each run (visual and auditory). To this end, we analyzed the specific interaction effect across groups, and identified the regions where the contrast of interest (neutral vs. facial expressions imagery) are significantly different for the NF group vs. alt-roi group (Table 3, based on the statistical map - two-sample t-test, active NF vs. alt-roi group, $t(18)$, $p<0.005$).

Table 3 – Whole brain assessment of the differences between NF group and alt-roi group during the visual feedback run and during the auditory feedback run

Region	Talairach coordinates (peak voxel coords X, Y, Z)			Number of voxels	t-statistic
Visual feedback run analysis					
Sub-Gyral (right)	30	-7	37	**7365**	-3.752799
Insula (right)	33	14	7	**584**	-3.445339
Lentiform Nucleus (right)	21	-13	1	**311**	-3.575890
Cingulate Gyrus (left)	-9	-10	34	**405**	-3.399608
Middle Frontal Gyrus (left)	-45	32	22	**3390**	-3.456471
Middle Frontal Gyrus (left)	-36	26	43	**1945**	-3.415913
Insula (left)	-36	8	19	**556**	-3.399863
Precentral Gyrus (left)	-60	-4	31	**1826**	-3.331889
Auditory feedback analysis					
Middle Temporal Gyrus (right)	45	-61	22	**416**	-3.584822
Anterior Cingulate (right)	24	32	22	**398**	-3.506509
Medial Frontal Gyrus (right)	12	44	25	**533**	-3.401492
Precuneus (left)	-9	-64	19	**5482**	-3.628287
Precuneus (left)	-21	-46	31	**2110**	-3.630086
Anterior Cingulate (left)	-12	20	22	**546**	-3.485696
Medial Frontal Gyrus (left)	-21	44	16	**1724**	-3.466876
Middle Frontal Gyrus (left)	-39	23	43	**1095**	-3.608613
Supramarginal Gyrus (left)	-36	-52	25	**703**	-3.511224
Precentral Gyrus (left)	-45	-7	22	**605**	-3.413738
Middle Temporal Gyrus (left)	-63	-10	-8	**407**	-3.507409

As a final positive control group, we performed the analysis considering a grey matter area for both groups — we considered a target region in the left anterior frontal cortex (BA 10, sphere around voxel with Talairach coordinates [-24, 49, -5], and a total of 257 voxels). The results show that neither group was able to modulate BOLD activity in this region. Taken together, this additional analysis reinforces the specificity of the proposed mental imagery strategy and pSTS localization.

4. Discussion

The aim of the current study was to investigate whether it is possible to reliably define a functional subdomain in pSTS that encodes dynamic facial expressions irrespective of the presence of motion and/or static faces and to probe this pSTS domain as a mechanistic neurofeedback target using a mental imagery task.

We proposed the participants to volitionally control the BOLD signal of this functionally defined subdomain with the help of a customized rt-fMRI neurofeedback interface developed in our laboratory. Possible clinical benefits from volitional control of BOLD activity of the pSTS region are especially relevant in social and emotion cognition disorders, such as ASD. Neurobiological theories on the mechanisms of the disorder commonly emphasize neuroactivation impairment in the STS, particularly concerning emotion recognition from perceptual analysis of faces (Silver and Rapin, 2012).

We used neurofeedback based on imagery of emotional facial expressions to get insight into the role of a specific region within STS. We were able to define a highly selective region, the pSTS subdomain which processes specific responses to facial expressions. This target region was specifically responsive to expression of emotions in faces and not just tomere motion or the presence of a face and its static features. We showed that volitional modulation of BOLD activity in pSTS ROI based on imagery of such emotional expressions can be successfully achieved, providing additional evidence for processing specificity. Additionally, we demonstrated that this was possible with two novel feedback approaches (visual or auditory) with distinct rules (mean or derivative based) in this selectively identified region.

No previous study addressed self-modulation of brain activity directly targeting facial expressions (both from the neuromodulation strategy point of view and processing specificity of the target region — a sub-cluster within the STS processing dynamic expressions). In a previous clinical study using neurofeedback based on the anterior insula, emotional face recognition was used as a clinical outcome measure (Ruiz et al., 2013a). Presentation of static faces as emotional stimuli was used to promote downregulation of activity of the amygdala (Brühl et al., 2014). None of these studies addressed self-modulation of brain activity based on dynamic facial expressions in selectively defined social recognition core regions.

Another recent study based on the concept of functional selectivity used relative up-regulation of the parahippocampal place area over the fusiform face area (Habes et al., 2016). The participants, based on scene imagery, were able to self-regulate higher visual areas. These results suggest the feasibility of using fMRI neurofeedback and ultimately unveil functional specificity of these visual areas. Our study addresses an area in the social and emotional cognition network and demonstrates that self-regulation of a selective core region involved in processing of dynamic facial expressions in the STS can be achieved and may represent a potential neurofeedback target region.

The proposed functional localizer enabled the identification of a specific functional domain in pSTS as well as brain regions specifically involved in the processing of dynamic aspects of facial expressions. The consistent identification of the target ROI across participants supports the notion that our paradigm allowed to functionally define a facial expression specific pSTS cluster that could be a potential target for imagery of emotions in faces.

An important factor influencing performance in neurofeedback studies is the engagement and motivation of the participants. To maximize this factor, we offered to the participants 2 novel alternative approaches in the feedback modality, 1 visual and the other auditory. Based on the ROI-GLM values, both modalities showed promising results. Most participants were able to modulate in at least 1 of the modalities (9 out of 10 in at least 1 of the runs). Our aim was not to compare both strategies, but to investigate whether the pSTS region is a suitable neurofeedback target considering different optional strategies. The results suggest that self-driven modulation is achievable considering the mental imagery of facial expressions coupled with the two different feedback interfaces. It is however important to note that given that this was a single session study, no inference can be made concerning long term learning effects.

We considered 2 controls to assess the specificity of the strategy and neurofeedback target: a within-subject (no feedback, control run at the end of the session, which can also be viewed as an approach suited to investigate learning in repeated paradigms) and a between-group control (alt-roi group). The results suggest that the proposed strategy enables self-modulation of the pSTS region, irrespectively of the feedback source. Moreover, this is a region specifically related with the mental imagery of dynamic facial expressions, since this region did not activate in previous neurofeedback studies using different tasks, such as simple dot motion, performed in our group (Banca et al., 2015; Sousa et al., 2016). During the feedback runs, both NF and alt-roi groups were able to achieve self-regulation of a pSTS region validating the efficacy of

the proposed strategy (mental imagery of facial expressions) irrespectively of the ROI used to provide feedback. During the no feedback run, only the NF group achieved statistically significant results at the group level in the pSTS ROI. Further experiments are required to better understand possible learning effects caused by the approach proposed here.

The present study provides evidence that a specific dynamic emotion expression subdomain in pSTS can be identified and it proved to be a suitable probe for a mental imagery task coupled with different neurofeedback modalities. Given the role of pSTS in social perception and emotional processing, and the evidence of abnormal functionality of this region in social cognition disorders such as ASD, we hypothesize that learned self-modulation of BOLD activity in this region could be tested in clinical trials using neurofeedback. A multiple session experiment taking advantage of pSTS neurofeedback target specificity would be valuable as a future approach supporting this idea; previous studies highlighted the impact of neurofeedback training in emotional processing (Zotev et al., 2014).

4.1 Limitations

Despite the encouraging preliminary results published with the use of rt-fMRI thus far, there is an ongoing debate on the limitations of these approaches and appropriate outcome measures or control conditions (Stoeckel et al., 2014; Mehler et al., 2018). It is therefore important to note the limitations of our study. The relatively small sample size limits generalization and future studies are necessary to replicate and extend our results. For that reason, we provide effect size measures. The use of a single neurofeedback session, to be expected from a proof-of-concept study, does not allow to further explore the learning effect of the neurofeedback experiment. The definition of appropriate controls in neurofeedback experiments is also a matter of debate (Sulzer et al., 2013; Sorger et al., 2019). Here, the rationale for a negative control region based on white matter voxels was to restrict the control over the trained signal as in the experimental group and a positive control based on a grey matter region was therefore also necessary. Despite these limitations our results point towards the possibility to use a functionally defined region in the pSTS for neuromodulation.

4.2 Conclusion

Given the relatively early stage of research in this field, there have been no large randomized controlled trials establishing clinical evidence of treatment efficacy. The encouraging results on the ability to self-modulate activity in pSTS as a neurofeedback target region, reinforce the need for further studies addressing the feasibility of using this region in a larger study, with multiple neurofeedback sessions, to formally evaluate the tolerance and efficacy of neurofeedback interventions, and ultimately design phase II/III clinical trials in clinical populations such as ASD.

REFERENCES

Alaerts K,Woolley DG, Steyaert J, Di Martino A, Swinnen SP, Wenderoth N. (2014) Underconnectivity of the superior temporal sulcus predicts emotion recognition deficits in autism. Soc. Cogn. Affect. Neurosci. 9:1589-1600.

Alino M, Gadea M, Espert R. (2016) A critical view of neurofeedback experimental designs: sham and control as necessary conditions. Int J Neurol Neurother 3:1-2.

Allison T, Puce A, McCarthy G. (2000) Social perception from visual cues: role of the STS region. Trends Cogn. Sci. 4:267-278.

Banca P, Sousa T, Catarina Duarte I, Castelo-Branco M. (2015) Visual motion imagery neurofeedback based on the hMT+/V5 complex: evidence for a feedback-specific neural circuit involving neocortical and cerebellar regions. J Neural Eng 12066003.

Baron-Cohen S, Wheelwright S, Hill J, Raste Y, Plumb I. (2001) The "reading the mind in the eyes" test revised version: a study with normal adults, and adults with Asperger syndrome or high-functioning autism. J. Child Psychol. Psychiatry. 42:241-251.

Brainard DH. (1997) The psychophysics toolbox. Spat. Vis. 10:433-436.

Bray S, Shimojo S, O'Doherty JP. (2007) Direct instrumental conditioning of neural activity using functional magnetic resonance imagingderived reward feedback. J. Neurosci. 27:7498-7507.

Brühl AB, Scherpiet S, Sulzer J, Stämpfli P, Seifritz E, Herwig U. (2014) Real-time neurofeedback using functional MRI could improve downregulation of amygdala activity during emotional stimulation: a proof-of-concept study. Brain Topogr. 27:138-148.

Cheng W, Rolls ET, Gu H, Zhang J, Feng J. (2015) Autism: reduced connectivity between cortical areas involved in face expression, theory of mind, and the sense of self. Brain 138(5):1382-1393.

deCharms RC, Christoff K, Glover GH, Pauly JM,Whitfield S, Gabrieli JD. (2004) Learned regulation of spatially localized brain activation using real-time fMRI. Neuroimage 21:436-443.

deCharms RC, Maeda F, Glover GH, Ludlow D, Pauly JM, Soneji D, Gabrieli JDE, Mackey SC. (2005) Control over brain activation and pain learned by using real-time functional MRI. Proc. Natl. Acad. Sci. U. S. A. 102:18626-18631.

Deen B, Koldewyn K, Kanwisher N, Saxe R. (2015) Functional organization of social perception and cognition in the superior temporal sulcus. Cereb. Cortex 25:4596-4609.

Fox Christopher J, Iaria Giuseppe, Barton Jason JS. (2009) Defining the face processing network: optimization of the functional localizer in fMRI. Hum. Brain Mapp. 30(5):1637-1651.

Friedrich EVC, Wood G, Scherer R, Neuper C. (2014) Mind over brain, brain over mind: cognitive causes and consequences of controlling brain activity. Front. Hum. Neurosci. 8:348.

Furl N, Henson RN, Friston KJ, Calder AJ. (2013) Top-down control of visual responses to fear by the amygdala. J. Neurosci. 33:17435-17443.

Habes I, Rushton S, Johnston SJ, Sokunbi MO, Barawi K, Brosnan M, Daly T, Ihssen N, Linden DEJ. (2016) fMRI neurofeedback of higher visual areas and perceptual biases. Neuropsychologia 85:208-215.

Hamilton JP, Glover GH, Hsu JJ, Johnson RF, Gotlib IH. (2011) Modulation of subgenual anterior cingulate cortex activity with real-time neurofeedback. Hum. Brain Mapp. 32:22-31.

Hein G, Knight RT. (2008) Superior temporal sulcus—it's my area: or is it? J. Cogn. Neurosci. 20:2125-2136.

Ishai A, Haxby JV, Ungerleider LG. (2002) Visual imagery of famous faces: effects of memory and attention revealed by fMRI. Neuroimage 17:1729-1741.

Johnston SJ, Boehm SG, Healy D, Goebel R, Linden DEJ. (2010) Neurofeedback: a promising tool for the self-regulation of emotion networks. Neuroimage 49:1066-1072.

Kim SE, Kim JW, Kim JJ, Jeong BS, Choi EA, Jeong YG, Kim JH, Ku J, Ki SW. (2007) The neural mechanism of imagining facial affective expression. Brain Res. 1145:128-137.

Krause F, Benjamins C, Lührs M, Eck J, Noirhomme Q, Rosenke M, Brunheim S, Sorger B, Goebel R. (2017) Real-time fMRI-based selfregulation of brain activation across different visual feedback presentations. Brain-Computer Interfaces 2621:1-15.

LaConte SM. (2011) Decoding fMRI brain states in real-time. Neuroimage 56:440-454.

LaConte SM, Peltier SJ, Hu XP. (2007) Real-time fMRI using brain-state classification. Hum. Brain Mapp. 28:1033-1044.

Logothetis NK. (2008) What we can do and what we cannot do with fMRI. Nature 453:869-878.

Mathiak, K a, Alawi, EM, Koush, Y, Dyck, M, Cordes, JS, Gaber, TJ, Zepf, FD, Palomero-Gallagher, et al., 2015. Social reward improves the voluntary control over localized brain activity in fMRI-based neurofeedback training. Front. Behav. Neurosci. 9.

Mehler DMA, Sokunbi MO, Habes I, Barawi K, Subramanian L, Range M, Evans J, Hood K, Lührs M, Keedwell P, Goebel R, Linden DEJ. (2018) Targeting the affective brain—a

randomized controlled trial of realtime fMRI neurofeedback in patients with depression. Neuropsychopharmacol 43:2578-2585.

Mishra J, Gazzaley A. (2015) Closed-loop cognition: the next frontier arrives. Trends Cogn. Sci. 19:1-2.

Muller R-A. (2007) The study of autism as a distributed disorder. Ment. Retard Dev Disabil Rev 13:85-95.

Pelphrey Ka, Carter EJ. (2008) Social perception: lessons from autism and typical developme, Brain mechanisms for social perception: lessons from autism and typical development. Ann. N. Y. Acad. Sci. 1145:283-299.

Pitcher D, Walsh V, Duchaine B. (2011) The role of the occipital face area in the cortical face perception network. Exp. Brain Res. 209:481-493.

Posse S, Fitzgerald D, Gao K, Habel U, Rosenberg D, Moore GJ, Schneider F. (2003) Real-time fMRI of temporolimbic regions detects amygdala activation during single-trial self-induced sadness. Neuroimage 18:760-768.

Radua Joaquim, Phillips Mary L, Russell Tamara, Lawrence Natalia, Marshall Nicolette, Kalidindi Sridevi, El-Hage Wissam, et al. (2010) Neural response to specific components of fearful faces in healthy and schizophrenic adults. NeuroImage 49(1):939-946.

Rebola J, Castelo-Branco M. (2014) Visual areas PPA and pSTS diverge from other processing modules during perceptual closure: Functional dichotomies within category selective networks. Neuropsychologia 61:135-142.

Reiner M, Gruzelier J, Bamidis PD, Auer T. (2018) The science of neurofeedback: learnability and effects. Neuroscience 378:1-10.

Ros T, Munneke MaM, Ruge D, Gruzelier JH, Rothwell JC. (2010) Endogenous control of waking brain rhythms induces neuroplasticity in humans. Eur. J. Neurosci. 31:770-778.

Ruiz S, Buyukturkoglu K, Rana M, Birbaumer N, Sitaram R. (2013) Realtime fMRI brain computer interfaces: self-regulation of single brain regions to networks. Biol. Psychol. 95:4-20.

Ruiz S, Lee S, Soekadar SR, Caria A, Veit R, Kircher T, Birbaumer N, Sitaram R. (2013) Acquired self-control of insula cortex modulates emotion recognition and brain network connectivity in schizophrenia. Hum. Brain Mapp. 34:200-212.

Sagi Y, Tavor I, Hofstetter S, Tzur-Moryosef S, Blumenfeld-Katzir T, Assaf Y. (2012) Learning in the fast lane: new insights into neuroplasticity. Neuron 73:1195-1203.

Saitovitch A, Bargiacchi A, Chabane N, Brunelle F, Samson Y, Boddaert N, Zilbovicius M. (2012) Social cognition and the superior temporal sulcus: implications in autism. Rev. Neurol. (Paris). 168:762-770.

Silver WG, Rapin I. (2012) Neurobiological basis of autism. Pediatr. Clin. North Am. 59:45-61.

Sitaram R, Veit R, Stevens B, Caria A, Gerloff C, Birbaumer N, Hummel F. (2012) Acquired control of ventral premotor cortex activity by feedback training: an exploratory real-time fMRI and TMS study. Neurorehabil. Neural Repair 26:256-265.

Sokunbi MO, Linden DEJ, Habes I, Johnston S, Ihssen N. (2014) Realtime fMRI brain-computer interface: development of a "motivational feedback" subsystem for the regulation of visual cue reactivity. Front. Behav. Neurosci. 8.

Sorger B, Scharnowski F, Linden DEJ, Hampson M, Young KD. (2019) Control freaks: Towards optimal selection of control conditions for fMRI neurofeedback studies. Neuroimage 186:256-265.

Sousa T, Direito B, Lima J, Ferreira C, Nunes U, Castelo-Branco M. (2016) Control of brain activity in hMT+/V5 at three response levels using fMRI-based neurofeedback/BCI. PLoS One 11e0155961.

Stoeckel LE, Garrison KA, Ghosh SS, Wighton P, Hanlon CA, Gilman JM, Greer S, Turk-Browne NB, et al. (2014) Optimizing real time fMRI neurofeedback for therapeutic discovery and development. NeuroImage Clin. 5:245-255.

Subramanian L, Hindle JV, Johnston S, Roberts MV, Husain M, Goebel R. (2011) Real-Time functional magnetic resonance imaging neurofeedback for treatment of Parkinson's disease. J. Neurosci. 31:16309-16317.

Sulzer J, Haller S, Scharnowski F, Weiskopf N, Birbaumer N., Blefari ML, Bruehl aB, Cohen LG, DeCharms RC, Gassert R, Goebel R, Herwig U, LaConte SM, Linden D, Luft A, Seifritz E, Sitaram R. (2013) Realtime fMRI neurofeedback: progress and challenges. Neuroimage 76:386-399.

Talairach J, Tournoux P. (1988) Co-planar stereotaxic atlas of the human brain, 3-dimensional proportional systems: an approach to cerebral imaging. New York: Thieme Medical Publishers, 1988.

Weiskopf N. (2012) Real-time fMRI and its application to neurofeedback. Neuroimage 62:682-692.

Weiskopf N, Scharnowski F, Veit R, Goebel R, Birbaumer N, Mathiak K. (2004) Self-regulation of local brain activity using real-time functional magnetic resonance imaging (fMRI). J. Physiol. Paris 98:357-373.

Weiskopf N, Sitaram R, Josephs O, Veit R, Scharnowski F, Goebel R, Birbaumer N, Deichmann R, Mathiak K. (2007) Functional magnetic resonance imaging: methods and applications. Magn. Reson. Imaging 25:989-1003.

Weiskopf N, Veit R, Erb M, Mathiak K, Grodd W, Goebel R, Birbaumer N. (2003) Physiological self-regulation of regional brain activity using real-time functional magnetic resonance imaging (fMRI): methodology and exemplary data. Neuroimage 19:577-586.

Zotev V, Phillips R, Yuan H, Misaki M, Bodurka J. (2014) Self-regulation of human brain activity using simultaneous real-time fMRI and EEG neurofeedback. Neuroimage. 85:985-995.

Appendix II

Training the social brain - clinical and neural effects of an 8-week real-time fMRI neurofeedback Phase IIa Clinical Trial in autism

This appendix is composed by the contents of the following publication:

Direito B*, Mouga S[a], Sayal A, Simões M, Quental Q, Playle R, McNamara R, Linden D, Oliveira G, Castelo-Branco M. Training the social brain - clinical and neural effects of an 8-week real-time fMRI neurofeedback Phase IIa Clinical Trial in autism

---

Abstract

Objective: Autism Spectrum Disorder (ASD) leads to abnormal activity patterns in core social brain regions. We aimed to demonstrate the feasibility of real-time fMRI volitional neurofeedback in targeting these regions in ASD.

Method: In this within-group design clinical trial, ASD patients (N=15) were enrolled in a program with 5- training sessions of rtfMRI-nf that targeted facial emotion expressions processing, using a ROI in the social cognition network, the posterior superior temporal sulcus.

Result: ASD participants were able to modulate brain activity in this ROI, over multiple sessions, using visual imagery strategies. Moreover, we identified relevant clinical and neural effects, as documented by neuroimaging results and neuropsychological measures, including emotion recognition, which were observed immediately after the intervention and retained after 6 months. Different neuromodulation profiles demonstrated subject-specificity in face perception in ASD: some participants regulated brain activity for happy, sad and neutral facial expressions in opposite directions – modulation occurred in positive or negative directions in

different patients. Striatal regions involved in operant learning (previously associated to success and failure of controlling neurofeedback signal), parts of the saliency (insula and Anterior Cingulate Cortex) and emotional control (medial Prefrontal Cortex) networks were recruited during neurofeedback.

Conclusions: All patients showed significant absolute neuromodulation regardless of the modulation profile. The involvement of the operant learning network supports the notion of engagement of the participants. Moreover, the potential behavioral benefits after the intervention and the persistence of these benefits after 6 months pave the way for future phase IIb/III clinical trials.

1. Introduction

Autism Spectrum Disorder (ASD) is a severe neurodevelopmental disorder characterized by an early onset, life-long set of clinical features, that include deficits in social interaction and communication, as well as repetitive patterns of behavior (1). Despite these core features, there is a characteristic etiological and phenotypic heterogeneity, in particular, regarding intellectual function and medical comorbidities (2–7).

Insights into the neurobiology of ASD have been provided by developments of structural, functional and spectroscopic neuroimaging methodologies (8). Functional magnetic resonance imaging (fMRI) opened a new era of research into the understanding of the neural correlates, pathophysiology, and etiology of ASD. The use of neuroimaging for intervention purposes is an emerging attractive opportunity (9). The current work addresses this gap in the context of ASD by providing proof-of-concept for a therapeutic application of (real-time) fMRI, using volitional neurofeedback. The concept behind neurofeedback is that the training of self-regulation of disease-relevant areas or neural circuits can reinforce positive psychological processes and promote neuroplasticity (10, 11).

The phenotypic (and genotypic) heterogeneity of ASD poses challenges to any unifying theory to explain core clinical features (4), which seems to involve disturbances in multiple and distinct neural systems (12). However, a large body of neuroimaging studies has addressed

social perception and cognition, which provide the rationale for our chosen target region for neurofeedback training, the superior temporal sulcus (STS).

The functional organization of the STS comprises distinct sub-regions. The posterior STS (part of the face processing network, together with the fusiform face area (FFA) and the occipital face area (OFA)) has been strongly implicated in the processing of facial expressions and other social cues (13). The role of the STS in other cognitive processes, such as Theory of mind, audiovisual integration, face processing and imagery of emotional facial expressions is also well established (14–19). Moreover, it has strong functional and anatomical connections with the extended face processing system, which includes the amygdala, inferior frontal gyrus (IFG), precuneus and anterior STS. Behavioral impairments in joint attention, eye contact and face emotion recognition, hallmarks of ASD, have been strongly linked to this circuit. The impact of putatively impaired STS responses in ASD has also been documented in several studies (20–23) (for a review see (24)). A decrease in structural connectivity has also been documented in tracts arising from grey matter in the STS (DTI-based studies) (for a review see (9)).

Training approaches based on volitional neurofeedback, using real-time fMRI, have been proposed for depression (25), addiction (26) and attention deficit hyperactivity disorder (27) but so far not for ASD. We have recently shown in healthy controls that neurofeedback focusing on the posterior STS (pSTS) is feasible and concluded that this region showed promise as a mechanistic neurofeedback target (28). This previous study in a control group paved the way for the present clinical study.

In this proof-of-principle longitudinal study, we aimed to assess the feasibility of using the pSTS as a target region for real-time fMRI neurofeedback (rtfMRI-nf), in ASD participants. The rationale for the selection of the target region is the importance of social face perception in typical cognition and social interaction, and the pivotal role of pSTS in this process with potential clinical benefits. To this end, we aimed to evaluate the efficacy of neurofeedback over multiple therapeutic sessions in ASD, and to assess efficacy measures derived from neuropsychological evaluation and imaging data.

2.Methods

The study consisted of a single-arm, within-group "before-after" design and aimed to examine the neuroimaging and behavioral effects of an intervention protocol including five sessions of rtfMRI-nf.

The research protocol was approved in January 2016 by the Institutional Ethics commission (Comissão de Ética da Faculdade de Medicina), the National Authority on medical devices (INFARMED - National Authority of Medicines and Health Products, I.P.) and National Ethics committee (CEIC - Portuguese Ethics Committee for Clinical Research) and registered in the clinicaltrials.gov platform.

2.1 Participants

Fifteen male participants (19 years and 11 months, ± 3 years and 3 months) with high-functioning ASD (Full-Scale Intelligence Quotient [FSIQ] superior to 80; FSIQ: Mean = 103; SD = 10.7) participated in the study. All participants had normal or corrected to normal vision, based on their clinical history. During the trial, participants were instructed to follow the treatment as usual, if any, and to not make major alterations in their activities.

Prior to participation, subjects were informed about the research protocol and gave written informed consent. All procedures are in accordance with the Declaration of Helsinki.

2.2 Procedures

The neurofeedback training intervention lasted for eight weeks and comprised five sessions of rtfMRI-nf (four weekly sessions and the last approximately one month later). During visit 1, participants also completed a neuropsychological evaluation. The Facial Expressions of Emotion - Stimuli and Tests - FEEST (The Emotion Hexagon test) (29), was the primary behavioral outcome.. The relation between FEEST, basic emotion recognition and abnormal brain activity in specific components of the response to emotional faces in patients with ASD has been previously reported (30). Additionally, the participants also completed two secondary outcome measures - Autism Treatment Evaluation Checklist (ATEC) (31) and the Vineland

Adaptive Behavior Scale (VABS) (32). Other neuropsychological measures related to mood, anxiety and depression were also assessed: Profile of Mood States (POMS) (33, 34); Hospital Anxiety & Depression Scale (HADS) (35, 36) and Beck Depression Inventory (BDI) (37–39). The evaluations were repeated at the primary endpoint - after the last training session, and at follow-up - 6 months after the last training session.

2.3 rtfMRI-nf paradigm

Data acquisition was performed on a 3T Siemens Magnetom Tim Trio scanner with a 12-channel head coil, at the Portuguese Brain Imaging Network. Each scanning session started with a high-resolution magnetization-prepared rapid acquisition gradient echo sequence for co-registration of functional data (176 slices; TE: 3.42 ms; TR: 2530 ms; voxel size 1 mm^3 isotropic, FA: 7°; matrix size: 256×256).

2.3.1 Localizer

After the structural sequence, we performed a functional localizer to identify the target region-of-interest (ROI) using an echo planar imaging sequence (160 volumes, TR = 2 s, TE = 30 ms, flip angle = 75°, 32 slices, matrix size 64×70, in-plane voxel size = 3×3 mm, slice thickness = 2.5 mm, gap of 0.5 mm) (a detailed explanation of the protocol is presented in (28)).

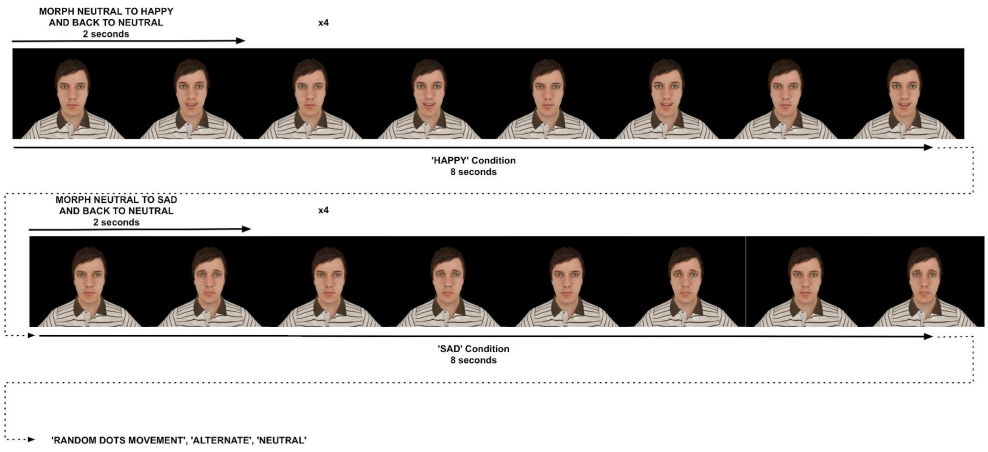

Figure 1 - Localizer run design.

The ROI was defined based on a block-based design with 40 blocks of eight seconds and five different conditions: Neutral - static neutral face; to subtract static aspects of face processing; Happy - morphing face from neutral to happy; Sad - morphing face from neutral to sad; Alternate expressions - alternating between sad and happy; Moving dots - randomly moving dots, to subtract motion processing (Figure 1) (see Supplementary Methods and (28) for further details).

2.3.2 Imagery Runs

The localizer was followed by four imagery task-based fMRI runs (300 volumes with the same EPI sequence parameters of the localizer run). The patients were asked to modulate BOLD activity in the target region. The first and the last runs were control runs without feedback, and the second and third were neurofeedback training runs. The first run establishes a baseline and the last is a control run (also known as transfer run) to test if patients retained the ability to self-regulate BOLD signal in the target ROI without feedback.

To facilitate operant learning, explicit strategies were suggested to the patients to modulate pSTS BOLD signal activity (40), e.g. imagining facial expressions morphing, of an avatar or real person, with or without a context. Nevertheless, patients were given the freedom to explore other strategies that would maximize the presented feedback.

The blocks included three randomly presented "conditions" featuring suggested neurofeedback strategies: IH) Imagery of a happy facial expression, IS) Imagery of a sad facial expression, IA) Alternate between the imagery of happy and sad facial expression, interleaved with IN) imagery of static neutral facial expressions.

Visual feedback was presented in runs two and three through an interface based on the expression of an avatar. The expression of the avatar on the screen was continuously updated based on the mean ROI activation of the neurofeedback target.

2.4 Data analysis and statistical evaluation

2.4.1 Outcome measures analysis

Primary Outcome Measures were characterized in terms of Confidence Intervals (CIs) and relative frequency, respectively. Statistical Package for Social Sciences (SPSS, Version 24) was used to analyze data. To assess differences between outcome measures at baseline, primary and secondary endpoints, 95% CI were determined (baseline vs. primary endpoint, and baseline vs. secondary endpoint - follow up), as well as the p-values corresponding to paired sample t-tests.

2.4.2 Imaging data

The fMRI data were analyzed using BrainVoyager QX (Version 2.8, Brain Innovation, Maastricht, Netherlands).

Our main goal was to assess the statistical significance of the modulation achieved within the neurofeedback target region. To this end, we performed t-tests to assess significance of neuromodulation. We performed additional group-analyses to explore whole-brain patterns associated with the neurofeedback training.

3. Results

3.1 Patient flow

A total of 15 patients completed the protocol and were included in the analyses (see CONSORT flow chart as Supplemental material)

3.2 Feasibility measures

The first important aspects to assess were fidelity (*were intervention sessions delivered as intended?*), feasibility (*was delivery of the intervention feasible in terms of time, group size, amount of sessions?*) and acceptability (*did participants and researchers evaluate the session positively?*) of the intervention sessions, by evaluating measures such as retention, compliance and adherence. Table 1 summarizes feasibility measures.

Table 1 - Feasibility measures summary.

	% (n/n)
Recruitment/Consent	100% (15/15)
Retention (primary end point)	100% (15/15)
Retention (secondary end point)	93% (14/15)
Intervention uptake	100% (15/15)
Adherence/ Completion	100% (15/15)
Compliance	100% (15/15)
Intervention delivery	100% (15/15)
Acceptability	100% (15/15)

The results for all feasibility measures, except the secondary endpoint, are 100%.

3.3 Safety

There were no adverse events reported during the study period by any of the participants.

3.4 Outcome measures

The results regarding clinical outcome measures are summarized in Table S1 (reported as 95% CIs). Considering global ability to recognize expressions using the FEEST, defined as our primary outcome measure, 10 out of 15 patients improved (the higher the result, the better is the ability to recognize the expressions). At the group level, the 95% CI for the difference between the global endpoint and baseline (i.e. the mean increase from baseline to primary

endpoint) is [-0.88, 5.41] (p = 0.144). Improvements at group level turned out to be specific and significant for fear conditions (see below)

Regarding the secondary outcome measures, for the VABS the 95% CI for the difference between the primary endpoint and baseline is [1.40, 6.07] (p = 0.004) (the higher the score, the better is the adaptive behavior) and for the global ATEC, the 95% CI for the difference between the primary endpoint and baseline is [-9.31, 0.11] (p = 0.055) (the lower the score, the better).

A detailed analysis of the subscales of the clinical outcome measures showed relevant improvements (regardless of the polarity of the scores, results presented as the difference between primary endpoint - after the last intervention session - and baseline): FEEST fear expression presented a mean increase from baseline to primary endpoint of 1.67 (95% CI [0.27, 3.07] (p = 0.023)), ATEC Sensory/Cognitive Awareness a decrease of 2.07 (95% CI [-3.52, -0.61] (p = 0.009)), ATEC Health/Physical/Behavior a decrease of 2.40 (95% CI [-4.44, -0.36] (p = 0.024)), VABS Communication an increase of 4.27 (95% CI [1.09, 7.44] (p = 0.012)), VABS Daily Living Skills an increase of 2.93 (95% CI [0.50, 5.37] (p = 0.022)),VABS ABC an increase of 3.73 (95% CI [1.40, 6.07] (p = 0.004)), VABS Socialization an increase of 3.33 (95% CI [0.98, 5.69] (p = 0.009)).

Considering the secondary follow-up time point, 6 months after the last training session, and comparing to the baseline, the patients sustained and improved the abovementioned variations reported in the primary follow-up time point, and even presented improvements in other measures such as ATEC Total (95% CI [-20.96, -12.19] (p < 0.001)) ATEC Speech/Language/Communication (95% CI [-1.76, -0.10] (p = 0.031)) and ATEC Sociability (95% CI [-7.17, -3.98] (p < 0.001)) (see Supplemental Material for a full account of improvement in additional measures, such as mood).

3.5 Imaging Results

3.5.1 Localizer

The target ROIs for neurofeedback training were defined, in each session, according to functional and anatomical principles. In this sense, the identification of a homogeneous ROI

within and across participants was an important goal of the intervention. The average position in Talairach space was x = 54 ± 5, y = 39 ± 7, z = 8 ± 5, and the size (measured in number of 1 mm^3 voxels) was 693 ± 325 voxels. Figure 2 shows the probabilistic distribution of the selected target regions. There was no significant effect of session on the size of the ROI, proving stability. We have also not found significant effect of session of the percent signal change (PSC) (Table S2).

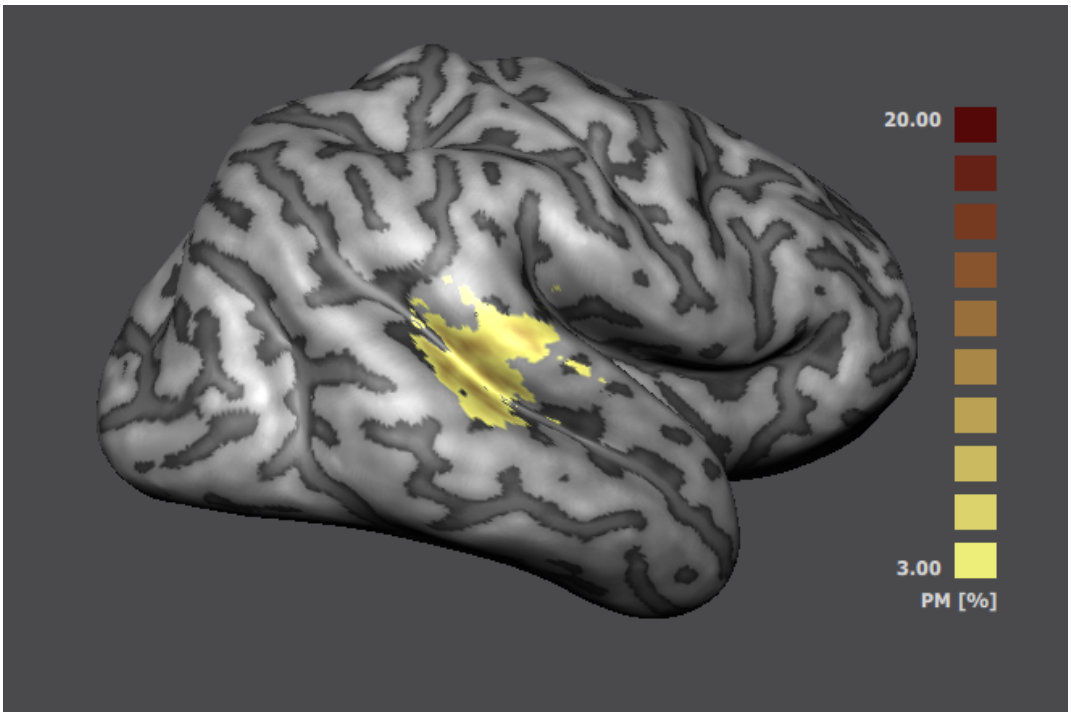

Figure 2 - Probabilistic map of the pSTS ROI locations.

3.5.2 Region of Interest Neurofeedback Analysis

Considering the feedback runs, we found that the participants could modulate brain activity based on the imagery of distinct facial expressions, but in subject- and stimulus-specific directions. In fact, some subjects could modulate the conditions IH, IS and IA expressions in different directions and this could even occur for IN imagery. We therefore opted to consider the absolute value of the t-statistic based on the facial expression contrast. Since the goal was to modulate ROI activity, irrespective of direction, we interpreted both modulation directions (IH, IS, IA > IN and IN > IH, IS, IA) as viable strategies. One-sample t-tests as well as 95% CIs characterized absolute BOLD % change within each ROI at the group level - session 1:

t(29) = 8.1151, 95% CIs for the BOLD % change [0.2887, 0.5190], session 2: t(29) = 6.5398, 95% CIs for the BOLD % change [0.2784, 0.5727], session 3: t(29) = 6.7730, 95% CIs for the BOLD % change [0.2619, 0.5075], session 4: t(29) = 6.2360, 95% CIs for the BOLD % change [0.3390, 0.6610], session 5: t(29) = 6.8469, 95% CIs for the BOLD % change [0.2907, 0.7339].

Considering all imagery runs (300 runs, 150 with and 150 without feedback), 128 runs presented statistically significant ROI-GLM (42% of the runs). Considering the 150 feedback runs, 70 runs presented statistically significant modulation values. Without feedback, significant modulation was only achieved in 58 runs, suggesting nevertheless that patients can readily use an instructed strategy to modulate brain activity even in the absence of feedback. Moreover, the number of successful training runs was close to the number of successful transfer runs (30 and 28 respectively). All patients were able to modulate ROI activity in at least 5 runs irrespective of feedback presentation; 4 patients achieved significance in more than 10 runs.

3.5.3 Post-hoc assessment

We further investigated individual profiles in the block-related average curves, given the evidence for different modulation strategies (participants could modulate either positively or negatively to distinct regulation conditions). We present the block-related average of a session from two patients in Figure 3, showing distinct directions in successful modulation. The first example (Figure 3.A) shows upregulation during condition IH and downregulation during condition IS. In the second example (Figure 3.B), the patient downregulates all non-neutral conditions.

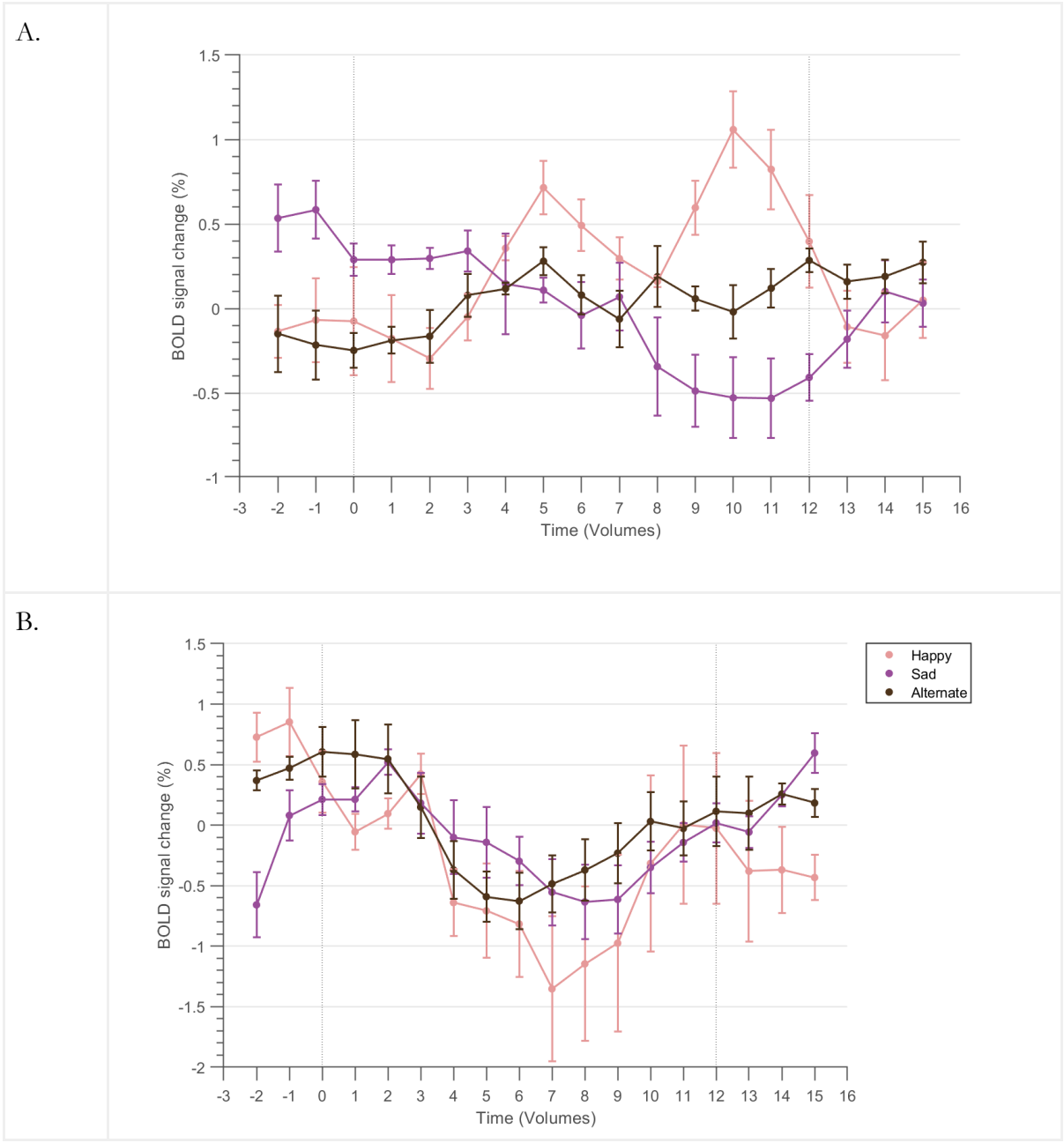

Figure 3 - Individual analysis of block-related averages of the target region for two different sessions (mean over imagery runs), showing that patients can modulate brain activity in the target region but in distinct directions. A. Patient #10, session #2 and B. Patient #5, session #4.

3.5.4 Whole-Brain Analysis

Figure 4 presents the most active brain regions during the neurofeedback session, using the balanced contrast (IH, IS, IA > IN) (RFX-GLM, FDR corrected, t(14), $p<0.0014$), for the 15

patients, 5 sessions and 2 runs with feedback. In this analysis, we found regions in the saliency network such as the anterior insula and anterior cingulate cortex (ACC) and subcortical structures involved in reward, feedback processing and operant learning such as the body of the caudate and putamen. Regions involved in emotional control in the medial prefrontal cortex (MPFC) were also activated.

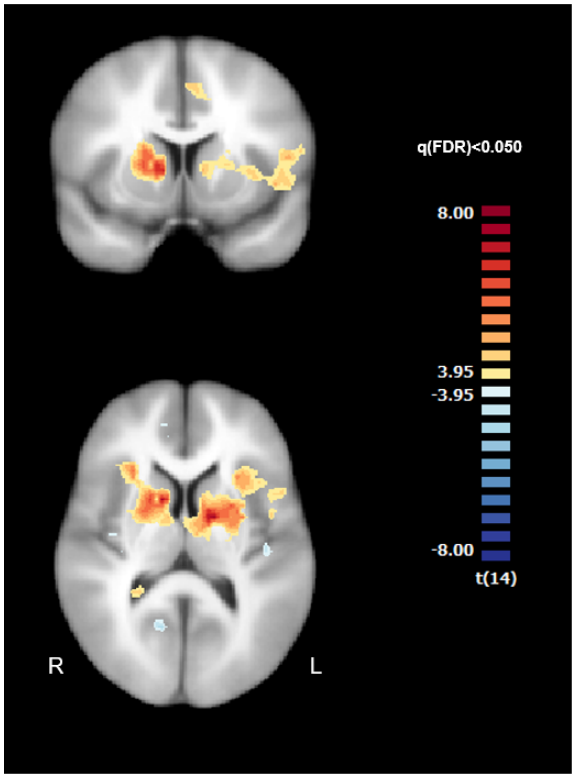

Figure 4 – Group RFX-GLM activation map for the neurofeedback runs, contrasting the imagery of happy, sad and alternate conditions with the neutral condition (FDR corrected, $q<0.05$) – Talairach coordinates of the slices are Y=9 (top) and Z=10(bottom).

4.Discussion

We demonstrate the feasibility of volitional rtfMRI-nf multiple session training in patients with ASD. This was attempted through training of a core feature in ASD, the processing of facial emotion expressions, in the pSTS, a region of the social cognition network. Moreover,

we identified relevant clinical and neural effects, as documented by neuroimaging results and improvement in neuropsychological measures of emotion recognition, adaptive behavior, and mood, which were observed immediately after the intervention and were sustained after 6 months. These findings pave the way for phase IIb/III clinical trials.

Volitional neurofeedback has been previously attempted in ASD only using EEG (37) which limits the targeting of specific brain regions, unlike fMRI. A previous fMRI study provided real-time covert (non-volitionally controlled) incidental feedback provided by the presentation of abstract nonsocial stimuli and did not address amplitude modulation (41) but instead induced subsequent changes in (resting state) connectivity. Behavioral effects in that study were modest, because as stated by the authors, it was designed as a proof of principle that aberrant connectivity can be addressed through neurofeedback, rather than as a clinical intervention. The ability of patients with ASD to undergo a complete (volitional) rtfMRI-nf intervention, targeting their social brain circuitry, is, therefore a novel approach, here tested through a clinical trial. All patients successfully participated and finished the 5-session intervention. We were able to evaluate all participants at the primary endpoint and only one patient did not complete the follow-up 6-month evaluation (the patient left the country). Recruitment satisfied the planned number of participants for the study and followed the recruitment rate schedule as planned (one participant every three weeks).

Neurobehavioral effects related to the chosen primary global efficacy outcome measure (emotion recognition - FEEST), were mainly observed for some subscales related to this measure and interesting effects were also observed for pre-defined secondary measures. Concerning the specific expression types assessed by FEEST, we note that the "Fear" condition presented a significant improvement. The secondary outcome measures, reflecting the generalization of learned skills to general aspects in social cognition, also suggest global significant improvements (VABS and ATEC) and in specific clinical subscales of ATEC, VABS, and POMS. Taken together, the results are in line with previous studies reporting that social cognition interventions can improve performance in emotion recognition tasks (42–44).

In our approach, using a neurofeedback training intervention, the patients are instructed to self-regulate brain activity/networks, ultimately aiming to change neural activity in a controlled manner. This approach can be useful to improve the ability of patients to achieve stable behavioral and neuropsychological benefits in neurodevelopmental disorders (for a review see (45)). The use of fMRI-based neurofeedback in ASD creates the opportunity to target novel

brain regions (such as pSTS, a social cognition specific region which is not accessible using alternative imaging techniques) and clinical symptoms associated with their function. The results do therefore suggest that fMRI-based volitional neurofeedback using pSTS and social cognition features may have a therapeutic future.

4.1 *Imaging results – insights into the neural effects of NF*

Imaging results provide interesting insights into the putative mechanisms of action of the intervention. The pSTS ROI could reliably be identified and selected online across sessions. Patients could modulate activity in this ROI during the neurofeedback. Interestingly, we found evidence for distinct modulation profiles, which are consistent with the heterogeneity of the cognitive styles of ASD patients. Some patients upregulated for imagery of neutral expressions and downregulated for imagery of sad and happy expressions, suggesting that perception of neutral faces is intrinsically distinct in ASD. Taken together, our results show distinct individual profiles, possibly related to different modes of perceptual experience and personal interpretation of the feedback. Future studies should exploit these individual differences and address whether these distinct profiles do indeed require tailored NF approaches.

4.2 *The role of reward and affective processing regions during NF*

There is an ongoing debate addressing the mechanisms of action underlying volitional control and success in neurofeedback (46, 47). Neurofeedback learning is possibly supported by operant learning systems, which are intrinsically related to motivation related networks (48). Spontaneous strategies (49) may emerge during NF training, with trial and error learning, in such an operant manner. These mechanisms are supported by the observed activation of striatal circuits, such as the caudate nucleus, involved in operant learning and reward. These neural systems may be particularly relevant in patients with ASD. The importance of striatal brain regions (implicated in reward and feedback processing) has been established across

neurofeedback experiments with different mental tasks (50). The identification of a similar network substantiates the contribution of the reward value of feedback to self-regulation in ASD patients. Even when participants modulated with different patterns of activity (in terms of direction of modulation), the similar contribution of such reward regions seemed relevant to achieve self-modulation of the target regions.

Another important aspect is that ASD participants seem to be highly motivated and engaged with information and communication technologies (ICTs) (51). ICTs allow them to explore a wide range of (self-driven) volitional strategies without disruptive social signals or intimidation.

Whole brain analysis during neurofeedback showed regions involved in operant learning and reward such as the caudate, and in the saliency network, such as the ACC and the anterior insula, which is decisive during feedback guided imagery irrespective from the task (50). In ASD, this network is especially relevant. The anterior insula has been previously implicated in ASD and is functionally related to emotional processing and cognitive control (52–54). In addition to the ACC, the MPFC may represent a hub between affective and cognitive processing (54). According to the same authors, ACC and the insula are also associated with emotional recall and imagery tasks, which is also supported by our findings. The identification of circuits involved in operant learning, reward and saliency processing sheds light into mechanisms of action-guided motivated behavior during volitional neurofeedback. Taken together, the results suggest that the patients were highly motivated and actively engaged in imagery/emotional self-control tasks. Moreover, we believe that the current findings provide enough evidence of behavioral improvements to motivate future phase IIb/III clinical trials.

References

1. Psychiatric A, Association: Diagnostic and Statistical Manual of Mental Disorders. 5th editio. Arlington, US, American Psychiatric Publishing., 2013

2. Mouga S, Almeida J, Café C, et al.: Adaptive Profiles in Autism and Other Neurodevelopmental Disorders. J Autism Dev Disord 2015; 45:1001–1012

3. Mouga S, Café C, Almeida J, et al.: Intellectual Profiles in the Autism Spectrum and Other Neurodevelopmental Disorders. J Autism Dev Disord 2016; 46:2940–2955

4. Charman T, Jones CRG, Pickles A, et al.: Defining the cognitive phenotype of autism [Internet]. Brain Res 2011; 1380:10–21Available from: http://dx.doi.org/10.1016/j.brainres.2010.10.075

5. Pinto D, Delaby E, Merico D, et al.: Convergence of genes and cellular pathways dysregulated in autism spectrum disorders. Am J Hum Genet 2014; 94:677–694

6. Pinto D, Pagnamenta AT, Klei L, et al.: Functional impact of global rare copy number variation in autism spectrum disorders [Internet]. Nature 2010; 466:368–372Available from: http://www.nature.com/doifinder/10.1038/nature09146

7. Weiss LA, Arking DE, Consortium TGDP of JH the A: A Genome-wide linkage and association scan reveals novel loci for autism2009; 461:802–808

8. Silver WG, Rapin I: Neurobiological basis of autism. [Internet]. Pediatr Clin North Am 2012; 59:45–61, x[cited 2013 Oct 25] Available from: http://www.ncbi.nlm.nih.gov/pubmed/22284792

9. Stigler KA, McDonald BC, Anand A, et al.: Structural and functional magnetic resonance imaging of autism spectrum disorders [Internet]. Brain Res 2011; 1380:146–161Available from: http://dx.doi.org/10.1016/j.brainres.2010.11.076

10. Seitz AR: Cognitive neuroscience: Targeting neuroplasticity with neural decoding and biofeedback [Internet]. Curr Biol 2013; 23:R210–R212Available from: http://dx.doi.org/10.1016/j.cub.2013.01.015

11. Papoutsi M, Weiskopf N, Langbehn D, et al.: Stimulating neural plasticity with real-time fMRI neurofeedback in Huntington's disease: A proof of concept study. Hum Brain Mapp 2017; 39:1339–1353

12. Muller R-A: The study of autism as a distributed disorder. Ment Retard Dev Disabil Rev 2007; 13:85–95

13. Fox CJ, Iaria G, Barton JJS: Defining the face processing network: optimization of the functional localizer in fMRI. [Internet]. Hum Brain Mapp 2009; 30:1637–51[cited 2013 Nov 7] Available from: http://www.ncbi.nlm.nih.gov/pubmed/18661501

14. Allison T, Puce A, McCarthy G: Social perception from visual cues: Role of the STS region. Trends Cogn Sci 2000; 4:267–278

15. Deen B, Koldewyn K, Kanwisher N, et al.: Functional Organization of Social Perception and Cognition in the Superior Temporal Sulcus. [Internet]. Cereb Cortex 2015; 25:4596–4609Available from: http://www.ncbi.nlm.nih.gov/pubmed/26048954

16. Kim SE, Kim JW, Kim JJ, et al.: The neural mechanism of imagining facial affective expression. Brain Res 2007; 1145:128–137

17. Hein G, Knight RT: Superior temporal sulcus--It's my area: or is it? J Cogn Neurosci 2008; 20:2125–2136

18. Pitcher D, Walsh V, Duchaine B: The role of the occipital face area in the cortical face perception network. [Internet]. Exp Brain Res 2011; 209:481–93[cited 2013 Dec 11] Available from: http://www.ncbi.nlm.nih.gov/pubmed/21318346

19. Rebola J, Castelo-Branco M: Visual areas PPA and pSTS diverge from other processing modules during perceptual closure: Functional dichotomies within category selective networks [Internet]. Neuropsychologia 2014; 61:135–142Available from: http://dx.doi.org/10.1016/j.neuropsychologia.2014.06.010

20. Iidaka T, Miyakoshi M, Harada T, et al.: White matter connectivity between superior temporal sulcus and amygdala is associated with autistic trait in healthy humans [Internet]. Neurosci Lett 2012; 510:154–158Available from: http://linkinghub.elsevier.com/retrieve/pii/S0304394012000717

21. Alaerts K, Woolley DG, Steyaert J, et al.: Underconnectivity of the superior temporal sulcus predicts emotion recognition deficits in autism. Soc Cogn Affect Neurosci 2014; 9:1589–1600

22. Pierce K, Mu R, Ambrose J, et al.: Face processing occurs outside the fusiform ' face area ' in autism : evidence from functional MRI. Brain 2001; 124:2059–2073

23. Saitovitch A, Bargiacchi A, Chabane N, et al.: Social cognition and the superior temporal sulcus: implications in autism. [Internet]. Rev Neurol (Paris) 2012; 168:762–70[cited 2014 Feb 11] Available from: http://www.ncbi.nlm.nih.gov/pubmed/22981269

24. Dichter GS: functional magnetic resonance imaging of autism spectrum disorders. Dialogues Clin Neurosci 2012; 14:319–30

25. Linden DEJ, Habes I, Johnston SJ, et al.: Real-time self-regulation of emotion networks in patients with depression. [Internet]. PLoS One 2012; 7:e38115[cited 2013 Nov 7] Available from: http://www.pubmedcentral.nih.gov/articlerender.fcgi?artid=3366978&tool=pmcentr

ez&rendertype=abstract

26. Karch S, Keeser D, Hümmer S, et al.: Modulation of craving related brain responses using real-time fMRI in patients with alcohol use disorder. PLoS One 2015; 10

27. Alegria AA, Wulff M, Brinson H, et al.: Real-time fMRI neurofeedback in adolescents with attention deficit hyperactivity disorder. Hum Brain Mapp 2017; 38:3190–3209

28. Direito B, Lima J, Simões M, et al.: Targeting dynamic facial processing mechanisms in superior temporal sulcus using a novel fMRI neurofeedback target [Internet]. Neuroscience 2019; 406:97–108Available from: https://linkinghub.elsevier.com/retrieve/pii/S0306452219301332

29. Young AW, Perrett DI, Calder a J, et al.: Facial expressions of emotion: stimuli and tests (FEEST). Psychology 2002; 126:420

30. Wright B, Alderson-Day B, Prendergast G, et al.: Gamma activation in young people with autism spectrum disorders and typically-developing controls when viewing emotions on faces. PLoS One 2012; 7

31. Rimland B, Edelson M: Autism Treatment Evaluation Checklist. 4812 Adams Avenue, San Diego, CA 92116., Autism Research Institute, 1999

32. Sparrow S, Balla A, Cicchetti V: Vineland adaptive behavior scales. Circle Pines, MN, American Guidance Service, 1984

33. Faro Viana M, Almeida P, Santos RC: Adaptação portuguesa da versão reduzida do Perfil de Estados de Humor – POMS [Internet]. Análise Psicológica 2012; 19:77–92Available from: http://publicacoes.ispa.pt/index.php/ap/article/view/345

34. McNair D, Lorr M, Droppleman L: Profile of mood states manual. San Diego, Educational and Industrial Testing Service, 1992

35. Pais-Ribeiro J, Silva I, Ferreira T, et al.: Validation study of a Portuguese version of the Hospital Anxiety and Depression Scale. Psychol Health Med 2007; 12:225–227

36. Zigmond AS, Snaith RP: The hospital anxiety and depression scale. Acta Psychiatr Scand 1983; 67:361–370

37. Beck AT, Ward CH, Mendelson M, et al.: An inventory for measuring depression. Arch Gen Psychiatry 1961; 4:561–571

38. A. Steer R, T. Beck A: Beck anxiety inventory manual. Behav Res Ther 1993; 3

39. Vaz Serra A, Pio Abreu JL: Aferição dos quadros clínicos depressivos: I. Ensaio de aplicação do "inventário Depressivo de Beck" a uma amostra portuguesa de doentes deprimidos. Coimbra Med 1973; 20:623–644

40. Sulzer J, Haller S, Scharnowski F, et al.: Real-time fMRI neurofeedback: progress and

challenges. [Internet]. Neuroimage 2013; 76:386–99[cited 2013 Nov 8] Available from: http://www.ncbi.nlm.nih.gov/pubmed/23541800

41. Ramot M, Kimmich S, Gonzalez-Castillo J, et al.: Direct modulation of aberrant brain network connectivity through real-time NeuroFeedback. Elife 2017; 6:1–23

42. Didehbani N, Allen T, Kandalaft M, et al.: Virtual Reality Social Cognition Training for children with high functioning autism [Internet]. Comput Human Behav 2016; 62:703–711Available from: http://dx.doi.org/10.1016/j.chb.2016.04.033

43. Silver M, Oakes P: Evaluation of a New Computer Intervention to Teach People with Autism or Asperger Syndrom to Predict Emotions in Others. Autism 2001; 5:299

44. LaCava PG, Golan O, Baron-Cohen S, et al.: Using assistive technology to teach emotion recognition to students with Asperger syndrome a pilot study. Remedial Spec Educ 2007;

45. Cohen R, Evans JR, editors: Neurofeedback and Neuromodulation Techniques and Applications. Elsevier, 2011

46. Wood G, Kober SE, Witte M, et al.: On the need to better specify the concept of "control" in brain-computer-interfaces/neurofeedback research [Internet]. Front Syst Neurosci 2014; 8:1–4Available from: http://journal.frontiersin.org/article/10.3389/fnsys.2014.00171/abstract

47. Schabus M, Griessenberger H, Gnjezda M-T, et al.: Better than sham? A double-blind placebo- controlled neurofeedback study in primary insomnia. Brain 2017; 140:1041–1052

48. Kleih SC, Nijboer F, Halder S, et al.: Motivation modulates the P300 amplitude during brain-computer interface use [Internet]. Clin Neurophysiol 2010; 121:1023–1031Available from: http://dx.doi.org/10.1016/j.clinph.2010.01.034

49. Kober S, Witte M, Ninaus M: Learning to modulate one's own brain activity: the effect of spontaneous mental strategies [Internet]. Front Hum … 2013; 7:695Available from: http://www.pubmedcentral.nih.gov/articlerender.fcgi?artid=3798979&tool=pmcentrez&rendertype=abstract%5Cnhttp://www.ncbi.nlm.nih.gov/pmc/articles/PMC3798979/

50. Skottnik L, Sorger B, Kamp T, et al.: Success and failure of controlling the fMRI-neurofeedback signal are reflected in the striatum2019; 1–15

51. Shic F, Goodwin M: Introduction to Technologies in the Daily Lives of Individuals with Autism. J Autism Dev Disord 2015; 45:3773–3776

52. Eckert M a, Menon V, Walczak A, et al.: At the Heart of the Ventral Attention System: the Right Anterior Insula. Hum Brain Mapp 2009; 30:2530–2541

53. Zaki J, Davis JI, Ochsner KN: Overlapping activity in anterior insula during interoception and emotional experience [Internet]. Neuroimage 2012; 62:493–499Available from: http://dx.doi.org/10.1016/j.neuroimage.2012.05.012

54. Phan KL, Wager T, Taylor SF, et al.: Functional neuroanatomy of emotion: A meta-analysis of emotion activation studies in PET and fMRI. Neuroimage 2002; 16:331–348

Supplementary Materials

Participants additional details

Fifteen male participants (19 years and 11 months, ± 3 years and 3 months) with high-functioning ASD (Full-Scale Intelligence Quotient [FSIQ] superior to 80; FSIQ: Mean = 103; SD = 10.7) participated in the study. ASD diagnosis was assigned based on: parental or caregiver interview (Autism Diagnostic Interview - Revised, ADI-R (1, 2)), direct structured subject assessment (Autism Diagnostic Observation Schedule, ADOS (3)), and the current diagnostic criteria for ASD according to the DSM-5 (4). Exclusion criteria included FSIQ inferior to 80, any associated medical condition such as epilepsy, or other usual comorbidities in ASD. Eight patients were medicated for ASD-related symptomatology, in particular irritability and agitation, at the time of the study. Three of them were polymedicated (risperidone n = 6; methylphenidate n = 3; sertraline = 1; lorazepam = 1).

Participants recruitment details

The participants were recruited based on a collaborative recruitment effort between ICNAS, the Autism Unit of the Pediatric Hospital integrated into the University Hospital of Coimbra and local ASD associations.

Sample size estimation

For guidance purposes, we calculated the sample size based on the hypothetical improvement on the FEEST test (primary outcome measure) based on the effects reported in (5). To this end, we followed a more conservative non-parametric approach. In a within-subject design with a standardized effect size of 0.82, the required sample size was 15, at an alpha level of 0.05 and power of 0.8. To determine these values, we used the G*Power tool (6).

Feasibility and efficacy measures

The intervention was assessed based on recruitment rate, retention (at primary and secondary endpoints), adherence, compliance, acceptability and ability to understand (and follow/engage

on) the protocol, i.e. ability to self-modulate brain activity. As primary efficacy measures, also used to calculate the sample size, we chose emotion recognition scores.

Procedures

Localizer

After the structural sequence, we performed a functional localizer to identify the target ROI for neurofeedback using an echo planar imaging (EPI) sequence (160 volumes, TR = 2 s, TE = 30 ms, flip angle = 75°, 32 slices, matrix size 64×70, in-plane voxel size = 3×3 mm, slice thickness = 2.5 mm, gap of 0.5 mm) (a detailed explanation of the protocol is presented in (7)).

The ROI was defined based on a block-based design with 40 blocks of eight seconds and five different conditions: N) Neutral - static neutral face; to subtract static aspects of face processing; H) Happy - morphing face from neutral to happy; S) Sad - morphing face from neutral to sad; A) Alternate expressions - alternating between sad and happy; M) Moving dots - randomly moving dots, to subtract motion processing (Figure 5).

Acquired fMRI data were exported in real-time to Turbo-BrainVoyager (TBV) software (Version 3.2, Brain Innovation, Maastricht, Netherlands), for data preprocessing (including 3D motion correction, spatial Gaussian smoothing and temporal filtering). Additionally, the incremental general linear model (GLM) routines in TBV, allowed rapid/real-time definition of the ROI based on the localizer run data. Our contrast featured the balanced subtraction of conditions N and M from emotion expression conditions H, S and A. Video clips of an avatar performing a facial expression (Vizard Virtual Reality Software Toolkit, Worldviz) were used as stimuli for conditions H, S and A.

Note that, because of the contrast-based subtraction by the static expression (N) and motion (M) conditions, the suggested localizer is quite stringent, since basic processing regions of static facial features will be elicited by the non-dynamic face stimuli, whose corresponding activation is subtracted. With this balanced contrast, we aim to capture the brain areas responsible specifically for processing of dynamic facial expressions. A three-dimensional box was visually selected over the cluster displaying the strongest response in the statistical

activation maps around the right posterior portion of the STS. We used the anatomical definition of the first sulcus inferior to the lateral fissure. The voxels significantly activated in this three-dimensional box defined our region of interest for the neurofeedback runs.

Imagery runs

Each run consisted of 25 blocks (12 regulation blocks featuring imagery of non-neutral expressions alternating with 13 regulation blocks of neutral expression imagery), each block with a duration of 24 seconds. At the beginning of each block, an auditory instruction was given to the participants presenting the condition, followed by a beep informing the start of each block.

The blocks included three randomly presented "conditions" featuring suggested neurofeedback strategies: IH) Imagery of a happy facial expression, IS) Imagery of a sad facial expression, IA) Alternate between the imagery of happy and sad facial expression, interleaved with IN) imagery of static neutral facial expressions, whereby the objective was to keep a neutral expression in the avatar. These possible strategies were instructed, taking into account that neurofeedback is also a skill that requires strategy learning, which can be speeded up with biologically inspired strategies.

Neurofeedback was presented in runs two and three with an interface providing the expression of an avatar. The expression of the avatar on the screen was continuously updated based on the mean ROI activation of the neurofeedback target. The avatar's expression was discretized into 15 levels (between neutral and the endpoint expression). The expression level displayed is determined considering the mean level of the ROI signal variation, in the direction of the instruction of the condition. In the IA condition, the feedback morphed in the "happy" axis. Real-time statistical analysis was performed with a custom MATLAB script and used to determine PSC. PSC value was discretized (considering 15 levels of the morphing), considering a maximum value of 1.5%.

The first and last runs were performed without feedback, but the stimuli and instructions were similar (the feedback was removed).

Data analysis – Imaging data details

The fMRI data were analyzed using BrainVoyager QX (Version 2.8, Brain Innovation, Maastricht, Netherlands). Pre-processing of single-subject fMRI data included slice-time

correction, realignment to the first image to compensate for head motion and temporal high-pass filtering (GLM-Fourier, 2 cycles) to remove low-frequency drifts. Co-registration of the functional data with the anatomical scan and normalization into Talairach coordinate space (8) were also performed as preliminary steps for group analyses.

In the first-level analysis of the functional runs, we used a standard GLM analysis for each run. Predictors were modelled as a boxcar function with the length of each condition (24 seconds), convolved with the canonical hemodynamic response function. Six motion parameters (three translational and three rotational) and predictors based on spikes (outliers in the BOLD time course) were also included in the GLM as covariates.

Our main goal was to assess the statistical significance of activation achieved within the neurofeedback target region. To this end, we used a ROI-GLM to retrieve the ROI activation level for the balanced contrast IN vs. IH, IS and IA.

Second-level analysis of the functional data was performed to better understand the mechanisms involved in neurofeedback at the group level. To this end, we performed a 3D spatial smoothing with a Gaussian filter of 6 mm. The resulting p-values were adjusted based on the false discovery rate (FDR) to correct for multiple testing.

Supplementary Results

The patient flow is presented in the CONSORT flow diagram (Figure S1). No dropouts were observed. Recruitment started on February 11, 2016 and ended on February 10, 2017, when the required sample size was reached, and the last interventional session was performed. Follow-up assessment was completed for the last participant on September 8, 2017.

Additional clinical measures

Additionally, other clinical measures also present improvements BDI total a decrease of 4.07 (95% CI [-7.41, -.72] (p = 0.021)) (the lower the score, the fewer the depression symptoms), POMS Tension a decrease of 3.20 (95% CI [-6.00, -0.41] (p = 0.028)) (the lower the score, the fewer the tension symptoms), POMS Anger a decrease of 1.80 (95% CI [-3.44, -0.16] (p = 0.033)) (the lower the score, the fewer the anger symptoms).

Imaging data - ROI analysis

Patients performed five neurofeedback training sessions. Each session included four imagery runs (the first - training run - and the last - transfer run - without feedback and the two in-between with feedback). Patients were asked to self-regulate the target ROI activity, use the feedback to optimize the modulation strategy and apply the best strategy in the runs without feedback.

Concerning variation within session, i.e. among runs, there is no evidence of run effect – repeated measures ANOVA [$F(3,222) = 1.685$, $p = 0.171$] (95% CI, training run [0.3694, 0.5525], first feedback run [0.3199, 0.5219], second feedback run [0.3769, 0.5625], transfer run [0.4070, 0.6456]).

There was no across session variability effect associated with the PSC within each imagery run – repeated measures ANOVA (training run: [$F(4,56) = 0.564$, $p = 0.690$]; neurofeedback 1: [$F(4,56) = 1.596$, $p = 0.188$]; neurofeedback 2: [$F(4,56) = 0.464$, $p = 0.762$]; transfer: [$F(4,56) = 0.332$, $p = 0.856$]).

Supplementary Figures

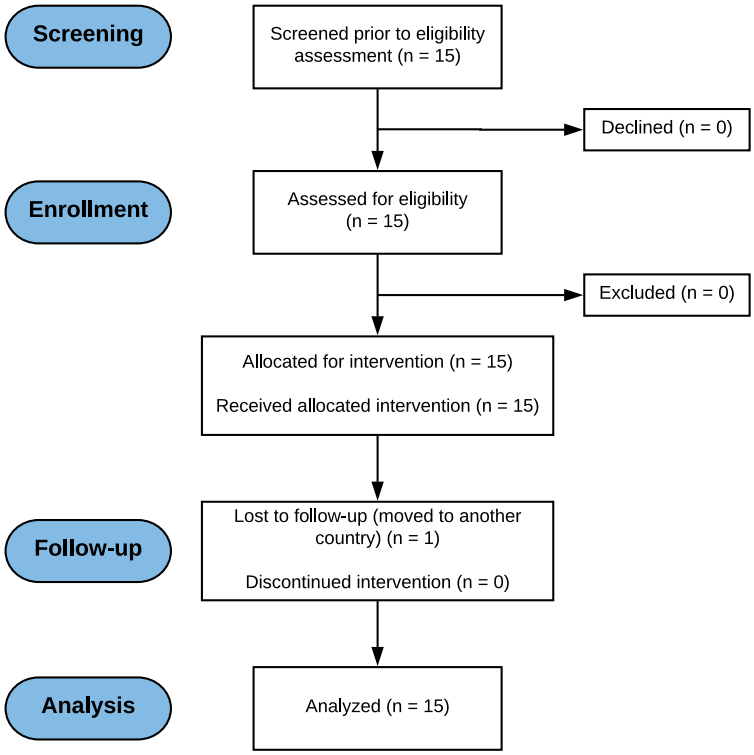

Figure S1 - Patient Flow, according to the CONSORT template. Follow-up assesses long-term effects of the intervention at 6 months (second evaluation, after the one occurring just post-intervention).

Supplementary Tables

Table S1– Outcome measure results (with a focus on confidence intervals - CIs).

	Baseline/Session 1		Primary follow-up time point (Session 5 - post-intervention)		Mean difference and 95% CI		Secondary follow-up time point (6 months after last training session)		Mean difference and 95% CI	
	n	Mean (SD)	n	Mean (SD)	Mean difference	95% CI	n	Mean (SD)	Mean difference	95% CI
FEEST _Anger	15	16.00 (6.80)	15	15.60 (7.08)	.40	(-.64, 1.44)	14	16.71 (6.22)	-1.00	(-2.18, .18)
FEEST _Disgust	15	11.60 (8.49)	15	13.33 (8.32)	-1.73	(-3.74, .27)	14	14.07 (7.92)	-2.71	(-5.80, .37)
FEEST _Fear	15	16.60 (2.26)	15	18.27 (1.98)	-1.67	(-3.07, -.27)	14	17.64 (3.39)	-1.21	(3.26, .83)

FEEST _Happiness	15	19.27 (2.84)	15	19.53 (0.99)	-.27	(-1.51, .98)	14	19.14 (3.21)	.07	(-.08, .23)
FEEST _Sadness	15	17.73 (2.69)	15	17.40 (4.82)	.33	(-1.73, 2.40)	14	17.36 (4.77)	.36	(-1.60, 2.31)
FEEST _Surprise	15	16.80 (4.63)	15	16.20 (6.26)	.60	(-.56, 1.76)	14	15.86 (5.90)	.71	(-.99, 2.42)
FEEST _Total	15	98.00 (19.30)	15	100.27 (19.29)	-2.27	(-5.41, .88)	14	100.79 (20.01)	-3.79	(-8.34, .77)
ATEC_SPEECH/LANGUAGE/COMMUNICATION	15	2.93 (1.71)	15	2.67 (1.76)	.27	(-.13, .66)	14	1.93 (1.30)	.93	(.10, 1.76)
ATEC_SOCIABILITY	15	13.60 (7.85)	15	13.73 (9.77)	-.13	(-3.00, 2.74)	14	7.79 (6.17)	5.57	(3.98, 7.17)
ATEC_SENSORY/COGNITIVE AWARENESS	15	8.87 (5.04)	15	6.80 (3.80)	2.07	(.61, 3.52)	14	4.86 (3.06)	4.21	(2.47, 5.96)
ATEC_HEALTH/PHYSICAL/BEHAVIOR	15	11.20 (6.17)	15	8.80 (5.13)	2.40	(.36, 4.44)	14	5.07 (2.81)	5.86	(3.27, 8.45)
ATEC_Total	15	36.60 (13.94)	15	32.00 (14.66)	4.60	(-.11, 9.31)	14	19.64 (8.13)	16.58	(12.19, 20.96)
VABS_COM	15	70.60 (15.65)	15	74.87 (14.95)	-4.27	(-7.44, -1.09)	14	79.79 (13.70)	-8.43	(-12.62, -4.24)
VABS_DLS	15	74.00 (17.15)	15	76.93 (16.46)	-2.93	(-5.37, -.50)	14	83.14 (17.00)	-8.64	(-12.31, -4.98)
VABS_SOC	15	63.40 (14.21)	15	66.73 (16.43)	-3.33	(-5.69, .98)	14	71.43 (15.36)	-7.07	(-9.60, -4.55)
VABS_ABC	15	63.40 (13.52)	15	67.13 (15.22)	-3.73	(-6.07, -1.40)	14	73.57 (16.67)	-9.50	(-12.13, -6.87)
HADS_Total	15	10.27 (4.81)	15	8.27 (4.10)	2.00	(-.47, 4.47)				
BDI_Total	15	9.40 (7.41)	15	5.33 (4.30)	4.07	(.72, 7.41)				
POMS_Tension	15	7.27 (4.27)	15	4.07 (2.87)	3.20	(.41, 6.00)				
POMS_Depression	15	5.93 (8.49)	15	1.07 (2.46)	4.87	(-.07, 9.81)				
POMS_Anger	15	2.80 (2.76)	15	1.00 (1.41)	1.80	(.16, 3.44)				
POMS_Vigour	15	15.20 (4.92)	15	12.73 (6.42)	2.47	(-.48, 5.41)				
POMS_Fatigue	15	3.53 (4.49)	15	2.27 (3.04)	1.27	(-1.49, 4.02)				
POMS_Confusion	15	6.20 (3.41)	15	5.40 (3.85)	.80	(-1.99, 3.59)				
POMS_Total	15	110.53 (20.39)	15	101.07 (13.25)	9.47	(-3.50, 22.44)				

Table S2 – Session effect on ROI size and PSC

Session number		number of voxels		PSC	
	n	Mean	95% CI	Mean	95% CI
1	15	734.0667	[578.0849, 890.0484]	1.7857	[1.2542, 2.3173]
2	15	687.2	[501.7434, 872.6566]	2.6417	[1.6347, 3.6486]
3	15	660.8	[462.4300, 859.1700]	2.3843	[1.6718, 3.0968]
4	15	689.6667	[495.3640, 883.9693]	2.3646	[1.4181, 3.3110]
5	15	692.2667	[507.2407, 877.2926]	1.8578	[1.0977, 2.6179]

References

1. Rutter M, Le Couteur AS, Lord C: ADI-R: Autism Diagnostic Interview Revised : Manual. Western Psychological Services, 2013

2. Lord C, Rutter M, Couteur A Le: Autism Diagnostic Interview-Revised : A Revised Version of a Diagnostic Interview for Caregivers of Individuals with Possible Pervasive Developmental Disorders. J Autism Dev Disord 1994; 24:659–685

3. Lord C, Rutter ML, DiLavore P, et al.: Autism Diagnostic Observation Schedule. Western Psychological Services, 1999

4. Psychiatric A, Association: Diagnostic and Statistical Manual of Mental Disorders. 5th editio. Arlington, US, American Psychiatric Publishing., 2013

5. Philip RCM, Whalley HC, Stanfield AC, et al.: Deficits in facial, body movement and vocal emotional processing in autism spectrum disorders. Psychol Med 2010; 40:1919–1929

6. Faul F, Erdfelder E, Lang A-G, et al.: G*Power 3: A flexible statistical power analysis program for the social, behavioral, and biomedical sciences. IOP Conf Ser Earth Environ Sci 39:175–191

7. Direito B, Lima J, Simões M, et al.: Targeting dynamic facial processing mechanisms in superior temporal sulcus using a novel fMRI neurofeedback target [Internet]. Neuroscience 2019; 406:97–108Available from: https://linkinghub.elsevier.com/retrieve/pii/S0306452219301332

8. Talairach J, Tournoux P: Co-planar Stereotaxic Atlas of the Human Brain, 3-Dimensional Proportional Systems: An Approach to Cerebral Imaging. New York, Thieme Medical Publishers, 1988

Appendix III

Correlated alpha activity with the facial expression processing network in a simultaneous EEG-fMRI experiment

This appendix is composed by the contents of the following publication:

Simoes, M., Direito, B., Lima, J., Castelhano, J., Ferreira, C., Couceiro, R., Carvalho, P., Castelo-Branco, M. (2017). Correlated alpha activity with the facial expression processing network in a simultaneous EEG-fMRI experiment. in *2017 39th Annual International Conference of the IEEE Engineering in Medicine and Biology Society (EMBC)* (IEEE), 2562–2565. doi:10.1109/EMBC.2017.8037380.

Abstract

The relationship between EEG and fMRI data is poorly covered in the literature. Extensive work has been conducted in resting-state and epileptic activity, highlighting a negative correlation between the alpha power band of the EEG and the BOLD activity in the default-mode-network. The identification of an appropriate task-specific relationship between fMRI and EEG data for predefined regions-of-interest, would allow the transfer of interventional paradigms (such as BOLD-based neurofeedback sessions) from fMRI to EEG, enhancing its application range by lowering its costs and improving its flexibility.

In this study, we present an analysis of the correlation between task-specific alpha band fluctuations and BOLD activity in the facial expressions processing network. We characterized the network ROIs through a stringent localizer and identified two clusters on the scalp (one frontal, one parietal-occipital) with marked alpha fluctuations, related to the task. We then check whether such power variations throughout the time correlate with the BOLD activity in the network.

Our results show statistically significant negative correlations between the alpha power in both clusters and for all the ROIs of the network. The correlation levels have still not met the requirements for transferring the protocol to an EEG setup, but they pave the way towards a better understand on how frontal and parietal-occipital alpha relates to the activity of the facial expressions processing network.

1. Introduction

Electroencephalography (EEG) and functional Magnetic Resonance Imaging (fMRI) are two non-invasive neuroimaging techniques. They are complementary and not supplementary, since their characteristics provide different types of measures of the brain activity. On the one hand, fMRI conveys detailed spatial information, with resolutions at the sub-millimetre level, but with a much more limited temporal resolution, with sampling rates around the second. On the other hand, EEG has poor spatial resolution (around 3 cm (Burle et al., 2015)), but presents high temporal resolution data (sub-millisecond). The differences go beyond their intrinsic characteristics: the costs associated with each imaging technique are very different. Although prices vary over location and institution, conducting a MRI recording session is much more expensive than an EEG session (DellaBadia Jr et al., 2002). Therefore, when considering therapeutically interventions - which usually require several sessions -, the EEG solution conveys better chances of widespread implementation based on its lower costs, portability and ease of use. However, since the characteristics of each technique are very different of the other, interventions using such methods tend also to be different.

The most common rehabilitation interventions using these techniques are neurofeedback. Neurofeedback refers to the method of self-regulation of brain activity based on real-time information provided by a neuroimaging method (for in-depth review, see (Sitaram et al., 2016)). The main concept behind it relies on the connection between behavior and neuronal activity: if there is a change in one activity pattern that is related to a behavior, changing that activity pattern should create a variation in the corresponding behavior. Thus, neurofeedback targets specific neuronal substrates of behavior and, providing real-time information about those neuronal substrates empowers the patient with the possibility of self-regulate the activity of those regions/patterns/signals and, hopefully, create a behavioral improvement.

The two major categories of neurofeedback signals used are electrophysiological and hemodynamic. The electrophysiological methods use EEG, magnetoencephalography (MEG) or invasive electrocorticography (ECoG) to capture the electrical activity of the brain, while the hemodynamic methods use fMRI or functional near-infrared spectroscopy (fNIRS) to capture changes in the Blood-Oxygenation-Level-Dependent (BOLD) activity. From those, the most used are scalp EEG and fMRI.

One of the main difficulties of using fMRI-based neurofeedback is the cost and setup inflexibility, which makes current studies using this technique limited in the number of sessions (they vary significantly between studies, from one up to ten sessions (Shibata et al., 2011), but the majority consisted of a single session). When comparing with EEG-based neurofeedback studies, where the number of sessions is significantly higher (most studies use more than 10 sessions), the need of transferring fMRI-based neurofeedback protocols to EEG setups becomes clear, in order to achieve a broader and wider application of those.

The relationship between the EEG alpha band (oscillatory activity with frequency between 8 and 15Hz) and the BOLD activity has been studied mostly for resting-state data. Negative correlations between the occipital alpha activity and the default-mode-network have been found in several studies (for a review, see (Murta et al., 2015)). However, it remains unclear if such relation exists when participants are performing a task. The literature on task-specific correlations is scarce (Meir-Hasson et al., 2016).

In this paper, we present a correlation analysis between spectral scalp activity and BOLD responses in task-specific regions-of-interest (ROI), for a simultaneous EEG-fMRI experiment of neurofeedback based on facial expressions imagery. To the best of our knowledge, our study is the first one to analyze EEG-fMRI correlations at the single-trial level for the facial expression processing network. We analyze how the alpha power band in the EEG signal correlate with activity in the regions of Occipital Face Area (OFA), Fusiform Face Area (FFA) and posterior Superior Temporal Sulcus (pSTS) (Fox et al., 2009), during a task of neurofeedback based on mental imagery of facial expressions.

2. Methods

In order to analyze the relationship between the different frequency bands and the BOLD signal at the different brain regions of the facial processing network, we conducted a neurofeedback session, recording simultaneously EEG and fMRI signals. The paradigm is fully described in (Simoes et al., 2015), and will be shortly overviewed here.

2.1 Participants

Ten healthy volunteers were enrolled in a one-session long fMRI-based neurofeedback experiment, where we captured simultaneously EEG signals (mean age: 26 ± 3 years; 9 males). All participants had normal or corrected-to-normal vision, presented no history of neurological disorders and were naive to the purpose of the study. The study was approved by the Ethics Commission of the Faculty of Medicine of the University of Coimbra and was conducted in accordance with the declaration of Helsinki. All subjects provided written informed consent to participate in the study.

2.2 Session Protocol

The session consisted of one localizer run and three runs of neurofeedback (imagery with auditory feedback, imagery with visual feedback and transfer run). The order of auditory and visual feedback was randomized between subjects.

2.2.1 Localizer

For the localization of the facial expression processing network, dynamic stimuli of a realistic avatar performing happy and sad facial expressions (see the facial expressions in Figure 2.1) was contrasted with the same avatar with a neutral expression and a generic motion stimulus (randomly moving dots). Such stringent contrast recovers the areas that respond to the facial expression, but do not respond to the face itself nor to isolated movement.

Figure 2.1 - Screenshots of the different facial expressions used in the stimuli (neutral, happy and sad).

2.2.2 Neurofeedback runs

The neurofeedback runs consisted of alternating blocks of up and down regulation of the activity over the right pSTS ROI, with duration of 24 seconds. As feedback, a visual (avatar morphing the facial expression) or auditory (positive or negative sound) were provided to the participant. To modulate the activity in the target ROI, the subject was suggested to use a strategy of mental imagery of the avatar performing the facial expression. In the baseline blocks, participants were instructed to imagine a neutral face in the avatar, while in the expression blocks they were instructed to imagine repeatedly the morphing of the expression (happy, sad or alternating from happy and sad).

2.3 MRI data recording and processing

Scanning was performed on a 3T Siemens Magnetom TimTrio scanner, at the Portuguese Brain Imaging Network, using a 12-channel head coil. To create a structural reference to map the functional data, the beginning of each scanning session included the acquisition of a high-resolution magnetization-prepared rapid acquisition gradient echo (MPRAGE) sequence for co-registration of functional data (176 slices; TE: 3.42ms; TR: 2530ms; voxel size 1.0×1.0×1.0 mm3.

Functional MR volumes were recorded consisting of 33 slices (in-plane resolution: 4×4 mm2, field of view (FOV): 256×256 mm^2, slice thickness: 3 mm, flip angle (FA): 90°) yielding a total

coverage of the occipital and posterior temporal lobe. Repetition time (TR) was 2000 ms (Echo Time (TE): 30 ms). Start of each trial was synchronized with the acquisition of the fMRI volumes.

For the localizer run, 160 volumes were acquired for a total duration of approximately 5 minutes. In the neurofeedback runs, the technical aspects of the functional MR volumes were similarly to the localizer run. Each run had a total duration of 10 minutes, corresponding to a total of 300 volumes.

Pre-processing of single-subject fMRI data included co-registration with structural data and normalization into Talairach coordinate space, temporal high-pass filtering, space domain 3D motion correction with intra-session alignment and slice scan time correction with cubic spline interpolation. A 3D spatial smoothing with a Gaussian filter of 5 mm was also applied.

2.4 EEG signal recording and processing

We used the MRI-compatible 64-channels Neuroscan system (MagLinkTM, NeuroScan, USA) to record the electrophysiological signal during the neurofeedback experiment. The EEG system was applied to the participants before they entered the scanner: scalp was cleaned with abrasive gel and alcohol, the EEG cap was placed in the participant head and conductive gel was added to each of the 64Ag/AgCl nonmagnetic electrodes positioned according to the 10/10 system to reduce impedance. Electrodes' impedance was kept under 10 kΩ during the recordings. The recording reference was set to an electrode close to CZ and EEG and fMRI data were acquired in a continuous way. The electrocardiogram signal (EKG) was also recorded, simultaneously with the EEG. EEG and EKG signals were amplified and recorded at a sampling rate (SR) of 10 kHz.

Simultaneous EEG/fMRI recording presents two major interferences in the EEG signal: gradient artifacts, corresponding to interference added by the magnetic field, and ballistocardiogram (BCG) artifacts, corresponding to physiological cardiac-related artifacts (Allen et al., 2000).

We used the average subtraction gradient correction implemented in Maglink RT Edit software (v4.5, NeuroScan, USA) to correct the artifacts added by the MR gradient switch.

That method creates an average template of the artifact and then subtracts it from the recorded EEG (Castelhano et al., 2014). The correction algorithm includes a low-pass filter of 75 Hz.

For the correction of BCG artifacts, we ran an independent component analysis (ICA). Data were high-pass filtered by 1Hz. "Bad" channels were removed and data were re-referenced to average reference. ICA components were computed using the EEGLAB (Matlab toolbox v13_3_3b) implementation of infomax algorithm (Bell and Sejnowski, 1995). The independent components were inspected and the ones with higher correlation with the EKG signal recorded during the acquisition were removed from the signal (around 3 to 5 components). Similarly, components related to other artifacts (such as blinking and eye movements) were also removed.

2.5 Analysis pipeline

For the correlation analysis, we extracted time-frequency activity related to the frequency bands of interest, average the data from the electrodes on our clusters of interest, convolve the final time-frequency values with the hemodynamic function and then correlate the data with the functional data from the MRI. Peak correlation values are then extracted from the facial expression network ROIs and, finally, final ROI correlation values are averaged across subjects, using a Fisher transformation (Figure 2.2).

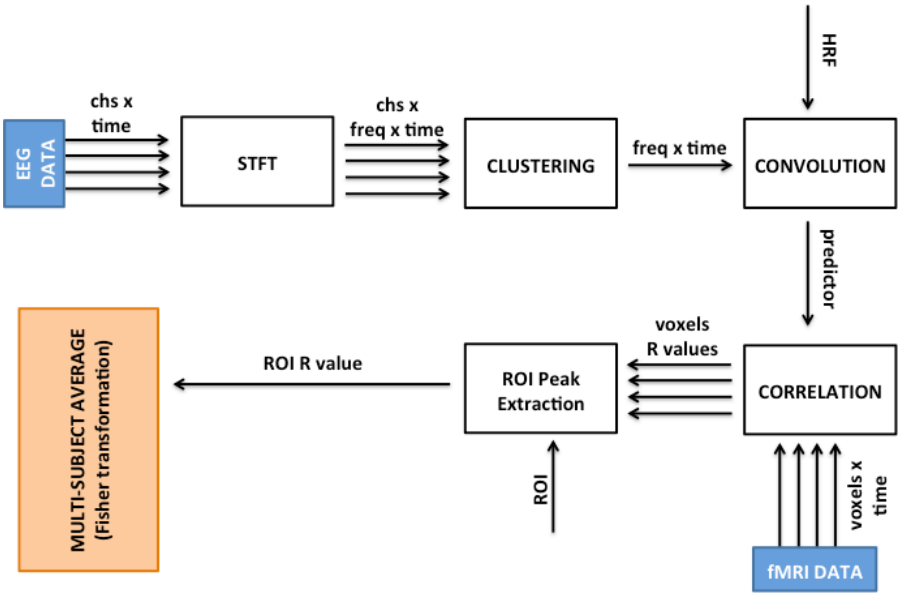

Figure 2.2 – Analysis Pipeline, describing all the steps from the preprocessed EEG and fMRI data to the correlation.

2.5.1 ROI selection

We used the localizer fMRI data to create a fixed-effects analysis. The statistical activation map was determined with the balanced contrast (i. randomly moving dots, ii. static neutral face) < (iii. morphing face from neutral to sad, iv. morphing face from neutral to happy, v. alternating between sad and happy). P-values were thresholded at $p = 0.001$. We were able to extract clusters from each of the regions of interest (FFA, OFA and pSTS, both hemispheres), guided by the literature locations. We then extracted the statistical peak of each ROI and generated spherical ROIs of 10mm diameter around each peak. As a result, ROI sizes became more homogeneous.

2.5.2 Power extraction, cluster selection and correlation

We calculated the Short-Time Fourier Transform with a window of 2 seconds and no overlap, in order to match the TR of the fMRI data, and extract the spectrogram for the alpha band (8-15Hz). That way we get a value of alpha activity for every TR and every channel. We then cluster the channels of interest and get a representation of the time-course of the alpha throughout the neurofeedback run.

For the selection of the clusters of interest, we looked for the task-related alpha variation throughout the scalp in order to identify the cluster who maximized those variations.

In order to account for the hemodynamic delay in the fMRI data, alpha values were convolved with the standard hemodynamic response function (HRF). After that, correlation was computed between our alpha predictor and the volume time course data from each voxel of brain. Correlation peaks from each ROI were extracted and added for the multi-subject analysis. We then transform the R values of each run through a Fisher z-transformation, average them and transform them back to R values through its inverse.

3. Results

Regarding the fixed-effects analysis for the extraction of the facial expression processing ROIs, Table 3.1 summarizes the peak Talairach coordinates, t and p-values achieved. As previously referred, spherical ROIs were applied centered on those coordinates.

Table 3.1 - Peak ROI coordinates and statistical values.

ROI	X	Y	Z	t	p
Right OFA	36	-67	-8	5,08	< 0.001
Left OFA	-39	-67	-8	9,21	< 0.001
Right FFA	36	-40	-23	4,59	< 0.001
Left FFA	-39	-49	-14	4,87	< 0.001
Right pSTS	48	-31	1	8,49	< 0.001
Left pSTS	-51	-46	10	8,29	< 0.001

Regarding the electrodes clustering, Figure 3.1 evidences the alpha task-related response through the time-frequency plot and the topographic map highlight the regions from where the alpha variations were manifested. From that analysis, we selected a frontal and a parietal-occipital cluster, described in Table 3.2.

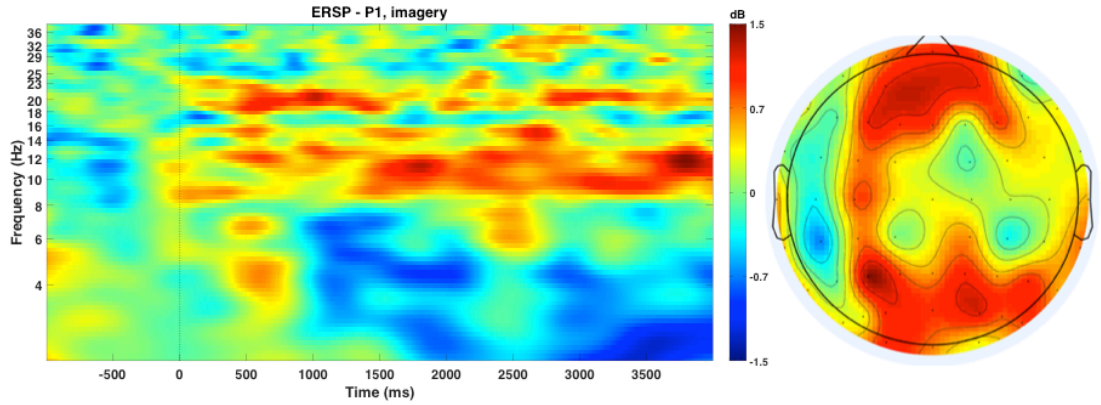

Figure 3.1 – Relative power between neutral and facial expression mental imagery. Left: time-frequency pattern normalized by the time after instruction and before cue. Right: spatial distribution of alpha power at t=2s.

Table 3.2 –Electrode clusters.

Cluster	Electrodes
Frontal	F1 F2 F3 F4 FC1 FC2 FC3 FC4
Parietal-Occipital	O1 O2 PO3 PO5 PO7 PO4 PO6 PO8 P1 P3 P5 P7 P2 P4 P6 P8

Parietal-Occipital and Frontal alpha correlations provided similar results. Figure 3.2 shows the correlations distributions for each ROI by cluster. Negative correlations were statistically significant for every ROI of the facial expression processing network, for both frontal and parietal-occipital clusters, as shown in Table 3.3.

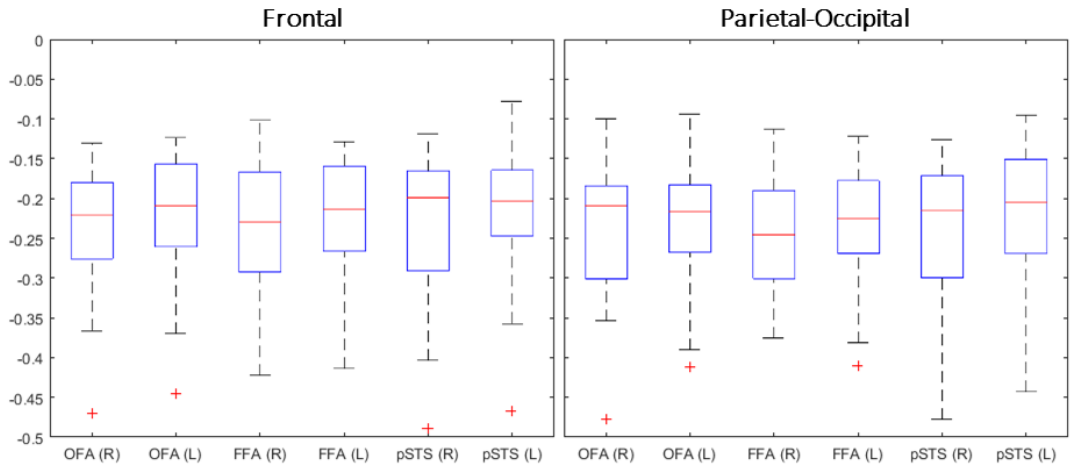

Figure 3.2 – Pearson R distribution across subjects. Each column represents one ROI and each plot one EEG cluster. Outliers marked by red cross.

Table 3.3 – Mean correlation values achieved for each ROI based on the alpha predictors of each cluster.

	Frontal		Parietal-Occipital	
ROI	**R**	**z**	**R**	**z**
OFA (R)	-.24	-4.21**	-.24	-4.18**
OFA (L)	-.23	-4.01**	-.23	-4.07**
FFA (R)	-.24	-4.31**	-.26	-4.51**
FFA (L)	-.22	-3.90**	-.23	-4.09**
pSTS (R)	-.23	-4.12**	-.24	-4.19**
pSTS (L)	-.22	-3.84**	-.22	-3.79**

****p < 0.01, FWE corrected for multiple comparisons**

4. Discussion

The negative correlation between alpha oscillations and BOLD activity have been studied in the default-mode-network, especially for the occipital cortex. However, it was unclear if such a relationship would be present in task paradigms. Our study shows a significant correlation between a frontal and a parietal-occipital alpha and the facial expression processing network.

Although correlations are not very high, it should be highlighted the fact that the facial expression processing ROIs are extracted from the group analysis. It is expected that subject-specific ROIs would elicit higher correlation values, although sometimes it is not possible to elicit a full network localization for each subject (Fox et al., 2009). Despite presenting already statistically significant correlation values, in order to transfer this paradigm to an EEG setup, the correlation values presented have to improve further. In this sense, additional work is needed in order to look for a better metric to represent the activity in the facial expressions processing network. A predictive model of the fMRI data could increase the correlation coefficients.

The similar results between clusters are justified by a high alpha power correlation between both clusters. Future work should assess that relation exploring, for instance, the source of both activities. Furthermore, task-performance might influence the correlation values, considering that better performers should present wider variation in the ROIs activity and therefore produce signals more easily measured at the scalp. Therefore, the relation between task performance and correlation levels should be addressed in future studies.

References

Allen PJ, Josephs O, Turner R (2000) A method for removing imaging artifact from continuous EEG recorded during functional MRI. Neuroimage 12:230–239. doi: 10.1006/nimg.2000.0599.

Bell AJ, Sejnowski TJ (1995) An Information-Maximization Approach to Blind Separation and Blind Deconvolution. Neural Comput 7:1129–1159. doi: 10.1162/neco.1995.7.6.1129.

Burle B, Spieser L, Roger C, Casini L, Hasbroucq T, Vidal F (2015) Spatial and temporal resolutions of EEG: Is it really black and white? A scalp current density view. Int J Psychophysiol 97:210–220. doi: 10.1016/j.ijpsycho.2015.05.004.

Castelhano J, Duarte IC, Wibral M, Rodriguez E, Castelo-Branco M (2014) The dual facet of gamma oscillations: Separate visual and decision making circuits as revealed by simultaneous EEG/fMRI. Hum Brain Mapp 00:1–17. doi: 10.1002/hbm.22545.

DellaBadia Jr J, Bell WL, Keyes Jr JW, Mathews VP, Glazier SS (2002) Assessment and cost comparison of sleep-deprived EEG, MRI and PET in the prediction of surgical treatment for epilepsy. Seizure 11:303–309. doi: 10.1053/seiz.2001.0648.

Fox CJ, Iaria G, Barton JJSS (2009) Defining the face processing network: Optimization of the functional localizer in fMRI. Hum Brain Mapp 30:1637–1651. doi: 10.1002/hbm.20630.

Meir-Hasson Y, Keynan JN, Kinreich S, Jackont G, Cohen A, Podlipsky-Klovatch I, Hendler T, Intrator N (2016) One-class FMRI-inspired EEG model for self-regulation training Schmahl C, ed. PLoS One 11:e0154968. doi: 10.1371/journal.pone.0154968.

Murta T, Leite M, Carmichael DW, Figueiredo P, Lemieux L (2015) Electrophysiological correlates of the BOLD signal for EEG-informed fMRI. Hum Brain Mapp 36:391–414. doi: 10.1002/hbm.22623.

Shibata K, Watanabe T, Sasaki Y, Kawato M (2011) Perceptual Learning Incepted by Decoded fMRI Neurofeedback Without Stimulus Presentation. Science (80-) 334:1413–1415. doi: 10.1126/science.1212003.

Simoes M, Lima J, Direito B, Castelhano J, Ferreira C, Carvalho P, Castelo-Branco M (2015) Feature analysis for correlation studies of simultaneous EEG-fMRI data: A proof of concept for neurofeedback approaches. In: 2015 37th Annual International Conference of the IEEE Engineering in Medicine and Biology Society (EMBC), pp 4065–4068.

IEEE. doi: 10.1109/EMBC.2015.7319287.

Sitaram R, Ros T, Stoeckel L, Haller S, Scharnowski F, Lewis-Peacock J, Weiskopf N, Blefari ML, Rana M, Oblak E, Birbaumer N, Sulzer J (2016) Closed-loop brain training: the science of neurofeedback. Nat Rev Neurosci 18:86–100. doi: 10.1038/nrn.2016.164.

Appendix IV

Neurohab: A Platform for Virtual Training of Daily Living Skills in Autism Spectrum Disorder.

This appendix is composed by the contents of the following publication:

Simões M, Mouga S, Pedrosa F, Carvalho P, Oliveira G, Branco MC (2014) Neurohab: A Platform for Virtual Training of Daily Living Skills in Autism Spectrum Disorder. In: HCIST 2014 - International Conference on Health and Social Care Information Systems and Technologies (João Varajão, Manuela Cunha, Niels Bjørn-Andersen, Rodney Turner, Duminda Wijesekera, Ricardo Martinho RR, ed), pp 1417–1423. Procedia Technology. Troia, Portugal doi: 10.1016/j.protcy.2014.10.161.

Abstract

Autism spectrum disorder (ASD) is a neurodevelopmental disorder that besides the core symptoms of impairment in communication, social interaction and repetitive behavior, seriously compromises adaptive functioning limiting social inclusion. A number of studies also support executive dysfunction in ASD, although its specificity remains controversial. Furthermore, recent studies point to the relevance of ecologically valid executive tasks that match patient's daily lives and therefore address the correlation with social cognition and learning of adaptive behavior. These disabilities are usually addressed in rehabilitation therapies, usually performed in a scheme of one therapist for individual, having high costs for the individuals and patient associations in human resources. This usually results in lesser hours of intervention, leading to lesser impact of the behavior training. To avoid this impact, some technological responses have been arising in the literature to perform training of individuals with ASD, although lacking scientific validity. In this work, we propose a platform for training daily activities in controlled environments, which allow caregivers and therapists to follow the patients' performances and improvements along the time. This platform contains several

serious games, which target specific adaptive and executive dysfunctions. Games can be added to the platform and become automatically available for the users.

1. Introduction

Autism spectrum disorder (ASD) is a severe, early-onset and life-long neurodevelopmental disorder with a high prevalence worldwide and also in Portugal, and a distribution of four males (M) to one female (F) [1-3]. ASD is characterized by deficits in social interaction and communication as well as by the presence of a repetitive pattern of behavior and interests [4]. These core symptoms compromise functioning across multiple domains, including cognitive functioning and adaptive behavior (AB), affecting multiple areas of a person's life [4-6]. AB refers to the capacity to accomplish conceptual, social and practical demands on a daily basis [7]. To be successful in those demands and therefore support personal, domestic and social self-sufficiency, individuals have to perform daily activities that require adaptive skills [8-9]. Deficits in this area are a primary barrier to a wide range of tasks that go from basic personal and domestic autonomy (such as hygiene, dressing, making meals) to self-sufficiency (such as having a competitive employment or managing your money) [12]. Difficulties in AB appear early in life [5-6] and, without appropriate and effective intervention, persist throughout life [13]. Humans are deeply social creatures living in highly collective environments, which mean that adaptive behaviors require social imitation learning. Social cognition usually refers to the fundamental abilities to perceive, categorize, remember, analyze, reason with, and behave toward other individuals [14]. Executive functions (EF) are necessary for goal-directed and adaptive behavior and include the ability to initiate and finish actions, to monitor and change behavior as needed, and to plan future behavior when faced with novel tasks and situations [15]. EF allows us to anticipate outcomes and adapt to changing situations. The ability to form concepts and think abstractly is also considered a component of EF. These life-long disabilities are one of the most important in the prognosis of the people with ASD and consequently have social and economic repercussion with large cost to the society [16]. ASD has a significant economic and social impact due to its high prevalence, absence of specific therapeutic intervention, comorbidity, outcome and impact on families. Discarding medical costs, intensive behavioral interventions for children with ASD are estimated to cost between $40,000 and $60,000 per year for each child, in the United States of America [17]. This

economic burden is very difficult to support for both parents and governments. The main problem is related to the fact that therapy must be intensive, which required specialized human resources allocated for long time with children, which is very expensive. In order to lower these costs and increase the access of families to economically viable therapy solutions, technology has been targeted as a potential help. Inside the technology field, virtual reality (VR) has gained a particular focus. VR addresses the possibility of creating computer simulations of real environments, providing safer learning experiences for individuals with ASD [18]. Its use in autism therapy is argued by the characteristics of VR allowing the control of the stimuli provided to users, reducing the complexity of the real world, along with the safety, control, repetition and some preference found in ASD people for computer interactions [19-20]. Furthermore, the realism of virtual environments increases the probability of transferring learning skills to the real life [19, 21-22]. There are also some works proposing guidelines for the development of such applications, addressing most issues autism patients have with interactive learning software [23]. In this direction, we present in this paper the development of the Neurohab platform. It is an integrated solution of serious games for individuals with ASD, which allows users and caregivers to train in virtual environments daily activities, in order to improve their autonomy. Here we describe the requirements identified together with patient associations and clinical staff, as well as the way they were addressed and incorporated in the current solution. The paper is structured in four sections. After this introduction, the methods section presents how we established the requirements of the system, the results section describes the solution developed and then we discuss the results in the final section.

2. Methods

For the development of the platform, requirements were defined together with two local autism patients' associations – Associação Portuguesa para as Perturbações do Desenvolvimento e Autismo (APPDA) of Coimbra and Viseu – and clinical staff from the Unidade de Neurodesenvolvimento e Autismo, Centro de Desenvolvimento da Criança, Pediatric Hospital, Centro Hospitalar e Universitário de Coimbra. Such interactions yielded, in a first phase, the main characteristics of the platform.

- **Aim:** It should enable participants to train daily living activities in virtual environments.
- **Interoperability:** Solutions for different types of platforms.
- **Self-incremental:** It should be possible to incrementally add new training tasks to the platform.
- **Reporting:** Caregivers should be able to remotely follow the progress of the patients.
- **Enabled for Immersion:** When immersion technology is available, the platform should be able to use it.

Requirements focused on two distinct user types: the patient and the caregiver. For the patient, basic needs were identified regarding not only the basic features for the platform and its interface, but also for the main serious games to be included on the system. For the caregiver, there were identified the type of follow up needed to monitor the progress of the users. On a second phase, the principal areas of interest for the daily routines to rehabilitate were identified, in order to direct the development of the serious games to include in the platform. Those areas are:

- **Hygiene:** teeth brushing, hand washing after using the toilet, choose clothes adapted to the weather, etc.
- **Privacy:** inter-personal distance regulation, keeping secret codes private, etc.
- **Employment:** train different professions, job interviews, etc.
- **Social:** adapt dialogs to the relationship with the other person, questions you should not ask, questions you should not answer, etc.
- **Housekeeping:** cooking, cleaning, place groceries, wash dishes, etc.
- **Outdoors:** deal with loud noises, exposure to animals, crossing the street safely, etc.
- **Money:** identify the money, use the debit card, attach costs to products value, etc.

Using those requirements, we built the platform we present in the next section.

3. Results

Following the requirements identified with the clinical partners, we developed the architecture defined in Figure 3.1. It incorporates a backbone of serious games, interfaced with different

devices with different levels of immersion. For the caregivers, a web interface allows access to the monitoring of the patients' information and their progress and usage of the platform along the time.

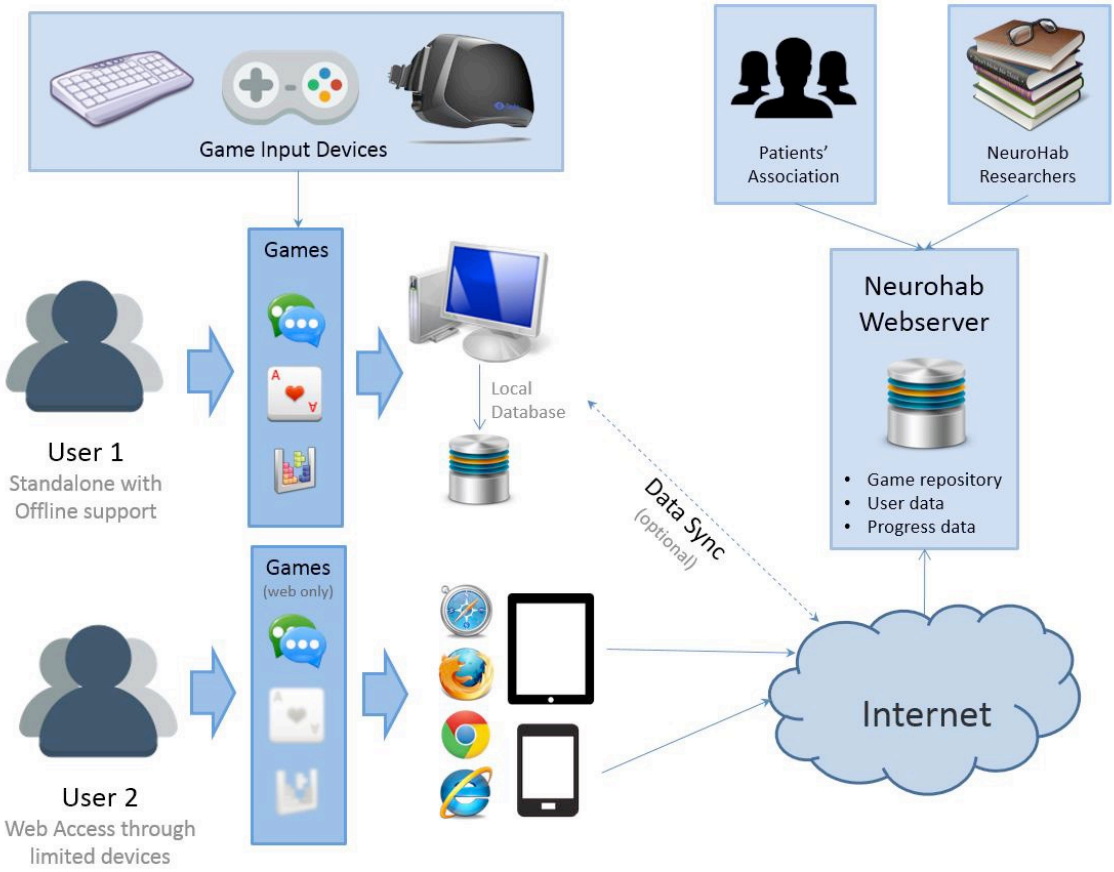

Figure 3.1 – Architecture of the system.

Therefore, Neurohab is a software platform that provides access to a growing catalog of **rehabilitation games** on **multiple platforms** with focus on **ubiquitous access** and **real-time feedback**. The software has several features which allow caregivers and therapists to closely follow the patients' performance along their usage timeline.

Ubiquitous access is achieved by having the same software run on multiple platforms like the desktop computer, the smartphone and the increasingly popular tablet. This allows for subjects to perform their training more frequently as they don't require any specific device or location. Using a centralized server, the user can automatically synchronize their progress across all devices, so they can continue as they left it. This synchronization is optional, as the

software does not require the server to run locally on any device, although required for the therapeutic follow up.

The serious games provided in the platform can be parameterized. Subjects are able to directly (through the settings configuration) or indirectly (throughout progress) affect how the games are played. From changing the controls, the ability to enable the use of specialized hardware for virtual reality scenarios, for instance, as well as several aspects affecting the difficulty of the game. There is a special emphasis on adaptive learning. Therapists can take advantage of this feature to enforce a more personalized learning, tailored to the user's needs.

The ability to run games in a cross-platform environment with shared state comes from the Neurohab architecture as shown in Figure 1. Running on the personal computers there is a standalone application that runs an embedded webserver that serves a simple UI navigation website, where users can automatically maintain an updated catalog of games and their progress data. Having the UI built on HTML5 and JavaScript, standard languages for web applications, makes it easy to share the same code between the standalone (running a machine executable) and the tablet use case (where patients access a public address serving the same UI website). When games are started from the standalone version, communication between games only happens locally. Optionally the user can have the standalone application automatically synchronizing their progress data with the Neurohab main server, allowing for other platforms to retrieve this progress and monitoring by the caregivers. In limited devices such as tablets and smartphones, access to games are restricted to web games as the user are given access to the application through their web-browsers.

Using the Neurohab website, both caregivers and therapists can watch closely how their assigned subjects are improving on the available games. For instance, on a conversations game, where subjects roam a virtual world engaging in conversations with digital avatars, caregivers are able to see how many conversations the subject performed, for how long, and how much confidence he gained with that individual avatar from the conversations made. These data are only available in the cases where the subject enables synchronization with the server (see Figure 3.2).

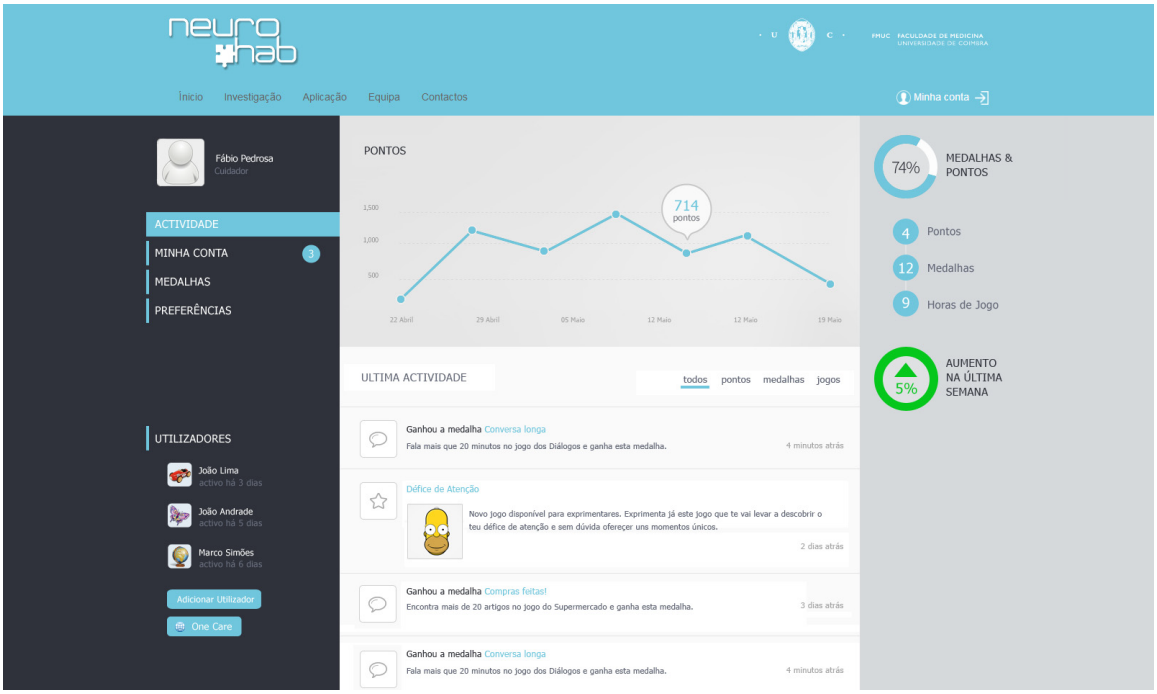

Figure 3.2 - Web interface for the caregivers to monitor the progress of the users.

There is an emphasis on data privacy in the system, resulting in a number of security features regarding the access to subjects' data, both personal information and progress record. Access to a subjects' data can only be permitted after a therapists and/or caregiver been given a secret token generated by the subject himself. This access can be revoked by the subject at any time.

The serious games are being developed as a continuous process, since the application provides the option of adding new games gradually. The games under development focus mainly daily routines targeting specific adaptive and executive dysfunctions. These games try to achieve a highly interactive and active learning experience for the user by leveraging the use of 3D virtual worlds and digital avatars to mimic subjects' real-world settings and offer ecologically valid tasks. Instructions are made available both on-screen and using text-to-speech.

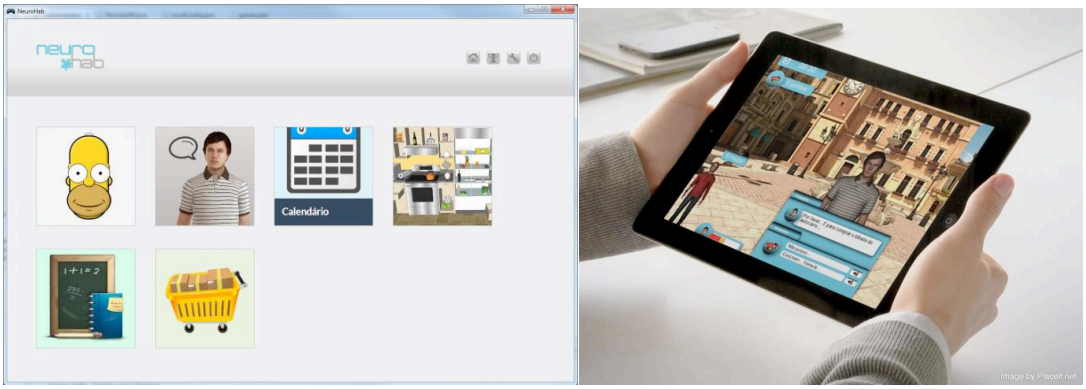

Figure 3.3 – NeuroHab platform for ASD users. On the left (a) is the main interface for selecting a serious game to practice. On the right (b) it is shown the application running on a tablet device

4. Discussion

Neurohab is both aimed at ASD patients who want to develop target specific adaptive and executive dysfunctions and therapists who want to follow on these developments and complement their rehabilitation programs with complementary autonomous training. Running the platform in several devices and integrating the data from wherever the participant is playing, it enhances the possibilities of usage and may adapt so each patient uses their preferred devices.

Furthermore, more immersive solutions can be provided by the autistic patients associations as a service, adding to their current rehabilitation offers. We believe this platform has the potential to be a complement to current therapies, reducing the costs of interventions and enhancing the follow-up of patients.

Next steps involve the validation of the serious games and the continuous improvement and development of new games to add to the catalog.

References

[1] Center for Disease Control and Prevention. Prevalence of autism spectrum disorders - Autism and Developmental Disabilities Monitoring Network, United States, 2006. MMWR Surveill Summ. 2009 Dec 18;58(10):1-20.

[2] Oliveira G, Ataide A, Marques C, Miguel TS, Coutinho AM, Mota-Vieira L, et al. Epidemiology of autism spectrum disorder in Portugal: prevalence, clinical characterization, and medical conditions. Dev Med Child Neurol. 2007 Oct;49(10):726-33.

[3] Fombonne E. Epidemiological surveys of autism and other pervasive developmental disorders: an update. J Autism Dev Disord. 2003 Aug;33(4):365-82.

[4] American Psychiatric Association. Diagnostic and Statistical Manual of Mental Disorders. 5th edition ed. Arlington, US: American Psychiatric Publishing; 2013

[5] Ventola P, Saulnier CA, Steinberg E, Chawarska K, Klin A. Early-emerging social adaptive skills in toddlers with autism spectrum disorders: an item analysis. J Autism Dev Disord. 2014 Feb;44(2):283-93.

[6] Paul R, Loomis R, Chawarska K. Adaptive behavior in toddlers under two with autism spectrum disorders. J Autism Dev Disord. 2014 Feb;44(2):264-70.

[7] American Association on Mental Retardation. Mental retardation: definition, classification, and systems of supports. . Washington, DC, USA2002.

[8] Tasse MJ, Schalock RL, Balboni G, Bersani H, Jr., Borthwick-Duffy SA, Spreat S, et al. The construct of adaptive behavior: its conceptualization, measurement, and use in the field of intellectual disability. Am J Intellect Dev Disabil. 2012 Jul;117(4):291-303.

[9] Sparrow S, Balla D, Cicchetti D. Vineland Adaptative Behaviour Scales: Interview edition, Survey form. Circle Pines, MN: American Guidance Service; 1984.

[10] Goldberg MR, Dill CA, Shin JY, Nguyen VN. Reliability and validity of the Vietnamese Vineland Adaptive Behavior Scales with preschool-age children. Res Dev Disabil. 2009 May-Jun;30(3):592-602.

[11] Soenen S, Van Berckelaer-Onnes I, Scholte E. Patterns of intellectual, adaptive and behavioral functioning in individuals with mild mental retardation. Res Dev Disabil. 2009 May-Jun;30(3):433-44.

[12] Dawson JE, Matson JL, Cherry KE. An analysis of maladaptive behaviors in persons with autism, PDD-NOS, and mental retardation. Res Dev Disabil. 1998 Sep-Oct;19(5):439-48.

[13] Matson JL, Rivet TT, Fodstad JC, Dempsey T, Boisjoli JA. Examination of adaptive behavior differences in adults with autism spectrum disorders and intellectual disability. Res Dev Disabil. 2009 Nov-Dec;30(6):1317-25.

[14] Pelphrey KA, Carter EJ. Brain mechanisms for social perception: lessons from autism and typical development. Ann N Y Acad Sci. 2008 Dec;1145:283-99.

[15] Riggs NR, Jahromi LB, Razza RP, Dillworth-Bart JE, Mueller U. Executive function and the promotion of social-emotional competence. Journal of Applied Developmental Psychology. 2006 Jul-Aug;27(4):300-9.

[16] Knapp M, Romeo R, Beecham J. Economic cost of autism in the UK. Autism. 2009 May;13(3):317-36.

[17] Amendah D, Grosse SD, Peacock G, Mandell DS. The economic costs of autism: A review. In: David Amaral DG, and Geraldine Dawson, editors, editor. Autism Spectrum Disorders. Oxford: Oxford University Press; 2011. p. 1347-60.

[18] Bellani M, Fornasari L, Chittaro L, Brambilla P. Virtual reality in autism: state of the art. Epidemiol Psychiatr Sci. 2011 Sep;20(3):235-8.

[19] Strickland D. Virtual reality for the treatment of autism. Stud Health Technol Inform. 1997;44:81-6.

[20] Vera L, Campos R, Herrera G, Romero C. Computer graphics applications in the education process of people with learning difficulties. Computers & Graphics. 2007;31:649-58.

[21] McComas J, Pivik J, Laflamme M. Current uses of virtual reality for children with disabilities. Stud Health Technol Inform. 1998;58:161-9.

[22] Wang M, Reid D. Virtual reality in pediatric neurorehabilitation: attention deficit hyperactivity disorder, autism and cerebral palsy. Neuroepidemiology. 2011;36(1):2-18.

[23] Davis M, Dautenhahn K, Powell S, Nehaniv C. Guidelines for researchers and practitioners designing software and software trials for children with autism. Journal of Assistive Technologies. 2010;4(1):38-48.